Proceedings of the

Hamburg Neutrinos from Supernova Explosions HAνSE 2011

July 19-23, 2011

Hamburg, Germany

Editors: Alessandro Mirizzi, Pasquale Dario Serpico, Günter Sigl

Verlag Deutsches Elektronen-Synchrotron

Impressum

Proceedings of the Hamburg Neutrinos from Supernova Explosion (HAνSE 2011)

July 19-23, 2011, Hamburg, Germany

Conference homepage
`http://hanse2011.desy.de/`

Slides at
`http://hanse2011.desy.de/e119287/`

Online proceedings at
`http://www-library.desy.de/preparch/desy/proc/proc11-03.html`

Editors:
Alessandro Mirizzi, Pasquale Dario Serpico, Günter Sigl
December 2011
DESY-PROC-2011-03
ISBN 978-3-935702-53-9
ISSN 1435-8077

Published by
Verlag Deutsches Elektronen-Synchrotron
Printed by
Kopierzentrale Deutsches Elektronen-Synchrotron
Notkestraße 85
22607 Hamburg
Germany

Organizing Committee

Sovan Chakraborty, Alessandro Mirizzi (Chairman), Günter Sigl, Ricard Tomàs Bayo
II Institut für Theoretische Physik
Universität Hamburg
Luruper Chaussee 149
D-22761 Hamburg

Caren Hagner
I Institut für ExperimentalPhysik
Universität Hamburg
Luruper Chaussee 149
D-22761 Hamburg

Pasquale Dario Serpico
Laboratoire de Physique Theorique
Univ. de Savoie, CNRS
B.P.110
F-74941 Annecy-Le-Vieux

Conference Secretary and Local Organization

Wiebke Kircheisen and Marco Baumgartl
II Institut für Theoretische Physik
Universität Hamburg
Luruper Chaussee 149
D-22761 Hamburg

Preface

The Hamburg Neutrinos from Supernova Explosions (HAνSE 2011) Workshop was held in DESY-Hamburg from July 19th to July 23rd, 2011. The meeting was organized by DESY and Hamburg University, with the financial support of the State Excellence Initiative (LEXI) Hamburg and of the Collaborative Research Center SFB 676 "Particles, Strings, and the Early Universe".
The project underlying HAνSE 2011 was to organize a specialized meeting focused on recent progress and open problems in supernova neutrino physics, ranging from supernova modeling to particle physics aspects and detection strategies. The aim of this meeting was to bring together experts working on various aspects of these phenomena to review the progress in understanding them, and discuss future courses of action. In order to stimulate the exchange of opinions in a truly workshop-like atmosphere, the format of the meeting included few survey talks, short contributions and ample time for discussions among the participants. In particular, the topics addressed in the Workshop were discussed in three different sessions on (1) *Astrophysical Aspects*, (2) *Particle Physics Aspects*, and (3) *Phenomenology and Detection Strategies*, respectively. The outcome of each session was eventually discussed in a summary session. These Proceedings can thus be considered as an up-to-date survey of the status and prospects of Supernova Neutrino Physics in 2011.
We sincerely believe that this Workshop has surpassed the expectations from previous events. Therefore, we would like to thank all the participants, a total of about 50 physicists, and in particular the speakers and the conveners who, in collaboration with the members of the Organizing Committee, contributed with enthusiasm to the scientific success of the Workshop.

On behalf of the Organizing Committee
Alessandro Mirizzi
Pasquale Dario Serpico
Günter Sigl

Acknowledgements

The organizers would like to thank DESY, Hamburg University, the State Excellence Initiative (LEXI) Hamburg, and the Collaborative Research Center SFB 676 “Particles, Strings, and the Early Universe” the for support and infrastructure, and specially Wiebke Kircheisen, Marco Baumgartl and Ninetta Saviano for their help with the organization that made the workshop run smoothly and helped to create a relaxing atmosphere. The organizers also thank Kirsten Sachs for the help in the preparation of these Proceedings and Roberto Mirizzi for the graphical support.

Contents

Chapter 1

Astrophysical Aspects

Convenors:

Chris Cardall
Gail McLaughlin

Neutrinos and Supernovae

Stephen W Bruenn[1], *Eric J. Lentz*[3,2,4], *Eric J. Lingerfelt*[5], *Anthony Mezzacappa*[2,3,5], *W. Raphael Hix*[2,3], *John N. Blondin*[6], *O. E. Bronson Messer*[7,3], *Pedro Marronetti*[1]

[1]Florida Atlantic University, 777 Glades Road, Boca Raton, FL 33431-0991, USA
[2]Physics Division, Oak Ridge National Laboratory, P. O. Box 2008, Oak Ridge, TN 37831-6354, USA
[3]Department of Physics and Astronomy, University of Tennessee, Knoxville, TN 37996-1200, USA
[4]Joint Institute for Heavy Ion Research, Oak Ridge National Laboratory, P. O. Box 2008, Oak Ridge, TN 37831-6374, USA
[5]Computer Science and Mathematics Division, Oak Ridge National Laboratory, P. O. Box 2008, Oak Ridge, TN 37831-6164, USA
[6]Department of Physics, North Carolina State University, Raleigh, NC 27695-8202, USA
[7]National Center for Computational Sciences, Oak Ridge National Laboratory, P. O. Box 2008, Oak Ridge, TN 37831-6164, USA

DOI: http://dx.doi.org/10.3204/DESY-PROC-2011-03/bruenn

We review the current status of the core-collapse supernova (CCSN) mechanism, beginning with a very brief account of CCSN types, and of the growing number of observations of their corresponding progenitors. This is followed by a brief account of current developments in the modeling of CCSNe progenitors, and of the four main supernova mechanisms under current study. We then focus on the current status of the neutrino mechanism, describing its essential features, as this mechanism seems the most promising at this time. We follow with a brief description of current efforts at the very computationally demanding challenge of modeling the neutrino mechanism, ending with a brief description of our CHIMERA code and some recent results obtained with this code.

1 Progenitors of Core-Collapse Supernovae

1.1 Observations

One of the major observational goals of core-collapse supernovae (CCSNe) research is to determine what main sequence mass range of stars will end up as CCSNe. Computer simulations of stellar evolution indicate that stars between 8 $M_\odot$ and $\sim$ 140 $M_\odot$ end their normal thermonuclear evolution with a core collapse. Below 8 $M_\odot$, a star sheds its envelope and settles non-explosively into a white dwarf. Above $\sim$ 140 $M_\odot$ a star suffers a pair-instability, triggering explosive oxygen core burning which results in the complete disruption of the star.

CCSNe are classified, in order of increased envelope stripping prior to explosion, as II-P (plateau), II-L (linear), IIn (narrow lines) IIb (transitional), Ib (no H), and Ic (no H or He) [1]. Until the advent of SN1987A, estimates of progenitor masses for any of these types had to

rely on the correlations between these supernovae and regions of massive star formation (giant HII regions) in galaxies, or estimating the ejected mass by modeling light curves and ejection velocities. Because of the nearness of SN1987A (a type II pec at $\sim$ 48 kpc) it was possible for the first time to identify the progenitor (a blue supergiant of mass $\sim$ 18 $M_\odot$). In addition, the detection of a total of 19 neutrinos in the Kamioka and IMB detectors confirmed the basic CCSN scenario, namely, that a core collapse of a massive star does indeed occur, and that the bulk of the gravitational binding energy is radiated away by neutrinos. It was also possible to detect the progenitor for the next nearest explosion, SN1993 in M81 ($\sim$ 3.6 Mpc), a type II which transformed to a type Ib, the data being best fit by a star of 15 $M_\odot$ main-sequence (MS) mass and tidally stripped of most of its hydrogen envelope by prior binary mass transfer.

The detection of other supernova progenitors has been made possible by high resolution archives of galaxy images built up over the past 15 or so years, mainly by the Hubble Space Telescope. By finding an image or an upper limit to an image on a high resolution pre-explosion galaxy image at the position of the SN it is possible, by comparing the color and magnitude of the image (or upper limit) with stellar models, to estimate the MS mass (or upper limit) and stellar type of the progenitor. For the progenitors of type II-P SNe, the most common type, this technique has netted 8 identifications (all red supergiants (RSGs), as expected) for which mass estimates are possible, and 12 upper limits (see [2] for a review through early 2009). Surprisingly, within the uncertainties of stellar modeling and the possible extinction of the progenitor by dust, no progenitor of a SN II-P greater than 21 $M_\odot$ has been found, and this upper limit is probably smaller. The lower limit appears to be about 8.5 $M_\odot$. Two progenitors of SNe II-L have been identified (tentatively) as yellow supergiants (YSGs) with inferred progenitor masses of 18 - 25 $M_\odot$, and only one progenitor of a SN IIn, a massive ($\geq$ 50 $M_\odot$) luminous blue variable (LBV). Several Type IIb SN progenitors have been identified; SN1993 mentioned above, and SN 2011dh whose progenitor has been identified as YSG of initial MS mass of 18–21 $M_\odot$ [3] or 13 $\pm$ 3 $M_\odot$ [4]. Unlike the above SN types, no progenitors of SNe Ib or Ic have been identified. They are expected to arise from Wolf-Rayet stars and/or from stars whose H or H/He envelope has been tidally stripped by Roche lobe overflow to a binary companion. Their correlation with regions of massive star formation suggest that at least some arise from the former.

It thus appears from observations that single stars in the MS mass range from $\sim$ 8.5 to 16 - 21 $M_\odot$ explode as SN II-P, and perhaps a subset of stars in this mass range that are tidally stripped in binaries and more massive single WR stars explode as SNe IIb, SNe Ib or Ic. On the basis of very limited observations, more massive stars explode as SN II-P when YSG's, and very massive LBV explode as SN IIn. Unanswered are the fate of RSG more massive than $\sim$ 21 $M_\odot$, whether some stars collapse directly to black holes with little or no optical display, whether there are distinct faint and bright branches of SN from a given mass range, and so on.

1.2 Modeling

The evolutions of massive stars from the main-sequence (MS) to the onset of core collapse have been computed in 1D by a number of groups ([5] and references therein). These calculations have all shown the development of a generic stellar structure consisting of nested burning shells of successively heavier elements from the hydrogen-helium envelope on the outside to the silicon-like shell overlying an inert iron-like core at the center. One of the great uncertainties attending 1D progenitor calculations is the modeling of turbulent mixing processes—e.g., turbulent mixing associated with thermal convection and/or rotational shear. Standard procedure is to use

some form of mixing length theory (MLT) in the turbulent regime with a prescription as to the location of the inner and outer boundaries, and to assume physically plausible diffusion coefficients for the transport of angular momentum due to rotational shear, magnetic torques, etc, ([6] and references therein). This introduces a number of ambiguities into the model, e.g., placement of the convective boundaries, mixing profiles, interaction with of convective plumes with the stable layers, diffusion coefficient magnitudes, etc.

It has now become possible with improved computing facilities to study the hydrodynamics of stellar interiors with two- and particularly three-dimensional simulations of space and time "windows" of the stellar interior (see [7] and references therein for modeling thermal convection, and [8] and references therein for modeling rotation). These studies have revealed shortcomings of current 1D modeling. In particular, they have shown that: (1) the traditional prescriptions for setting the locations of the inner and outer boundaries of a turbulent layer, e.g., the Schwarzschild or Ledoux criterion, should be replaced by a Richardson criterion, which is a measure of the boundary "stiffness" to the strength of the turbulence; (2) rather than convective overshooting, mixing occurs at convective boundaries and the convective region grows due to turbulent entrainment (shear instabilities and the scouring out of the stable layer by turbulent eddies); (3) wave generation at convective boundaries induces slow mixing in the stable layers; (4) shell burning, particularly O shell burning, can be violent, leading to asymmetries at the onset of core collapse; (5) smaller effective mixing lengths near the lower boundaries of a turbulent regions lead to steeper temperature gradients, affecting nuclear-reaction rates due to their stiff temperature dependence; (6) the large ratio of the size of rising high entropy plumes to low entropy downflows results in a large downward flux of kinetic energy (neglected in MLT) compensated by a correspondingly large upward enthalpy flux to maintain the requisite convective luminosity; (7) in rotating red giant envelopes, simulations do not approach the extreme cases of uniform mean radial specific angular momentum or angular velocity as has been typically assumed in 1D models.

It is clear from the above that the structure of core collapse progenitors may be expected to change in the near future as results of these multi-D computational experiments become incorporated into stellar evolutionary calculations.

2 The Core-Collapse Supernova Mechanism

Four explosion mechanisms have been the focus of CCSNe research during recent years: (1) the acoustic mechanism, (2) the MHD mechanism, (3) the hadron-quark mechanism, and (4) the neutrino-driven mechanism.

2.1 Acoustic Mechanism

The acoustic mechanism was discovered by [9] in the simulation of an 11 $M_\odot$ progenitor. They found that long after shock stagnation ($\gtrsim 0.6$ s post-bounce) turbulence and anisotropic accretion on the proto-neutron star excites and maintains vigorous g-mode oscillations which radiate intense sound waves, the energy coming from the gravitational binding energy of the accreted gas. As these sound waves propagate outward through the negative density gradient into the surroundings, they steepen into shocks and their energy and momentum are efficiently absorbed, powering up the supernova explosion. Thus, the proto-neutron star acts like a transducer converting the gravitational energy of infall into acoustic energy which propagates out

and deposits energy in the surroundings, in analogy with the neutrino transport mechanism. They subsequently found [10] that the acoustic mechanism is able to explode a variety of progenitors at late times ($\gtrsim 0.6$ s). The physical reality of this mechanism is debated, as it has not been observed in simulations by other investigators although their numerical techniques, though different, are capable of capturing this phenomenon. A further note of caution is cast by a recent study by [11] that finds that the damping of the primary $\ell = 1$ g-mode mode by the parametric instability causes this mode to saturate at an energy two orders of magnitude lower than that required to power a supernova.

2.2 MHD Mechanism

Magnetic fields threading a progenitor are frozen in the gas on all relevant core-collapse time scales. On core collapse these magnetic fields will be amplified both by flux conservation during matter compression and by being wound up toroidally by the differential rotation of the core. Simulations with increasing sophistication have shown that if the iron core before collapse is threaded by very strong magnetic fields (B $\geq 10^{12}$ gauss), then this in combination with rapid rotation can produce jet-like explosions magnetically on a prompt time scale (see [12, 13, 14, 15, 16, 17]). Furthermore, it has been recognized that initially weak magnetic fields can be amplified to equipartition values exponentially by the magnetorotational instability [18, 19, 20]. Notwithstanding all this, it must be appreciated that the maximum magnetic energy that can be achieved in a differentially rotating core is the free energy, $T_{\rm free}$, of the differential rotation, i.e., the difference between the energy of the differentially rotating core and the same core uniformly rotating with the same angular momentum, and

$$T_{\rm free} \leq T_{\rm rot} = 4 \times 10^{51} \left(\frac{\kappa_{\rm I}}{0.3}\right) \left(\frac{M}{1.4 M_\odot}\right) \left(\frac{R}{10 \text{ km}}\right)^2 \left(\frac{P_{\rm rot}}{2 \text{ ms}}\right)^{-2} \text{ ergs} \qquad (1)$$

[20]. Thus rather small initial rotation periods, ≤ 2 ms, for newly formed neutron stars are required if enough magnetic energy is to potentially arise to power up the typical supernova. These small rotation periods are at variance with the calculated rotational periods of the magnetized cores of supernova progenitors [6], and the extrapolated periods of newly formed neutron stars (≥ 10 ms). Both of these constraints are "soft" (stellar evolutionary calculations with rotation and magnetic fields are not ab initio, and we have not yet observed a newly formed neutron star), but if they hold, then the MHD mechanism will only be relevant to a subset of core collapse supernovae. However, the observations of magnetars, long-duration gamma-ray bursts, and hints of highly collimated material in some supernova remnants suggests a subclass of events that are magnetically driven.

2.3 Hadron-Quark Mechanism

A recently investigated ([21, 22, 23]) possible supernova mechanism obtains if a hadron-quark phase transition occurs at the $(\rho, , T, Y_{\rm e})$-values sampled by the core center at and around core bounce. As in all scenarios, the core bounce launches a shock which propagates out to 100 - 200 km and stalls, becoming an accretion shock (see below). The formation of a mixed phase softens the equation of state (EOS) and induces a further collapse of the protoneutron star (PNS) at some given period after the initial core bounce when this EOS softening encompasses enough of the core. A secondary accretion shock forms when this second core collapse is halted by the formation of a pure quark phase which stiffens the EOS again. The secondary accretion

shock becomes dynamic, propagates outward, and merges with the original accretion shock and the resulting shock propagates outward giving rise to a supernova. The viability of this model depends on a low critical density for the hadron-quark phase transition for proton fractions of 0.2 - 0.3 and temperatures of 10 - 30 MeV. At the present time this critical density is unknown.

2.4 Neutrino-Driven Mechanism

The neutrino-driven mechanism has a long pedigree extending back to the seminal paper of [24] and its more modern incarnation [25]. Following the collapse and bounce of the inner core of massive star at the endpoint of its normal thermonuclear evolution, the shock launched at core bounce stalls in the outer core, losing energy (and therefore post-shock pressure) to nuclear dissociation and electron neutrino losses. Within a short time ($\sim$ 50 ms) a thermodynamic profile is established in which infalling matter encountering the outward flow of neutrinos undergoes net heating between the shock and the so-called gain radius, and net cooling below, due to the different neutrino heating and cooling radial profiles. Crudely speaking, for neutrino heating to be successful in powering an explosion a fluid element must be heated sufficiently while it resides in the heating layer to reenergize the shock.

Energy deposition by neutrinos plays the primary role in the neutrino-driven mechanism, and the rate of energy deposition per nucleon, $\dot{q}$, can be written as

$$\dot{q} = \frac{X_{\rm n}}{\lambda^a_{\nu_{\rm e}}} \frac{L_{\nu_{\rm e}}}{4\pi r^2} \langle \epsilon^2_{\nu_{\rm e}} \rangle \frac{1}{f_{\nu_{\rm e}}} + \frac{X_{\rm p}}{\lambda^a_{\bar{\nu}_{\rm e}}} \frac{L_{\bar{\nu}_{\rm e}}}{4\pi r^2} \langle \epsilon^2_{\bar{\nu}_{\rm e}} \rangle \frac{1}{f_{\bar{\nu}_{\rm e}}}, \tag{2}$$

where the first and second terms express the absorption of electron neutrinos ($\nu_{\rm e}$'s) and antineutrinos ($\bar{\nu}_{\rm e}$'s), respectively. For the $\nu_{\rm e}$'s ($\bar{\nu}_{\rm e}$'s), $L_{\nu_{\rm e}}$ ($L_{\bar{\nu}_{\rm e}}$) is their luminosity, $\langle \epsilon^2_{\nu_{\rm e}} \rangle$ ($\langle \epsilon^2_{\bar{\nu}_{\rm e}} \rangle$) their mean square energy, and and $\frac{1}{f_{\nu_{\rm e}}}$ ($\frac{1}{f_{\bar{\nu}_{\rm e}}}$) their inverse flux factor (ratio of zeroth to first angular moment of the neutrino distribution), which is a measure of their anisotropy. The presence of the mean square neutrino energies and the inverse flux factors underscores the necessity of accurately calculating both the energy spectrum and the angular distribution of the neutrinos and antineutrinos.

3 Status of the Neutrino-Driven Mechanism

Simulations of core-collapse supernovae in spherical symmetry with considerable realism have been performed with Boltzmann neutrino transport, state-of-the-art neutrino interactions, and with/without general relativity [26, 27, 28, 29, 30]. Except for the smallest MS masses undergoing core collapse, these have not yielded explosions. Something was clearly missing.

An insight as to what might be the missing ingredient began to be appreciated during the 1990's, and is the essential role played by multidimensional effects. Analyses of immediate post-bounce core profiles given by computer simulations had for a long time indicated that a variety of fluid instabilities are present, driven by gradients in entropy and/or leptons. The most important of these for the neutrino-driven mechanism is the neutrino heating above the neutrinosphere. Because neutrinos heat the bottom of the heating layer most intensely, a negative entropy gradient builds up which renders the layer convectively unstable. In order for convection to grow, however, the fluid must remain in the heating layer for a critical length of time; roughly the ratio of the advective timescale to some averaged timescale of convective growth timescale must be $\gtrsim 3$ [31]. If convection can get established in the hearing layer, hot

gas from the neutrino-heating region will be transported directly to the shock, while downflows simultaneously will carry cold, accreted matter to the layer of strongest neutrino heating where a part of this gas, being cold, readily absorbs more energy from the neutrinos. The loss of energy accompanying the advection of matter through the gain radius is thereby reduced and more energy stays in the heating layer. A useful criterion for shock revival and successful neutrino driven explosions is the residency time of fluid elements in the heating layer [32]. Longer residency times, by allowing fluid elements to absorb more energy, are thus favorable for explosions. The lateral motions associated with convection lengthen the heating layer residency time of some fluid elements, thereby further enhancing the effects of convection.

Another important phenomenon missing in spherical symmetry was pointed out by [33] who discovered that the stalled shock is subject to low-mode aspherical oscillations, which is now referred to as the standing accretion shock instability or 'SASI.' The cause of this instability is still being debated, but it leads to enlargements of the heating layer in certain regions and its diminution in others. Where the heating region is enlarged, the residency times of fluid elements is lengthened, and the magnitude of neutrino heating is enhanced. Where the heating region is constricted, conditions are favorable for the establishment of down-flows or return-flows for large-scale convection. The diversion of infalling material by the distorted shock to the constricted regions adds to these effects. It has further been pointed out and supported by 2D simulations with parameterized neutrino sources that the development of the SASI leads to the large asymmetries observed for SN 1987A and other supernovae, and might account for the large observed velocities of neutron stars [34, 35].

A number of groups are actively engaged in modeling CCSNe with the aim of ascertaining the viability of the neutrino mechanism. These include the Princeton-CalTech-Israeli group using the Vulcan/2D code, the Swiss-Japanese group using the Zeus+IDSA code, the Garching group with using VERTEX code, and the FAU-NCSU-Oak Ridge group using the CHIMERA code, e.g., ([36, 37, 38, 39] and references therein to earlier work). Because modeling realistic neutrino transport in CCNSe is such a computational challenge, demanding exascale resources to fully implement, say, the solution for each neutrino specie of a multi-energy, multi-angle, GR Boltzmann transport in three spatial dimensions (i.e., the solution of the time evolution of neutrinos in a six-dimensional phase space), these groups have had to resort to various approximate approaches to reduce the dimensionality of the problem. Zeus+IDSA, VERTEX, and CHIMERA use a ray-by-ray approximation whereby the three spatial dimensions accessible to a neutrino are reduced to "one-and-one-half" dimensions—namely, a one-dimensional transport problem is solved along each of an ensemble of independent radial rays spanning the solid angle of the computational domain. Lateral neutrino pressure and advection, but not transport, are computed in neutrino optically thick regions. Vulcan/2D solves the transport equation along independent "energy rays," thus ignoring non-isoenergetic scattering, specie coupling, and observer corrections, the latter omission being potentially serious as it leads, among other things, to a substantial non-conservation of energy and leptons [40].

The codes also use different approximations in solving their respective transport equations. CHIMERA and Vulcan/2D use flux-limited diffusion (the latter also has an SN option), VERTEX uses a variable Eddington tensor closure with the latter calculated by the solution of a spherically averaged, model Boltzmann equation. Zeus+IDSA uses an Isotropic Diffusion Source Approximation (IDSA) [41], whereby the neutrino distribution is broken up into a trapped component and a streaming component. VERTEX and CHIMERA use approximate GR for both the gravity and transport, CHIMERA using a spherically symmetric post-Newtonian approximation gravitational potential supplemented by a Newtonian gravity

spectral Poisson solver described in [42], VERTEX having used the same until recently switching to the conformally flat approximation [43], while the other two codes use the Newtonian approximation in both gravity and transport. A full opacity set is used by both VERTEX and CHIMERA (VERTEX also includes neutrino-neutrino interactions), including non-isoenergetic scattering from nucleons, electrons, and positrons, ion-ion correlations, weak magnetism corrections, and electron capture on an ensemble of heavy nuclei using the improved data of [44]. Vulcan/2D and Zeus+IDSA omit non-isoenergetic scatterings, ion-ion correlations, and weak magnetism corrections, and treat electron captures on nuclei as described in [45]. Finally, CHIMERA independently transports four coupled neutrino species ($\nu_{\rm e}$'s, $\bar{\nu}_{\rm e}$'s, $\nu_{\mu\tau}$'s and $\bar{\nu}_{\mu\tau}$'s), VERTEX independently transports three coupled neutrino species ($\nu_{\rm e}$'s, $\bar{\nu}_{\rm e}$'s, and $\nu_{\rm x}$'s, where $\nu_{\rm x} = \{\nu_{\mu\tau}, \bar{\nu}_{\mu\tau}\}$), and Vulcan/2D and Zeus+IDSA transport two uncoupled species ($\nu_{\rm e}$'s, $\bar{\nu}_{\rm e}$'s).

Given the differences between the groups in the implementation of neutrino transport, and other differences, such as the grid geometry and resolution, the hydrodynamic scheme, equation of state used, and the progenitors chosen, it is not surprising that results from the above groups have not converged. The FNO group in has found, for example, fairly strong explosions for progenitor masses in the range of 12 - 25 $M_\odot$ [39], the G and SJ groups get, respectively, weak explosions for 11.2 and 15 $M_\odot$ progenitors [46], and a 13 $M_\odot$ progenitor [37], while the PCI group did not obtain any neutrino-driven explosions in their simulations [9, 10]. Clearly, much work needs to be done before the viability of the neutrino-driven mechanism is understood.

4 CHIMERA Code

The CHIMERA code has been extensively refined and updated since the last suite of core-collapse simulations were performed as described in [39]. Adding to the brief description of the code given above, the CHIMERA hydrodynamics consists of a Lagrangian remap implementation of the Piecewise Parabolic Method (PPM) [47]. A moving radial grid option and an adaptive mesh redistribution algorithm keeps the radial grid between the core center and the shock structured so as to maintain approximately constant $\Delta\rho/\rho$ both during collapse and the post-bounce evolutionary phases. The grid resolution for current 2D simulations is now 512 radial zones and 256 angular zones . Above 10^{11} g cm^{-3}, the equation of state (EOS) used is the Lattimer-Swesty EOS [48] with an incompressibility coefficient of 220 MeV. For matter in nuclear statistical equilibrium (NSE) below 10^{11} g cm^{-3} with proton fractions below 26/56 a modified Cooperstein EOS is used [49], and for a proton fraction above 26/56 the nuclei are treated as an ideal gas of 17 nuclear species in NSE (neutrons, protons, alpha particle nuclei from 4He to 60Zn, and 56He). In regions where nuclei are not in NSE, the same 17 nuclei are employed with the 14 alpha particle nuclei evolved by means of a nuclear reaction network.

5 2D Simulation Results

A suite of four 2D simulations are currently being computed by CHIMERA, initiated from the 12, 15, 20, and 25 $M_\odot$ core-collapse progenitors of [50]. The 15, 20, and 25 $M_\odot$ models have evolved less than 200 ms post-bounce, which is too early to ascertain whether an explosion will ensue. We will briefly describe the 12 $M_\odot$ model, which has evolved past 200 ms and seems to be exhibiting the beginnings of an explosion.

Following core bounce, which occurs 260.9 ms after the initiation of the simulation, the shock propagates rapidly out to $\sim$ 60 km in 10 ms and than pauses for a few ms. At this time

a brief but violent convection sets in initially at a radius of $\sim$ 38 km, driven by a negative lepton fraction (Y_ℓ) gradient. This gradient is established when the shock propagates through the neutrinosphere, and it occurs by the rapid electron capture and outward transport of ν_e's, which lowers the electron fraction (Y_e) and Y_ℓ below the values in the denser regions below where the ν_e's are fully trapped. The inner radius of this region of lowered Y_e is advected inward as the core compresses while the outer radius of this region advances with the shock. Consequently, in $\sim$ 5 ms the lepton-driven convection grows to encompass the region between 16 and 60 km, the shock in the mean time having resumed its outward propagation to $\sim$ 80 km. This convective episode only lasts only 10 – 15 ms, but it has the effect of perturbing the shock and exciting low-order SASI modes. During the next $\sim$ 30 ms the shock continues to propagate out and then stagnates at an average radius of $\sim$ 150 km, all the time sloshing from side to side in what appears to be a combination of $\ell = 1$ and $\ell = 2$ modes. This sloshing motion causes entropy fluctuations in the form of arcs to be formed behind the shock. Arcs of high entropy material form behind the shock when the shock front is moving outward and the relative velocity between the shock front and the infalling material is correspondingly large; arcs of low entropy material form behind the shock when the shock front moves inward and the relative velocity between the shock front and the infalling material is correspondingly small. Comparing the mean shock radius versus time of this 2D simulation with the shock radius versus time of a corresponding 1D simulation shows that the two radii track each other closely for the first 30 or so ms. After 30 ms, the mean shock radius of the 2D simulation begins to exceed that of the 1D simulation. The shock radius of the 2D simulation also exhibits a growing difference between its maximum and minimum values, reflecting the SASI and its increasing amplitude with time. The mean entropy of the fluid as a function radius in the 2D simulation at 30 ms post-bounce tracks closely that of the 1D simulation out to about 40 km, but rises slightly above that of the 1D simulation out to the shock, with a growing spread between maximum and minimum values.

At about 50 ms post-bounce the heating layer begins to become convectively unstable, and mushroom shaped plumes of high entropy material begin to appear, separated by narrow down-flows. These plumes slowly merge, and by 90 ms post-bounce a flow pattern from polar to equatorial regions becomes established. This is caused by the prolate shape assumed by the shock at this time. Infalling material encountering the prolate shock is deflected equatorially, driving the polar to equatorial flow. By 130 ms post-bounce smaller high entropy convective plumes have merged into three large high entropy plumes, two polar and one equatorial, with down-flows on either side of the equatorial plume. The residency time for material in the high-entropy plumes, particularly the polar plumes, becomes large, while newly shocked material is directed towards the down-flows and quickly reaches the surface of the nascent neutron star. The large residency time of the material in the high-entropy plumes causes the entropy to rise there, with the result that the plumes tend to push the shock farther out. The down-flows are deflected around the nascent neutron star by the SASI induced motion of the fluid there, and encounter the neutron star surface near the polar regions causing the accretion ν_e and $\bar{\nu}_e$ luminosities to peak there. The result is that at this time the ν_e and $\bar{\nu}_e$ luminosity as a function of angle is generally smaller in the equatorial region than in a corresponding 1D simulation at the same time, but larger in the polar regions. By 210 ms post-bounce the shock near the zero angle polar region passes 400 km, and the shock near the near the opposite pole passes this radius 20 ms later. A runaway situation has apparently been established and the shock continues to expand in a highly prolate fashion for the rest of the simulation. The simulation has only been carried out for 240 ms so it is much too early to ascertain the explosion energy.

6 Conclusions

Observations of CCSNe during the past decade are providing information as to the masses and evolutionary states of their stellar progenitors, and the types of stellar progenitors as a function of the SN spectral type. The statistics are still poor except for the type II-P SNe, which arise from a range of initial MS masses from ~ 8.5 $M_\odot$ to an uncertain maximum mass which is likely metalicity dependent. The low end of the initial MS mass of CCSNe progenitors, in fact, appears to be ~ 8.5 $M_\odot$, as expected from theory. Computer modeling of these progenitors can be expected to become more realistic as new multi-dimensional computations of fluid instabilities, induced by thermal convection and rotation, serve to guide their implementation in the stellar models. The most extensively studied CCSN mechanism, and perhaps the most promising at this time, is the neutrino-driven mechanism. The formidable computing challenges of realistically modeling the neutrino-driven mechanism, however, has compelled groups to make approximations in the physics and the numerics implemented in their codes, particularly in their neutrino transport algorithms, and this has led to disagreements between the results of different groups. It is expected that as more powerful computing resources become available enabling more realistic modeling to be done, these disagreements will diminish. The neutrino-driven mechanism will the either become the standard CCSN model, or will be shown to be in need of modification or replacement.

7 Acknowledgments

S.W.B. and P.M. acknowledge partial support from NASA award 07-ATFP07-0011, E. J. Lentz. is supported NASA grant number NNH11AQ721 and NSF grant number OCI-0749242), A.M. and W.R.H. are supported by the Department of Energy Office of Nuclear Physics, and A.M., O.E.B.M., and E.J.Lingerfelt are supported by the Department of Energy Office of Advanced Scientific Computing Research. This research was supported in part by the National Science Foundation through TeraGrid resources provided by the National Institute for Computational Sciences under grant number TG-MCA08X010. This research used resources of the Oak Ridge Leadership Computing Facility at the Oak Ridge National Laboratory, which is supported by the Office of Science of the U.S. Department of Energy under Contract No. DE-AC05-00OR22725.

References

[1] A. V. Filippenko. *Annual Review of Astronomy and Astrophysics*, 35:309, 1997.

[2] S. J. Smartt. *Annual Review of Astronomy and Astrophysics*, 47:63, 2009.

[3] S. D. Van Dyk, W. Li, S. B. Cenko, M. M. Kasliwal, A. Horesh, E. O. Ofek, A. L. Kraus, J. M. Silverman, L Arcavi, A. V. Filippenko, A. Gal-Yam, R. M. Quimby, S. R. Kulkarni, O. Yaron, and D. Polishook. *eprint arXiv:1106.2897*, 2011.

[4] J. R. Maund, M. Fraser, M. Ergon, A. Pastorello, S. J. Smartt, J. Sollerman, S. Benetti, M.-T. Botticella, F. Bufano, I. J. Danziger, R. Kotak, L. Magill, A. W. Stephens, and S. Valenti. *Astrophysical Journa Letters*, 739:L37, 2011.

[5] S.-C. Yoon and S. E. Woosley. *Astrophysical Journal*, 725:940, 2010.

[6] A. Heger, S. E. Woosley, and H. C. Spruit. *Astroparticle Physics*, 626:350, 2005.

[7] W. D. Arnett and C. Meakin. *Astrophysical Journal*, 733:78, 2011.

[8] A. S. Brun and A. Palacios. *Astrophysical Journal*, 702:1078, 2009.

[9] A. Burrows, E. Livne, L. Dessart, C. D. Ott, and J Murphy. *Astrophysical Journal*, 640:878, 2006.

[10] A. Burrows, E. Livne, L. Dessart, C. D. Ott, and J Murphy. *Astrophysical Journal*, 655:416, 2007.

[11] N. N. Weinberg and E. Quataert. *Monthly Notices of the Royal Astronomical Society, Letters*, 387:L64, 2007.

[12] A. Burrows, L. Dessart, E. Livne, C. D. Ott, and J. Murphy. *Astrophysical Journal*, 664:416, 2007.

[13] L. Dessart, A. Burrows, E. Livne, and C. D. Ott. *Astrophysical Journal*, 669:585, 2007.

[14] H. Mikami, Y. Sato, T. Matsumoto, and T. Hanawa. *Astrophysical Journal*, 683:357, 2008.

[15] S. G. Moiseenko and S. Bisnovatyi-Kogan, G. *Astrophysics and Space Science*, 311:191, 2007.

[16] H. Sawai, K. Kotake, and S. Yamada. *Astrophysical Journal*, 672:465, 2008.

[17] T. Takiwaki, K. Kotake, and K. Sato. *Astrophysical Journal*, 691:1360, 2009.

[18] S. A. Balbus and J. F. Hawley. *Astrophysical Journal*, 376:214, 1991.

[19] S. A. Akiyama, J. C. Wheeler, D. L. Meier, and I. Lichtenstadt. *Astrophysical Journal*, 584:954, 2003.

[20] M. Shibata, Y. T. Liu, S. L. Shapiro, and B. C. Stephens. *Physical Review D*, 74:104026, 2006.

[21] I. Sagert, T. Fischer, M. Hempel, G. Pagliara, J. Schaffner-Bielich, A. Mezzacappa, F.-K. Thielemann, and M. Liebendörfer. *Physical Review Letters*, 102:article id. 081101, 2009.

[22] T. et al. Fischer. *Classical and Quantum Gravity*, 27:114102, 2010.

[23] T. Fischer, I. Sagert, M. Hempel, G. Pagliara, J. Schaffner-Bielich, and M. Liebendörfer. *Astrophysical Journal Supplement*, 194:article id. 39, 2011.

[24] S. A. Colgate and R. H. White. *Astrophysical Journal*, 143:626, 1966.

[25] H. A. Bethe and J. R. Wilson. *Astrophysical Journal*, 295:14, 1985.

[26] M. Rampp and H.-Th. Janka. *Astrophysical Journal Letters*, 539:L33, 2000.

[27] A. Mezzacappa, M. Liebendörfer, O. E. Messer, W. R. Hix, F.-K. Thielemann, and S. W. Bruenn. *Physical Review Letters*, 86:1935, 2001.

[28] T. A. Thompson, A. Burrows, and P. A. Pinto. *Astrophysical Journal*, 592:434, 2003.

[29] M. Liebendörfer, A. Mezzacappa, F.-K. Thielemann, O. E. Messer, W. R. Hix, and S. W. Bruenn. *Physical Review D*, 63:103004, 2001.

[30] M. Liebendörfer, M. Rampp, H.-Th. Janka, and A. Mezzacappa. *The Astrophysical Journal*, 620:840, 2005.

[31] T. Foglzzo, L. Scheck, and H.-Th. Janka. *The Astrophysical Journal*, 652:1436, 2006.

[32] J. W. Murphy and A. Burrows. *Astrophysical Journal*, 688:1159, 2008.

[33] J. M. Blondin, A. Mezzacappa, and C. DeMarino. *Astrophysical Journal*, 584:971, 2003.

[34] K. Kifonidis, T. Plewa, H.-Th. Janka, and E. Müller. *Astronomy and Astrophysics*, 453:661, 2006.

[35] L. Scheck, T. Plewa, H.-TH. Janka, K. Kifonidis, and E. Müller. *Astronomy and Astrophysics*, 457:963, 2007.

[36] T. D. Brandt, A. Burrows, C. D. Ott, and E. Livne. *Astrophysical Journal*, 728:article id. 8, 2011.

[37] Y. Suwa, K. Kotake, T. Takiwaki, S. C. Whitehouse, M. Liebendörfer, and K. Sato. *Publications of the Astronomical Society of Japan*, 62:L49, 2010.

[38] F. Hanke, A. Marek, B. Müller, and H.-Th. Janka. *eprint arXiv:1108.4355*, 2011.

[39] S. W. Bruenn, A. Mezzacappa, W. R. Hix, J. M. Blondin, O. E. B. Messer, C. J. Dirk, and S. Yoshida. In *Journal of Physics*, volume 180 of *Conference Series*, page 012018. IOP, 2006.

[40] E. Lentz, A. Mezzacappa, O. E. B. Messer, M. Liebendörfer, W. R. Hix, and S. W. Bruenn. *Submitted to ApJ*, 2011.

[41] M. Liebendörfer, S. C. Whitehouse, and T. Fischer. *Astrophysical Journal*, 698:1174, 2009.

[42] E. Müller and M. Steinmetz. *Computer Physics Communications*, 89:45, 1994.

[43] B. Müller, H.-Th. Janka, and H. Dimmelmeier. *Astrophysical Journal Supplement*, 189:104, 2010.

[44] K. Langanke, G. Martínez-Pinedo, J. M. Sampaio, D. J. Dean, W. R. Hix, O. E. B. Messer, A. Mezzacappa, M. Liebendörfer, H.-Th. Janka, and M. Rampp. *Physical Review Letters*, 90:241102, 2003.

[45] S. W. Bruenn. *Astrophysical Journal Supplement*, 58(4):771, 1985.

[46] A. Marek and H.-Th. Janka. *Astrophysical Journal*, 694:664, 2009.

[47] P. Colella and P. R. Woodward. *Journal of Computational Physics*, 54:174, 1984.

[48] J.M. Lattimer and D. F. Swesty. *Nuclear Physics A*, 535:331, 1991.

[49] J. Cooperstein. *Nuclear Physics A*, 438:722, 1986.

[50] S. E. Woosley and A. Heger. 442:269, 2007.

Core-Collapse Supernovae: Explosion Dynamics, Neutrinos and Gravitational Waves

Bernhard Müller[1], *Hans-Thomas Janka*[1], *Andreas Marek*[1], *Florian Hanke*[1], *Annop Wongwathanarat*[1], *Ewald Müller*[1]

[1]Max-Planck-Institut für Astrophysik, Karl-Schwarzschild-Str. 1, 85748 Garching, Germany

DOI: http://dx.doi.org/10.3204/DESY-PROC-2011-03/mueller

The quest for the supernova explosion mechanism has been one of the outstanding challenges in computational astrophysics for several decades. Simulations have now progressed to a stage at which the solution appears close and neutrino and gravitational wave signals from self-consistent explosion models are becoming available. Here we focus one of the recent advances in supernova modeling, the inclusion of general relativity in multi-dimensional neutrino hydrodynamics simulations, and present the latest simulation results for an $11.2M_\odot$ and a $15M_\odot$ progenitor. We also mention 3D effects as another aspect in supernova physics awaiting further, more thorough investigation.

1 Introduction

Massive stars end their lives as a core-collapse supernova (SN), a violent event that involves the collapse of the iron core of the progenitor to a proto-neutron star and the subsequent expulsion of the outer layers of the star with a kinetic energy on the order of 10^{51} erg, which is associated with a spectacularly bright optical display. Currently, there is still no final consensus on the supernova explosion mechanism that operates in the optically obscured supernova core, and a number of competing ideas are under discussion. The delayed neutrino-driven mechanism [1, 2], which relies on neutrino energy deposition in the gain region to revive the stalled shock, remains the most promising candidate, provided that the efficiency of neutrino heating can be sufficiently enhanced by multi-dimensional hydrodynamical instabilities such as convection and the so-called standing accretion shock instability SASI [3, 4]. This mechanism has worked successfully in several recent 2D simulations [5, 6, 7] (some of which appeared to be only marginally successful [6]), but has failed in others [8, 9]. Alternatives to the neutrino-driven mechanism have also been proposed, such as the acoustic mechanism [8, 9] (whose viability has been called into question by [10], however), magnetohydrodynamically driven supernovae [11, 12], and explosions triggered by a QCD phase transition [13].

As the "engine" driving this explosion is not directly accessible by classical, photon-based astronomical observations, our understanding of the supernova explosion mechanism has largely rested on numerical simulations in the past ever since the pioneering work of [14]. Over the years, a variety of ambitious numerical approaches has been developed to cope with the challenging interplay of neutrino transport, multidimensional hydrodynamics, general relativity (GR), neutrino physics, and nuclear physics in the supernova problem. The currently most advanced models rely on sophisticated multi-group neutrino transport schemes (e.g. ray-by-ray

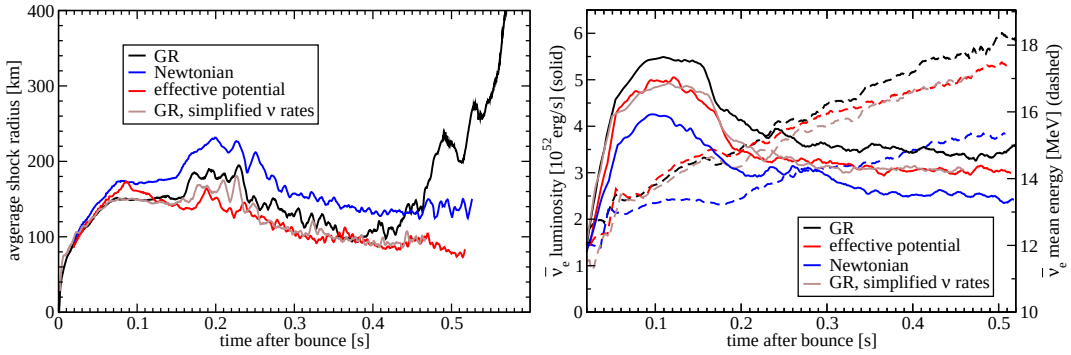

Figure 1: (color online) Left: Average shock radius for the $15M_\odot$ model as obtained in GR with our best set of opacities (black curve) and with simplified neutrino rates (light brown curve), in the purely Newtonian approximation (blue), and with an effective gravitational potential (red). Right: Electron antineutrino luminosities (solid) and mean energies (dashed) at the gain radius for these three cases.

variable Eddington factor transport [15, 16], ray-by-ray-diffusion [7], 2D multi-angle transport without energy bin coupling [17], or the isotropic diffusion source approximation [18]) with different strengths and weaknesses, and there have only been very tentative attempts to venture forth to 3D models with these methods [7, 19]. Elements missing or only partially included in current state-of-the-art-models, such as 3D effects (whose potential is presently being debated [20, 19, 21]) or general relativity may hold the key to a better understanding of the explosion mechanism. Moreover, an improved treatment of such as yet poorly explored aspects is also indispensable for accurate predictions of the neutrino and gravitational wave signal – the only *observables* that directly probe the dynamics in the supernova core.

Among the aspects that have not yet been thoroughly investigated in self-consistent multi-D neutrino hydrodynamics simulations of core-collapse supernovae, our group has recently begun to study the influence of GR in more detail. Although the importance of relativistic effects in core-collapse supernovae (due to the compactness of the proto-neutron star and the occurrence of high velocities) has long been recognized an demonstrated [22], the combination of GR hydrodynamics and multi-group neutrino transport has long been feasible only in spherical symmetry [22, 23, 24]. With the relativistic generalization of the ray-by-ray variable Eddington factor method [25] used in our neutrino hydrodynamics code VERTEX, we are now able to present first results about the impact of GR on the explosion dynamics and, in particular, the neutrino and gravitational wave emission in axisymmetric (2D) supernova models.

2 General Relativistic Effects in Multi-Dimensional Supernova Models

Our group has recently conducted relativistic supernova simulations for progenitors with $11.2M_\odot$ [26] and $15M_\odot$ [27] well into the explosion phase, which were supplemented by three additional runs for the $15M_\odot$ star. In order to estimate the magnitude of GR effects, two complementary models were computed using either the purely Newtonian approximation or the "effective po-

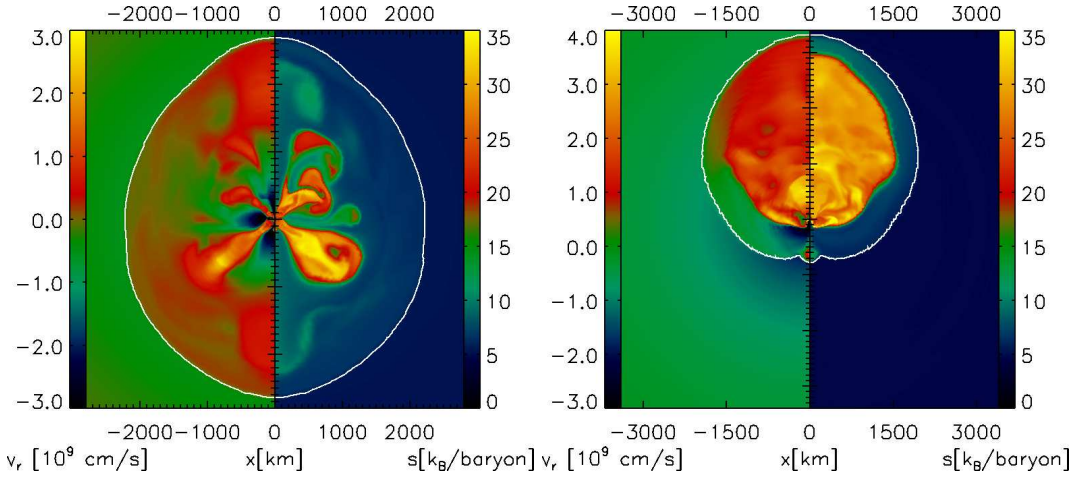

Figure 2: (color online) Explosion geometry for the GR simulations of the $11.2M_\odot$ (left panel, almost spherical shock) and the $15M_\odot$ progenitor (right panel, strong dipolar shock deformation) 658 ms and 745 ms after bounce, respectively. The left and right half of the panels show the electron fraction Y_e and the entropy s, respectively, and the shock is indicated as a white curve.

tential" approach [28], which has long been the only means of including some GR corrections in multi-D neutrino hydrodynamics simulations. In addition, we also calculated a model with a simplified set of neutrino opacities (neglecting the effects of recoil, high-density correlations and weak magnetism in neutrino-nucleon reactions and ignoring reactions between different neutrino flavors), which serves to illustrate the importance of the neutrino microphysics for the dynamics in the supernova core and provides a scale of reference for the GR effects. As a marginal case close to the threshold between explosion and failure [6], the $15M_\odot$ progenitor is ideally suited for such a comparative analysis.

Interestingly, we find that among the $15M_\odot$ models, the GR run with improved rates is the only one to develop an explosion with shock revival occurring some 450 ms after bounce (Fig. 1), indicating the relevance of both GR effects *and* of the neutrino microphysics. The different evolution of the three models with a different treatment of gravity is a consequence of the different compactness and surface temperature of the proto-neutron star, which leads to a clear hierarchy of the electron neutrino and antineutrino luminosities and mean energies (which determine the heating conditions) between the three cases (cp. [22, 29, 25] for this effect in 1D simulations) as illustrated by Fig. 1 for the electron antineutrinos, where the enhancement in GR is most pronounced. The beneficial effect of higher local heating rates as compared to the Newtonian case is, however, counterbalanced by the faster advection of material through the gain layer around a more compact proto-neutron star in the effective potential run, but in the GR case, the enhanced heating is strong enough to overcome this adverse effect.

It is noteworthy that the neutrino emission and the shock evolution are similarly sensitive to the neutrino interaction rates (in agreement with the findings of [30, 7]). In the run with improved microphysics, weak magnetism and nucleon correlations lower the opacities for $\bar{\nu}_e$, shift the neutrinosphere into deeper and hotter regions of the proto-neutron star surface [31], and thus result in harder $\bar{\nu}_e$ spectra (by up to ~ 1 MeV during the late phases) and increased $\bar{\nu}_e$

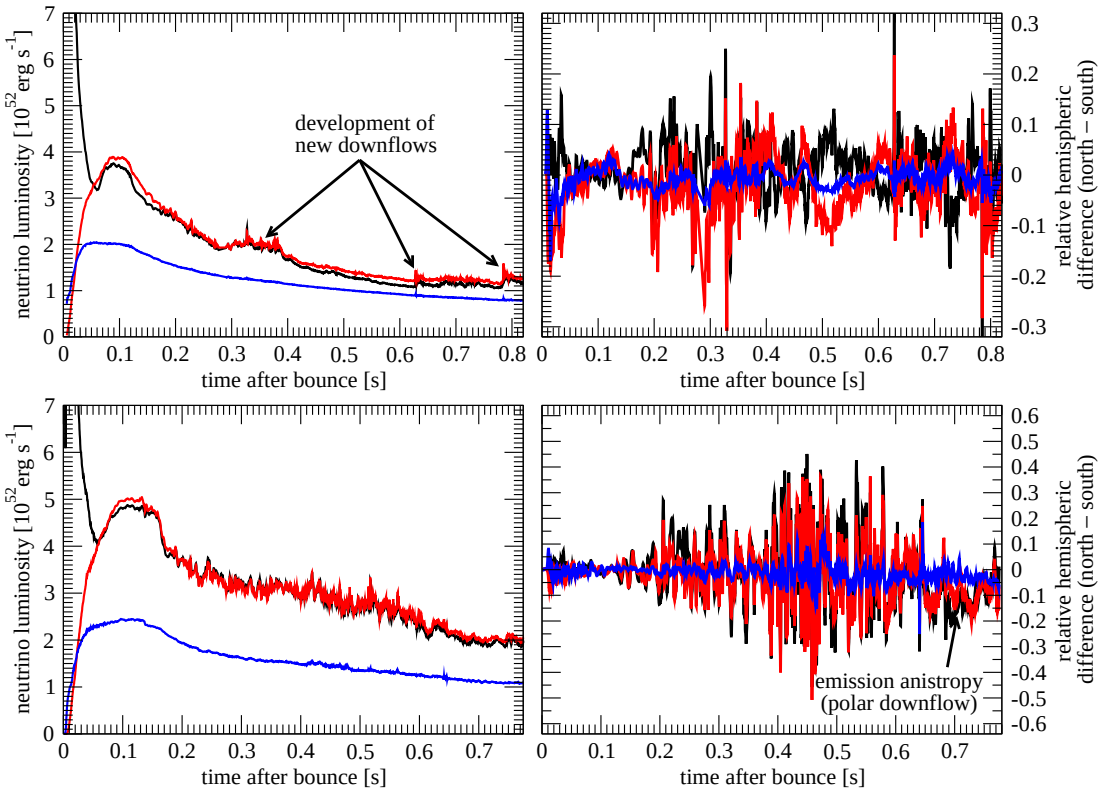

Figure 3: (color online) Left panels: Neutrino luminosities (defined as the total angle-integrated neutrino flux from the supernova) for the relativistic $11.2M_\odot$ (top) and $15M_\odot$ (bottom) models. Right panels: Relative differences of the angle-integrated neutrino fluxes $L_{\rm north}$ and $L_{\rm south}$ in the northern and southern hemisphere, computed as $2(L_{\rm north}-L_{\rm south})/(L_{\rm north}+L_{\rm south})$. Black, red, and blue curves are used for ν_e, $\bar{\nu}_e$, and $\nu_{\mu/\tau}$, respectively.

luminosities, which also allows for more efficient heating in the gain layer. Neglecting possible effects of flavor conversion and MSW, this would also imply somewhat higher detection rates for $\bar{\nu}_e$ (by $\sim 15\%$).

3 Neutrino and Gravitational Wave Signals from Supernovae

Both the $11.2M_\odot$ and the $15M_\odot$ models have been evolved well into the post-explosion phase until ~ 0.8 s after bounce, and thus provide a good illustration of the impact of multi-dimensional effects on the neutrino and gravitational wave signal during the different stages of the evolution. Prior to the onset of the explosion the neutrino luminosities of both models (Fig.3, left panels) are characterized by the familiar large contribution of the accretion luminosity for ν_e and $\bar{\nu}_e$. As soon as the SASI starts to grow vigorously, we also observe the strong angle-dependent time

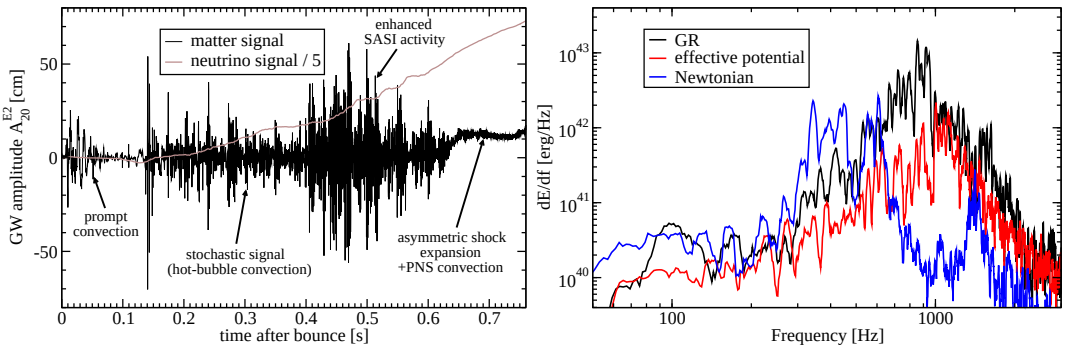

Figure 4: (color online) Left: Matter (black) and neutrino (light brown) gravitational wave signals for the general relativistic $15M_\odot$ explosion model. Right: Influence of the treatment of gravity (black: GR hydro, red: Newtonian hydro + effective potential, blue: purely Newtonian) on the gravitational wave energy spectrum for the first 500 ms of the post-bounce evolution of the $15M_\odot$ progenitor.

variations in the neutrino flux (particularly in ν_e and $\bar{\nu}_e$, see Fig. 3, right panels) that have been discussed in [17, 32, 33, 34] and can potentially be used to extract the frequencies of the SASI from the neutrino signal using detectors with high temporal resolution such as Icecube [33]. In our simulations, these fluctuations are present in similar strength as in Newtonian and effective potential models [17, 32, 34] with the hemispheric flux fluctuating by several tens of percent; and the dominant frequencies (45 Hz and 75 Hz for the $\ell = 1$ and $\ell = 2$ mode) are in excellent agreement with [32, 33].

It is interesting to note that our results suggest that the neutrino signal changes its character only gradually over several hundreds of milliseconds after the onset of the explosion. The temporal fluctuations are actually strongest during the first ~ 200 ms after shock revival, and the luminosities of ν_e and $\bar{\nu}_e$ do not show any abrupt decline correlated with the time of the explosion. This behavior is in marked contrast to the abrupt drop in the ν_e and $\bar{\nu}_e$ luminosities in 1D models with artificial explosions [35], and is due to the fact that quite large accretion rates can still be maintained through the downflows at late times in multi-dimensional models (Fig. 2). As long as the shock does not expand too rapidly, new downflows may still form and channel fresh material into the cooling region (see [6], as in the case of the $11.2M_\odot$ progenitor, which leads to noticeable "bumps" in the neutrino luminosity (Fig. 3, top left panel). For the $15M_\odot$ progenitor, an even higher accretion luminosity can be maintained continuously because of the presence of a stable polar downflow in an extremely asymmetric explosion geometry (Fig. 2). With a single downflow, the neutrino emission exhibits a strong directional dependence with sustained hemispheric flux differences of up to several tens of percent (Fig. 3). On the other hand, the strong high-frequency fluctuations subside during the late phases as the expansion of the shock quenches further SASI activity. The neutrino signal thus still reflects the dynamical evolution of explosion models in multi-D, albeit in a form very different from artificial 1D explosions.

Naturally, the determination of gravitational wave signals has also been among the major goals of the simulations with the relativistic version of VERTEX. Qualitatively, we obtain similar waveforms as computed in the Newtonian or effective potential approximation [32, 36, 37]

with clearly distinct phases in the signal corresponding to the dynamics (Fig. 4, cp. with ref. [36]). Shortly after bounce, prompt convection and early SASI activity produce a low-frequency, quasi-periodic signal, which is followed by a more quiescent period until hot-bubble convection and strengthening SASI sloshing motions gives rise to a stochastic signal with typical frequencies rising from 500 Hz to over 1000 Hz during a phase of $\sim$ 200 ms around shock revival revival, when gravitational wave emission is strongest. Afterwards, proto-neutron star convection becomes the dominant source of high-frequency gravitational waves. In the case of the $15M_{\odot}$ progenitor with a rather extreme explosion geometry, asymmetric shock expansion and neutrino emission also give rise to a monotonously rising "tail signal" which contributes somewhat to the low-frequency part of the spectrum. Despite the qualitative similarities of waveforms in GR and the Newtonian approximation, GR effects have a considerable impact on the power spectrum, however. The integrated signal for the first 500 s (Fig. 4) peaks at considerably higher frequencies in GR ($\sim$ 900 Hz) compared to the purely Newtonian case ($\sim$ 500 Hz). On the other hand, the effective potential approximation even overestimates the peak frequency ($\sim$ 1100 Hz), because the lower proto-neutron star surface temperature leads to a higher Brunt-Väisälä frequency and therefore to a more abrupt braking of convective bubbles at the lower boundary of the hot-bubble convection region (cp. with the interpretation of the characteristic frequencies given in [36]).

4 Outlook – 3D Supernova Modeling

The results presented here demonstrate that both GR effects and variations in the neutrino microphysics have a significant impact on the neutrino emission and, consequently, and on the dynamics in the supernova core. As illustrated by the marginal $15M_{\odot}$ progenitor, a detailed and sophisticated treatment of gravity and neutrino interactions can very well be crucial for the success of the neutrino-driven explosion mechanism. Such improvements in the models also bring up the perspective of reliable, non-parametrized predictions for the neutrino and gravitational wave signal *beyond* the accretion phase (cp. also [37]), whose salient features have been pointed out in the last section.

One of the major limitations of the models discussed here is their restriction to axisymmetry, which presently remains a necessary compromise for simulations with the most advanced multi-group neutrino transport methods. In the meantime, 3D effects can already be explored with the help of parametrized approaches and cheaper approximative methods to gain insights into their potentially important role for the explosion mechanism [20, 19, 21] and the expected changes in the neutrino and gravitational wave signals [38]. On the background of the strong sensitivity of the heating conditions on the neutrino treatment, conclusions about the implications of 3D effects for the viability of the neutrino-driven mechanism can only be drawn with some caution, however. Recent studies by [19] and by our own group [21] have indeed demonstrated that models do not necessarily explode more easily in 3D than in 2D [19, 21], and have rather pointed out issues that require further investigation, such as the role of feedback effects of convection and the SASI on the neutrino emission[19, 21], dimensionality-dependent resolution effects due to the different direction of the turbulent cascade [21], and the growth and saturation of the SASI in 3D [21].

While the influence of the dimensionality on the explosion conditions remains a controversial topic, the gravitational wave [39, 40, 41, 42] and neutrino signatures of non-radial hydrodynamic instabilities developing during the post-bounce phase will undoubtedly be affected by going from

2D to 3D. First predictions based on models with simplified semi-parametrized neutrino transport have recently become available [38], and suggest that the lack of a preferred direction in 3D and weaker activity of the $l = 1$ SASI sloshing mode reduce both the gravitational wave amplitude and the fast temporal variations of the neutrino signal by a factor of several. Even these findings are still subject to uncertainties about the dynamics in the supernova core (in particular concerning the behavior of the SASI in 3D), and in the end, accurate signal predictions will also require self-consistent simulations with at least the same level of sophistication as currently available in 2D.

Acknowledgments

This work was supported by the Deutsche Forschungsgemeinschaft through the Transregional Collaborative Research Centers SFB/TR 27 "Neutrinos and Beyond" and SFB/TR 7 "Gravitational Wave Astronomy" and the Cluster of Excellence EXC 153 "Origin and Structure of the Universe" (http://www.universe-cluster.de). The simulations of the MPA core-collapse group were performed on the IBM p690 of the Computer Center Garching (RZG), the NEC SX-8 at the HLRS in Stuttgart (within the SUPERN project), the Juropa Cluster at the John von Neumann Institute for Computing (NIC) in Jülich (partially through a DECI-6 grant of the EU), and on the IBM p690 at Cineca in Italy through a DECI-5 grant of the DEISA initiative.

References

[1] J. R. Wilson, Supernovae and Post-Collapse Behavior, in *Numerical Astrophysics*, edited by J. M. Centrella, J. M. Leblanc, and R. L. Bowers, pp. 422–434, 1985.

[2] H. A. Bethe and J. R. Wilson, Astrophys. J. **295**, 14 (1985).

[3] J. M. Blondin, A. Mezzacappa, and C. DeMarino, Astrophys. J. **584**, 971 (2003).

[4] T. Foglizzo, L. Scheck, and H.-T. Janka, Astrophys. J. **652**, 1436 (2006).

[5] R. Buras, H.-T. Janka, M. Rampp, and K. Kifonidis, Astron. Astrophys. **457**, 281 (2006).

[6] A. Marek and H.-T. Janka, Astrophys. J. **694**, 664 (2009).

[7] S. W. Bruenn *et al.*, ArXiv e-prints (2010), arXiv:1002.4914.

[8] A. Burrows, E. Livne, L. Dessart, C. D. Ott, and J. Murphy, Astrophys. J. **640**, 878 (2006).

[9] A. Burrows, E. Livne, L. Dessart, C. D. Ott, and J. Murphy, Astrophys. J. **655**, 416 (2007).

[10] N. N. Weinberg and E. Quataert, Mon. Not. R. Astron. Soc.**387**, L64 (2008).

[11] S. Akiyama, J. C. Wheeler, D. L. Meier, and I. Lichtenstadt, Astrophys. J. **584**, 954 (2003).

[12] A. Burrows, L. Dessart, E. Livne, C. D. Ott, and J. Murphy, Astrophys. J. **664**, 416 (2007).

[13] I. Sagert *et al.*, Physical Review Letters **102**, 081101:1 (2009).

[14] S. A. Colgate and R. H. White, Astrophys. J. **143**, 626 (1966).

[15] M. Rampp and H.-T. Janka, Astron. Astrophys. **396**, 361 (2002).

[16] R. Buras, M. Rampp, H.-T. Janka, and K. Kifonidis, Astron. Astrophys. **447**, 1049 (2006).

[17] C. D. Ott, A. Burrows, L. Dessart, and E. Livne, Astrophys. J. **685**, 1069 (2008).

[18] M. Liebendörfer, S. C. Whitehouse, and T. Fischer, Astrophys. J. **698**, 1174 (2009).

[19] T. Takiwaki, K. Kotake, and Y. Suwa, ArXiv e-prints (2011), arXiv:1108.3989.

[20] J. Nordhaus, A. Burrows, A. Almgren, and J. Bell, Astrophys. J. **720**, 694 (2010).

[21] F. Hanke, A. Marek, B. Müller, and H.-T. Janka, ArXiv e-prints (2011), arXiv:1108.4355.

[22] S. W. Bruenn, K. R. De Nisco, and A. Mezzacappa, Astrophys. J. **560**, 326 (2001).

[23] S. Yamada, H.-T. Janka, and H. Suzuki, Astron. Astrophys. **344**, 533 (1999).

[24] M. Liebendörfer *et al.*, Astrophys. J. Suppl. **150**, 263 (2004).

[25] B. Müller, H.-T. Janka, and H. Dimmelmeier, Astrophys. J. Suppl. **189**, 104 (2010).

[26] S. E. Woosley, A. Heger, and T. A. Weaver, *Rev. Mod. Phys.* **74**, 1015 (2002).

[27] S. E. Woosley and T. A. Weaver, Astrophys. J. Suppl. **101**, 181 (1995).

[28] A. Marek, H. Dimmelmeier, H.-T. Janka, E. Müller, and R. Buras, Astron. Astrophys. **445**, 273 (2006).

[29] M. Liebendörfer, M. Rampp, H.-T. Janka, and A. Mezzacappa, Astrophys. J. **620**, 840 (2005).

[30] M. Rampp, R. Buras, H.-T. Janka, and G. Raffelt, Core-collapse supernova simulations: variations of the input physics, in *Nuclear Astrophysics*, edited by W. Hillebrandt & E. Müller, pp. 119–125, 2002.

[31] C. J. Horowitz, Phys. Rev. D **65**, 043001 (2002).

[32] A. Marek, H.-T. Janka, and E. Müller, Astron. Astrophys. **496**, 475 (2009).

[33] T. Lund, A. Marek, C. Lunardini, H.-T. Janka, and G. Raffelt, Phys. Rev. D **82**, 063007 (2010).

[34] T. D. Brandt, A. Burrows, C. D. Ott, and E. Livne, Astrophys. J. **728**, 8 (2011).

[35] T. Fischer, S. C. Whitehouse, A. Mezzacappa, F. Thielemann, and M. Liebendörfer, Astron. Astrophys. **517**, A80+ (2010).

[36] J. W. Murphy, C. D. Ott, and A. Burrows, Astrophys. J. **707**, 1173 (2009).

[37] K. N. Yakunin *et al.*, Classical and Quantum Gravity **27**, 194005 (2010).

[38] E. Müller, H.-T. Janka, and A. Wongwathanarat, ArXiv e-prints (2011), arXiv:1106.6301.

[39] S. Scheidegger, T. Fischer, S. C. Whitehouse, and M. Liebendörfer, Astron. Astrophys. **490**, 231 (2008).

[40] K. Kotake, W. Iwakami, N. Ohnishi, and S. Yamada, Astrophys. J. **697**, L133 (2009).

[41] S. Scheidegger, R. Käppeli, S. C. Whitehouse, T. Fischer, and M. Liebendörfer, Astron. Astrophys. **514**, A51+ (2010).

[42] K. Kotake, W. Iwakami-Nakano, and N. Ohnishi, Astrophys. J. **736**, 124 (2011).

New Aspects and Boundary Conditions of Core-Collapse Supernova Theory

Christian D. Ott[1,2,3], *Evan P. O'Connor*[1], *Basudeb Dasgupta*[4]

[1]TAPIR, California Institute of Technology, Pasadena, CA, USA

[2]Center for Computation and Technology, Louisiana State University, Baton Rouge, LA, USA

[3]Institute for the Physics and Mathematics of the Universe (IPMU), The University of Tokyo, Kashiwa, Japan

[4]CCAPP, The Ohio State University, Columbus, OH, USA

DOI: http://dx.doi.org/10.3204/DESY-PROC-2011-03/ott

Core-collapse supernovae are among Nature's grandest explosions. They are powered by the energy released in gravitational collapse and include a rich set of physical phenomena involving all fundamental forces and many branches of physics and astrophysics. We summarize the current state of core-collapse supernova theory and discuss the current set of candidate explosion mechanisms under scrutiny as core-collapse supernova modeling is moving towards self-consistent three-dimensional simulations. Recent work in nuclear theory and neutron star mass and radius measurements are providing new constraints for the nuclear equation of state. We discuss these new developments and their impact on core-collapse supernova modeling. Neutrino-neutrino forward scattering in the central regions of core-collapse supernovae can lead to collective neutrino flavor oscillations that result in swaps of electron and heavy-lepton neutrino spectra. We review the rapid progress that is being made in understanding these collective oscillations and their potential impact on the core-collapse supernova explosion mechanism.

1 Overview: Core-Collapse Supernova Theory

The ultimate goal of core-collapse supernova theory is to understand the mechanism driving supernova explosions in massive stars, connect initial conditions to the final outcome of collapse, and make falsifiable predictions of observable signals and explosion features. These include neutrino, gravitational wave, and electromagnetic signals, nucleosynthetic yields, compact remnant masses, explosion morphologies, and pulsar kicks, spins, and magnetic fields.

Baade and Zwicky, in their seminal 1934 article [1], first hypothesized that a "supernova represents the transition of an ordinary star into a neutron star, consisting mainly of neutrons." This basic picture still holds today and the road to its refinement has been, at best, meandering and bumpy. When the nuclear fuel at the core of a massive star is exhausted, the core becomes electron degenerate and, upon reaching its effective Chandrasekhar mass, undergoes dynamical collapse. Electron capture on free protons and protons bound in heavy nuclei reduces the electron fraction (Y_e; the number of electrons per baryon) and accelerates the collapse of the inner core. When the latter reaches nuclear density, $\rho_{\rm nuc} \approx 2.7 \times 10^{14}\,{\rm g\,cm^{-3}}$, the nuclear equation of state (EOS) stiffens[1], leading to core bounce and the formation of the bounce shock

[1]The stiffening of the EOS near $\rho_{\rm nuc}$ is due to the repulsive effect of the strong force at small distances and $\Gamma = d\ln P/d\ln\rho$ jumps from $\sim$4/3 to $\gtrsim 2$. Neutron degeneracy, which is non-relativistic at bounce, only gives $\Gamma \approx 5/3$.

at the interface of inner and outer core. The shock initially rapidly propagates out in radius and mass coordinate, but the work done to break up infalling heavy nuclei and energy losses to neutrinos quickly sap its might. The shock stalls within tens of milliseconds of bounce and turns into an accretion shock at a radius of $\sim 100 - 200\,\mathrm{km}$ [2].

Core collapse liberates $\sim 3 \times 10^{53}\,\mathrm{erg} = 300\,\mathbf{B}ethe$ of gravitational binding energy of the neutron star, $\sim$99% of which is radiated in neutrinos over tens of seconds. The *supernova mechanism* must revive the stalled shock and convert $\sim$1% of the available energy into energy of the explosion, which must happen within less than $\sim 0.5 - 1\,\mathrm{s}$ of core bounce in order to produce a typical core-collapse supernova explosion and leave behind a neutron star with the canonical neutron star gravitational mass of $\sim 1.4\,M_\odot$ [3, 4].

The *neutrino mechanism* [2, 5] for core-collapse supernova explosions relies on the deposition of net neutrino energy (heating > cooling) in the region immediately behind the stalled shock, heating this region and eventually leading to explosion (for details, see the excellent discussion in [6]). While having great appeal and being most straightforward, given the huge release of neutrino energy in core collapse, the simplest, spherically-symmetric form of this mechanism fails to revive the shock in all but the lowest-mass massive stars (O-Ne cores) [7–10].

Indications are strong that multi-dimensional effects, principally turbulent convective overturn and the standing-accretion-shock instability (SASI, e.g., [11, 12] and references therein) increase the efficacy of the neutrino mechanism by boosting neutrino heating [13–16] or, as suggest by [6], by reducing neutrino cooling. This is generally borne out by recent fully self-consistent axisymmetric (2D) neutrino radiation-hydrodynamics simulations with an energy-dependent treatment of neutrinos, but their detailed results vary significantly from group to group and a clear picture has yet to emerge. Marek *et al.* [17] reported the onset of explosions in a nonrotating 11.2-$M_\odot$ (at zero-age main sequence [ZAMS]) and in a slowly spinning 15-$M_\odot$ star, setting in at $\sim$200 ms and $\sim$600 ms after bounce, respectively, and the estimate explosion energies are on the lower side of what is expected from observations. The exploding simulations used the softest variant of the EOS by Lattimer & Swesty (LS) [18] and included a stronger quasi-relativistic monopole term in the gravitational potential. A similar, so far unpublished [19], calculation of core collapse in a 11.2-$M_\odot$ star with the stiffer EOS of H. Shen *et al.* [20] also produced an explosion while simulations with the very stiff EOS by Hillebrand & Wolff [21] did not. Bruenn *et al.* [22], also using the softest LS EOS variant and quasi-relativistic gravity, found strong explosions setting in within $\sim$250 ms after bounce in progenitors with ZAMS masses of (12, 15, 20, and 25) $M_\odot$. Suwa *et al.* [23], using Newtonian gravity and the soft LS EOS variant, found early, but weak explosions in a 13-$M_\odot$ progenitor star. Ott *et al.* [24] and Burrows *et al.* [25, 26], on the other hand, who performed purely Newtonian calculations using the stiffer H. Shen EOS, did not find neutrino-driven explosions in progenitors of $11.2 - 25\,M_\odot$.

Given that Nature has a way to robustly (without fine tuning) explode at least a significant fraction, but probably most stars with ZAMS masses of $\sim 10 - 20\,M_\odot$ [27, 28], the large range of differing and sometimes disagreeing results of 2D simulations is dissatisfactory, if not disturbing.

There are essentially three possible ways out:
(*1*) The neutrino mechanism, while getting much closer to being viable in 2D than in 1D, may still not be reaching its full efficacy. In 3D, an additional fluid motion degree of freedom is available and the nature of turbulence changes[2]. This may allow accreting material to stay even longer in the region of net heating, resulting in a greater heating efficiency and, thus,

[2]Provided that the turbulent cascade is resolved, turbulent power will cascade towards small scales in 3D while it cascades to large scales in 2D, which is unphysical.

potentially make the neutrino mechanism robust. Results to this effect have been obtained by Nordhaus *et al.* [29] who performed 1D, 2D, and 3D calculations with parameterized neutrino heating and cooling using spherical Newtonian gravity and the H. Shen EOS. This work confirmed the results of [13] for the 1D→2D case and found another big increase in efficacy when going from 2D to 3D. However, a similar parameterized study, carried out by Hanke *et al.* [16], found no significant difference between 2D and 3D. The debate thus remains open and more work will be needed before the final word on the neutrino mechanism can be spoken. For this, fully self-consistent 3D simulations with reliable energy-dependent neutrino transport will be necessary. The first steps towards such self-consistent 3D models have already been taken [30, 31] and their results, while not definite, are encouraging.

(*2*) If dimensionality is not the key to robust neutrino-driven core-collapse supernova explosions, then could there be physics missing from current 1D and 2D simulations that, once included, could render 2D, or perhaps even 1D, neutrino-driven explosions robust? A key example for this are self-induced (by ν-ν scattering) collective neutrino oscillations and we will discuss their potential effect on the neutrino mechanism in §3.

(*3*) If 3D and/or new physics cannot save the neutrino mechanisms, alternatives must be sought. Potential ones include the *magnetorotational mechanism* (e.g., [32]), the *acoustic mechanism* [25, 26, 33], and the *phase-transition-induced* mechanisms [34]. The *magnetorotational mechanism* requires very rapid rotation in combination with non-linear magnetic field amplification after bounce by the magnetorotational instability (e.g., [32, 35]). Pulsar birth spin estimates [36] and stellar evolution calculations that take into account magnetic fields (e.g., [37]) suggest that it may be active in no more than ∼1% of massive stars that produce very energetic explosions and are related to the hyper-energetic core-collapse supernova explosions associated with a growing number of long gamma-ray bursts [38–40].

The *acoustic mechanism*, proposed by [25, 26], relies on the excitation of protoneutron star pulsations by turbulence and SASI-modulated accretion downstreams. These pulsations reach large amplitudes at $600-1000$ ms after bounce and damp via the emission of strong sound waves that steepen to secondary shocks as they propagate down the radial density gradient in the region behind the stalled shock. They dissipate and heat the postshock region, robustly leading to explosions, which, however, tend to be weak and occur late. This mechanism has not been confirmed by other groups, has been studied only in 2D simulations, and, most importantly, [41] have shown via non-linear perturbation theory that a parametric instability between the main mode of pulsation and abound higher-order modes, which are not resolved by the numerical models of [25, 26], is likely to limit the mode amplitude to dynamically negligible magnitudes.

The *phase-transition-induced mechanism* (e.g., [34, 42]) requires a hadron-quark phase transition occurring within the first few 100 ms after core bounce (hence, at moderate protoneutron-star central densities). This phase transition leads to an intermittent softening of the EOS, a short collapse phase followed by a second bounce launching a secondary shock wave that runs into the stalled shock and launches an explosion even in spherical symmetry. However, the needed early onset of the phase transition requires fine tuning of the quark EOS and leads to maximum cold neutron star gravitational masses inconsistent with observations [3, 43].

In the remainder of this contribution to the proceedings of the HAmburg Neutrinos from Supernova Explosions 2011 (HAνSE 2011) conference, we discuss, in §2, new boundary conditions of core-collapse supernova theory set by neutron star mass and radius constraints, and, in §3, we summarize the recent rapid progress made by studies considering the potential effect of collective neutrino oscillations on the core-collapse supernova mechanism. In §4, we cricially

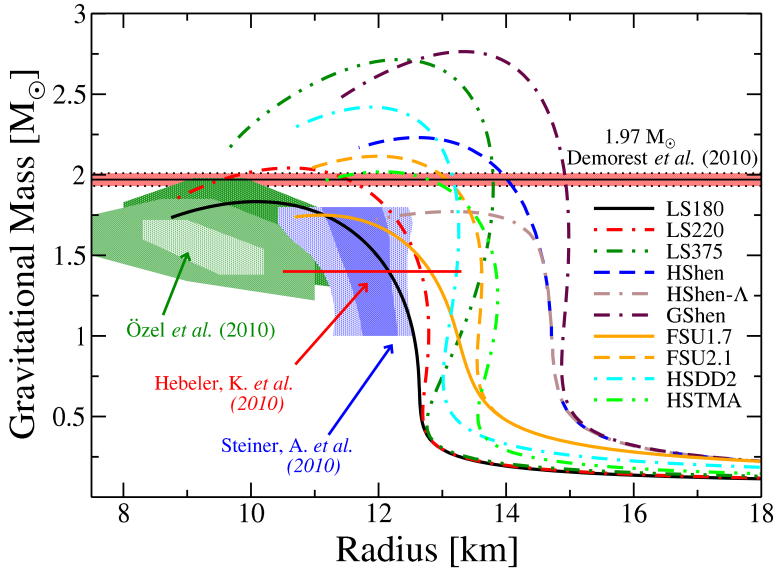

Figure 1: (color online) Mass-radius relations for 10 publically available finite-temperature EOS along with several constraints. The EOS are taken from [18, 44–48] and the Tolman-Oppenheimer-Volkoff equation is solved with $T = 0.1\,\mathrm{MeV}$ and neutrino-less β-equilibrium imposed. The family of LS EOS is based on the compressible liquid-droplet model [18] while all other EOS are based on relativistic mean field theory. The nuclear theory constraints of Hebeler *et al.* [49] assume a maximum mass greater than $2\,M_\odot$ and do not take into account a crust (which would increase the radius by $\sim$400 m). EOS that do not support a mass of at least $1.97 \pm 0.04\,M_\odot$ are ruled out [3, 43]. Özel *et al.* [50] analyzed three accreting and bursting neutron star systems and derived mass-radius regions shown in green. Steiner *et al.* [51] performed a combined anaylsis of six accreting neutron star systems, shown are 1-σ and 2-σ results in blue.

summarize our discussion and highlight the new frontiers of core-collapse supernova theory.

2 New Constraints on the Supernova Equation of State

An important ingredient in any core-collapse supernova model is the nuclear EOS. It provides the crucial closure for the set of (magneto-)hydrodynamics equations used to describe the evolution of the collapsing stellar fluid and strongly influences the structure of the protoneutron star and the thermodynamics of the overall problem. Nuclear statistical equilibrium (NSE) prevails above temperatures of $\sim$0.5 MeV, which corresponds to densities above $\sim 10^7\,\mathrm{g\,cm^{-3}}$ in the core-collapse supernova problem. In this regime, the EOS is derived from the Helmholtz free energy and thus is expressed as a function of density ρ, temperature T, and electron fraction Y_e. The NSE part of the core-collapse supernova EOS must cover tremendous ranges of density ($10^7 - 10^{15}\,\mathrm{g\,cm^{-3}}$), temperature ($0.5 - 100\,\mathrm{MeV}$), and electron fraction (0–$\sim$0.6). Constraints from experimental nuclear physics on the nuclear EOS are few and generally limited to only

small regions of the needed (ρ, T, Y_e) space (see the discussions in [47, 52]).

A stringent constraint on the nuclear EOS is set by precision mass measurements of neutron stars in binary systems. The 2-$M_\odot$ ($[1.97 \pm 0.04]\, M_\odot$) neutron star of Demorest *et al.* [43] rules out a large range of soft hadronic, mixed hadronic-exotic, and strange-quark matter EOS [3, 53].

Recently, Hebeler *et al.* [49] have carried out chiral effective field theory calculations of neutron-rich matter below nuclear saturation density, strongly constraining the $P(\rho)$ relationship in this regime. They derived a radius constraint for a 1.4-$M_\odot$ neutron star of $10.5\,\mathrm{km} \lesssim R \lesssim 13.3\,\mathrm{km}$ (these numbers would be shifted up by $\sim$400 m if a detailed crust treatment was included) by requiring that all EOS support neutron stars with mass $\gtrsim 2\,M_\odot$ and pass through the $P(\rho)$ range allowed by their calculations.

Steiner *et al.* [51] and Özel *et al.* [50] analyzed observations from accreting and bursting neutron stars to obtain neutron star mass-radius constraints. Such observations and their interpretations should be taken with a grain of salt, since large systematic uncertainties are attached to the models that are required to infer mass and radius and to the assumptions made in their statistical analysis. For example, [51] and [50], starting with different assumptions, derive rather different 2-σ mass-radius constraints from the same set of sources.

In Fig. 1, we contrast the various observational constraints on the neutron star mass and radius with a range of EOS used in core-collapse supernova modeling. The LS family of EOS is based on the compressible liquid droplet model [18], while all other EOS (drawn from [44–48]) are based on relativistic mean field (RMF) theory. The details of the $M - R$ curves depend on multiple EOS parameters such as nuclear incompressibility, symmetry energy and their derivatives and we must refer the reader to [47] and to the primary EOS references for details for each EOS. Fig. 1 shows that none of the current set of available EOS allow for a 2-$M_\odot$ neutron star while at the same time being consistent with the current mass-radius constraints from observations. The crux is that the EOS needs to be sufficiently stiff to support 2-$M_\odot$ neutron stars *and* at the same time sufficiently soft to make neutron stars with moderate radii in the canonical mass range. This balance appears to be difficult to realize. The stiff set of RMF EOS produce systematically too large neutron stars. The soft compressible liquid-droplet LS180 EOS [18] agrees well with the mass-radius constraints, but is ruled out by its failure to support a 2-$M_\odot$ neutron star. Closest to satisfying all constraints are the LS220 EOS of [18] and the yet unpublished HSDD2 EOS of [48] based on the RMF model of [54].

The stiffness of the nuclear EOS at high and intermediate densities has important consequences for the postbounce evolution of core-collapse supernovae. In simple terms: the stiffer the EOS, the more extended the protoneutron star and the larger the radius and the lower the matter temperature at which neutrinos decouple from the protoneutron star matter. Assuming a Fermi-Dirac spectrum with zero degeneracy, the mean-squared energy of the emitted neutrinos is approximately given by $\langle \epsilon_\nu^2 \rangle \approx 21 T_\nu^2$ [55], where T_ν is the matter temperature (in units of MeV) at the neutrinosphere (where the optical depth $\tau \approx 2/3$). Hence, a softer EOS will lead to systematically harder neutrino spectra than a stiffer EOS (as born out by the simulations of [17]). Since the charged-current neutrino heating rate Q_ν^+ scales $\propto \langle \epsilon_\nu^2 \rangle$, a soft EOS leads to a higher neutrino heating efficiency than a stiff EOS. This is at least part of the explanation why some published 2D simulations using the soft, now ruled-out LS180 EOS have shown neutrino-driven explosions [17, 22, 23] while simulations with stiffer EOS have generally failed to yield such explosions in stars more massive than $\sim$11 $M_\odot$ [17, 19, 25].

3 New Physics: Collective Neutrino Oscillations

Neutrinos and antineutrinos of all three flavors are produced in core-collapse supernovae and can oscillate from one flavor to another. ν_e and $\bar{\nu}_e$ are made and interact via charged-current and neutral-current interactions, while ν_μ and ν_τ and their antineutrinos experience only neutral-current processes, since no muons or tauons are present in the core-collapse supernova environment. Hence, their interaction cross sections are very similar and one generally lumps them together as $\nu_x = \{\nu_\mu, \nu_\tau\}$ and $\bar{\nu}_x = \{\bar{\nu}_\mu, \bar{\nu}_\tau\}$.

The oscillations between ν_e and ν_x or $\bar{\nu}_e$ and $\bar{\nu}_x$ are driven by their mass differences, forward scattering off background electrons, and forward scattering off other neutrinos and antineutrinos. These limiting regimes are called neutrino oscillations in vacuum [56], matter-enhanced oscillations through the MSW effect [57], and collective oscillations [58], respectively. Quantitatively, the nature of neutrino flavor conversions depends on an interplay of vacuum neutrino oscillation frequency $\omega = \Delta m^2/(2E)$ with the matter potential $\lambda = \sqrt{2} G_F n_e$ due to background electrons (where n_e is the electron number density) and with the collective neutrino potential $\mu \sim \sqrt{2} G_F (1 - \cos\theta) n_{\nu+\bar{\nu}}$ generated by the neutrinos themselves (where $n_{\nu+\bar{\nu}}$ is the neutrino and antineutrino number density). In a typical core-collapse supernova environment, the matter potential falls off with radius as $n_e \propto 1/r^3$, whereas the collective potential falls off faster with $n_{\nu+\bar{\nu}} \langle 1 - \cos\theta \rangle \propto 1/r^4$. So, when the neutrinos travel outward from the core, they generally first experience collective effects and then matter effects, which may be modified by shock wave effects [59]. After they leave the star, the mass eigenstates travel independently and are detected on Earth as an incoherent superposition. There can be distinctive effects due to additional conversions during propagation inside the Earth (e.g., [60]).

3.1 Collective Oscillations due to ν-ν Interactions

The neutrino density creates a potential that is not flavor diagonal [58]; $n_\nu, n_{\bar{\nu}}$ are density matrices in flavor space and depend on the flavor composition of the entire neutrino ensemble! Flavor evolution of such dense neutrino gases [61] can be understood to good accuracy without considering many-particle effects [62]. Calculations in spherical symmetry showed that the collective oscillations can affect neutrino flavor conversions substantially [63, 64]. The main features observed were large flavor conversions for inverted hierarchy (neutrinos masses $m_1, m_2 > m_3$), and a surprisingly weak dependence on the mixing angle and the matter density.

These features can be understood analytically. A dense gas of neutrinos displays collective flavor conversion [65], i.e., the flavor oscillations of all neutrinos and antineutrinos become coupled to each other and all of them undergo flavor conversion together. Neutrinos of all energies oscillate almost in phase, through synchronized [66]/parametrically resonant [67]/bipolar oscillations [68, 69]. The effect of the bipolar oscillations with a decreasing collective potential μ is a partial or complete swap of the energy spectra of two neutrino flavors [70, 71]. The "$1 - \cos\theta$" structure of weak interactions can give rise to a dependence of flavor evolution on the neutrino emission angle [64] or even flavor decoherence, i.e., neutrinos acquire uncorrelated phases, and the neutrino fluxes for all flavors become almost identical [72]. For a realistic excess of ν_e, compared to $\bar{\nu}_e$ fluxes, such angle-dependent effects are likely to be small [73, 74]. Even non-spherical source geometries can often be captured by an effective single-angle approximation [75] in the coherent regime. While most of these results were obtained for neutrino oscillations between two flavors, it was shown that with three flavors one can usually treat the oscillation problem by factorizing it into simpler two-flavor oscillation problems, since the mass-

squared differences between the mass eigenstates obey $\Delta m^2_{12} \ll |\Delta m_{13}|$ and the mixing angle $\theta_{13} \ll 1$ [76], and the previous results are easily generalized. Effects of potential CP violation are expected to be small with realistic differences between μ and τ neutrino fluxes [77]. On the other hand, similar realistic departures are sufficient to trigger collective effects even for a vanishing mixing angle [78, 79].

3.2 Results obtained with Core-Collapse Supernova Toy-Models

Although the inherent nonlinearity and the presence of multi-angle effects make the analysis rather complicated, the final outcome for the neutrino fluxes turns out to be rather straightforward, at least in the spherically symmetric scenario. Synchronized oscillations with a frequency $\langle\omega\rangle$ take place just outside the neutrinosphere at $r \sim 10 - 40$ km. These cause no significant flavor conversions since the mixing angle, which determines the extent of flavor conversion, is highly suppressed by the large matter potential due to the high electron density in these inner regions [80, 81]. A known exception occurs for the ν_e burst phase in low-mass progenitor stars that have a very steep density profile [82]. In such a situation, neutrinos of all energies undergo MSW resonances *before* collective effects become negligible [83, 84]. At larger radii, $r \sim 40 - 100$ km, bipolar or pendular oscillations $\nu_e \leftrightarrow \nu_x$ with a higher frequency $\sqrt{2\omega\mu}$ follow. These oscillations are instability-driven and thus depend logarithmically [68] on the mixing angle, occurring where the fluxes for the two flavors are very similar [71]. As μ decreases, so that $\langle\omega\rangle \sim \mu$, neutrinos near this instability may relax to the lower neutrino mass (energy) state. As a result, one finds one or more spectral swaps demarcated by sharp discontinuities or "spectral splits" in the oscillated flux.

These simple explanations do not take into account the fact that neutrinos are emitted at different angles from the neutrinosphere. As a result, radial neutrinos take a shorter path (while tangentially emitted neutrinos take a longer path), and thus experience less (more) background potentials from the electrons and from other neutrinos leading to an emission angle-dependent flavor evolution. These sort of effects are called *multi-angle effects*, and can suppress or delay flavor conversions either through multi-angle matter effects [85], or through multi-angle neutrino-neutrino interactions themselves [86].

3.3 Results obtained with more realistic Models

The observations outlined in the previous section 3.2 were mostly based on toy models of core-collapse supernova neutrino fluxes and background densities. Recently, several groups have tried to perform semi-realistic calculations of the oscillation physics, by injecting the output neutrino fluxes from supernova simulations into oscillation calculations [87–89]. Interesting results have also been obtained by performing a linear stability analysis of the equations used for calculating the flavor conversion, with the initial conditions taken from simulations [90, 91].

The simple picture given in §3.2 has therefore undergone further changes. Firstly, it has been recognized that matter effects suppress collective oscillations even in the bipolar regime through multi-angle effects as explained before [87, 88] (see also §3.4). This is most effective in the pre-explosion accretion phase, when the matter density is large in the region behind the stalled shock. In this case, it appears that one can simply ignore collective effects and only include the MSW effects which take place at larger radii. Of course, the result depends on details of the matter density and ratios of neutrino fluxes. In particular, for fluxes that are either highly symmetric in neutrinos and antineutrinos [89], or include flavor dependent angular

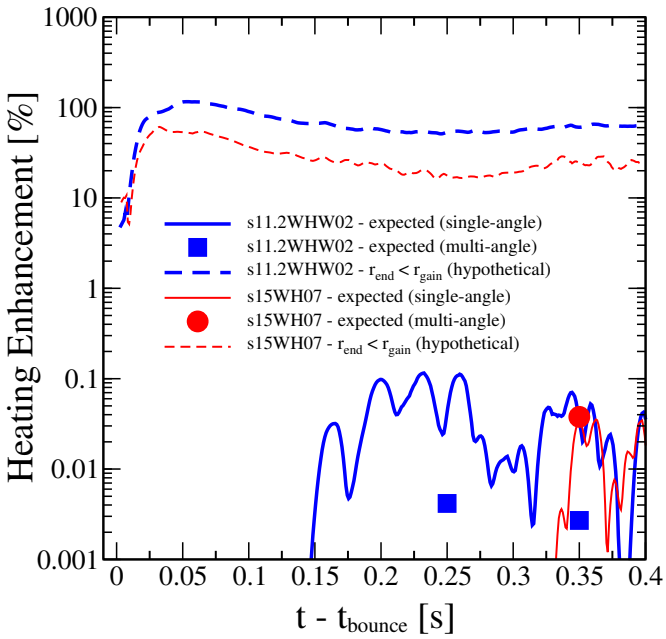

Figure 2: (color online) Time evolution (as a function of time after core bounce) of the potential percentage increase in the heating rate due to collective neutrino oscillations based on our recent simulations [89], in which we considered 11.2-$M_\odot$ and 15-$M_\odot$ progenitors. The dashed lines assume the naive case of complete conversion already below the gain radius where heating begins to dominate over cooling. This is the case assumed by by Suwa *et al.* [95]) and leads to an enhancement of up to 100%. In the our detailed oscillation calculations, conversion does not occur before the gain radius and our more realistic estimate of the heating enhancement is much lower and shown in solid lines. The points, blue squares for the 11.2-$M_\odot$ model and red circles for the 15-$M_\odot$ model, represent our estimate of the heating enhancement if multi-angle oscillation effects are included, which further increase the radii at which collective oscillations occur and thus decrease the heating enhancement even further, in general agreement with [87, 88]. This figure corresponds to Fig. 7 of [89].

emission that leads to an angular instability [89, 92], one finds the matter suppression to be less effective. Secondly, in the cooling phase of the explosion, $\nu_x/\bar{\nu}_x$ fluxes may be larger than $\nu_e/\bar{\nu}_e$ fluxes. This can lead to additional instabilities which cause multiple spectral splits [71]. These features survive multi-angle effects in general, and with the inclusion of three-flavor effects can lead to a rich and complex phenomenology [93, 94].

The understanding of collective neutrino oscillations is still evolving, and we expect that more accurate numerical calculations and improved analytical understanding will yield new surprises and insights into the existing results we have summarized here.

3.4 Effect of Collective Oscillations on Neutrino-driven Explosions

From the core-collapse supernova theory point of view, the most intriguing result of collective oscillations is the almost complete exchange of ν_e and ν_x and $\bar{\nu}_e$ and $\bar{\nu}_x$ spectra in the inverted mass hierarchy. The ν_x and $\bar{\nu}_x$ are emitted by thermal processes deep inside the core and their spectra are much harder than those of their electron-flavor counterparts. Due to the ϵ_ν^2-dependence of the charged-current absorption cross section, a swap of $\nu_x/\bar{\nu}_x$ and $\nu_e/\bar{\nu}_e$ spectra could dramatically enhance neutrino heating and may be the crucial ingredient missing in core-collapse supernova models, provided that the oscillations occur at sufficiently small radii to have an effect in the region behind the shock. To our knowledge, this point, in the context of collective oscillations, was first made by one of us [96].

Suwa *et al.* [95] recently performed a set of 1D and 2D core-collapse supernova simulations in which they considered *ad-hoc* spectral swaps above 9 MeV for neutrinos and antineutrinos occurring at a fixed radius of 100 km, which is close to the gain radius (where heating begins to dominate over cooling) in their simulations. They considered a range of progenitor models and found that the heating enhancement by collective oscillations can indeed turn duds into explosions. This result was corroborated in a semi-analytic study by Pejcha *et al.* [97] in which the authors also considered different radii for the oscillations to become effective.

Chakraborty *et al.* [87, 88] carried out the first multi-angle single-energy neutrino oscillations based on realistic neutrino radiation fields from 1D core-collapse supernova simulations. They discovered that the rather high matter density between protoneutron star and stalled shock strongly suppresses collective neutrino oscillations in the pre-explosion phase when multi-angle effects are taken into account. Hence, the authors excluded any impact of collective oscillations on neutrino heating.

In Dasgupta *et al.* [89], we carried out single-angle multi-energy and multi-angle single-energy oscillation calculations based on neutrino radiation fields from 2D core-collapse supernova simulations performed with the `VULCAN/2D` code [26]. In 2D, convection and SASI lead to complicated flow patterns and large-scale shock excursions not present in 1D simulations. Even in our single-angle calculations and in the most optimistic case, we find that collective oscillations do not set in at radii sufficiently deep in the heating region to have a significant effect on neutrino heating. When including multi-angle effects, we also observe a suppression of collective oscillations, though not at the level argued for by [87, 88], who made different assumptions about the angular distribution of the neutrino radiation fields emitted from the neutrinosphere (ours are based on the angle-dependent neutrino transport results of [24]).

As depicted by Fig. 2, we find that the heating enhancement due to collective oscillations, if present at all, stays below $\sim$0.1% at all times in both considered progenitor models when oscillation radii from full oscillation calculations are taken into account. This shows, in agreement with [87, 88], that the strong positive effect on the neutrino mechanism reported by Suwa *et al.* [95] is artificial and due primarily to their ad-hoc choice of a small oscillation radius.

3.5 Collective Oscillations after the Onset of Explosion

In Dasgupta *et al.* [89], we studied the suppression of collective oscillations by multi-angle effects at high matter density using multi-angle single-energy oscillation calculations for select simulation snapshots of the pre-explosion phase in 11.2-$M_\odot$ and 15-$M_\odot$ progenitors. We also, in a more heuristic approach, studied the potential for suppression of collective oscillations by comparing the MSW potential $\lambda(r)$ with the expression $\lambda_{\rm MA} = 2\sqrt{2}G_F\Phi_{\nu,\bar{\nu}}(R_{\nu_e}^2/r^2)\mathcal{F}_-$,

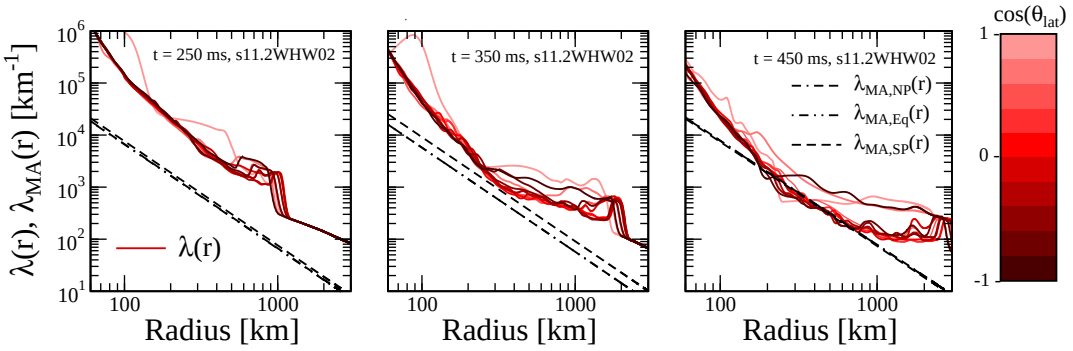

Figure 3: (color online) The MSW potential $\lambda(r)$ along various directions (solid lines, 10 rays equally spaced in $\cos[\theta_{\rm lat}]$), in comparison to the minimum $\lambda(r)$ needed for multi-angle suppression, $\lambda_{\rm MA} = 2\sqrt{2}G_F\Phi_{\nu,\bar{\nu}}(R^2_{\nu_e}/r^2)\mathcal{F}_-$. Dot-dashed-dashed, dot-dot-dashed, and dashed lines, indicated $\lambda_{\rm MA}$ taken along the North pole (NP), equator (Eq), and South pole (SP), respectively. The steep rise in the $\lambda(r)$ profiles at 250 ms and 350 ms occurring around $r \sim 1000$ km and $r \sim 2000$ km, respectively, is the location of the shock. At 450 ms the shock is close to 3000 km.

where $\Phi_{\nu,\bar{\nu}}$ is the neutrino number density at the ν_e neutrino sphere radius R_{ν_e} and $\mathcal{F}_- = (\Phi_{\nu_e} - \Phi_{\bar{\nu}_e})/(\Phi_{\nu_e} + \Phi_{\bar{\nu}_e} + 4\Phi_{\nu_x})$ is the relative lepton asymmetry of the neutrinos. If $\lambda \gg \lambda_{\rm MA}$, collective oscillations are suppressed [85].

In [89], we compared λ and $\lambda_{\rm MA}$ at various pre-explosion times, radii, and spatial angular directions in our simulations using 11.2-$M_\odot$ and 15-$M_\odot$ progenitors. Based on this, we concluded, in agreement with [87, 88], that suppression of collective oscillations is likely highly relevant in the pre-explosion phase and must be carefully studied even in relatively low-mass progenitors with steep density profiles such as the 11.2-$M_\odot$ progenitor model.

The situation after the onset of explosion, however, may be quite different: The explosion rarefies the region behind the expanding shock and shuts off the large $\nu_e/\bar{\nu}_e$ accretion luminosity, changing the neutrino flux asymmetry. Extending our previous results to the explosion phase, we have repeated our simulations for the 11.2-$M_\odot$ progenitor, but included an additional neutrino heating term in order to drive an early explosion. The heating term is equivalent to the prescription used in [13] with $L_{\nu_e} = L_{\bar{\nu}_e} = 0.5 \times 10^{52}$ ergs/s.

In Figure 3, we compare the MSW potential $\lambda(r)$ along multiple angular directions with $\lambda_{\rm MA}$. As the explosion clears out the region behind the shock, the MSW potential decreases in strength. In this model, within a few 100 ms of the onset of the explosion, the MSW potential becomes comparable to $\lambda_{\rm MA}$, which indicates that the suppression is lifted and collective oscillations may now occur at radii as small as ∼200 km. At this point, the core-collapse supernova explosion has already been launched, but collective neutrino oscillations may still affect the evolution and various observable features, for example, via the neutrino-driven wind from the protoneutron star and r-process nucleosynthesis [98, 99].

4 Summary and Outlook

In this contribution to the proceedings of the HAmburg Neutrinos from Supernova Explosions (HAνSE) 2011 conference, we have summarized the recent rapid progress in various aspects of core-collapse supernova theory. While 2D simulations continue to be perfected [22, 24, 100, 101], self-consistent 3D simulations with energy-dependent neutrino radiation hydrodynamics are now the frontier of core-collapse supernova modeling [30] and are made possible by the first generation of petascale supercomputers. General relativity is also beginning to be included in 2D [100–102] and 3D simulations [103, 104], which will eventually allow for first-principles studies of multi-D black hole formation and the relationship between massive star collapse and long gamma-ray bursts. Also, open-source codes and microphysics inputs (EOS, neutrino opacities) are gaining traction [48, 105–112]. They allow for code verification and physics benchmarking and are lowering the technological hurdle for new groups with new ideas trying to enter core-collapse supernova modeling.

After ten years with little activity, improved modeling capabilities, faster computers, and the discovery of the 2-$M_\odot$ neutron star, have spawned a flurry of activity in the nuclear EOS community, which has already resulted in multiple new finite-temperature EOS for core-collapse supernova modeling [44–47].

The realization that collective neutrino oscillations may occur in the core-collapse supernova environment [63, 64, 68] has led to a plethora of work since $\sim$2005. As we have outlined in this article, the current state of affairs is that collective oscilations are unlikely to be dynamically relevant in driving the explosion, but their effects are crucial in predicting and understanding the neutrino signal that will be seen in detectors from the next nearby core collapse event. The current frontier of oscillation calculations in the core-collapse supernova context is marked by detailed multi-energy multi-angle calculations that take their input spectra and angular distributions from core-collapse supernova models. Significant progress towards this has recently been made [87–89, 113], but more will be needed to assess the potentially strong impact of neutrino-matter interactions and only partially-decoupled neutrino radiation fields in the oscillation regime.

The broad range of current and near-future advances in theory will be matched and tested by observations of the next galactic (or Magellanic-cloud) core-collapse supernova. This event will most likely be observed in electromagnetic waves, neutrinos, and, with the upcoming advanced generation of gravitational-wave observatories, for the first time also in gravitational waves. Gravitational waves carry dynamical information on the intricate multi-D processes occuring in the supernova core [114, 115] and will complement the structural and thermodynamic information carried by neutrinos. Together, neutrinos and gravitational waves may finally shed observational light on the details of the core-collapse supernova mechanism.

5 Acknowledgments

The authors wish to thank the organizers of the HAνSE 2011 conference. The authors furthermore acknowledge helpful discussions with A. Burrows, L. Dessart, C. Horowitz, H.-T. Janka, J. Lattimer, E. Livne, A. Mirizzi, B. Müller, J. Murphy, J. Nordhaus, C. Reisswig, A. Schwenk, G. Shen, H. Shen, A. Steiner, and S. Woosley. CDO and EPO are partially supported by the Sherman Fairchild Foundation and the National Science Foundation under award numbers AST-0855535 and OCI-0905046. Results presented in this article were obtained through com-

putations on the Caltech compute cluster "Zwicky" (NSF MRI award No. PHY-0960291), on the NSF XSEDE network under grant TG-PHY100033, on machines of the Louisiana Optical Network Initiative under grant loni_numrel07, and at the National Energy Research Scientific Computing Center (NERSC), which is supported by the Office of Science of the US Department of Energy under contract DE-AC03-76SF00098.

References

[1] W. Baade and F. Zwicky. *Proc. Nat. Acad. Sci.*, 20:259, 1934.

[2] H. A. Bethe. *Rev. Mod. Phys.*, 62:801, 1990.

[3] J. M. Lattimer and M. Prakash. What a Two Solar Mass Neutron Star Really Means. In S. Lee, editor, *From Nuclei to Stars: Festschrift in Honor of Gerald E. Brown. arXiv:1012.3208*. World Scientific Publishing, UK, 2011.

[4] E. O'Connor and C. D. Ott. *Astrophys. J.*, 730:70, 2011.

[5] H. A. Bethe and J. R. Wilson. *Astrophys. J.*, 295:14, 1985.

[6] O. Pejcha and T. A. Thompson. *Submitted to ApJ. arXiv:1103.4865*, 2011.

[7] T. A. Thompson, A. Burrows, and P. A. Pinto. *Astrophys. J.*, 592:434, 2003.

[8] M. Liebendörfer, M. Rampp, H.-T. Janka, and A. Mezzacappa. *Astrophys. J.*, 620:840, 2005.

[9] R. Buras, M. Rampp, H.-T. Janka, and K. Kifonidis. *Astron. Astrophys.*, 447:1049, 2006.

[10] F. S. Kitaura, H.-T. Janka, and W. Hillebrandt. *Astron. Astrophys.* , 450:345, 2006.

[11] J. M. Blondin, A. Mezzacappa, and C. DeMarino. *Astrophys. J.*, 584:971, 2003.

[12] L. Scheck, H.-T. Janka, T. Foglizzo, and K. Kifonidis. *Astron. Astrophys.* , 477:931, 2008.

[13] J. W. Murphy and A. Burrows. *Astrophys. J.*, 688:1159, 2008.

[14] R. Fernández and C. Thompson. *Astrophys. J.*, 703:1464, 2009.

[15] J. W. Murphy and C. Meakin. *Astrophys. J.*, 742:74, 2011.

[16] F. Hanke, A. Marek, B. Müller, and H.-T. Janka. *Submitted to the Astrophys. J., arXiv:1108.4355*, 2011.

[17] A. Marek and H.-T. Janka. *Astrophys. J.*, 694:664, 2009.

[18] J. M. Lattimer and F. D. Swesty. *Nucl. Phys. A*, 535:331, 1991.

[19] H.-T. Janka. private communication, 2011.

[20] H. Shen, H. Toki, K. Oyamatsu, and K. Sumiyoshi. *Prog. Th. Phys.*, 100:1013, 1998.

[21] W. Hillebrandt and R. G. Wolff. Models of Type II Supernova Explosions. In W. D. Arnett and J. W. Truran, editors, *Nucleosynthesis : Challenges and New Developments*, page 131, 1985.

[22] S. W. Bruenn, A. Mezzacappa, W. R. Hix, J. M. Blondin, P. Marronetti, O. E. B. Messer, C. J. Dirk, and S. Yoshida. Mechanisms of Core-Collapse Supernovae and Simulation Results from the CHIMERA Code. In G. Giobbi, A. Tornambe, G. Raimondo, M. Limongi, L. A. Antonelli, N. Menci, and E. Brocato, editors, *AIP Phys. Conf. Ser.*, volume 1111 of *AIP Phys. Conf. Ser.*, page 593, 2009.

[23] Y. Suwa, K. Kotake, T. Takiwaki, S. C. Whitehouse, M. Liebendörfer, and K. Sato. *Pub. Astr. Soc. Jap.*, 62:L49, 2010.

[24] C. D. Ott, A. Burrows, L. Dessart, and E. Livne. *Astrophys. J.*, 685:1069, 2008.

[25] A. Burrows, E. Livne, L. Dessart, C. D. Ott, and J. Murphy. *Astrophys. J.*, 640:878, 2006.

[26] A. Burrows, E. Livne, L. Dessart, C. D. Ott, and J. Murphy. *Astrophys. J.*, 655:416, 2007.

[27] N. Smith, W. Li, A. V. Filippenko, and R. Chornock. *Mon. Not. Roy. Astron. Soc.* , 412:1522, 2011.

[28] S. J. Smartt. *Ann. Rev. Astron. Astroph.* , 47:63, 2009.

[29] J. Nordhaus, A. Burrows, A. Almgren, and J. Bell. *Astrophys. J.*, 720:694, 2010.

[30] T. Takiwaki, K. Kotake, and Y. Suwa. *Submitted to the Astrophys. J., arXiv:1108.3989*, 2011.

[31] C. L. Fryer and M. S. Warren. *Astrophys. J. Lett.*, 574:L65, 2002.

[32] A. Burrows, L. Dessart, E. Livne, C. D. Ott, and J. Murphy. *Astrophys. J.*, 664:416, 2007.

[33] C. D. Ott, A. Burrows, L. Dessart, and E. Livne. *Phys. Rev. Lett.*, 96:201102, 2006.

[34] I. Sagert, T. Fischer, M. Hempel, G. Pagliara, J. Schaffner-Bielich, A. Mezzacappa, F.-K. Thielemann, and M. Liebendörfer. *Phys. Rev. Lett.*, 102:081101, 2009.

[35] M. Obergaulinger, P. Cerdá-Durán, E. Müller, and M. A. Aloy. *Astron. Astrophys.* , 498:241, 2009.
[36] C. D. Ott, A. Burrows, T. A. Thompson, E. Livne, and R. Walder. *Astrophys. J. Suppl. Ser.*, 164:130, 2006.
[37] A. Heger, S. E. Woosley, and H. C. Spruit. *Astrophys. J.*, 626:350, 2005.
[38] S.-C. Yoon, N. Langer, and C. Norman. *Astron. Astrophys.* , 460:199, 2006.
[39] S. E. Woosley and A. Heger. *Astrophys. J.*, 637:914, 2006.
[40] M. Modjaz. *Astron. Nachr.*, 332:434, 2011.
[41] N. N. Weinberg and E. Quataert. *Mon. Not. Roy. Astron. Soc.* , 387:L64, 2008.
[42] N. A. Gentile, M. B. Aufderheide, G. J. Mathews, F. D. Swesty, and G. M. Fuller. *Astrophys. J.*, 414:701, 1993.
[43] P. B. Demorest, T. Pennucci, S. M. Ransom, M. S. E. Roberts, and J. W. T. Hessels. *Nature*, 467:1081, 2010.
[44] H. Shen, H. Toki, K. Oyamatsu, and K. Sumiyoshi. *Submitted to Astrophys. J., arXiv:1105.1666*, 2011.
[45] G. Shen, C. J. Horowitz, and S. Teige. *Phys. Rev. C*, 83:035802, 2011.
[46] G. Shen, C. J. Horowitz, and E. O'Connor. *Phys. Rev. C*, 83:065808, 2011.
[47] M. Hempel, T. Fischer, J. Schaffner-Bielich, and M. Liebendörfer. *ArXiv:1108.0848*, 2011.
[48] M. Hempel. URL `http://phys-merger.physik.unibas.ch/~hempel/eos.html`. Matthias Hempel's EOS webpage.
[49] K. Hebeler, J. M. Lattimer, C. J. Pethick, and A. Schwenk. *Phys. Rev. Lett.*, 105:161102, 2010.
[50] F. Özel, G. Baym, and T. Güver. *Phys. Rev. D.*, 82:101301, 2010.
[51] A. W. Steiner, J. M. Lattimer, and E. F. Brown. *Astrophys. J.*, 722:33, 2010.
[52] F. J. Fattoyev, C. J. Horowitz, J. Piekarewicz, and G. Shen. *Phys. Rev. C*, 82:055803, 2010.
[53] F. Özel, D. Psaltis, S. Ransom, P. Demorest, and M. Alford. *Astrophys. J. Lett.*, 724:L199, 2010.
[54] S. Typel, G. Röpke, T. Klähn, D. Blaschke, and H. H. Wolter. *Phys. Rev. C*, 81:015803, 2010.
[55] H.-T. Janka. *Astron. Astrophys.* , 368:527, 2001.
[56] B. Pontecorvo. *Sov.Phys.JETP*, 26:984, 1968.
[57] S.P. Mikheev and A.Yu. Smirnov. *Sov.J.Nucl.Phys.*, 42:913, 1985.
[58] J. T. Pantaleone. *Phys. Lett. B.*, 287:128, 1992.
[59] R. C. Schirato and G. M. Fuller. *astro-ph/0205390*, 2002.
[60] M. Cribier, W. Hampel, J. Rich, and D. Vignaud. *Phys. Lett. B*, 182:89, 1986.
[61] G. Sigl and G. Raffelt. *Nucl. Phys. B*, 406:423, 1993.
[62] A. Friedland and C. Lunardini. *Phys. Rev. D.*, 68:013007, 2003.
[63] H. Duan, G. M. Fuller, and Y.-Z. Qian. *Phys. Rev. D.*, 74(12):123004, 2006.
[64] H. Duan, G. M. Fuller, J. Carlson, and Y.-Z. Qian. *Phys. Rev. D.*, 74(10):105014, 2006.
[65] V. A. Kostelecky and S. Samuel. *Phys. Rev. D.*, 52:621, 1995.
[66] S. Pastor, G. G. Raffelt, and D. V. Semikoz. *Phys. Rev. D.*, 65:053011, 2002.
[67] G. G. Raffelt. *Phys. Rev. D.*, 78:125015, 2008.
[68] S. Hannestad, G. G. Raffelt, G. Sigl, and Y. Y. Y. Wong. *Phys. Rev. D.*, 74(10):105010, 2006.
[69] H. Duan, G. M. Fuller, J. Carlson, and Y.-Z. Qian. *Phys. Rev. D.*, 75:125005, 2007.
[70] G. G. Raffelt and A. Y. Smirnov. *Phys. Rev. D.*, 76:081301, 2007.
[71] B. Dasgupta, A. Dighe, G. G. Raffelt, and A. Y. Smirnov. *Phys. Rev. Lett.*, 103:051105, 2009.
[72] G.G. Raffelt and G. Sigl. *Phys. Rev. D.*, 75:083002, 2007.
[73] A. Esteban-Pretel, S. Pastor, R. Tomas, G. G. Raffelt, and G. Sigl. *Phys. Rev. D.*, 76:125018, 2007.
[74] G. L. Fogli, E. Lisi, A. Marrone, and A. Mirizzi. *JCAP*, 0712:010, 2007.
[75] B. Dasgupta, A. Dighe, A. Mirizzi, and G. G. Raffelt. *Phys. Rev. D.*, 78:033014, 2008.
[76] B. Dasgupta and A. Dighe. *Phys. Rev. D.*, 77:113002, 2008.
[77] J. Gava and C. Volpe. *Phys. Rev. D.*, 78:083007, 2008.
[78] M. Blennow, A. Mirizzi, and P. D. Serpico. *Phys. Rev. D.*, 78:113004, 2008.
[79] B. Dasgupta, G. G. Raffelt, and I. Tamborra. *Phys. Rev. D.*, 81:073004, 2010.

[80] L. Wolfenstein. *Phys. Rev. D.*, 17:2369, 1978.

[81] S. P. Mikheev and A. Y. Smirnov. *Yad. Fiz.*, 42:1441, 1985.

[82] H. Duan, G. M. Fuller, J. Carlson, and Y.-Z. Qian. *Phys. Rev. Lett.*, 100:021101, 2008.

[83] H. Duan, G. M. Fuller, and Y.-Z. Qian. *Phys. Rev. D.*, 77:085016, 2008.

[84] B. Dasgupta, A. Dighe, A. Mirizzi, and G. G. Raffelt. *Phys. Rev. D.*, 77:113007, 2008.

[85] A. Esteban-Pretel, A. Mirizzi, S. Pastor, R. Tomàs, G. G. Raffelt, P. D. Serpico, and G. Sigl. *Phys. Rev. D.*, 78:085012, 2008.

[86] H. Duan and A. Friedland. *Phys. Rev. Lett.*, 106(9):091101, 2011.

[87] S. Chakraborty, T. Fischer, A. Mirizzi, N. Saviano, and R. Tomàs. *Phys. Rev. Lett.*, 107:151101, 2011.

[88] S. Chakraborty, T. Fischer, A. Mirizzi, N. Saviano, and R. Tomàs. *Phys. Rev. D.*, 84:025002, 2011.

[89] B. Dasgupta, E. P. O'Connor, and C. D. Ott. *Submitted to Phys. Rev. D., arXiv:1106.1167*, 2011.

[90] A. Banerjee, A. Dighe, and G. Raffelt. *Phys. Rev. D.*, 84:053013, 2011.

[91] S. Sarikas, G. G. Raffelt, L. Hudepohl, and H.-T. Janka. *arXiv:1109.3601*, 2011.

[92] A. Mirizzi and P. D. Serpico. *arXiv:1110.0022*, 2011.

[93] A. Friedland. *Phys. Rev. Lett.*, 104:191102, 2010.

[94] B. Dasgupta, A. Mirizzi, I. Tamborra, and R. Tomas. *Phys. Rev. D.*, 81:093008, 2010.

[95] Y. Suwa, K. Kotake, T. Takiwaki, M. Liebendörfer, and K. Sato. *Astrophys. J.*, 738:165, 2011.

[96] C. D. Ott. Talk at the Joint Indo-German Supernova Astroparticle Physics Workshop (JIGSAW) 2010 at TIFR, Mumbai, India, 2010. URL `http://theory.tifr.res.in/~jigsaw10/talks/ott.pdf`.

[97] O. Pejcha, B. Dasgupta, and T. A. Thompson. *Submitted to the Astrophys. J., arXiv:1106.5718*, 2011.

[98] H. Duan, A. Friedland, G. C. McLaughlin, and R. Surman. *J. Phys. G Nuc. Phys.*, 38:035201, 2011.

[99] R. Surman, G. C. McLaughlin, A. Friedland, and H. Duan. *Nuc. Phys. B Proc. Suppl.*, 217:121, 2011.

[100] B. Müller, H.-T. Janka, and H. Dimmelmeier. *Astrophys. J. Supp. Ser.* , 189:104, 2010.

[101] P. Cerdá-Durán, J. A. Font, L. Antón, and E. Müller. *Astron. Astrophys.* , 492:937, 2008.

[102] Y. Sekiguchi and M. Shibata. *Astrophys. J.*, 737:6, 2011.

[103] C. D. Ott, H. Dimmelmeier, A. Marek, H.-T. Janka, I. Hawke, B. Zink, and E. Schnetter. *Phys. Rev. Lett.*, 98:261101, 2007.

[104] C. D. Ott, C. Reisswig, E. Schnetter, E. O'Connor, U. Sperhake, F. Löffler, P. Diener, E. Abdikamalov, I. Hawke, and A. Burrows. *Phys. Rev. Lett.*, 106:161103, 2011.

[105] M. Liebendörfer. URL `http://www.physik.unibas.ch/~liebend/download/index.html`. Numerical Algorithms for Supernova Dynamics.

[106] URL `http://www.stellarcollapse.org`. `stellarcollapse.org`: A Community Portal for Stellar Collapse, Core-Collapse Supernova and GRB Simulations.

[107] E. O'Connor and C. D. Ott. *Class. Quantum Grav.*, 27:114103, 2010.

[108] F. Timmes. URL `http://cococubed.asu.edu/code_pages/codes.shtml`. Cococubed – Astronomy Codes.

[109] URL `http://www.einsteintoolkit.org`. EinsteinToolkit: A Community Toolkit for Numerical Relativity.

[110] F. Löffler, J. Faber, E. Bentivegna, T. Bode, P. Diener, R. Haas, I. Hinder, B. C. Mundim, C. D. Ott, E. Schnetter, G. Allen, M. Campanelli, and P. Laguna. *ArXiv:1111.3344*, 2011.

[111] H. Shen. URL `http://physics.nankai.edu.cn/grzy/shenhong/EOS/index.html`. Homepage of Relativistic EOS Table.

[112] G. Shen. URL `http://cecelia.physics.indiana.edu/gang_shen_eos/`. Gang Shen's EOS webpage.

[113] H. Duan, G. M. Fuller, and Y.-Z. Qian. *Ann. Rev. Nuc. Part. Sc.*, 60:569, 2010.

[114] C. D. Ott. *Class. Quantum Grav.*, 26:063001, 2009.

[115] K. Kotake. *submitted to a special issue of Comptes Rendus Physique "Gravitational Waves (from detectors to astrophysics)", ArXiv:1110.5107*, 2011.

Long-term evolution of massive star explosions

T. Fischer[1,2], *M. Liebendörfer*[3], *F.-K. Thielemann*[3], *G. Martínez-Pinedo*[2,1], *B. Ziebarth*[1] *and K. Langanke*[1,2,4]

[1] GSI Helmholtzzentrum für Schwerionenforschung, Planckstraße 1, 64291 Darmstadt, Germany
[2] Technische Universität Darmstadt, Schlossgartenstraße 9, 64289 Darmstadt, Germany
[3] University Basel, Department of Physics, Klingelbergstraße 82, 4056 Basel, Switzerland
[4] Frankfurt Institute for Advanced Studies, Ruth-Moufang Straße 1, Frankfurt, Germany

DOI: http://dx.doi.org/10.3204/DESY-PROC-2011-03/fischer

We examine simulations of core-collapse supernovae in spherical symmetry. Our model is based on general relativistic radiation hydrodynamics with three-flavor Boltzmann neutrino transport. We discuss the different supernova phases, including the long-term evolution up to 20 seconds after the onset of explosion during which the neutrino fluxes and mean energies decrease continuously. In addition, the spectra of all flavors become increasingly similar, indicating the change from charged- to neutral-current dominance. Furthermore, it has been shown recently by several groups independently, based on sophisticated supernova models, that collective neutrino flavor oscillations are suppressed during the early mass-accretion dominated post-bounce evolution. Here we focus on the possibility of collective flavor flips between electron and non-electron flavors during the later, on the order of seconds, evolution after the onset of an explosion with possible application for the nucleosynthesis of heavy elements.

1 Introduction

Explosions of massive stars are related to the formation of a shock wave, which forms when the collapsing stellar core bounces back at nuclear matter density. During collapse, the stellar core deleptonizes so that a low central proton-to-baryon ratio, given by the electron fraction of $Y_e \simeq 0.3$, is reached at bounce. The conditions obtained at bounce depend sensitively on the weak interaction scheme and the equation of state used. Fig. 1 illustrates the radial evolution of selected mass elements. Before bounce, the infalling mass elements correspond to the central iron-core while the outer layers of the progenitor are basically unaffected from the central happenings. After bounce, the shock wave propagates outwards and stalls on a timescale of 5–20 ms due to energy losses from heavy-nuclei dissociation and ν_e-escapes emitted via large numbers of electron captures during the shock passaged across the neutrinospheres. As a result of energy loss, the expanding dynamic bounce shock turns into a standing accretion shock (SAS). For the early shock propagation and the position of the ν_e-sphere, see the red solid and magenta dash-dotted lines in Fig. 1. The post-bounce evolution is given by mass accretion onto the SAS and neutrino heating, dominantly via ν_e and $\bar{\nu}_e$ absorption at the dissociated free nucleons, behind the SAS on timescales on the order of 100 ms.

Several explosion mechanisms have been explored; the magneto-rotational [1], the dumping of acoustic energy [2] and the standard scenario due to neutrino heating [3]. Recently, it has been

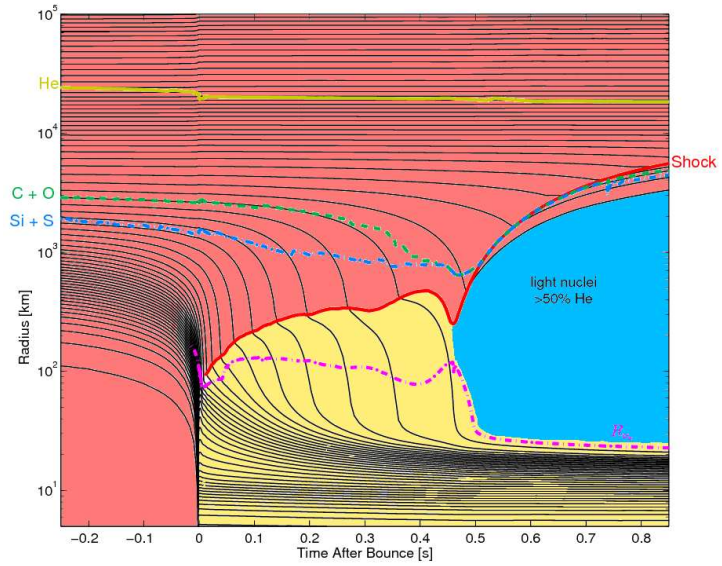

Figure 1: (color online) Sketching the evolution of selected mass elements during core collapse, bounce, post-bounce accretion and onset of explosion. Color coding is according to the dominant composition (light red: heavy nuclei, blue: ^{4}He, yellow: light nuclei and free nucleons). The solid red and dash-dotted magenta lines mark the positions of shock and neutrinosphere. The dashed lines mark the evolution of interfaces between different composition layers of the progenitor.

shown that a quark-hadron phase transition can lead to the formation of an additional shock wave that can trigger explosions [4, 5]. In this article, we explore standard neutrino-driven explosions in spherical symmetry of the low-mass 8.8 $M_\odot$ O-Ne-Mg-core and more massive iron-core progenitors. For the latter, where neutrino-driven explosions cannot be obtained in spherical symmetry, we enhance neutrino heating in order to trigger explosions. Fig. 1 illustrates the standard neutrino-driven explosion of a 15 $M_\odot$ progenitor, for which the accretion phase ends at about 450 ms post bounce with the onset of explosion. The SAS turns into a dynamic shock which expands continuously to increasingly larger radii (see the red solid line in Fig. 1). It has been speculated that collective neutrino flavor oscillations, during the post-bounce accretion phase, may affect neutrino luminosities and hence heating and cooling. Recently, it has been shown that matetr dominance suppresses collective flavor oscillations during the accretion phase [6, 7]. It has been confirmed by several different groups based on different supernova models [8, 9].

At the onset of explosion, mass accretion vanishes and the central proto-neutron star contracts rapidly (see the magenta dash-dotted line in Fig. 1). It formed at core bounce and is hot and lepton-rich, in which terms it differs from the final supernova remnant neutron star. Between the expanding shock wave and the central proto-neutron star forms a region of low density and high entropy, where the surface of the proto-neutron star is subject to continued neutrino heating. There, a low-mass outflow develops known as *neutrino-driven wind*. The first sophisticated radiation-hydrodynamics study of the neutrino-driven wind was a milestone of research in the field [10]. It could explain the solar r-process abundances, due to the obtained strong wind with high entropies per baryon $\sim$ 300 k_B and generally neutron-rich conditions with $Y_e \simeq$0.35–0.48. The neutrino-driven wind has also long been explored in static steady-state models [11, 12, 13, 14] and dynamic studies [15, 10, 16, 17], as possible site for the nucleosynthesis of heavy elements [18, 19, 20]. However, recent supernova simulations that include Boltzmann neutrino transport cannot confirm the early results. They obtain generally proton-rich

conditions and entropies per baryon on the order of 100 k_B [21, 22]. The main difference to the early studies is related to the evolution of neutrino luminosities and mean energies. Within the current models, they reduce continuously during the proto-neutron star deleptonization on timescales on the order of 10 seconds after the onset of explosion. Furthermore, the ν_e and $\bar{\nu}_e$ spectra become increasingly similar. Charged-current dominace reduces, because final state electrons become Pauli-blocked and nucleons become degenerate at the neutrinospheres, due to the increasing density. Instead, the spectra become dominated by neutral-current processes during the proto-neutron star deleptonization.

The relevance of collective neutrino flavor oscillations has long been investigated in various astrophysical applications. Although collective neutrino flavor oscillations are suppressed during the accretion phase, they may be relevant after the onset of explosion due to the continuously decreasing matter density in the presence of still high neutrino densities.Here, we explore the possibility of complete spectral flips of $\bar{\nu}_e$ and $\bar{\nu}_{\mu/\tau}$ at a fixed flip energy and their impact to νp-process nucleosynthesis for a selected trajectory from a supernova simulation of a massive iron-core progenitor. We find that it enhances the neutron production rate which in turn increases the production of heavy nuclei with $A > 90$.

The manuscript is organized as follows. We will summarize main aspects of our core-collapse model in § 2. In § 3 we will illustrate standard neutrino-driven explosions of massive stars in spherical symmetry as well as the neutrino-driven wind phase after the onset of an explosion. § 4 is devoted to the evolution of neutrino luminosities and spectra. Illustration of our simplified neutrino flavor flip analysis and the impact to nucleosynthesis will be discussed in § 5. We close with a summary in § 6.

2 Core-collapse supernova model

The simulations under investigation are based on general relativistic radiation hydrodynamics and three-flavor Boltzmann neutrino transport in spherical symmetry. For details, see the following references [23, 24, 25, 26, 27, 28, 29]. Recent improvements of the adaptive mesh have been added in ref. [21]. It enables large stable timesteps and allows for long simulation times on the order of 10 seconds. The list of weak processes considered is given in Table 1, including references. In addition, the implementation of the following weak process, $\nu_e + \bar{\nu}_e \leftrightarrows \nu_{\mu/\tau} + \bar{\nu}_{\mu/\tau}$, has been discussed in ref [30], following ref. [31]. For the current study, weak magnetism corrections as well as N–N–recoil and ion-ion-correlations have not been included in the weak processes.

For matter in nuclear statistical equilibrium (NSE), the equation of state from ref. [34] was used. It is based on relativistic mean field approach and the Thomas-Fermi approximation for heavy nuclei, with a simplified composition of neutrons, protons, α-particles and a single representative heavy nucleus with average atomic mass A and charge Z. Baryon contributions for matter in non-NSE are added using a slim nuclear reaction network for 20 nuclei (see [21] and references therein). It is used only for energy production. On top of the baryons, contributions from (e^-, e^+) and photons as well as ion-ion-correlations for non-NSE are added [35].

Our core-collapse simulations are launched from the low-mass 8.8 $M_\odot$ O-Ne-Mg-core [36, 37] and from more massive iron-cores of 10.8, 15 and 18 $M_\odot$ [38]. Their evolution during accretion and explosion, as well as the long-term evolution on timescales on the order of seconds after the onset of explosion, will be discussed in the next section.

	weak process[1]	References
1	$\nu_e + n \leftrightarrows p + e^-$	[32]
2	$\bar{\nu}_e + p \leftrightarrows n + e^+$	[32]
3	$\nu_e + (A, Z-1) \leftrightarrows (A, Z) + e^-$	[32]
4	$\nu + N \leftrightarrows \nu' + N$	[32]
5	$\nu + (A, Z) \leftrightarrows \nu' + (A, Z)$	[32]
6	$\nu + e^\pm \leftrightarrows \nu' + e^\pm$	[32, 25]
7	$\nu + \bar{\nu} \leftrightarrows e^- + e^+$	[32, 25]
8	$\nu + \bar{\nu} + N + N \leftrightarrows N + N$	[33]

[1] Notes: $\nu = \{\nu_e, \bar{\nu}_e, \nu_{\mu/\tau}, \bar{\nu}_{\mu/\tau}\}$, $N = \{n, p\}$

Table 1: Neutrino reactions considered, including references.

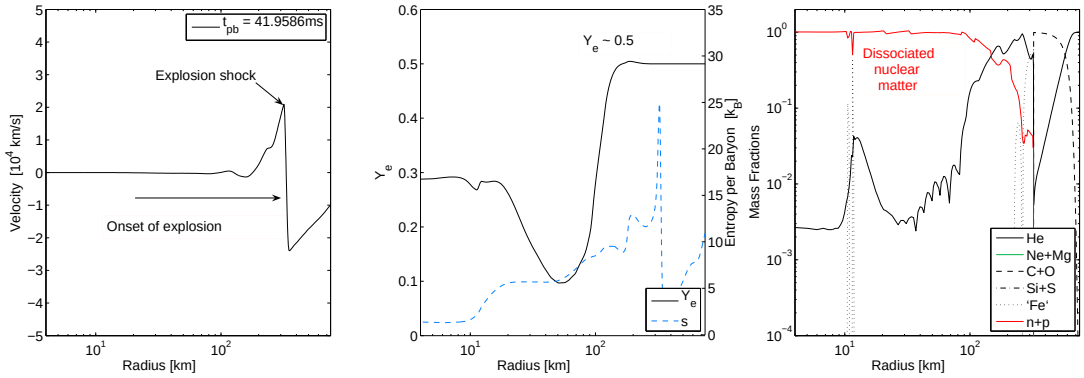

Figure 2: (color online) Radial profiles of selected quantities at the onset of explosion, for the 8.8 $M_\odot$ O-Ne-Mg-core progenitor (data are taken form ref. [21]).

3 Explosions and long-term evolution

Neutrino-driven explosions of the low-mass 8.8 $M_\odot$ O-Ne-Mg-core can be obtained even in spherically symmetric supernova models [39, 21]. The success of this model is related to the special structure of the progenitor. Only about 0.1 $M_\odot$ of the 1.376 $M_\odot$ core is composed of iron-group nuclei, at the onset of collapse. The outer layers are dominated by ^{20}Ne and ^{24}Mg as well as further out ^{12}C and ^{16}O. During collapse, the Ne and Mg layers are partly burned to iron-group elements and hence the enclosed mass inside the iron-core grows. Moreover, when the standing accretion shock reaches the interface between C-O and He-layers, where the density drops over more than 10 orders of magnitude, it turns into a dynamic shock with positive velocities. It determines the onset of explosion, at about 35 ms post bounce, after which the shock expands continuously to larger radii. Fig. 2 illustrates the onset of explosion for this model (see ref. [21] and references therein). During the early explosion phase the $\bar{\nu}_e$and ν_e-spectra are very similar. Note further, for this low-mass progenitor the shock wave expands basically into vacuum due to the extremely low density of the He-rich hydrogen envelop, where velocities on the order of the speed of light are reached. The competition between reactions (1) and (2) in Table 1, lead to even slightly neutron-rich conditions with $Y_e \simeq 0.4681$–0.4986

during the initial shock expansion after the onset of explosion between about 200–400 ms post bounce. The timescale for $\bar{\nu}_e$ captures to turn material to the proton-rich side is not sufficient. In axially symmetric simulations, matter becomes even more neutron-rich early after the onset of explosion, developing mushroom-like pockets with $Y_{e,\,\mathrm{min}} \simeq 0.404$ [43]. It may be a possible site for the weak r-process, producing elements with atomic mass between $A >$56–90, for which the production problem based on standard chemical evolution models has been discovered in ref. [44]. Recently, the question of an additional nucleosynthesis process required in order to explain the observed abundances of these elements has been addressed. It became known as light-element primary process (LEPP) [45] and is an active subject of research.

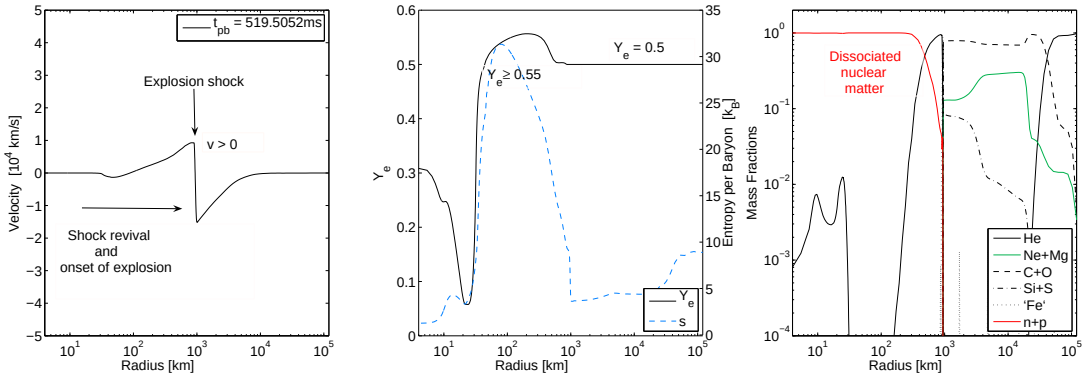

Figure 3: (color online) Radial profiles of selected quantities at the onset of explosion, for the 15 $M_\odot$ iron-core progenitor.

The situation is different for more massive stars, illustrated in Fig. 3 at the example of a 15 $M_\odot$ iron-core progenitor. The extended high-density Si-S-layer surrounding the more massive iron-core, leads to a post-bounce accretion phase that can last for several 100 ms (depending on the progenitor model). The central proto-neutron star is much more compact at the onset of explosion. The luminosities of ν_e and $\bar{\nu}_e$ are very similar during the post-bounce accretion phase as well as at the onset of explosion. Hence, due to the rest-mass difference between neutrons and protons, matter becomes proton-rich with $Y_e \simeq$0.5–0.57. The magnitude of the differences between ν_e and $\bar{\nu}_e$ luminosities and mean energies, and consequently Y_e, is an active subject of research. It may change taking corrections from weak magnetism and improved weak rates into account. Note that the explosions for the iron-core progenitors under investigation are obtained applying enhanced heating and cooling rates (detailed balance is fulfilled), in order to trigger the explosions. For more details, see ref. [21]. Core-collapse simulations based on multi-dimensional models, that include sophisticated neutrino transport [40, 41, 42], are required for simulation times on the order of several seconds after the onset of explosion.

After the onset of explosion a region of low density and high entropy develops between the expanding explosion shock and the central proto-neutron star. Moreover, at the surface of the proto-neutron star establishes net-heating, illustrated in Fig. 4(b). It leads to a low-mass outflow, known as the neutrino-driven wind. Compared to the very fast initial expansion of the 8.8 $M_\odot$ model, the situation is different for more-massive iron-core progenitors. There, the neutrino-driven ejecta expand into the extended C-O and He-layers with baryon densities between 10^1 g cm^{-3} to 10^3 g cm^{-3}, where also the shock expansion slows down. For illustration,

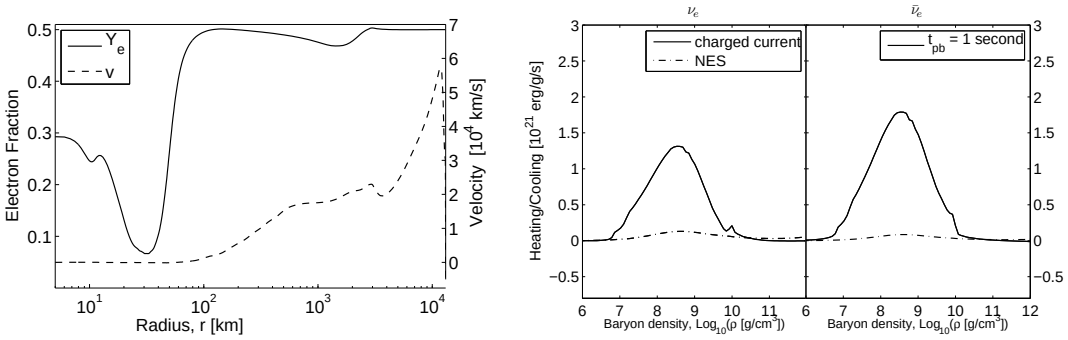

(a) Radial profiles of Y_e and velocity.

(b) Heating rate during the neutrino-driven wind

Figure 4: Electron fraction and velocity profiles at the early explosion phase at about 200 ms post bounce for the 8.8 $M_\odot$ model in graph 4(a) and net energy-deposition rates at the onset of the neutrino-driven wind phase at about 1 second post bounce in graph 4(b) (data are taken form ref. [21]).

see the radial profiles at a selected post-bounce time during the neutrino-driven wind phase in Fig. 5(a) at the example of the 10.8 $M_\odot$ progenitor. Moreover, the neutrino-driven wind collides with the slower moving explosion shock. Note that in case of a super-sonic neutrino-driven wind, a reverse shock forms as shown in Fig. 5(b). This leads to an additional temperature and entropy increase (see Figs. 5(a) and 5(b) between 5000-6000 km). The impact of the reverse shock on possible nucleosynthesis has been investigated recently [46]. At late times, neutrino heating reduces and the neutrino-driven wind turns back to sub-sonic velocities before it vanishes completely.

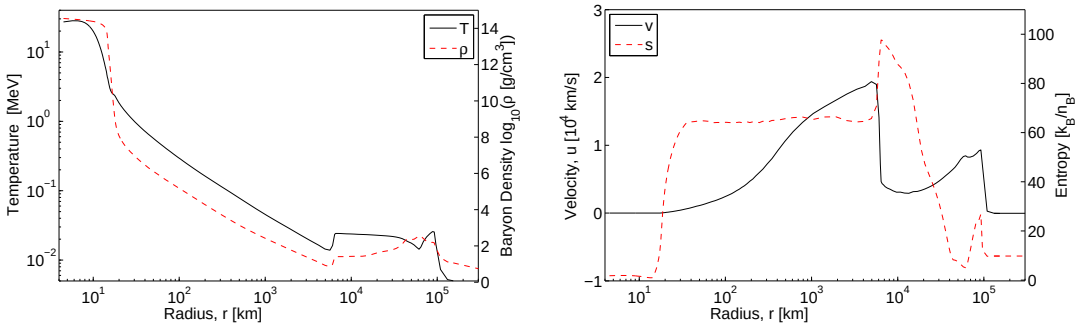

(a) Baryon density and Temperature

(b) Velocity and entropy per baryon.

Figure 5: (color online) Radial profiles of selected quantities during the neutrino-driven wind phase for the 10.8 $M_\odot$ progenitor model under investigation (data are taken form ref. [21]).

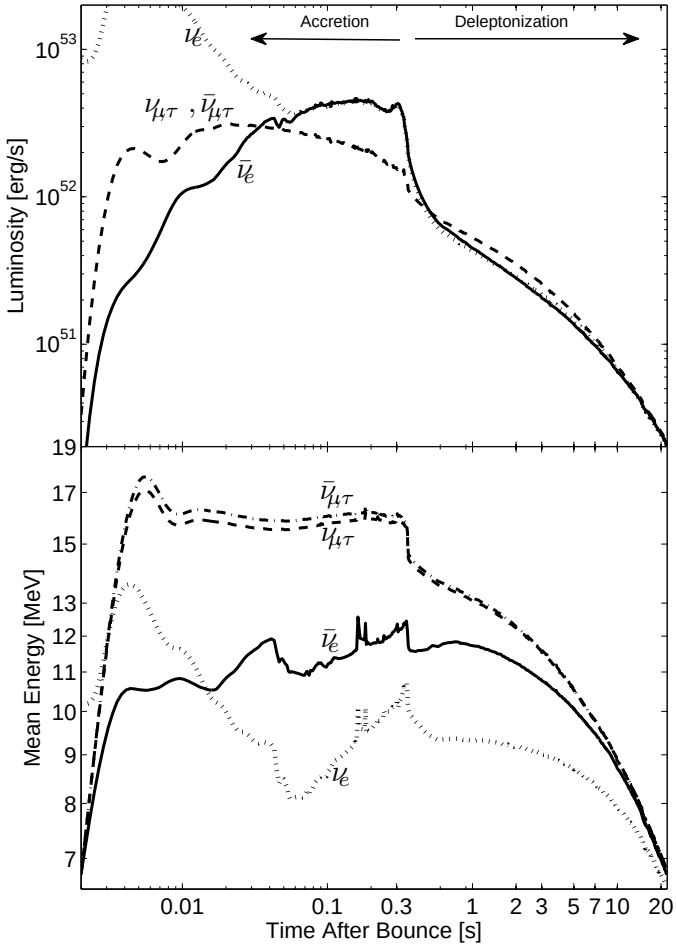

Figure 6: Post bounce evolution of neutrino (dotted lines: ν_e, solid lines: $\bar{\nu}_e$, dashed lines: $\nu_{\mu/\tau}$, dash-dotted lines: $\bar{\nu}_{\mu/\tau}$) luminosities (top) and mean energies (bottom) for the 18 $M_\odot$ progenitor model (data are taken form ref. [21]). At the end of the accretion phase, indicated by the sharp jumps at about 350 ms post bounce, the luminosities of all flavors decrease continuously. The same holds for the mean energies. Furthermore, neutrino luminosities and spectra become increasingly similar for all flavors during the deleptonization phase. They converge for this model at about 20 seconds post bounce. It is related to the reducing dominance of charged-current reactions during the proto-neutron star deleptonization. Instead, the spectra are dominated by neutral-current reactions (neutrino-neutron scattering).

4 Neutrino spectra evolution

The evolution of neutrino luminosities and mean energies is shown in Fig. 6 at the example of the 18 $M_\odot$ progenitor up to 22 seconds post bounce. The observables are sampled in the co-moving reference frame at a distance of 500 km, well outside the neutrinospheres.

The ν_e-luminosity, $\mathcal{O}(10^{52})$ erg/s, rises slowly after the deleptonization burst has been launched at 20 ms post bounce. $\bar{\nu}_e$ and $\nu_{\mu/\tau}$ are produced only after bounce. The $\nu_{\mu/\tau}$-luminosities rises until about 20 ms post bounce and the $\bar{\nu}_e$-luminosity rises continuously. After reaching their maximum, the $\nu_{\mu/\tau}$-luminosity decreases slowly continued during the accretion phase on timescales of 100 ms. Furthermore, the ν_e and $\bar{\nu}_e$ luminosities are determined by mass accretion at the neutrinospheres. They rise slowly on a timescale of 100 ms and reach their maximum of several 10^{52} erg/s at the onset of explosion at about 350 ms post bounce. After

that, mass accretion vanishes and the electron flavor luminosities decrease rapidly one order of magnitude within the first second after the onset of explosion. The $\nu_{\mu/\tau}$-luminosity reduces accordingly and takes similar values as the electron flavor luminosities. The magnitude of the differences between the different flavors is an active subject of research. It depends sensitively on the weak processes considered and the dimensionality of the model. On a long timescale on the order of several 10 seconds, i.e. the proto-neutron star deleptonization, the neutrino luminosities of all flavors reduce below 10^{50} erg/s. Furthermore, they become practically indistinguishable. In multi-dimensional models, and in the presence of aspherical explosions, mass accretion is still possible after the onset of an explosion. A possible enhancement of the neutrino fluxes remains to be shown for simulation times on the order of several seconds.

The mean energies, shown at the bottom of Fig. 6, have a similar behavior as the neutrino fluxes. They rise during the early post bounce phase up to 12, 14 and 19 MeV for ν_e, $\bar{\nu}_e$ and $\nu_{\mu/\tau}$ respectively, at the onset of explosion. After that, $\langle E\rangle_{\nu_{\mu/\tau}}$ decreases continuously. $\langle E\rangle_{\nu_e}$ and $\langle E\rangle_{\bar{\nu}_e}$ stay about constant until about 2 seconds post bounce, after which they decrease as well. The spectra of all flavors converge during the evolution after the onset of explosion, i.e. the difference between the mean energies of all flavors reduces continuously during the proto-neutron star deleptonization. For the 18 $M_\odot$ progenitor model under investigation, the spectra have converged at about 20 seconds post bounce. It is related to the reduced dominance of charged-current reactions, due to final-state electron blocking and increasing nucleon degeneracy. Instead, the spectra are dominated by neutral-current reactions, in particular neutrino-neutron scattering.

The small, and even reducing, difference between ν_e and $\bar{\nu}_e$ luminosities and spectra has important consequences for the composition. It leads to generally proton-rich conditions with $Y_e \simeq$0.52–0.56 for matter that becomes gravitationally unbound during the proto-neutron star deleptonization in the neutrino-driven wind. The results obtained for the low-mass O-Ne-Mg-core are in qualitative agreement with the results of the Garching group [22]. The magnitude of Y_e obtained for the models under investigation depends sensitively on the equation of state and the weak processes used.

5 Nucleosynthesis under proton-rich conditions

Matter at the surface of the proto-neutron star is in NSE, due to the high temperatures and densities. During the expansion in the neutrino-driven wind, matter cools until reaching larger distance from the proto-neutron star surface, where nucleons recombine into heavy nuclei. This nucleosynthesis depends sensitively on the initial proton-to-baryon ratio. It is determined via the competition of reactions (1) and (2) from Table 1 in the dissociated regime at the proto-neutron star surface. It depends on the above discussed electron flavor luminosities and spectra. In the presence of similar ν_e and $\bar{\nu}_e$ luminosities and mean energies[1], matter becomes proton-rich due to the neutron-proton rest-mass difference [47]. The proton-rich conditions obtained lead to isospin symmetric nuclei, mainly ^{56}Ni, as well as ^{4}He and free protons. However, the further nucleosynthesis stops at, e.g., ^{64}Ge which has a long beta-decay half-life of $\simeq$ 64 s (known as waiting-point nucleus) and because ^{65}As has a low proton separation energy of $\simeq$ 90 keV.

The situation changes including neutrino reactions, mostly $\bar{\nu}_e$ because isospin symmetric

[1]For neutron-rich conditions, $\varepsilon_{\bar{\nu}_e} - \varepsilon_{\bar{\nu}_e} \lesssim 4\Delta$, where $\varepsilon = \langle E^2\rangle/\langle E\rangle$. $\langle E\rangle$ is the mean neutrino energy and $\langle E^2\rangle$ is the square value of the root-mean-square (rms) energy and the neutron-proton rest-mass difference $\Delta = 1.2935$ MeV

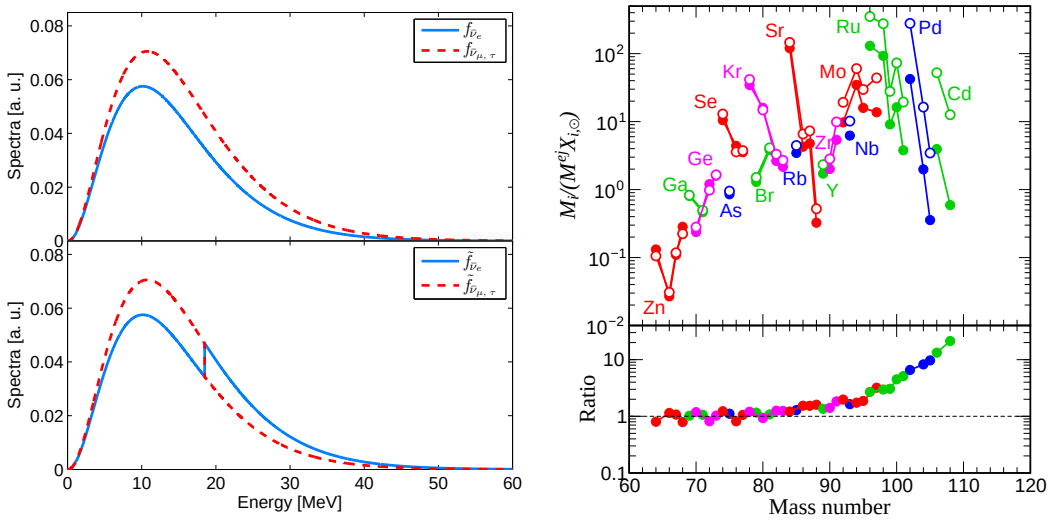

(a) (b)

Figure 7: (color online) Anti-neutrino spectra with (bottom) and without (top) spectral split in graph 7(a) and overproduction factors based on νp-process nucleosynthesis in graph 7(b) (both figures are taken from ref. [48]).

nuclei are inert to ν_e captures. $\bar{\nu}_e$ can be captured at mainly protons as well as nuclei on timescales of seconds at distances of several 100 km when temperatures are as low as several 10^9 K. With the consequently increased neutron density, waiting-point nuclei can be overcome via (n,p)-reactions, and the mass flow can continue to heavier nuclei. This process is know as νp process [49, 50, 20]. Which heaviest nuclei can be reached depends on the conditions obtained in the neutrino-driven wind. The full circles in the upper panel of Fig. 7(b) illustrate the final abundances of a particular mass element from a simulation of a 15 $M_\odot$ progenitor star [51, 52, 50], labelled "1116 ms". The figure shows the ratio $M_i/(M^{\rm ej}X_{i,\odot})$, where M_i is the produced mass of isotope i with the corresponding solar mass fraction $X_{i,\odot}$ and total mass ejected (taken form ref. [52]). The neutrino spectra required are taken from ref. [50] and approximated by an α-fit (for details, see [48] and references therein).

Collective neutrino flavor oscillations have long been investigated in the context of core-collapse supernovae. Here, we explore possible effects of complete collective flavor flips between $\bar{\nu}_e$ and $\bar{\nu}_{\mu/\tau}$ on the νp process, assuming normal mass hierarchy. Following ref. [53], Fig. 7(a) illustrates the spectral flip taking place at energy of about 18 MeV (bottom) in comparison to the unmodified spectra (top). Note that including nucleon recoil, especially for heavy-lepton neutrinos, will decrease high-energy spectral differences between $\bar{\nu}_e$ and $\bar{\nu}_{\mu/\tau}$ and hence the enhanced high-energy tail of the oscillated $\bar{\nu}_e$ as illustrated in Fig. 7(a) will be reduced.

For the νp process, $\bar{\nu}_e$ spectra are required. In addition to the unmodified neutrino spectra, we include the oscillated spectra into the nucleosynthesis analysis and repeat the calculation. Relevant is the change of the neutron production rate due to the inclusion of the spectral flip. It increases the neutron production due to the enhanced high-energy tail of the flipped $\bar{\nu}_e$ spectra. Furthermore, we parametrized the flip energy [48]. We found that the enhancement

of the neutron production rate is a robust result which is independent from the flip energy. It depends on the characteristics of the neutrino spectra obtained in particular simulations. Result of the nucleosynthesis outcome, including the complete spectral flip, is shown in Fig. 7(b) (open circles). The neutron-production rate is enhanced by a factor of 1.4, according to the spectra taken from ref [52]. It significantly increases the production of heavy elements with $A > 90$. Furthermore, overproduction factors for nuclei with $A = 64$, 68 and 76 are reduced slightly. It has been discussed in more details in ref. [48].

6 Summary

Core-collapse supernova simulations are investigated in spherical symmetry. We focused on the post-bounce accretion phase and the evolution after the onset of explosion, illustrating different conditions comparing the two intrinsically different core-collapse progenitors with an O-Ne-Mg-core and an iron-core. The explosion of the first one is a combination of neutrino heating and energy deposition from nuclear burning, on a short timescale of only few 10 ms post bounce. Furthermore, matter remains slightly neutron-rich for this progenitor only during the early explosion phase. On the other hand, the massive Si-layer surrounding the iron-core for more massive progenitors leads to an extended post-bounce accretion phase. It can last several 100 ms (depending on the progenitor model) during which the central proto-neutron star, which formed at core bounce, contracts continuously. The resulting similar electron flavor neutrino luminosities lead to generally proton-rich conditions at the onset of explosion.

After an explosion has been launched, continued neutrino heating at the proto-neutron star surface leads to a low-mass outflow on a timescale on the order of seconds. It became known as neutrino-driven wind, for which we discussed and illustrated typical conditions. Furthermore, the neutrino luminosities and spectra of all flavors become increasingly similar during the long-term proto-neutron star deleptonization. It is a consequence of the decreasing importance of charged-current reactions, because at the neutrinospheres (a) electrons become Pauli-blocked, (b) the number of neutrinos reduces continuously and (c) nucleons become degenerate. Instead, the spectra are dominated by scattering at neutrons. The reducing difference between ν_e and $\bar{\nu}_e$ leads to generally proton-rich conditions. It has important consequences for the nucleosynthesis of heavy elements and may allow for the νp process.

Recently, it has been shown that neutrino oscillations are dominated by matter terms and hence collective flavor oscillations are suppressed during the accretion phase [6, 7, 8, 9]. However, they may be possible during the later evolution after the onset of an explosion, during which the matter density decreases continuously. In addition to the standard nucleosynthesis in proton-rich conditions, we explore the possibility of the νp process assuming a complete spectral flip between $\bar{\nu}_e$ and $\bar{\nu}_{\mu/\tau}$ at a certain split energy. We used neutrino spectra from recent supernova simulations. It results in enhanced $\bar{\nu}_e$ captures, due??to the enhanced high-energy tail of $\bar{\nu}_e$, which in turn increases the number of neutrons present during νp-process nucleosynthesis. It allows the matter flow to proceed to heavier nuclei and results in larger abundances of nuclei with $A > 64$. The current analysis has to be improved, using full energy- and angle-dependent neutrino oscillation techniques, in order to compute the spectral evolution consistently in massive star explosions.

Acknowledgement

The work was supported by the Swiss National Science Foundation under project numbers PBBSP2-133378, PP00P2-124879/1 and 200020-122287 as well as HIC for FAIR and the Helmholtz Alliance EMMI and the SFB 634 at the Technical University Darmstadt. Parts of the work has been initiated during the GSI Summer School Program. B.Z. thanks the program for financial support. The authors are additionally supported by CompStar, a research networking program of the European Science Foundation.

References

[1] LeBlanc, J. M. and Wilson, J. R., *Astrophys. J.*, 161, 541, 1970

[2] Burrows, A.; Livne, E.; Dessart, L.; Ott, C. and Murphy, J., *Astrophys. J.*, 640, 878, 2006

[3] Bethe, H. A. and Wilson, R. J., *Astrophys. J.*, 295, 14, 1985

[4] Sagert, I.; Fischer, T.; Hempel, M.; Pagliara, G. Schaffner-Bielich, J.; et al. *Phys. Rev. Lett.*, 102, 081101, 2009.

[5] Fischer, T.; Sagert, I.; Pagliara, G.; Hempel, M.; Schaffner-Bielich, J.; Rauscher, T.; Thielemann, F.-K.; Käppeli, R.; Martínez-Pinedo, G. and Liebendörfer, M, *Astrophys. J. Suppl.*, 194, 39, 2011

[6] Chakraborty, S.; Fischer, T.; Mirizzi, A.; Saviano, N. and Tomas, R., *Phys. Rev. Lett.*, 107, 151101, 2011

[7] Chakraborty, A.; Fischer, T.; Mirizzi, A.; Saviano, N. and Tomàs, R., *Pys. Rev. D*, 84, 025002, 2011

[8] Dasgupta, B.; O'Connor, E. P. and Ott, C. D., *ArXiv e-prints*, astro-ph.SR/1106.1167, 2011

[9] Sarikas, S.; Raffelt, G. G.; Hüdepohl, L. and Janka, H.-Th., *ArXiv e-prints*, astro-ph.SR/1109.3601, 2011

[10] Woosley, S. E.; Wilson, J. R.; Mathews, G. J.; Hoffman, R. D. and Meyer, B. S., *Astrophys. J.*, 433, 229, 1994

[11] Duncan, R. C.; Shapiro, S. L. and Wasserman, I., *Astrophys. J.*, 309, 141, 1986

[12] Hoffman, R. D.; Woosley, S. E. and Qian, Y.-Z., *Astrophys. J.*, 482, 951,1997

[13] Thompson, T. A. and Burrows, A., *Nucl. Phys.*, A688, 377, 2001

[14] Thompson, T. A.; Burrows, A. and Meyer, B. S., *Astrophys. J.*, 562, 887, 2001

[15] Woosley, S. E. and Baron, E., *Astrophys. J.*, 391, 228, 1992

[16] Takahashi, K.; Witti, J. and Janka, H.-Th., *Astron. Astrophys.*, 286, 857, 1994

[17] Witti, J.; Janka, H.-Th. and Takahashi, K., *Astron. Astrophys.*, 286, 841, 1994

[18] Otsuki, K.; Tagoshi, H.; Kajino, T. and Wanajo, S., *Astrophys. J.*, 533, 424, 1999

[19] Wanajo, S., *Astrophys. J. Lett.*, 650, 79, 2006

[20] Wanajo, S., *Astrophys. J.*, 647, 1323, 2006.

[21] Fischer, T.; Whitehouse, S. C.; Mezzacappa, A.; Thielemann, F.-K. and Liebendörfer, M., *Astron. Astrophys.*, 517, A80, 2010

[22] Hüdepohl, L.; Müller, B.; Janka, H.-Th.; Marek, A. and Raffelt, G.-G., *Phys. Rev. Lett.*, 104, 251101, 2010

[23] Mezzacappa, A. and Bruenn, S. W., *Astrophys. J.*, 405, 669, 1993

[24] Mezzacappa, A. and Bruenn, S. W., *Astrophys. J.*, 405, 637, 1993

[25] Mezzacappa, A. and Bruenn, S. W., *Astrophys. J.*, 410, 740, 1993

[26] Liebendörfer, M.; Mezzacappa, A. and Thielemann, F.-K., *Phys. Rev.*, D63, 104003, 2001

[27] Liebendörfer, M.; Mezzacappa, A.; Thielemann, F.-K.; Messer, O. E. B.; Hix, R. W.; et al. *Phys. Rev.*, D63, 103004, 2001

[28] Liebendörfer, M.; Rosswog, S. and Thielemann, F.-K., *Astrophys. J. Suppl.*, 141,229, 2002

[29] Liebendörfer, M.; Messer, O. E. B.; Mezzacappa, A.; Bruenn, S. W.; Cardall, C. Y. et al. *Astrophys. J. Suppl.*, 150, 263, 2004

[30] Fischer, T.; Whitehouse, S. C.; Mezzacappa, A.; Thielemann, F.-K. and Liebendörfer, M., *Astronom. Astrophys.*, 499,1, 2009

[31] Buras, R.; Janka, H.-Th.; Keil, M., T.; Raffelt, G. G. and Rampp, M., *Astrophys. J.*, 587, 320, 2003

[32] Bruenn, S. W., *Astrophys. J. Suppl.*, 58, 771, 1985

[33] Hannestad, A. and Raffelt, G. G., *Astrophys. J.*, 507, 339, 1998

[34] Shen, H.; Toki, H.; Oyamatsu, K. and Sumiyoshi, K., *Nucl. Phys.*, A637, 435, 1998

[35] Timmes, F. X. and Arnett, D., *Astrophys. J. Suppl.*, 125, 277, 1999

[36] Nomoto, K., *Astrophys. J.*, 277, 791, 1984

[37] Nomoto, K., *Astrophys. J.*, 322, 206, 1987

[38] Woosley, S. E.; Heger, A. and Weaver, T. A., *Rev. Mod. Phys.*, 74, 1015, 2002

[39] Kitaura, F. S.; Janka, H.-Th. and Hillebrandt, W., *Astron. Astrophys.*, 450, 345, 2006

[40] Ott, C. D.; Burrows, A.; Dessart, L.; Murphy, J. and Livne, E, *Astrophys. J.*, 685, 1069, 2008

[41] Marek, A. and Janka, H.-Th., *Astrophys. J.*, 694, 664, 2009

[42] Bruenn, S. W.; Mezzacappa, A.; Hix, W. R.; Blondin, J. M.; Marronetti, P.; et al., *ArXiv e-print* astro-ph/1002.4914, 2010

[43] Wanajo, S.; Janka, H.-Th. and Müller, B., *Astrophys. J. Lett.*, 726, 15, 2011

[44] Qian, Y.-Z. and Wasserburg, G. J., *Astrophys. J.*, 559, 925, 2001

[45] Travaglio, C.; Gallino, R.; Arnone, E.; Cowan, J.; Jordan, F. and Sneden, C., *Astrophys. J.*, 601, 864, 2004

[46] Arcones, A. and Janka, H.-Th., *Astron. Astrophys.*, 526,A160, 2011

[47] Qian, Y.-Z. and Woosley, S. E., *Astrophys. J.*, 471, 331, 1996

[48] Martínez-Pinedo, G.; Ziebarth, B.; Fischer, T. and Langanke, K., *Europ. Phys. J.*, A 47, 98, 2011

[49] Fröhlich, C.; Martínez-Pinedo, G.; Liebendorfer, M.; Thielemann, F.-K.; Bravo, E.; et al. *Phys. Rev. Lett.*, 96, 142502, 2006

[50] Pruet, J.; Hoffman, R. D.; Woosley, S. E.; Janka, H.-Th. and Buras, R., *Astrophys. J.*, 644, 1028, 2006

[51] Buras, R.; Rampp, M.; Janka, H.-Th. and Kifonidis, K., *Astron. Astrophys.*, 447, 10491, 2006

[52] Pruet, J.; Woosley, S. E.; Buras, R.; Janka, H.-Th. and Hoffman, R. D., *Astrophys. J.*, 623, 325, 2005

[53] Dasgupta, B.; Dighe, A.; Raffelt, G. G. and Smirnov, A. Y., *Phys. Rev. Lett.*, 103, 051105, 2009

Neutrino-driven winds and nucleosynthesis of heavy elements

Almudena Arcones[1, 2]

[1]Department of Physics, University of Basel, Klingelbergstraße 82, 4056, Switzerland
[2]Feodor Lynen Fellow, Alexander von Humboldt Foundation

DOI: http://dx.doi.org/10.3204/DESY-PROC-2011-03/arcones

Heavy r-process elements ($Z > 56$) cannot be synthesized in the neutrino-driven winds because their entropy is too low and ejected matter is proton-rich. Neutrinos play thus a key role in determining the neutron or proton richness of the wind. We have shown that the lighter heavy elements (e.g., Sr, Y, Zr) are produced in neutron- and proton-rich winds and could explain the abundance observed in some very old halo stars.

1 Introduction

The astrophysical site where half of the heavy elements are produced by the r-process (rapid neutron capture compared to beta decay) remains unknown. The necessary neutron-rich conditions point to violent events like core-collapse supernovae and neutron star mergers (see [1] for a review). Core-collapse supernovae and the subsequent neutrino-driven winds have attracted vast attention as candidates for the production of r-process elements because they occur early and frequently enough to account for the abundances observed in old halo stars and in the solar system [2]. The necessary conditions to produce heavy elements ($A > 130$) are identified [3] (high entropies, low electron fractions, and short expansion timescales), however these are not found in the most recent long-time supernova simulations [4, 5, 6, 7].

Most of the recent progress in understanding the origin of elements commonly associated with the r-process is due to observations of ultra metal-poor (UMP) stars (see [8] for recent review). The elemental abundances observed in the atmosphere of these very old stars come from a few nucleosynthesis events. These stars generally present a robust pattern for heavy r-process elements $56 < Z < 83$, in agreement with the expected contribution of the r-process to the solar system, but show some scatter for lighter heavy elements $Z < 47$ [8]. This suggests that at least two types of events contribute to the r-process abundances (see e.g., [9]). The process leading to elements with $A < 130$ has been called in the literature the weak r-process [10], charged-particle reaction (CPR) process [11, 12, 13], and Lighter Elemental Primary Process (LEPP) [14, 15].

2 Neutrino-driven wind simulations

Recently, we have extended our spherically symmetric study [4] to two dimensional simulations [7]. In these multidimensional explosions we have shown that the neutrino-driven wind

remains spherically symmetric due to the isotropic neutrino emission from a neutron star. However, the position of the wind termination shock is angle dependent due to the anisotropic distribution of early supernova ejecta (Fig. 1).

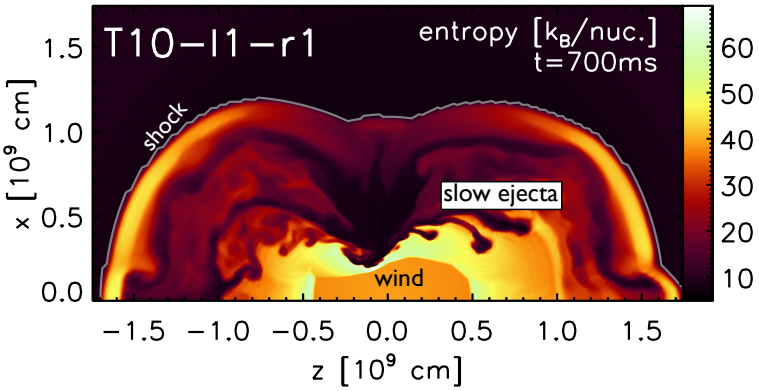

Figure 1: (color online) The neutrino-driven wind is the region of constant entropy in this two-dimensional simulation [7]. Notice the anisotropic distribution of the slow, early supernova ejecta.

In most recent hydrodynamic simulations with detailed neutrino transport, the neutrino-driven wind has relative low entropy and is proton-rich [5, 6]. The electron fraction is extremely sensitive to details of the neutrino interactions and transport around the neutrinosphere where neutrinos decouple from matter. The evolution of this region depends on the nuclear equation of state and on neutrino interactions, which are both key inputs for supernova simulations, but still very uncertain. Therefore, the electron fraction is only known approximately (see Fig. 2) and its variation can lead to different nucleosynthesis.

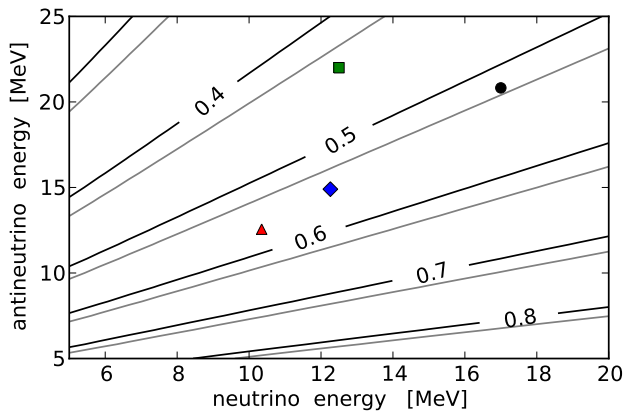

Figure 2: (color online) Contours represent the electron fraction based on the approximation of Ref. [17]. The points indicate approximately the electron neutrino and antineutrino energies for different supernova models: the green square from Ref. [18], the black circle from model M15-l1-r6 of Ref. [4], the red triangle is from a 10 $M_\odot$ progenitor of Ref. [5], and the blue diamond from Ref. [6], all at 10 s after bounce. For more details see Ref. [16].

3 Lighter heavy elements in neutrino-driven winds

The lighter heavy elements (Sr, Y, Zr) can be synthesized in neutrino-driven winds [16] as suggested in Ref. [13]. We have performed the first comparison between the LEPP abundances observed in some UMP stars and nucleosynthesis calculations based on long-time hydrodynamic simulations of core-collapse supernovae. Our results show that neutrino-driven winds can explain the observed LEPP pattern in proton- and neutron-rich conditions.

The exact calculation of the electron fraction remains a very challenging open problem [6]. As shown in Fig. 2, the antineutrino energy has decreased as the neutrino reactions and transport have been improved leading to proton-rich winds in the most recent simulations as shown by the electron fraction contours. This motivated our exploration of the impact of the electron fraction on the production of the LEPP elements. Figure 3 illustrates that the LEPP elements can be obtained for different proton- and neutron-rich conditions. Left panel in Fig. 3 shows that the LEPP pattern is reproduced in proton-rich winds. Moreover, we found that this abundance pattern is quite robust under variations of the evolution of the electron fractions. However, elements heavier than iron-group nuclei can be produced only when the neutrino fluxes are high enough to allow a successful νp-process (see, e.g., [19]). Moreover, almost only neutron-deficient isotopes are produced suggesting that proton-rich winds contribute to synthesize light p-nuclei. When the electron fraction is assumed to evolve towards neutron-rich conditions, the LEPP pattern can also be reproduced but it is very sensitive to variations of the electron fraction (right panel, Fig. 3). Moreover, in this case, there is an overproduction around $A \sim 90$. This together with the fact that most recent supernova simulations [5, 6] favor proton-rich winds could suggests that neutron-rich winds are rare events.

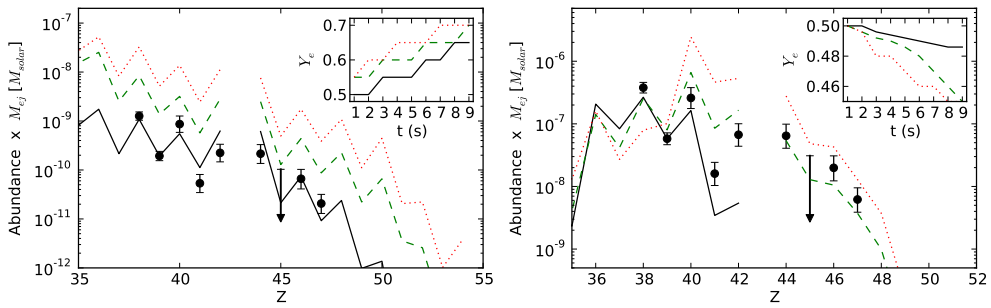

Figure 3: (color online) Elemental abundances are shown for different electron fraction evolutions and compared to observations from UMP stars (dots). See Ref. [16].

4 Conclusions

Recent long-time supernova simulations do not produce r-process elements because the wind entropy is too low and the electron fraction high, even staying proton rich during several seconds [6]. However, lighter heavy elements (e.g., Sr, Y, Zr) can be produced in proton- and neutron-rich neutrino-driven winds reproducing the abundance of UMP stars. Observation of isotopic abundances in UMP stars are very promising to constraint the neutron richness of the

neutrino-driven wind and thus the evolution of the electron fraction and the neutrino properties in supernovae.

References

[1] M. Arnould, S. Goriely, and K. Takahashi. The r-process of stellar nucleosynthesis: Astrophysics and nuclear physics achievements and mysteries. *Phys. Repts.*, 450:97–213, 2007.

[2] D. Argast, M. Samland, F.-K. Thielemann, and Y.-Z. Qian. Neutron star mergers versus core-collapse supernovae as dominant r-process sites in the early Galaxy. *Astron. & Astrophys.*, 416:997–1011, March 2004.

[3] B. S. Meyer, G. J. Mathews, W. M. Howard, S. E. Woosley, and R. D. Hoffman. R-process nucleosynthesis in the high-entropy supernova bubble. *Astrophys. J.*, 399:656–664, November 1992.

[4] A. Arcones, H.-T. Janka, and L. Scheck. Nucleosynthesis-relevant conditions in neutrino-driven supernova outflows. I. Spherically symmetric hydrodynamic simulations. *Astron. & Astrophys.*, 467:1227–1248, June 2007.

[5] T. Fischer, S. C. Whitehouse, A. Mezzacappa, F.-K. Thielemann, and M. Liebendörfer. Protoneutron star evolution and the neutrino-driven wind in general relativistic neutrino radiation hydrodynamics simulations. *Astron. & Astrophys.*, 517:A80, July 2010.

[6] L. Hüdepohl, B. Müller, H.-T. Janka, A. Marek, and G. G. Raffelt. Neutrino Signal of Electron-Capture Supernovae from Core Collapse to Cooling. *Phys. Rev. Lett.*, 104(25):251101, 2010.

[7] A. Arcones and H.-T. Janka. Nucleosynthesis-relevant conditions in neutrino-driven supernova outflows. II. The reverse shock in two-dimensional simulations. *Astron. & Astrophys.*, 526:A160, February 2011.

[8] C. Sneden, J. J. Cowan, and R. Gallino. Neutron-Capture Elements in the Early Galaxy. *Ann. Rev. Astron. & Astrophys.*, 46:241–288, September 2008.

[9] Y.-Z. Qian and G. J. Wasserburg. A Model for Abundances in Metal-poor Stars. *Astrophys. J.*, 559:925–941, 2001.

[10] G. J. Wasserburg, M. Busso, and R. Gallino. Abundances of actinides and short-lived nonactinides in the interstellar medium: Diverse supernova sources for the r-processes. *Astrophys. J.*, 466:L109, August 1996.

[11] S. E. Woosley and R. D. Hoffman. The alpha-process and the r-process. *Astrophys. J.*, 395:202–239, 1992.

[12] C. Freiburghaus, J.-F. Rembges, T. Rauscher, E. Kolbe, F.-K. Thielemann, K.-L. Kratz, B. Pfeiffer, and J. J. Cowan. The Astrophysical r-Process: A Comparison of Calculations following Adiabatic Expansion with Classical Calculations Based on Neutron Densities and Temperatures. *Astrophys. J.*, 516:381–398, May 1999.

[13] Y.-Z. Qian and G. J. Wasserburg. Where, oh where has the r-process gone? *Phys. Repts.*, 442:237–268, April 2007.

[14] C. Travaglio, R. Gallino, E. Arnone, J. Cowan, F. Jordan, and C. Sneden. Galactic Evolution of Sr, Y, And Zr: A Multiplicity of Nucleosynthetic Processes. *Astrophys. J.*, 601:864–884, 2004.

[15] F. Montes, T. C. Beers, J. Cowan, T. Elliot, K. Farouqi, R. Gallino, M. Heil, K.-L. Kratz, B. Pfeiffer, M. Pignatari, and H. Schatz. Nucleosynthesis in the Early Galaxy. *Astrophys. J.*, 671:1685–1695, December 2007.

[16] A. Arcones and F. Montes. Production of Light-element Primary Process Nuclei in Neutrino-driven Winds. *Astrophys. J.*, 731:5, April 2011.

[17] Y.-Z. Qian and S. E. Woosley. Nucleosynthesis in Neutrino-driven Winds. I. The Physical Conditions. *Astrophys. J.*, 471:331–351, 1996.

[18] S. E. Woosley, J. R. Wilson, G. J. Mathews, R. D. Hoffman, and B. S. Meyer. The r-process and neutrino-heated supernova ejecta. *Astrophys. J.*, 433:229–246, September 1994.

[19] C. Fröhlich, G. Martínez-Pinedo, M. Liebendörfer, F.-K. Thielemann, E. Bravo, W. R. Hix, K. Langanke, and N. T. Zinner. Neutrino-Induced Nucleosynthesis of A>64 Nuclei: The νp Process. *Phys. Rev. Lett.*, 96(14):142502, April 2006.

Equation of State for Supernova

Gang Shen[1]

[1]Theoretical Division, Los Alamos National Laboratory, Los Alamos, NM, 87545, USA

DOI: http://dx.doi.org/10.3204/DESY-PROC-2011-03/shen

In this contribution we discuss several new complete EoS for supernova, whose detailed composition is important for the neutrino dynamics. We focus on one important distinction for various EoS - the density dependence of symmetry energy E'_{sym}, and its interesting correlation with the radii of neutron star, as well as properties of neutron distribution in neutron rich nuclei.

1 Introduction

The equation of state (EoS) for hot, dense matter relates energy and pressure to temperature, density, and composition. The properties of hot dense matter, for example its pressure at high baryon density - larger than normal nuclear density 3×10^{14} g/cm^3, have been the focus of many extradinary terrestrial experiments, including heavy ion collisions with Au [1]. The pressure of nuclear matter at high density determines how large a neutron star our nature could realize.

The properties of nuclear matter depends on its composition, particularly the proton-neutron number asymmetry, or iso-spin dependence, conveniently characterized by the parameter called (a)symmetry energy E_{sym}. Most stable nuclei have a small such asymmetry and tell us little about how the EoS changes with the asymmetry. The neutron/proton rich isotopes will be studied with new tools like the Facility for Rare Isotope Beams (FRIB) [2], a heavy ion accerelator to be built in Michigan State University. Studies by these new tools will help us understand when the nuclei would become unstable upon too many neutrons (or protons) added, and ultimately tell us the composition of nuclear matter in supernova given temperature, density, and proton-neutron asymmetry.

Density dependence of symmetry energy E'_{sym} is one key unknown in nuclear physics and nuclear astrophysics, where neutron rich matter is particularly relevant. There are many interesting correlations with E'_{sym} that have been studied in recent years. The pressure of nuclear matter is proportional to E'_{sym}. With a higher pressure if E'_{sym} is large , neutron rich nucleus, such as ^{208}Pb, is found to have a larger neutron radius [3]. This has motivated the Lead Radius Experiment (PREX) [4] to accurately measure the neutron radius in ^{208}Pb with parity violating electron scattering [5]. On the other hand, the radius of a canonical 1.4 solar mass neutron star is determined by the nuclear matter at similar density inside ^{208}Pb, therefore a larger pressure at such density tends to give a bigger radius for 1.4 solar mass neutron star [6]. Current large uncertainties in the EoS lead us to generate several big tables of EoS based on dinstinct properties of nuclear matter at high densities, which could be used in astrophysical simulations such as proto-neutron star evolution to identify astrophysical observables with related nuclear matter properties.

Table 1: Range of temperature T, density n_B, and proton fraction Y_p in the finely spaced interpolated EoS table.

Parameter	minimum	maximum	number of points
T [MeV]	0, $10^{-0.8}$	$10^{1.875}$	109
$\log_{10}(n_B)$ [fm^{-3}]	-8.0	0.175	328
Y_P	0, 0.05	0.56	1(Y_P=0)+52

2 Complete EoS for Supernova

We used a relativistic mean field (RMF) model to self-consistently calculate non-uniform matter at intermediate density and uniform matter at high density, and used a virial expansion for nonideal gas of nucleons and thousands of different nuclei to obtain the EoS at low densities. Altogether these two EoS models cover the large range of temperatures, densities, and proton fractions. Discussion of matching the two results can be found in Ref. [7]. There are 73,840 data points from the virial calculation at low densities, 17,021 data points from the nonuniform Hartree calculation, and 90,478 data points from uniform matter calculations. The overall calculations took 7,000 CPU days in Indiana University's supercomputer clusters.

We use a hybrid interpolation scheme to generate a full EoS table on a fine grid that is thermodynamically consistent. The range of parameter spaces is shown in Table 1. This insures that the first law of thermodynamics is satisfied and that entropy is conserved during adiabatic compression. Our EoS is an improvement over the existing Lattimer-Swesty [8] and H. Shen *et al.* [9, 10] equations of state, because our EoS includes thousands of heavy nuclei and is exact in the low density limit.

We also generated a second EoS based on the RMF effective interaction FSUGold [11, 12], whereas our earlier EoS was based on the RMF effective interaction NL3. The FSUGold interaction has a lower pressure at high densities compared to the NL3 interaction. The original FSUGold interaction produces an EoS, that we call FSU1.7, that has a maximum neutron star mass of 1.7 solar masses. A modification in the high density EoS is introduced to increase the maximum neutron star mass to 2.1 solar masses and results in a slightly different EoS that we call FSU2.1. Finally, the EoS tables for NL3, FSU1.7 and FSU2.1 are available for download.

3 Symmetry Energy in Various EoS

The bulk properties of infinite nuclear matter have been collected in Table 2, for NL3, FSUGold, as well as a new effective RMF interaction IUFSU [13]. One important distinction among various EoS is the slope of the symmetry energy at saturation density, $L/3 = \rho_0 E'_{sym}(\rho_0)$. The pressure around saturation density is proportional to L, which plays a crucial role both in the terrestial context where it affects the neutron density distribution in neutron rich nuclei and in astrophysics where it affects the structure and thermal evolution of neutron stars.

Brown first realized the correlation between L and the neutron skin thickness of ^{208}Pb [3], which has 126 neutrons and 82 protons. A larger pressure - due to larger L inside the nucleus will push neutrons to the surface, therefore leads to a bigger neutron skin thickness. This is clearly demonstrated in left panel of Fig. 1, where the proton and neutron densities inside ^{208}Pb are shown from several model predictions. The proton density is well constrained to 1%. In contrast the neutron density has sizable variations among different model predictions. The

Model	ρ_0 (fm^{-3})	ε_0 (MeV)	K_0 (MeV)	E_{sym} (MeV)	L (MeV)
NL3	0.148	−16.24	271.5	37.29	118.2
FSU	0.148	−16.30	230.0	32.59	60.5
IU-FSU	0.155	−16.40	231.2	31.30	47.2

Table 2: Bulk parameters characterizing the behavior of infinite nuclear matter at saturation density ρ_0. The quantities ε_0 and K_0 represent the binding energy per nucleon and incompressibility coefficient of symmetric nuclear matter, whereas E_{sym} and L represent the energy and slope of the symmetry energy at saturation density.

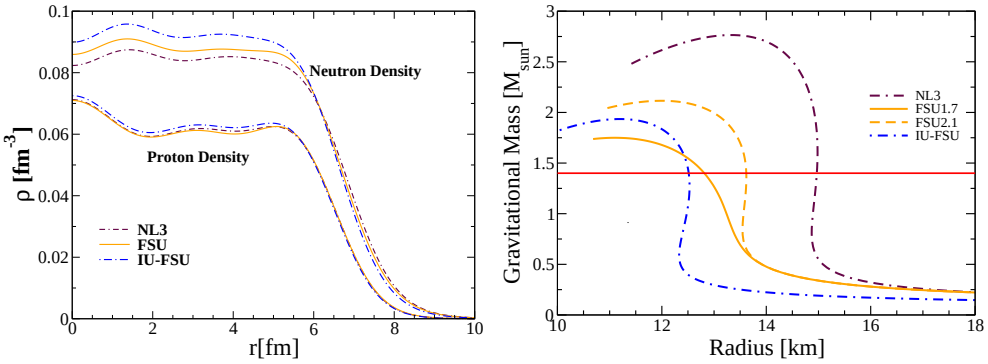

Figure 1: (color online) Left: model predictions for the proton and neutron densities of ^{208}Pb. Right: Neutron Star *Mass-vs-Radius* relation predicted by the relativistic mean-field models discussed in the text.

values of L are 118.2, 60.5, and 47.2 MeV for NL3, FSU, and IUFSU, respectively. The resulting neutron skin thickness is 0.28, 0.21, and 0.16 fm for NL3, FSU, and IUFSU, respectively. The pressure of neutron matter around saturation density also influences the radius of cold neutron star [6]. In the right panel of Fig. 1, we show the neutron star mass-radius relation for various RMF models. For 1.4 solar mass neutron star, the corresponding radii are 15, 12.8, and 12.5 km for NL3, FSU, and IUFSU, respectively. FUS2.1 has a larger pressure than FSU1.7 at density above 0.2 fm^{-3}, and gives rise to larger radius for 1.4 solar mass neutron star, 13.6 km. Due to their common relation to the derivative of symmetry energy L, there exists a correlation between the neutron skin thickness and neutron star radius [6].

It's our goal to calculate EoS tables with different pressures. This will allow one to correlate features of astrophysical simulations with EoS properties. In this work we discussed two new EoS based on different RMF effective interactions NL3 and FSUGold. In future we will present a third EoS based on IU-FSU like effective interaction which has a softer symmetry energy L.

4 Conclusions

Equation of state of nuclear matter at finite temperature and its dynamics is the key to understand the evolution of supernova. The pressure at high densities determines how big and large a neutron star nature could make. The composition of matter in supernova and its dynamical

response with neutrinos is important for the evolution of supernova. The emergent neutrino spectra from neutrino-sphere is crucial for the neutron fraction in the neutrino-driven wind and possible r-process that could make heavy nuclei beyond iron. The EoS of nuclear matter has been the focus of heavy ion collision experiments and a future heavy ion accelerator FRIB.

We construct several new EoS of nuclear matter for a wide range of temperatures, densities, and proton fractions. We employ fully microscopic relativistic mean field calculation for matter at intermediate density and high density, and the virial expansion of a nonideal gas (with nucleons and 8981 kinds of nuclei) for matter at low density. The EoS was obtained at over 180,000 grid points in 3-dimensional parameter spaces (temperature, density, and proton fraction). We used hybrid interpolation scheme to generate the final table, as shown in Table 1. The thermodynamic consistency in our table is checked via usual adiabatic compression test, where the oscillation in entropy is limited to 1% using the finer table Ref. [7, 12].

Due to the rather large uncertainties in the EoS at high density, particularly the density dependence of symmetry energy, we generated two EoS tables based on a stiff EoS at high density, NL3, and a softer EoS at low density, FSU1.7, and the modified FSU2.1 which could support a 2.1 solar mass neutron star. In future we will generate a third EoS based on IU-FSU like interaction, which is soft around saturation density but stiff at higher densities. Altogether these EoS tables could cover the uncertainties in the properties of nuclear matter at high density, and astrophysical simulations with them could identify observational phenomena with dinstinct nuclear matter property.

5 Acknowledgments

The author acknowledges supports by a grant from the DOE under the contract DE-AC52-06NA25396 and the DOE topical collaboration to study “Neutrinos and nucleosynthesis in hot and dense matter” during write-up of this work.

References

[1] P. Danielewicz, R. Lacey, and W. G. Lynch, Science **22**, 1592 (2002).

[2] Facility for Rare Isotope Beams project, http://www.frib.msu.edu.

[3] B. A. Brown, Phys. Rev. Lett. **85**, 5296 (2000) .

[4] Jefferson Laboratory Experiment E-06-002, Spokespersons K. Kumar, R. Michaels, P. A. Souder, and G. M. Urciuoli.

[5] C. J. Horowitz, S. J. Pollock, P. A. Souder, and R. Michaels, Phys. Rev. **C 63**, 025501 (2001).

[6] C. J. Horowitz and J. Piekarewicz, Phys. Rev. Lett. **86**, 5647 (2001).

[7] G. Shen, C. J. Horowitz, and S. Teige, Phys. Rev. C **83**, 035802 (2011).

[8] J. M. Lattimer and F. D. Swesty, Nucl. Phys. **A 535**, 331 (1991).

[9] H. Shen, H. Toki, K. Oyamatsu, and K. Sumiyoshi, Nucl. Phys. **A 637**, 435 (1998).

[10] H. Shen, H. Toki, K. Oyamatsu, and K. Sumiyoshi, Prog. Theo. Phys. **100**, 1013 (1998).

[11] B. G. Todd-Rutel and J. Piekarewicz, Phys. Rev. Lett. **95**, 122501 (2005).

[12] G. Shen, C. J. Horowitz, and E. O’Connor, Phys. Rev. C **83**, 065808 (2011).

[13] F. J. Fattoyev, C. J. Horowitz, J. Piekarewicz, and G. Shen, Phys. Rev. C **82**, 055803 (2010).

Chapter 2

Particle Physics Aspects

Convenors:

Amol Dighe
Eligio Lisi

Supernova as Particle-Physics Laboratory

Georg Raffelt

Max-Planck-Institut für Physik (Werner-Heisenberg-Institut)
Föhringer Ring 6, 80805 München, Germany

DOI: http://dx.doi.org/10.3204/DESY-PROC-2011-03/raffelt

The neutrino signal of supernova (SN) 1987A has provided numerous particle-physics constraints, primarily by the signal duration that precludes excessive energy losses in new channels. Improving these results with the neutrino signal from the next galactic SN requires a better understanding of the expected standard signal duration and in particular of neutrino opacities. Independently of neutrino observations, one should perform SN simulations including nonstandard flavor changing and lepton-number violating processes to understand their impact on SN dynamics.

1 Introduction

A high-statistics neutrino observation of the next nearby supernova (SN) is one of the major physics motivations for low-energy neutrino astronomy [1, 2, 3]. Above all it would provide detailed information on the core collapse phenomenon and test the delayed explosion scenario [4, 5]. Moreover, the IceCube detector may be able to resolve fast time variations caused by SASI activity and convective overturns [6, 7]. The simultaneous observation with the upcoming round of gravitational wave detectors would provided crucial additional information [8].

On the other hand, SN neutrinos hold crucial particle-physics information [9, 10, 11, 12]. Neutrino flavor oscillations form one central topic, but will be covered mostly by other speakers at this conference. I will here primarily review the traditional SN 1987A constraints and how these would be affected by new theoretical developments and a high-statistics observation of the next nearby SN. Independently of such an observation, I will argue that SN simulations with nonstandard flavor changing and lepton-number violating processes should be performed.

2 Time-of-flight constraints

It was Georgiy Zatsepin who first pointed out that the neutrino burst from SN collapse offers an opportunity to measure the neutrino mass by the energy-dependent time-of-flight delay [13]

$$\Delta t = 5.1\ \mathrm{ms} \left(\frac{D}{10\ \mathrm{kpc}}\right) \left(\frac{10\ \mathrm{MeV}}{E_\nu}\right)^2 \left(\frac{m_\nu}{1\ \mathrm{eV}}\right)^2 .$$

However, when the SN 1987A burst was measured, it provided a mass limit of about 20 eV [14, 15, 16], which even at that time was only marginally interesting and was soon superseded by laboratory limits. The neutrino signal of the next nearby SN could improve this at best

to the eV range [17]. It is more interesting to note that the restrictive sub-eV cosmological neutrino mass limits [18] assure that fast time variations at the source will not be washed out by time-of-flight effects and thus are, in principle, detectable at IceCube [6, 7]. In this sense the forthcoming KATRIN direct neutrino mass measurement (or mass limit) [19] will be of interest to the interpretation of a SN neutrino signal.

A putative neutrino electric charge would lead to deflection in the galactic magnetic field and thus to an energy-dependent pulse dispersion in analogy to m_ν, providing the bound $e_\nu \lesssim 3\times10^{-17}\,e$ [20, 21].

From a present-day perspective, the most interesting time-of-flight constraint, however, is the one between neutrinos and photons, testing the equality of the relativistic limiting propagation speed between the two species. SN physics dictates that the neutrino burst should arrive a few hours earlier than the optical brightening, in agreement with SN 1987A. Given the distance of about 160.000 light years one finds [22, 23]

$$\left|\frac{c_\nu - c_\gamma}{c_\gamma}\right| \lesssim 2\times10^{-9}\,.$$

At the time of this writing, this result plays a crucial role for possible interpretations of the apparent superluminal neutrino speed reported by the OPERA experiment [24], $(c_\nu - c_\gamma)/c_\gamma = (2.48 \pm 0.28_{\rm stat} \pm 0.30_{\rm sys})\times10^{-5}$.

Both neutrinos and photons should be delayed by their propagation through the gravitational potential of the galaxy (Shapiro time delay) which is estimated to be a few months toward the Large Magellanic Cloud. The agreement between the arrival times within a few hours confirms a common time delay within about $0.7\text{–}4\times10^{-3}$, i.e. neutrinos and photons respond to gravity in the same way [25, 26]. This is the only experimental proof that neutrinos respond to gravity in the usual way.

It is intriguing that these results could be extended to include the propagation speed of gravitational waves if the next nearby SN is observed both in neutrinos and with gravitational wave detectors. The onset of both bursts would coincide with the SN bounce time to within a few ms and the coincidence could be measured with this precision [27, 28]. In view of the current discussion of superluminal neutrino propagation, such a measurement would provide important additional constraints on possible interpretations.

3 Novel SN energy loss and neutrino signal duration

After core collapse, neutrinos are trapped in the SN core and energy is emitted on a neutrino diffusion time scale of a few seconds [29]. This basic picture was confirmed by the SN 1987A neutrino burst, indicating that the gravitational binding energy was not carried away in the form of some other radiation, more weakly coupled than neutrinos, that would escape directly without diffusion [30, 31, 32]. This "energy-loss argument" has been applied to a large number of cases, notably axions, Majorons, and right-handed neutrinos, often providing the most restrictive limits on the underlying particle-physics model; extensive reviews are Refs. [9, 10, 11, 12]. More recently, the argument was applied to Kaluza-Klein gravitons [33, 34, 35, 36], light neutralinos [37], light dark matter particles [38], and unparticles [39, 40, 41].

While there is no good reason to doubt the validity of this widely used argument, it is based on very sparse data. Measuring a high-statistics neutrino signal from the next nearby SN would put these crucial results on much firmer experimental ground.

Another question is what to use as a theoretical benchmark for comparison with the data. The pioneering work of the Livermore group combined relativistic hydrodynamics with multi-group three-flavor neutrino diffusion in spherical symmetry (1D), simulating the entire evolution self-consistently [4]. These models, however, included significant numerical approximations and omitted neutrino reactions that were later recognized to be important [42]. A crucial ingredient to enhance the early neutrino fluxes was a neutron-finger mixing instability, which today is disfavored [43]. Relativistic calculations of proto neutron star (PNS) cooling were performed with a flux-limited equilibrium [44, 45] or multi-group diffusion treatment [46]. Pons et al. [47] studied PNS cooling for different equations of state and masses, using flux-limited equilibrium transport with diffusion coefficients adapted to the underlying equation of state.

New opportunities to study the neutrino signal consistently from collapse to late-time cooling arise from the class of "electron-capture SNe" or "O-Ne-Mg core SNe." These low-mass stars (8–10 $M_\odot$) collapse because of rapid electron capture on Ne and Mg and could represent up to 30% of all SNe. They are the only cases where 1D simulations obtain neutrino-powered explosions [48]. It has become possible to carry hydrodynamic simulations with modern neutrino Boltzmann solvers in 1D all the way to PNS cooling. Very recently, the Basel group has circulated first results of the PNS evolution [49] for a representative 8.8 $M_\odot$ progenitor and subsequently the Garching group has simulated explosions with the same progenitor [50]. The multi-flavor neutrino signal is shown in Fig. 1.

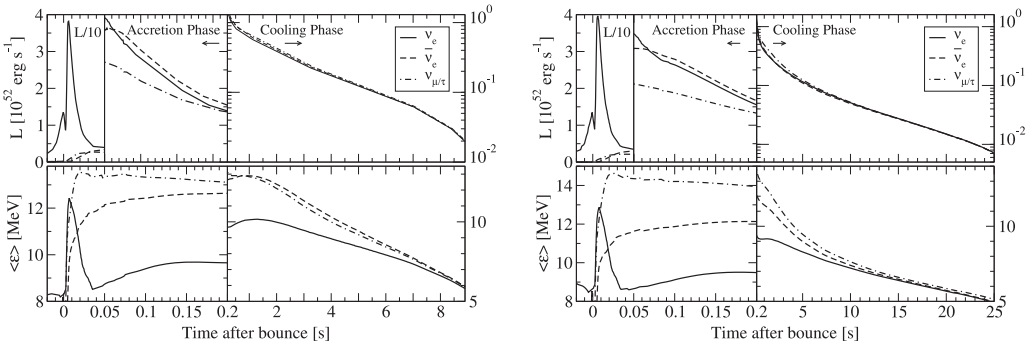

Figure 1: Neutrino emission from a spherically symmetric electron-capture SN according to a Garching simulation [50]. *Left:* Full set of neutrino opacities. *Right:* Reduced set, primarily excluding nucleon-nucleon correlations and nucleon recoils.

The Garching group has performed this simulation with two different sets of neutrino opacities. The full set includes, in particular, nucleon recoil and nucleon-nucleon correlations that can strongly reduce the interaction rate and thus increase the neutrino mean free path. Their reduced set, essentially without these effects, is close to what is used by other groups. The late-time signal duration is quite different between the two cases (left and right panel of Fig. 1). For the "full case" (left panel), the cooling time is so short that it is just barely compatible with the SN 1987A signal duration. In other words, how much energy loss by new particles is allowed by SN 1987A or a future high-statistics signal depends on the treatment of neutrino transport. With long-term cooling calculations, based on a Boltzmann transport scheme, becoming a routine task, improving the microscopic treatment of neutrino interaction in the dense SN medium should be more systematically studied.

4 Flavor and lepton number violation

Conventional SN simulations are based on standard particle-physics assumptions that are not necessarily tested in the laboratory. In particular, lepton-number conservation is crucial in the collapse process because it ensures that the liberated gravitational energy is at first stored primarily in the degeneracy energy of electrons and electron neutrinos, i.e. the SN core after collapse is relatively cold. On the other hand, it is now commonly assumed that lepton number is not conserved in that neutrino masses are widely assumed to be of Majorana type. While neutrino Majorana masses would not suffice for significant lepton-number violating effects in a SN core, other sources of lepton-number violation may well be strong enough, e.g. R-parity violating supersymmetric models that in turn can induce Majorana masses. Therefore, it would be intriguing to study core collapse with "internal" deleptonization, leading to a hot SN core immediately after collapse.

In a SN core, the matter potentials are so large that flavor conversion by oscillation is strongly suppressed even though some of the mixing angles are large. Therefore, the initial ν_e Fermi sea is conserved—in a SN core, flavor lepton number is effectively conserved. On the other hand, certain non-standard interactions (NSI) [51] that are not diagonal in flavor space would allow for flavor lepton number violation in collisions and therefore lead to a quick equipartition among flavors of the trapped lepton number. The required interaction strength is much smaller than what is typically envisioned for NSI effects on long-baseline neutrino oscillation experiments. In other words, a SN core is potentially the most sensitive laboratory for NSI effects. While it has been speculated that such effects would strongly modify the physics of core collapse [52, 53], a numerical simulation including the quick equipartition of flavors has never been performed.

Therefore, one should perform numerical studies of core collapse, allowing for the violation of lepton number and of flavor or both on a dynamical SN time scale. As a first step, a parametric study would be enough—detailed microscopic models are probably not important to understand the possible impact on SN dynamics. Also, such a programme would not depend on measuring neutrinos from the next nearby SN.

5 Conclusions

We have briefly reviewed the role of core-collapse SNe as particle physics laboratories and have discussed time-of-flight and energy-loss arguments. Moreover, we have suggested that simulations should be performed that include lepton and flavor violation. Of course, the field is much broader. For example, we have not touched upon flavor oscillations or the role of sterile neutrinos because these topics are covered by other speakers at this workshop. Measuring a high-statistics neutrino signal from the next nearby SN would greatly help us to put the existing SN 1987A limits on a firm observational footing, but also requires a better theoretical understanding, for example of neutrino transport and particle emission processes.

Acknowledgements

This work was partly supported by the Deutsche Forschungsgemeinschaft under grants TR-27 and EXC-153.

References

[1] D. Autiero *et al.*, JCAP **0711** (2007) 011 [arXiv:0705.0116].

[2] M. Wurm *et al.* (LENA Working Group), arXiv:1104.5620.

[3] K. Scholberg, J. Phys. Conf. Ser. **203** (2010) 012079.

[4] T. Totani, K. Sato, H. E. Dalhed and J. R. Wilson, Astrophys. J. **496** (1998) 216 [astro-ph/9710203].

[5] H.-T. Janka, K. Langanke, A. Marek, G. Martínez-Pinedo and B. Müller, Phys. Rept. **442** (2007) 38 [astro-ph/0612072].

[6] T. Lund, A. Marek, C. Lunardini, H.-T. Janka and G. Raffelt, Phys. Rev. D **82** (2010) 063007 [arXiv:1006.1889].

[7] R. Abbasi *et al.* (IceCube Collaboration), arXiv:1108.0171.

[8] A. Marek, H.-T. Janka and E. Müller, Astr. Astrophys., **496** (2009) 475 [arXiv:0808.4136].

[9] D. N. Schramm, Comments Nucl. Part. Phys. **17**, 239 (1987).

[10] G. G. Raffelt, Phys. Rept. **198** (1990) 1.

[11] G. G. Raffelt, Ann. Rev. Nucl. Part. Sci. **49** (1999) 163 [hep-ph/9903472].

[12] G. G. Raffelt, astro-ph/0701677.

[13] G. T. Zatsepin, Pisma Zh. Eksp. Teor. Fiz. **8** (1968) 333 [JETP Lett. **8** (1968) 205].

[14] T. J. Loredo and D. Q. Lamb, Annals N. Y. Acad. Sci. **571** (1989) 601.

[15] T. J. Loredo and D. Q. Lamb, Phys. Rev. D **65** (2002) 063002 [astro-ph/0107260].

[16] P. J. Kernan and L. M. Krauss, Nucl. Phys. B **437** (1995) 243 [astro-ph/9410010].

[17] J. F. Beacom and P. Vogel, Phys. Rev. D **58** (1998) 053010 [hep-ph/9802424].

[18] K. N. Abazajian *et al.*, Astropart. Phys. **35** (2011) 177 [arXiv:1103.5083].

[19] G. Drexlin, J. Phys. Conf. Ser. **136** (2008) 022031.

[20] G. Barbiellini and G. Cocconi, Nature **329** (1987) 21.

[21] J. N. Bahcall, *Neutrino Astrophysics* (Cambridge University Press, 1989).

[22] M. J. Longo, Phys. Rev. D **36** (1987) 3276.

[23] L. Stodolsky, Phys. Lett. B **201** (1988) 353.

[24] T. Adam *et al.* (OPERA Collaboration), arXiv:1109.4897.

[25] M. J. Longo, Phys. Rev. Lett. **60** (1988) 173.

[26] L. M. Krauss and S. Tremaine, Phys. Rev. Lett. **60** (1988) 176.

[27] G. Pagliaroli, F. Vissani, E. Coccia and W. Fulgione, Phys. Rev. Lett. **103** (2009) 031102 [arXiv:0903.1191].

[28] F. Halzen and G. G. Raffelt, Phys. Rev. D **80** (2009) 087301 [arXiv:0908.2317].

[29] R. F. Sawyer, D. J. Scalapino and A. Soni, "The neutrino pulse from a newly born neuton star", Proc. Neutrino 1979, Bergen, Norway, 18–22 June 1979, vol. 2, pg. 429.

[30] G. Raffelt and D. Seckel, Phys. Rev. Lett. **60** (1988) 1793.

[31] M. S. Turner, Phys. Rev. Lett. **60** (1988) 1797.

[32] R. Mayle, J. R. Wilson, J. R. Ellis, K. A. Olive, D. N. Schramm and G. Steigman, Phys. Lett. B **203** (1988) 188; Phys. Lett. B **219** (1989) 515.

[33] S. Cullen and M. Perelstein, Phys. Rev. Lett. **83** (1999) 268 [hep-ph/9903422].

[34] C. Hanhart, D. R. Phillips, S. Reddy and M. J. Savage, Nucl. Phys. B **595**, 335 (2001) [nucl-th/0007016].

[35] C. Hanhart, J. A. Pons, D. R. Phillips and S. Reddy, Phys. Lett. B **509**, 1 (2001) [astro-ph/0102063].

[36] S. Hannestad and G. G. Raffelt, Phys. Rev. D **67** (2003) 125008; Erratum *ibid.* **69** (2004) 029901 [hep-ph/0304029].

[37] H. K. Dreiner, C. Hanhart, U. Langenfeld and D. R. Phillips, Phys. Rev. D **68**, 055004 (2003) [hep-ph/0304289].

[38] P. Fayet, D. Hooper and G. Sigl, Phys. Rev. Lett. **96**, 211302 (2006) [hep-ph/0602169].

[39] H. Davoudiasl, Phys. Rev. Lett. **99** (2007) 141301 [arXiv:0705.3636 [hep-ph]].

[40] S. Hannestad, G. Raffelt and Y. Y. Y. Wong, Phys. Rev. D **76** (2007) 121701 [arXiv:0708.1404 [hep-ph]].

[41] S. Dutta and A. Goyal, JCAP **0803** (2008) 027 [arXiv:0712.0145].

[42] M. T. Keil, G. G. Raffelt and H.-T. Janka, Astrophys. J. **590**, 971 (2003) [astro-ph/0208035].

[43] S. W. Bruenn and T. Dineva, Astrophys. J. **458**, L71 (1996).

[44] A. Burrows and J. M. Lattimer, Astrophys. J. **307** (1986) 178.

[45] W. Keil and H.-T. Janka, Astron. Astrophys. **296** (1995) 145.

[46] H. Suzuki, Num. Astrophys. in Japan **2**, 267 (1991); in *Frontiers of Neutrino Astrophysics*, ed. by Y. Suzuki and K. Nakamura (Univ. Acad, Press, Tokyo, 1993), p. 219.

[47] J. A. Pons, S. Reddy, M. Prakash, J. M. Lattimer and J. A. Miralles, Astrophys. J. **513** (1999) 780. [astro-ph/9807040].

[48] F. S. Kitaura, H.-T. Janka and W. Hillebrandt, Astron. Astrophys. **450**, 345 (2006) [astro-ph/0512065].

[49] T. Fischer, S. C. Whitehouse, A. Mezzacappa, F. K. Thielemann and M. Liebendörfer, Astron. Astrophys. **517** (2010) A80 [arXiv:0908.1871].

[50] L. Hüdepohl, B. Müller, H.-T. Janka, A. Marek and G. G. Raffelt, Phys. Rev. Lett. **104** (2010) 251101; Erratum *ibid.* **105** (2010) 249901 [arXiv:0912.0260].

[51] C. Biggio, M. Blennow and E. Fernandez-Martinez, JHEP **0908** (2009) 090 [arXiv:0907.0097].

[52] P. S. Amanik and G. M. Fuller, Phys. Rev. D **75**, 083008 (2007) [astro-ph/0606607].

[53] O. Lychkovskiy, S. Blinnikov and M. Vysotsky, Eur. Phys. J. C **67** (2010) 213 [arXiv:0912.1395].

Supernova neutrino flavor evolution at high densities

A.B. Balantekin[1,2]

[1]University of Wisconsin, Department of Physics, Madison, WI 53706 USA*

[2]Nuclear Science Division, Lawrence Berkeley National Laboratory, Berkeley, CA 94720 USA

DOI: http://dx.doi.org/10.3204/DESY-PROC-2011-03/balantekin

These conference proceedings cover various aspects of neutrino propagation through the high matter and neutrino densities near the proto-neutron star in a core-collapse supernova. A significant feature of this regime is the impact of neutrino-neutrino interactions. Properties of this non-linear many-neutrino system are discussed with a particular emphasis on its symmetries.

1 Introduction

Almost all the gravitational binding energy of the pre-supernova star is converted into neutrinos and antineutrinos in a core-collapse supernova, yielding a very large neutrino flux [1]. Consequently neutrino properties play a very important role, not only in the dynamics of a core-collapse supernova, but also in the r-process nucleosynthesis if supernovae are the appropriate sites [2]. Neutrinos traveling through supernovae undergo matter-enhanced neutrino oscillations (due to the MSW effect resulting from neutrinos interacting with the background electrons and positrons) much like neutrinos traveling through the Sun or the Earth [3]. However, unlike these latter sites, in a supernova environment it is possible to have matter-enhanced antineutrino flavor transformations [4]. It was ascertained that, because of the large number of neutrinos ($\sim 10^{58}$) emitted by the proto-neutron star, background neutrinos also contribute to the coherent forward scattering of neutrinos in a core-collapse supernova [3, 5]. Once the importance of the flavor-mixing non-diagonal terms coming from neutrino-neutrino interactions was highlighted [6], it became clear that one deals with a genuine many-body problem with one- and two-body interactions.

The significance of the neutrino-neutrino interactions in core-collapse supernovae [7] and the possibility of the occurrence of collective effects due to those interactions were recognized early on [8]. In a supernova environment neutrino-neutrino interactions [6] play a crucial role both for neutrinos and antineutrinos [7, 8, 9, 10]. Since such collective neutrino oscillations dominate the neutrino propagation much deeper than the conventional matter-induced MSW effect, it would impact the r-process nucleosynthesis [11, 12, 13]. There is an extensive literature on this subject [14], a good starting point is several recent surveys [15, 16, 17]. An algebraic approach to this problem was worked out in Ref. [18] from a many-body point of view. Such an algebraic

*Permanent address.

approach is helpful in exploring the hidden symmetries of the system. Hamiltonian describing collective neutrino oscillations possesses an $SU(N)_f$ rotation symmetry in the neutrino flavor space [18, 19, 20]. Various collective modes, including spectral swappings or splittings arise from this symmetry even in the inhomogeneous or anisotropic environments [19]. One expects that such a complex nonlinear system may exhibit further symmetries. Indeed, several authors noted the presence of various conserved quantities in the collective neutrino oscillations [21, 22]. More recently, it was shown that collective oscillations that maintain coherence can be classified by a number of linearly-independent functions [23], implying that scalar products of a unique linear combination of the original polarization vectors are conserved. The flavor evolution of a dense neutrino system by taking into account both the vacuum oscillations and self interactions of neutrinos from a many-body perspective was considered in Ref. [24]. Using the similarity between the collective neutrino oscillation Hamiltonian and the BCS Hamiltonian one can show that, in the single angle approximation, both the full many-body picture and the commonly-used effective one-particle picture possess several constants of motion [25].

One appealing aspect of the core-collapse supernovae is that they are the laboratories where diverse aspects of neutrino physics come into play. Here we concentrate on the collective behavior arising from the neutrino-neutrino interactions in a supernova and omit other interesting topics such as the role of sterile neutrinos [26] or the neutrino magnetic moment [28] in the r-process nucleosynthesis, effects of the CP-violation [29], effects of turbulence and density fluctuations [30], the role of neutrinos in shock revival [31], and neutrino signatures of black hole formation [32].

The next chapter of this proceedings contribution describes the algebraic formulation of the neutrino-neutrino interactions in the many-neutrino system. Chapter 3 includes a discussion of the invariants of the Hamiltonian of this system. Brief concluding remarks are included in Chapter 4.

2 An Algebraic Formulation of the Neutrino-Neutrino Interactions

For simplicity, we first consider a neutrino gas with two flavors and no antineutrinos. Matter and flavor basis creation and annihilation operators for a neutrino with momentum $\mathbf{p}$ and spin s are related as

$$a_1(\mathbf{p},s) = \cos\theta\, a_e(\mathbf{p},s) - \sin\theta\, a_x(\mathbf{p},s) \tag{1}$$

$$a_2(\mathbf{p},s) = \sin\theta\, a_e(\mathbf{p},s) + \cos\theta\, a_x(\mathbf{p},s). \tag{2}$$

It is easy to show that the flavor isospin operators defined as

$$\hat{J}^+_{\mathbf{p},s} = a^\dagger_e(\mathbf{p},s)a_x(\mathbf{p},s)\ , \qquad \hat{J}^-_{\mathbf{p},s} = a^\dagger_x(\mathbf{p},s)a_e(\mathbf{p},s)\ ,$$

$$\hat{J}^0_{\mathbf{p},s} = \frac{1}{2}\left(a^\dagger_e(\mathbf{p},s)a_e(\mathbf{p},s) - a^\dagger_x(\mathbf{p},s)a_x(\mathbf{p},s)\right)$$

form an SU(2) algebra:

$$[\hat{J}^+_{\mathbf{p},s}, \hat{J}^-_{\mathbf{q},r}] = 2\delta_{\mathbf{pq}}\delta_{sr}\hat{J}^0_{\mathbf{p},s}\ , \qquad [\hat{J}^0_{\mathbf{p},s}, \hat{J}^\pm_{\mathbf{q},r}] = \pm\delta_{\mathbf{pq}}\delta_{sr}\hat{J}^\pm_{\mathbf{p},s}\ .$$

One can show that the particle mixing given in Eqs. (1) and (2) is generated by this algebra:

$$\hat{U}^\dagger a_1(\mathbf{p},s)\hat{U} = a_e(\mathbf{p},s)$$

with

$$\hat{U} = e^{\sum_p \tan\theta J_p^+}\ e^{-\sum_p \ln(\cos^2\theta) J_0^p}\ e^{-\sum_p \tan\theta J_p^-}. \tag{3}$$

After subtracting a term proportional to the identity, the one-body Hamiltonian including interactions with the electron background takes the form

$$\hat{H}_\nu = \sum_p \left(\frac{\delta m^2}{2p} \hat{B} \cdot \vec{J}_p - \sqrt{2} G_F N_e J_p^0 \right)$$

where one defines

$$\hat{B} = (\sin 2\theta, 0, -\cos 2\theta).$$

The neutrino-neutrino interaction term in the Hamiltonian is

$$\hat{H}_{\nu\nu} = \frac{\sqrt{2} G_F}{V} \sum_{\mathbf{p},\mathbf{q}} (1 - \cos\vartheta_{\mathbf{pq}})\, \vec{J}_{\mathbf{p}} \cdot \vec{J}_{\mathbf{q}} \tag{4}$$

where $\vartheta_{\mathbf{pq}}$ is the angle between neutrino momenta $\mathbf{p}$ and $\mathbf{q}$. In Eq. (4) $(1 - cos\vartheta)$ terms follow from the V-A nature of the weak interactions.

The evolution operator

$$i\frac{\partial \mathcal{U}}{\partial t} = (H_\nu + H_{\nu\nu})\,\mathcal{U}$$

can be calculated [18] as a path integral using SU(2) coherent states:

$$|z(t)\rangle = \exp\left(\int dp z(p,t) J_+(p) \right) |\phi\rangle, \quad |\phi\rangle = \prod_p a_e^\dagger(p)|0\rangle$$

to obtain

$$\langle z'(t_f)|\mathcal{U}|z(t_i)\rangle = \int \mathcal{D}[z, z^*] \exp\left(iS[z, z^*]\right)$$

where

$$S(z, z^*) = \int_{t_i}^{t_f} dt \frac{\langle z(t)|i\frac{\partial}{\partial t} - H_\nu - H_{\nu\nu})|z(t)\rangle}{\langle z(t)|z(t)\rangle} + \log\langle z'(t_f)|z(t_f)\rangle.$$

The stationary phase approximation to the path integral

$$\left(\frac{d}{dt}\frac{\partial}{\partial \dot{z}} - \frac{\partial}{\partial z} \right) L(z, z^*) = 0 \qquad \left(\frac{d}{dt}\frac{\partial}{\partial \dot{z}^*} - \frac{\partial}{\partial z^*} \right) L(z, z^*) = 0$$

yields the differential equation

$$i\dot{z}(p,t) = \beta(p,t) - \alpha(p,t) z(p,t) - \beta^*(p,t) z(p,t)^2 \tag{5}$$

where we defined

$$\alpha(p,t) = -\frac{\delta m^2}{2p}\cos 2\theta + \sqrt{2} G_F N_e + \sqrt{2} G_F \int dq (1 - \cos\vartheta_{pq}) \left(\frac{1 - |z(q,t)|^2}{1 + |z(q,t)|^2} \right)$$

and

$$\beta(p,t) = \frac{1}{2}\frac{\delta m^2}{2p}\sin 2\theta + \sqrt{2} G_F \int dq (1 - \cos\vartheta_{pq}) \left(\frac{z(q,t)}{1 + |z(q,t)|^2} \right).$$

Defining

$$z(p,t) = \frac{\psi_x(p,t)}{\psi_e(p,t)},$$

with the auxiliary condition $|\psi_e|^2 + |\psi_x|^2 = 1$, Eq. (5) reduces to

$$i\frac{\partial}{\partial t}\begin{pmatrix} \psi_e \\ \psi_x \end{pmatrix} = \frac{1}{2}\begin{pmatrix} A + D - \Delta\cos 2\theta & D_{e\mu} + \Delta \sin 2\theta \\ D_{\mu e} + \Delta \sin 2\theta & -A - D + \Delta\cos 2\theta \end{pmatrix}\begin{pmatrix} \psi_e \\ \psi_x \end{pmatrix} \tag{6}$$

where

$$\Delta = \frac{\delta m^2}{2p}, \qquad A = \sqrt{2}G_F N_e,$$

$$D = \sqrt{2}G_F \int dq(1-\cos\vartheta_{pq})\left[\left(|\psi_e(q,t)|^2 - |\psi_x(q,t)|^2\right)\right],$$

$$D_{ex} = 2\sqrt{2}G_F \int dq(1-\cos\vartheta_{pq})\left(\psi_e(q,t)\psi_x^*(q,t)\right).$$

In the stationary point approximation to the full quantum mechanical problem, the test neutrino interacts with an "average field" representing the effect of all the other neutrinos. This approximation is analogous to the random phase approximation (RPA), widely used in many-body physics. In the RPA one can approximate product of two commuting arbitrary operators $\hat{\mathcal{O}}_1$ and $\hat{\mathcal{O}}_2$ as

$$\hat{\mathcal{O}}_1\hat{\mathcal{O}}_2 \sim \hat{\mathcal{O}}_1\langle\xi|\hat{\mathcal{O}}_2|\xi\rangle + \langle\xi|\hat{\mathcal{O}}_1|\xi\rangle\hat{\mathcal{O}}_2 - \langle\xi|\hat{\mathcal{O}}_1|\xi\rangle\langle\xi|\hat{\mathcal{O}}_2|\xi\rangle,$$

provided that

$$\langle\xi|\hat{\mathcal{O}}_1\hat{\mathcal{O}}_2|\xi\rangle = \langle\xi|\hat{\mathcal{O}}_1|\xi\rangle\langle\xi|\hat{\mathcal{O}}_2|\xi\rangle. \tag{7}$$

This approximation reduces $H_{\nu\nu}$ to a *one-body* Hamiltonian:

$$\mathcal{H}_{\nu\nu} \sim 2\frac{\sqrt{2}G_F}{V}\int d^3p\, d^3q\, R_{pq}\left(J_0(p)\langle J_0(q)\rangle + \frac{1}{2}J_+(p)\langle J_-(q)\rangle + \frac{1}{2}J_-(p)\langle J_+(q)\rangle\right).$$

The pre-exponential determinant obtained in the stationary phase approximation to the path integral is rather complicated and an explicit evaluation is not yet available in the literature. For simplicity in the discussion above we omitted antineutrinos. Antineutrinos can be included by introducing a second set of SU(2) algebras [18]. Similarly incorporating three flavors requires introduction of SU(3) algebras [33]. Both extensions are straightforward, but tedious.

Introducing the polarization vectors

$$P_i(q) = \mathrm{Tr}(J_i(q)\rho) \tag{8}$$

with the density matrix

$$\rho = \begin{pmatrix} \rho_{ee} & \rho_{ex} \\ \rho_{xe} & \rho_{xx} \end{pmatrix} = \frac{1}{2}\left(P_0 + \mathbf{P}\cdot\sigma\right),$$

one can show that, in RPA and including antineutrinos, the evolution equation (6) takes the commonly-used forms

$$\partial_r \mathbf{P}_p = \left\{+\frac{\delta m^2}{2p}(\sin 2\theta\hat{\mathbf{x}} - \cos 2\theta\hat{\mathbf{z}}) + \sqrt{2}\,G_{\mathrm{F}}\left[N_e\hat{\mathbf{z}} + \int d\mathbf{q}\,(1-\cos\vartheta_{pq})\,(\mathbf{P}_{\mathbf{q}} - \overline{\mathbf{P}}_{\mathbf{q}})\right]\right\}\times\mathbf{P}_p$$

and

$$\partial_r \overline{\mathbf{P}}_p = \left\{-\frac{\delta m^2}{2p}(\sin 2\theta\hat{\mathbf{x}} - \cos 2\theta\hat{\mathbf{z}}) + \sqrt{2}\,G_{\mathrm{F}}\left[N_e\hat{\mathbf{z}} + \int d\mathbf{q}\,(1-\cos\vartheta_{pq})\,(\mathbf{P}_{\mathbf{q}} - \overline{\mathbf{P}}_{\mathbf{q}})\right]\right\}\times\overline{\mathbf{P}}_p.$$

3 Invariants of the neutrino-neutrino interaction Hamiltonian

We consider the limit where the neutrino-neutrino interactions dominate and neglect the interactions with the background electrons and positrons. The Hamiltonian then becomes

$$\hat{H} = \sum_p \frac{\delta m^2}{2p} \hat{B} \cdot \vec{J}_p + \frac{\sqrt{2} G_F}{V} \sum_{\mathbf{p},\mathbf{q}} (1 - \cos\vartheta_{\mathbf{pq}})\, \vec{J}_{\mathbf{p}} \cdot \vec{J}_{\mathbf{q}}.$$

We further limit this discussion to the so-called single-angle approximation where all the ϑ are the same. Defining $\mu = (1 - \cos\vartheta)\frac{\sqrt{2}G_F}{V}$, $\tau = \mu t$, and $\omega_p = \frac{1}{\mu}\frac{\delta m^2}{2p}$, the Hamiltonian takes the form

$$\hat{H} = \sum_p \omega_p \hat{B} \cdot \vec{J}_p + \vec{J} \cdot \vec{J}. \tag{9}$$

This Hamiltonian of Eq. (9) preserves the *length of each spin*

$$\hat{L}_p = \vec{J}_p \cdot \vec{J}_p \ , \qquad \left[\hat{H}, \hat{L}_p\right] = 0 \ ,$$

as well as the *total spin component* in the direction of the "external magnetic field", $\hat{B}$

$$\hat{C}_0 = \hat{B} \cdot \vec{J} \ , \qquad \left[\hat{H}, \hat{C}_0\right] = 0 \ . \tag{10}$$

It is possible to show that [25] the collective neutrino Hamiltonian of Eq. (9) has the following constants of motion:

$$\hat{h}_p = \hat{B} \cdot \vec{J}_p + 2 \sum_{q(\neq p)} \frac{\vec{J}_p \cdot \vec{J}_q}{\omega_p - \omega_q}. \tag{11}$$

The individual neutrino spin-length discussed before in an independent invariant. However $\hat{C}_0 = \sum_p \hat{h}_p$. The Hamiltonian itself is also a linear combination of these invariants.

$$\hat{H} = \sum_p w_p \hat{h}_p + \sum_p \hat{L}_p \ .$$

The maximal value of the neutrino flavor isospin quantum number is $J_{\max} = N/2$, where N is total number of neutrinos. For example a state with all electron neutrinos is $|\nu_e\ \nu_e\ \nu_e\ \ldots\rangle = |J_{\max}\ \ J_{\max}\rangle_f$. It is also easy to show that matter and flavor bases are connected with the unitary transformation of Eq. (3): $|J_{\max}\ \ J_{\max}\rangle_f = \hat{U}^\dagger |J_{\max}\ \ J_{\max}\rangle_m$. One has $|J_{\max}\ \ J_{\max}\rangle_m = \prod_{\mathbf{p},s} a_1^\dagger(\mathbf{p}, s)\ |0\rangle$ and $|J_{\max}\ -J_{\max}\rangle_m = \prod_{\mathbf{p},s} a_2^\dagger(\mathbf{p}, s)\ |0\rangle$, corresponding to the energies $E_{(+J_{\max})} = -\sum_p \frac{n_p}{2}\omega_p + J_{\max}\,(J_{\max}+1)$ and $E_{(-J_{\max})} = \sum_p \frac{n_p}{2}\omega_p + J_{\max}\,(J_{\max}+1)$, respectively. Energy eigenvalues can be obtained by introducing the raising operator [25]

$$\mathcal{Q}^\pm(\xi) == \sum_p \frac{1}{\omega_p - \xi} \left(\cos^2\theta \hat{J}_p^\pm + \sin 2\theta \hat{J}_p^0 - \sin^2\theta \hat{J}_p^\mp\right).$$

Applying the operator to the state $|J\ -J\rangle_m$ yields a term proportional to $\mathcal{Q}^+(\xi)|J\ -J\rangle_m$ and an additional term. Setting the coefficient of this latter term to zero gives the Bethe ansatz

equation $\sum_p \frac{-j_p}{w_p-\xi} = -\frac{1}{2}$ that needs to be satisfied if $\mathcal{Q}^+(\xi)|J\ -J\rangle_m$ is an eigenstate. The most general eigenstate is

$$|\xi_1, \xi_2, \ldots \xi_\kappa\rangle \equiv \mathcal{Q}^+(\xi_1)\mathcal{Q}^+(\xi_2)\ldots\mathcal{Q}^+(\xi_\kappa)|J\ -J\rangle_m$$

which corresponds to the eigenvalue

$$E(\xi_1, \xi_2, \ldots, \xi_\kappa) = E_{(-J)} - \sum_{\alpha=1}^{\kappa} \xi_\alpha - \kappa(2J - \kappa + 1)\ ,$$

provided that the following Bethe ansatz equations are satisfied:

$$\sum_p \frac{-j_p}{\omega_p - \xi_\alpha} = -\frac{1}{2} + \sum_{\substack{\beta=1 \\ (\beta\neq\alpha)}}^{\kappa} \frac{1}{\xi_\alpha - \xi_\beta}\ .$$

Using the polarization vector, $\vec{P}_{\mathbf{p},s} = 2\langle\vec{J}_{\mathbf{p},s}\rangle$, of Eq. (8) one can write the Hamiltonian of Eq. (9) as

$$\hat{H} \sim \hat{H}^{\rm RPA} = \sum_p \omega_p \hat{B}\cdot\vec{J}_p + \vec{P}\cdot\vec{J}. \tag{12}$$

This Hamiltonian yields the Heisenberg equations of motion for the operators $\vec{J}_p$:

$$\frac{d}{d\tau}\vec{J}_p = -i[\vec{J}_p, \hat{H}^{\rm RPA}] = (\omega_p\hat{B} + \vec{P})\times\vec{J}_p. \tag{13}$$

Applying the RPA consistency conditions of Eq. (7) to Eq. (13) one obtains the equations of motion in the RPA:

$$\frac{d}{d\tau}\vec{P}_p = (\omega_p\hat{B} + \vec{P})\times\vec{P}_p.$$

Note that this is the single-angle limit of Eq. (9) only with neutrinos. It turns out that expectation value of the invariants, Eq. (11), of the exact many-body Hamiltonian

$$I_p = 2\langle\hat{h}_p\rangle = \hat{B}\cdot\vec{P}_p + \sum_{q(\neq p)} \frac{\vec{P}_p\cdot\vec{P}_q}{\omega_p - \omega_q}, \tag{14}$$

is an invariant of the RPA Hamiltonian:

$$\frac{d}{d\tau}I_p = 0.$$

Introduction of antineutrinos is again straightforward utilizing a second SU(2) algebra (denoted below with a tilde over the appropriate quantity). The conserved quantities for the single-angle Hamiltonian with both neutrinos and antineutrinos

$$H = \sum_p \omega_p\hat{B}\cdot\vec{J}_p + \sum_{\bar{p}} \omega_{\bar{p}}\hat{B}\cdot\vec{\bar{J}}_p + \left(\vec{J} + \vec{\bar{J}}\right)\cdot\left(\vec{J} + \vec{\bar{J}}\right)$$

are

$$\hat{h}_p = \hat{B}\cdot\vec{J}_p + 2\sum_{q(\neq p)} \frac{\vec{J}_p\cdot\vec{J}_q}{\omega_p - \omega_q} + 2\sum_{\bar{q}} \frac{\vec{J}_p\cdot\vec{\bar{J}}_{\bar{q}}}{\omega_p - \omega_{\bar{q}}}$$

for each neutrino energy mode p and

$$\hat{h}_{\bar{p}} = \hat{B}\cdot\vec{\bar{J}}_p + 2\sum_{\bar{q}(\neq\bar{p})}\frac{\vec{\bar{J}}_{\bar{p}}\cdot\vec{\bar{J}}_{\bar{q}}}{\omega_{\bar{p}}-\omega_{\bar{q}}} + 2\sum_q\frac{\vec{\bar{J}}_{\bar{p}}\cdot\vec{J}_q}{\omega_{\bar{p}}-\omega_q}\ .$$

or each antineutrino energy mode. In the RPA these take the form

$$I_p = 2\langle\hat{h}_p\rangle = \hat{B}\cdot\vec{P}_p + \sum_{q(\neq p)}\frac{\vec{P}_p\cdot\vec{P}_q}{\omega_p-\omega_q} + \sum_{\bar{q}}\frac{\vec{P}_p\cdot\vec{\bar{P}}_{\bar{q}}}{\omega_p-\omega_{\bar{q}}}$$

and

$$I_{\bar{p}} = 2\langle\hat{h}_{\bar{p}}\rangle = \hat{B}\cdot\vec{\bar{P}}_{\bar{p}} + \sum_{\bar{q}(\neq\bar{p})}\frac{\vec{\bar{P}}_{\bar{p}}\cdot\vec{\bar{P}}_{\bar{q}}}{\omega_{\bar{p}}-\omega_{\bar{q}}} + \sum_q\frac{\vec{\bar{P}}_{\bar{p}}\cdot\vec{P}_q}{\omega_{\bar{p}}-\omega_q},$$

respectively.

Recently a lot of attention was paid to the spectral splitting (or spectral swapping) phenomenon [21, 34, 35, 36, 37]. To explore the origin of this phenomenon we note that the expectation value of the invariant in Eq. (10) which can be written in terms of the expectation value of the invariants in Eq. (14),

$$\sum_p I_p = \mathbf{B}\cdot\mathbf{P}, \tag{15}$$

is not conserved by the RPA Hamiltonian, Eq. (12). Its conservation needs to be enforced using a Lagrange multiplier. Since $\sum_p I_p$ is proportional to $\hat{J}^0$, one needs to diagonalize the quantity

$$\begin{aligned}\hat{H}^{\rm RPA} + \omega_c\hat{J}^0 &= \sum_p(\omega_c-\omega_p)\hat{J}^0_p + \vec{\mathcal{P}}\cdot\vec{J}\\ &= \sum_{\mathbf{p},s}2\lambda_p\hat{U}'^\dagger\hat{J}^0_p\hat{U}',\end{aligned}$$

where the transforming operator is parameterized as

$$\hat{U}' = e^{\sum_p z_p J^+_p}\ e^{\sum_p \ln(1+|z_p|^2)J^0_p}\ e^{-\sum_p z^*_p J^-_p} \tag{16}$$

with

$$z_p = e^{i\delta}\tan\theta_p$$

and

$$\cos\theta_p = \sqrt{\frac{1}{2}\left(1+\frac{\omega_c-\omega_p+\mathcal{P}^0}{2\lambda_p}\right)}.$$

This operator transforms matter-basis creation and annihilation operators into *quasi-particle* creation and annihilation operators:

$$\begin{aligned}\alpha_1(\mathbf{p},s) &= \hat{U}'^\dagger a_1(\mathbf{p},s)\hat{U}' = \cos\theta_p\ a_1(\mathbf{p},s) - e^{i\delta}\sin\theta_p\ a_2(\mathbf{p},s)\\ \alpha_2(\mathbf{p},s) &= \hat{U}'^\dagger a_2(\mathbf{p},s)\hat{U}' = e^{-i\delta}\sin\theta_p\ a_1(\mathbf{p},s) + \cos\theta_p\ a_2(\mathbf{p},s)\end{aligned}$$

so that we obtain a diagonal Hamiltonian:

$$\hat{H}^{\rm RPA} + \omega_c \hat{J}^0 = \sum_{\mathbf{p},s} \lambda_p \left(\alpha_1^\dagger(\mathbf{p},s)\alpha_1(\mathbf{p},s) - \alpha_2^\dagger(\mathbf{p},s)\alpha_2(\mathbf{p},s) \right).$$

Let us assume that initially ($\lim \mu \to \infty$) there are more ν_e's and all neutrinos are in flavor eigenstates. We then have

$$\lim \cos\theta_p = \lim \sqrt{\frac{1}{2}\left(1 + \frac{P^0}{|\vec{P}|}\cos 2\theta\right)} = \cos\theta,$$

i.e., the diagonalizing transformation of Eq. (16) reduces into the neutrino mixing transformation of Eq. (3) and the total Hamiltonian of Eq. (16) is diagonalized by the flavor eigenstates:

$$\alpha_1(\mathbf{p},s) = \hat{U}^\dagger a_1(\mathbf{p},s)\hat{U} = a_e(\mathbf{p},s).$$

After neutrinos propagate to a region with very low neutrino density ($\mu \to 0$) one gets

$$\cos\theta_p = \sqrt{\frac{1}{2}\left(1 + \frac{\omega_c - \omega_p}{|\omega_c - \omega_p|}\right)} \Rightarrow \left\{ \begin{array}{ll} 1 & \omega_p < \omega_c \\ 0 & \omega_p > \omega_c \end{array} \right.$$

yielding

$$\alpha_1(\mathbf{p},s) = \hat{U}^\dagger a_1(\mathbf{p},s)\hat{U} \Rightarrow \left\{ \begin{array}{ll} a_1(\mathbf{p},s) & \omega_p < \omega_c \\ -a_2(\mathbf{p},s) & \omega_p > \omega_c \end{array} \right. ,$$

i.e. neutrinos with $\omega_p < \omega_c$ and $\omega_p > \omega_c$ evolve into different mass eigenstates. In Ref. [21] it was shown that such an evolution leads to spectral splits.

4 Concluding Remarks

Neutrino propagation through the dense media in the core-collapse supernovae probes many interesting collective effects. Because of the neutrino-neutrino interactions, this many-body system is intrinsically non-linear, it can be linearized only in certain cases [38]. We examined this many-neutrino system both from the exact many-body perspective and from the point of view of an effective one-body description formulated with the application of the RPA method. To achieve this goal we exploited mathematical similarities between the neutrino-neutrino interaction Hamiltonian and the BCS pairing Hamiltonian. (Indeed, the N-mode collective oscillations of the neutrinos are related to the m-spin solutions of the BCS model [39]). In the limit of the single angle approximation, both the many-body and the RPA pictures possess many constants of motion manifesting the existence of associated dynamical symmetries in the system. Judicious use of these invariants could certainly help numerical calculations [40].

We treated the two-flavor neutrino-neutrino interaction in the single-angle approximation, and provided an interpretation of the critical energy in the spectral swap/split phenomenon as the Lagrange multiplier of the number conservation constraint. Recent numerical work with three flavors in the multi-angle approximation uncovers significant differences between single- and multi-angle formulations [41]. In particular, multi-angle formulation is found to reduce the adiabaticity of flavor evolution in the normal neutrino mass hierarchy, resulting in lower swap

energies. Thus it seems that single-angle approximation seems to be sufficient in some cases, but inadequate in other situations.

Other questions remain regarding the many-body behavior of the neutrino system. For example, in the calculations so far neutrinos are assumed to be emitted half-isotropically (only outward-moving modes are occupied with backward-moving modes being empty). However, recent realistic supernova simulations suggest that neutrino angular distributions are not half-isotropic [42]. Flavor-dependent angular distributions may lead to multi-angle instabilities [43, 44]. Future work could uncover even more interesting features of this many-neutrino system.

Acknowledgments

This work was supported in part by the U.S. National Science Foundation Grant No. PHY-0855082, and in part by the University of Wisconsin Research Committee with funds granted by the Wisconsin Alumni Research Foundation. I would like to thank the organizers of HAνSE 2011 for their hospitality.

References

[1] G. M. Fuller, W. C. Haxton, G. C. McLaughlin, Phys. Rev. **D59**, 085005 (1999) [astro-ph/9809164]; C. Lunardini, A. Y. .Smirnov, Astropart. Phys. **21**, 703-720 (2004) [arXiv:hep-ph/0402128 [hep-ph]]; J. F. Beacom, M. R. Vagins, Phys. Rev. Lett. **93**, 171101 (2004) [hep-ph/0309300]; L. Cadonati, F. P. Calaprice, M. C. Chen, Astropart. Phys. **16**, 361-372 (2002) [hep-ph/0012082]; M. K. Sharp, J. F. Beacom, J. A. Formaggio, Phys. Rev. **D66**, 013012 (2002) [hep-ph/0205035]; A. B. Balantekin and F. Loreti, Phys. Rev. D **45**, 1059 (1992); J. Ahrens *et al.* [AMANDA Collaboration], Astropart. Phys. **16**, 345-359 (2002). [astro-ph/0105460]; R. Abbasi *et al.* [IceCube Collaboration], [arXiv:1108.0171 [astro-ph.HE]]; D. Vaananen, C. Volpe, JCAP **1110**, 019 (2011). [arXiv:1105.6225 [astro-ph.SR]].

[2] A. B. Balantekin, G. M. Fuller, J. Phys. G **G29**, 2513-2522 (2003). [astro-ph/0309519].

[3] G. M. Fuller, R. W. Mayle, J. R. Wilson and D. N. Schramm, Astrophys. J. **322**, 795 (1987).

[4] Y. -Z. Qian, G. M. Fuller, Phys. Rev. **D52**, 656-660 (1995). [astro-ph/9502080].

[5] D. Notzold and G. Raffelt, Nucl. Phys. B **307**, 924 (1988).

[6] J. T. Pantaleone, Phys. Lett. B **287**, 128 (1992).

[7] Y. Z. Qian and G. M. Fuller, Phys. Rev. D **51**, 1479 (1995) [arXiv:astro-ph/9406073].

[8] S. Pastor, G. Raffelt, Phys. Rev. Lett. **89**, 191101 (2002). [astro-ph/0207281].

[9] A. Friedland and C. Lunardini, Phys. Rev. D **68**, 013007 (2003) [arXiv:hep-ph/0304055]; A. Friedland, B. H. J. McKellar and I. Okuniewicz, Phys. Rev. D **73**, 093002 (2006) [arXiv:hep-ph/0602016].

[10] J. Gava, J. Kneller, C. Volpe, G. C. McLaughlin, Phys. Rev. Lett. **103**, 071101 (2009). [arXiv:0902.0317 [hep-ph]].

[11] A. B. Balantekin and H. Yuksel, New J. Phys. **7**, 51 (2005) [arXiv:astro-ph/0411159].

[12] S. Chakraborty, S. Choubey, S. Goswami, K. Kar, JCAP **1006**, 007 (2010). [arXiv:0911.1218 [hep-ph]].

[13] H. Duan, A. Friedland, G. C. McLaughlin, R. Surman, J. Phys. G **G38**, 035201 (2011). [arXiv:1012.0532 [astro-ph.SR]].

[14] For a sampling of recent work on this subject see J. F. Cherry, M. -R. Wu, J. Carlson, H. Duan, G. M. Fuller, Y. -Z. Qian, [arXiv:1109.5195 [astro-ph.HE]]; S. Sarikas, G. G. Raffelt, L. Hudepohl, H. -T. Janka, [arXiv:1109.3601 [astro-ph.SR]]; S. Chakraborty, T. Fischer, A. Mirizzi, N. Saviano, R. Tomas, Phys. Rev. **D84**, 025002 (2011) [arXiv:1105.1130 [hep-ph]]; H. Duan, A. Friedland, Phys. Rev. Lett. **106**, 091101 (2011) [arXiv:1006.2359 [hep-ph]]; A. Friedland, Phys. Rev. Lett. **104**, 191102 (2010) [arXiv:1001.0996 [hep-ph]]; G. Fogli, E. Lisi, A. Marrone, I. Tamborra, JCAP **0904**, 030 (2009) [arXiv:0812.3031 [hep-ph]].

[15] H. Duan and J. P. Kneller, J. Phys. G **36**, 113201 (2009) [arXiv:0904.0974 [astro-ph.HE]].

[16] H. Duan, G. M. Fuller and Y. Z. Qian, *Annu. Rev. Nucl. Part. Sci.* **60**, 569 (2010) [arXiv:1001.2799 [hep-ph]].

[17] G. G. Raffelt, Prog. Part. Nucl. Phys. **64**, 393-399 (2010).

[18] A. B. Balantekin, Y. Pehlivan, J. Phys. G **G34**, 47-66 (2007). [astro-ph/0607527].

[19] H. Duan, G. M. Fuller and Y. Z. Qian, J. Phys. G **36**, 105003 (2009) [arXiv:0808.2046 [astro-ph]].

[20] A. B. Balantekin, Nucl. Phys. A **844**, 14C (2010) [arXiv:0910.1814 [nucl-th]].

[21] G. G. Raffelt and A. Y. Smirnov, Phys. Rev. D **76**, 081301 (2007) [Erratum-ibid. D **77**, 029903 (2008)] [arXiv:0705.1830 [hep-ph]]; Phys. Rev. D **76**, 125008 (2007) [arXiv:0709.4641 [hep-ph]].

[22] H. Duan, G. M. Fuller, J. Carlson and Y. Z. Qian, Phys. Rev. D **75**, 125005 (2007) [arXiv:astro-ph/0703776].

[23] G. G. Raffelt, Phys. Rev. **D83**, 105022 (2011). [arXiv:1103.2891 [hep-ph]].

[24] Y. Pehlivan, T. Kajino, A. B. Balantekin, T. Yoshida, T. Maruyama, AIP Conf. Proc. **1269**, 189-194 (2010).

[25] Y. Pehlivan, A. B. Balantekin, T. Kajino, T. Yoshida, Phys. Rev. D **84**, 065008 (2011). [arXiv:1105.1182 [astro-ph.CO]].

[26] G. C. McLaughlin, J. M. Fetter, A. B. Balantekin and G. M. Fuller, Phys. Rev. C **59**, 2873 (1999) [arXiv:astro-ph/9902106]; J. Fetter, G. C. McLaughlin, A. B. Balantekin and G. M. Fuller, Astropart. Phys. **18**, 433 (2003) [arXiv:hep-ph/0205029]; D. O. Caldwell, G. M. Fuller and Y. Z. Qian, Phys. Rev. D **61**, 123005 (2000) [arXiv:astro-ph/9910175];

[27] I. Tamborra, G. G. Raffelt, L. Huedepohl, H. -T. Janka, [arXiv:1110.2104 [astro-ph.SR]].

[28] A. B. Balantekin, C. Volpe and J. Welzel, JCAP **0709**, 016 (2007) [arXiv:0706.3023 [astro-ph]].

[29] A. B. Balantekin, J. Gava and C. Volpe, Phys. Lett. B **662**, 396 (2008) [arXiv:0710.3112 [astro-ph]]; J. Gava and C. Volpe, Phys. Rev. D **78**, 083007 (2008) [arXiv:0807.3418 [astro-ph]]; J. P. Kneller and G. C. McLaughlin, Phys. Rev. D **80**, 053002 (2009) [arXiv:0904.3823 [hep-ph]].

[30] F. N. Loreti, Y. Z. Qian, G. M. Fuller and A. B. Balantekin, Phys. Rev. D **52**, 6664 (1995) [arXiv:astro-ph/9508106]; A. Friedland and A. Gruzinov, arXiv:astro-ph/0607244; G. L. Fogli, E. Lisi, A. Mirizzi and D. Montanino, JCAP **0606**, 012 (2006) [arXiv:hep-ph/0603033]; J. P. Kneller and C. Volpe, Phys. Rev. D **82**, 123004 (2010) [arXiv:1006.0913 [hep-ph]]; J. F. Cherry, M. R. Wu, J. Carlson, H. Duan, G. M. Fuller and Y. Z. Qian, arXiv:1108.4064 [astro-ph.HE].

[31] B. Dasgupta, E. P. O'Connor, C. D. Ott, [arXiv:1106.1167 [astro-ph.SR]].

[32] T. Sasaqui, T. Kajino, A. B. Balantekin, Astrophys. J. **634**, 534-541 (2005). [astro-ph/0506100].

[33] R. F. Sawyer, Phys. Rev. D **72**, 045003 (2005) [arXiv:hep-ph/0503013].

[34] B. Dasgupta, A. Mirizzi, I. Tamborra, R. Tomas, Phys. Rev. **D81**, 093008 (2010). [arXiv:1002.2943 [hep-ph]]; B. Dasgupta, A. Dighe, G. G. Raffelt, A. Y. .Smirnov, Phys. Rev. Lett. **103**, 051105 (2009). [arXiv:0904.3542 [hep-ph]]; B. Dasgupta, A. Dighe, A. Mirizzi, G. G. Raffelt, Phys. Rev. **D77**, 113007 (2008). [arXiv:0801.1660 [hep-ph]].

[35] H. Duan, G. M. Fuller, J. Carlson, Y. -Q. Zhong, Phys. Rev. Lett. **99**, 241802 (2007). [arXiv:0707.0290 [astro-ph]]; H. Duan, G. M. Fuller, Y. -Z. Qian, Phys. Rev. **D77**, 085016 (2008). [arXiv:0801.1363 [hep-ph]].

[36] G. Fogli, E. Lisi, A. Marrone, I. Tamborra, JCAP **0910**, 002 (2009). [arXiv:0907.5115 [hep-ph]].

[37] S. Galais, C. Volpe, Phys. Rev. **D84**, 085005 (2011). [arXiv:1103.5302 [astro-ph.SR]].

[38] A. Banerjee, A. Dighe, G. Raffelt, Phys. Rev. **D84**, 053013 (2011). [arXiv:1107.2308 [hep-ph]].

[39] A.A. Yuzbashyan, B.L. Altshuler, V.B. Kuznetsov, and V.E. Enolskii, J. Phys. A **38**, 7831 (2005).

[40] H. Duan, G. M. Fuller, J. Carlson, Comput. Sci. Dis. **1**, 015007 (2008). [arXiv:0803.3650 [astro-ph]].

[41] J. F. Cherry, G. M. Fuller, J. Carlson, H. Duan, Y. -Z. Qian, Phys. Rev. **D82**, 085025 (2010). [arXiv:1006.2175 [astro-ph.HE]].

[42] C. D. Ott, A. Burrows, L. Dessart and E. Livne, Astrophys. J. **685**, 1069 (2008) [arXiv:0804.0239 [astro-ph]]; S. Chakraborty, T. Fischer, A. Mirizzi, N. Saviano and R. Tomas, Phys. Rev. D **84**, 025002 (2011) [arXiv:1105.1130 [hep-ph]].

[43] R. F. Sawyer, Phys. Rev. **D79**, 105003 (2009). [arXiv:0803.4319 [astro-ph]].

[44] A. Mirizzi, P. D. Serpico, [arXiv:1110.0022 [hep-ph]].

Supernova bound on keV-mass sterile neutrinos

Shun Zhou

Max-Planck-Institut für Physik (Werner-Heisenberg-Institut), 80805 München, Germany

DOI: http://dx.doi.org/10.3204/DESY-PROC-2011-03/zhou

In this talk, I first explain why the keV-mass sterile neutrinos, slightly mixing with ordinary neutrinos, are interesting in particle astrophysics. Then the production and oscillation of such sterile neutrinos in the supernova core are discussed. Assuming the ν_τ-ν_s mixing and implementing the standard energy-loss argument, I finally draw the supernova bound on the active-sterile mixing angle for a given sterile neutrino mass.

1 Motivation

It has been well established that the matter content of our Universe is dominated by the non-baryonic dark matter. A lot of attention has been so far focused on the cold dark matter (CDM), which has a negligible velocity dispersion and damps structures below the Earth mass scales [1]. The candidates for CDM arise from the well-motivated theories of elementary particle physics [2], such as the lightest supersymmetric particle and the axion. However, the CDM scenario suffers from several unsolved problems in the galaxy and small-scale structure formation, e.g., the overprediction of the observed satellites in the galaxy-scale halos [3] and the high concentration of dark matter in galaxies [4]. In the scenario of warm dark matter (WDM), a light-mass particle with a large velocity dispersion can suppress the structure formation up to the galaxy scales and thus solve the potential small-scale structure problems.

Sterile neutrinos of keV masses are a promising candidate for the WDM [5]. Dodelson and Widrow have proposed that sterile neutrinos with masses $m_s \sim$ keV can be produced via neutrino oscillations in the early Universe and account for all the dark matter [6], if they mix with the ordinary neutrinos via a small vacuum mixing angle $\theta \sim 10^{-(4\cdots5)}$. Due to such a tiny mixing angle, the sterile neutrinos have never been in thermal equilibrium. In the presence of a primordial lepton asymmetry, Shi and Fuller have observed that the production rate of sterile neutrinos could be enhanced by the Mikheyev-Smirnov-Wolfenstein (MSW) effect [7] and the correct relic abundance can be reproduced even for much smaller mixing angles [8]. One possible way to detect sterile-neutrino WDM is to look for the X-rays from their radiative decays [9]. Conversely, the non-observation of an X-ray line from the local group dwarf galaxies has placed restrictive limits on the mass and mixing angle of sterile neutrinos. Other limits can be obtained from the Lyman-alpha forest and Supernova (SN) 1987A [5]. Put all together, the window for the Dodelson-Widrow mechanism of non-resonant production is closed, while the Shi-Fuller mechanism of resonant production is still viable [10]. Roughly speaking, sterile neutrinos with $m_s = 1 \sim 10$ keV and $\theta = 10^{-(4\cdots6)}$ could be WDM. However, it should be noted that the observational constraints depend crucially on the production mechanisms of sterile neutrinos, so they can be evaded in various models [11].

Moreover, the WDM sterile neutrinos could play an important role in generating the supernova asymmetries and the pulsar kicks [12], and perhaps in the supernova explosions [13]. Hence it is interesting to reexamine the SN bound on the keV-mass sterile neutrinos.

2 Sterile neutrinos in SN cores

Sterile neutrinos with masses in the keV range can be copiously produced in the SN core. For $m_s \gtrsim 100$ keV, the vacuum mixing angle of sterile neutrinos is stringently constrained $\sin^2 2\theta \lesssim 10^{-9}$ in order to avoid excessive energy loss [14]. For smaller masses, however, the MSW effect on active-sterile neutrino mixing becomes very important and the SN bound on vacuum mixing angle is not that obvious. Note that the bounds on mixing angles depend on which neutrino species the sterile neutrino mixes with. We concentrate on the SN bound in ν_τ-ν_s-mixing case for simplicity, because ν_τ and $\bar{\nu}_\tau$ only have neutral-current interactions and essentially stay in thermal equilibrium with the ambient matter.

The matter density in the SN core is so high that the incoherent scattering of active neutrinos on matter particles may even dominate over flavor oscillations as the production mechanism for keV-mass sterile neutrinos. An elegant formalism to deal with both incoherent scattering and flavor oscillations has been developed in Ref. [15], where the evolution equations for the occupation numbers of different neutrino species have been derived. In the weak-damping limit, which is always valid for supernova neutrinos mixing with keV-mass sterile neutrinos, the evolution of ν_τ number density is determined by [16]

$$\dot{N}_{\nu_\tau} = -\frac{1}{4} \sum_a \int \frac{E^2 \mathrm{d}E}{2\pi^2} s^2_{2\theta_\nu} \int \frac{E'^2 \mathrm{d}E'}{2\pi^2} W^a_{E'E} f^\tau_{E'} \; , \tag{1}$$

where $s_{2\theta_\nu} \equiv \sin 2\theta_\nu$ with θ_ν being the neutrino mixing angle in matter, f^τ_E the occupation number of ν_τ, and $W^a_{E'E}$ the transition probability for $\nu(E') + a \to \nu(E) + a$ with a being background particles in the SN core. In a similar way, we can derive the evolution equation of the $\bar{\nu}_\tau$ number density, involving the mixing angle $\theta_{\bar{\nu}}$, the occupation number $f^{\bar{\tau}}_E$ and the transition probability $\bar{W}^a_{E'E}$. Due to the MSW effect, the mixing angle of neutrinos in matter is different from that of antineutrinos, i.e.,

$$\sin^2 2\theta_{\nu,\bar{\nu}} = \frac{\sin^2 2\theta}{\sin^2 2\theta + (\cos 2\theta \pm E/E_\mathrm{r})^2} \; , \tag{2}$$

where θ denotes the vacuum mixing angle, and the upper sign refers to ν and the lower to $\bar{\nu}$. The resonant energy $E_\mathrm{r} \equiv \Delta m^2/2|V_{\nu_\tau}|$ can be written as

$$E_\mathrm{r} = 3.25 \text{ MeV} \left(\frac{m_s}{10 \text{ keV}}\right)^2 \rho^{-1}_{14} \left|Y_0 - Y_{\nu_\tau}\right|^{-1} \; , \tag{3}$$

where ρ_{14} is the matter density ρ in units of 10^{14} g cm^{-3} and $Y_0 \equiv (1 - Y_e - 2Y_{\nu_e})/4$. Note that $Y_x \equiv (N_x - N_{\bar{x}})/N_\mathrm{B}$ with N_B being the baryon number density, N_x and $N_{\bar{x}}$ being the number densities of particle x and its antiparticle $\bar{x}$. For tau neutrinos, the matter potential $V_{\nu_\tau} = -(G_\mathrm{F}/\sqrt{2}) N_\mathrm{B} \left(1 - Y_e - 2Y_{\nu_e} - 4Y_{\nu_\tau}\right)$ is negative if the typical values of $Y_e = 0.3$, $Y_{\nu_e} = 0.07$ and $Y_{\nu_\tau} = 0$ for a SN core are taken. Therefore, the mixing angle for $\bar{\nu}_\tau$ is enhanced by matter effects, and the emission rate for $\bar{\nu}_\tau$ exceeds that for ν_τ, indicating that a ν_τ-$\bar{\nu}_\tau$ asymmetry (i.e., $Y_{\nu_\tau} \neq 0$) will be established. An interesting feedback effect emerges: (i) The chemical

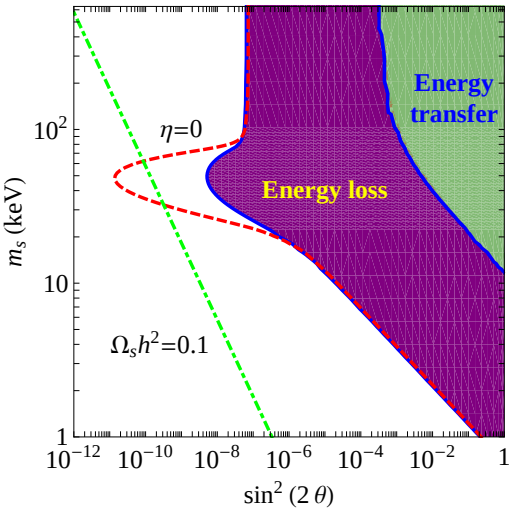

Figure 1: (color online) Supernova bound on sterile neutrino masses m_s and mixing angles θ, where the purple region is excluded by the energy-loss argument while the green one by the energy-transfer argument [16]. The excluded region will be extended to the dashed (red) line if the build-up of degeneracy parameter is ignored, i.e., $\eta(t) = 0$. The dot-dashed (green) line represents the sterile neutrinos as dark matter with the correct relic abundance $\Omega_s h^2 = 0.1$.

potential for tau neutrinos develops and thus changes the occupation numbers of ν_τ and $\bar{\nu}_\tau$; (ii) The ν_τ-$\bar{\nu}_\tau$ asymmetry shifts the resonant energy $E_{\rm r}$, and thus modifies the mixing angles θ_ν and $\theta_{\bar{\nu}}$; (iii) Both effects in (i) and (ii) will feed back on the emission rates. Hence a stationary state of this active-sterile neutrino system will be achieved if the emission rates for neutrinos and antineutrinos become equal to each other [16].

3 SN bound on sterile neutrinos

Given the sterile neutrino mass m_s and vacuum mixing angle θ, the energy loss rate $\mathcal{E}(t)$ due to sterile neutrino emission can be calculated by following the evolution of ν_τ-$\bar{\nu}_\tau$ asymmetry $Y_{\nu_\tau}(t)$. It has been found that the stationary state can be reached within one second and the feedback effect is very important for 20 keV $\lesssim m_s \lesssim$ 80 keV and $10^{-9} \lesssim \sin^2 2\theta \lesssim 10^{-4}$. To avoid excessive energy losses, we require that the average energy-loss rate $\langle \mathcal{E} \rangle \equiv \int_0^{\tau_{\rm d}} \mathcal{E}(t)\, {\rm d}t$ with $\tau_{\rm d} = 1$ s should be $\langle \mathcal{E} \rangle \lesssim 3.0 \times 10^{33}$ erg cm^{-3} s^{-1}. Otherwise, the duration of neutrino burst from SN 1987A would have been significantly reduced. In Fig. 1, we show the contours of energy-loss rates in the $(\sin^2 2\theta, m_s)$-plane, where we have assumed a homogeneous and isotropic core with matter density $\rho = 3.0 \times 10^{14}$ g cm^{-3} and temperature $T = 30$ MeV. Based on the energy-loss argument, the purple region has been excluded. The most stringent bound $\sin^2 2\theta \lesssim 10^{-8}$ arises for $m_s = 50$ keV. For the large-mixing angle region, the energy-loss rate is actually small, because sterile neutrinos have been trapped in the core and cannot carry away energies. However, the mean free path of sterile neutrinos is comparable to or even

larger than that of ordinary neutrinos, indicating that they may transfer energies in a more efficient way. As a consequence, the duration of neutrino burst will be shortened by emitting neutrinos more rapidly. In this sense, the excessive energy transfer should be as dangerous as the excessive energy loss. Hence the large-mixing angle region is excluded when the energy-transfer argument is applied. The green line in Fig. 1 indicates the relic abundance of dark matter $\Omega_s h^2 = 0.1$, where keV-mass sterile neutrinos are warm dark matter and the non-resonant production mechanism is assumed. If we ignore the feedback effect (i.e., a vanishing chemical potential for tau neutrinos $\eta = \mu_{\nu_\tau}/T = 0$), the excluded region will extend to the red line, which overlaps the relic-abundance line. However, the mixing angles are essentially unconstrained in the favored warm-dark-matter mass range 1 keV $\lesssim m_s \lesssim$ 10 keV.

As for the ν_μ-ν_s-mixing case, our discussions about the feedback effects are essentially applicable. However, the charged-current interactions of ν_μ and $\bar{\nu}_\mu$ should be taken into account, and the change of ν_μ-$\bar{\nu}_\mu$ asymmetry will be redistributed between muon neutrinos and charged muons. The ν_e-ν_s mixing in SN cores is more involved because of the large trapped electron number and high ν_e degeneracy. Besides energy loss, deleptonization by sterile neutrino emission is an effect to be taken into account.

Acknowledgements

The author would like to thank the organizers for such a wonderful workshop on supernova neutrinos, and Georg Raffelt for collaboration. This work was supported by the Alexander von Humboldt Foundation.

References

[1] S. Hofmann, D.J. Schwarz and H. Stoecker, Phys. Rev. D **64**, 083507 (2001).

[2] F.D. Steffen, Eur. Phys. J. C. **59**, 557 (2009).

[3] G. Kauffmann, S.D.M. White and B. Guiderdoni, Mon. Not. R. Astron. Soc. **264**, 201 (1993).

[4] P.J.E. Peebles, arXiv:astro-ph/0101127.

[5] A. Kusenko, Phys. Rept. **481**, 1 (2009).

[6] S. Dodelson and L.M. Widrow, Phys. Rev. Lett. **72**, 17 (1994).

[7] L. Wolfenstein, Phys. Rev. D **17**, 2369 (1978);
S.P. Mikheyev and A.Yu. Smirnov, Sov. J. Nucl. Phys. **42**, 913 (1985).

[8] X.D. Shi and G.M. Fuller, Phys. Rev. Lett. **82**, 2832 (1999).

[9] K.N. Abazajian, arXiv:0903.2040 [astro-ph.CO].

[10] A. Boyarsky *et al.*, Phys. Rev. Lett. **102**, 201304 (2009).

[11] A. Kusenko, Phys. Rev. Lett **97**, 241301 (2006);
F. Bezrukov, H. Hettmansperger and M. Lindner, Phys. Rev. D **81**, 085032 (2010).

[12] A. Kusenko and G. Segre, Phys. Lett. B **396**, 197 (1997).

[13] J. Hidaka and G.M. Fuller, Phys. Rev. D **74**, 125015 (2006);
J. Hidaka and G.M. Fuller, Phys. Rev. D **76**, 083516 (2007).

[14] K. Kainulainen, J. Maalampi and J.T. Peltoniemi, Nucl. Phys. B **358**, 435 (1991);
G. Raffelt and G. Sigl, Astropart. Phys. **1**, 165 (1993);
X. Shi and G. Sigl, Phys. Lett. B **323**, 360 (1994);
K. Abazajian, G.M. Fuller and M. Patel, Phys. Rev. D **64**, 023501 (2001).

[15] G. Sigl and G. Raffelt, Nucl. Phys. B **406**, 423 (1993).

[16] G.G. Raffelt and S. Zhou, Phys. Rev. D **83**, 093014 (2011).

Supernovae and sterile neutrinos

Irene Tamborra

Max-Planck-Institut für Physik, Föhringer Ring 6, 80805 München, Germany

DOI: http://dx.doi.org/10.3204/DESY-PROC-2011-03/tamborra

Motivated by the recent hints for sterile neutrinos from reactor anomalies, we discuss active-sterile conversions in an electron-capture supernova using a (2 active + 1 sterile) scenario. By including the feedback effect on the electron abundance due to neutrino oscillations, we study the impact of sterile neutrinos on both the oscillated neutrino fluxes and on Y_e.

1 Introduction

Sterile neutrinos are hypothetical gauge-singlet fermions that mix with one or more of the active states and thus show up in active-sterile flavor oscillations. Our study is motivated by the most recent indication for the possible existence of eV-mass sterile neutrinos coming from a new analysis of reactor $\bar{\nu}_e$ spectra [1, 2]. The data suggest a ν_e-ν_s mixing of $\sin^2 2\theta \sim 0.14$ with mass splitting of $\Delta m^2 \gtrsim 1.5$ eV^2.

Assuming that the sterile state is heavier than the active ones because of cosmological mass limits, in supernovae (SN) such parameters imply $\nu_e - \nu_s$ MSW conversions close to the SN core. Therefore, the ν_e flux arriving at Earth from the next SN explosion would be significantly modified by the presence of sterile neutrinos.

We here focus on a different aspect of ν_e-ν_s oscillations that could have an interesting impact during the SN cooling phase. The neutrino-driven matter outflow is a candidate site for r-process nucleosynthesis (it requires a neutron-rich environment, i.e. $Y_e < 0.5$, large entropy to favor lighter nuclei at high temperatures and fast timescales to lower the efficacy of converting alpha particles to heavier nuclei). We discuss whether sterile neutrinos might trigger the r-process or somehow affect the nuclei formation.

2 Neutrino and Y_e evolutions in electron-capture supernovae

We use long-term simulations for an electron-capture supernova of a representative progenitor with mass 8.8 $M_\odot$ [3] and we discuss here two representative cooling times ($t = 0.5, 2.9$ s). In Table 1, for each flavor ν_β, the neutrino-sphere radius, the luminosity L_{ν_β}, the average energies $\langle E_{\nu_\beta} \rangle$ are reported.

We consider a $2 + 1$ flavor scenario (ν_e, ν_x, ν_s) with mass differences $\delta m^2_{\rm S} = 2.35$ eV$^2 > 0$, $\delta m^2_{\rm atm} = -2 \times 10^{-3}$ eV$^2 < 0$. The mixing is driven by $\sin^2 \Theta_{13} = 10^{-4}$ and $\sin^2 2\Theta_S = 0.165$ assuming negligible the other mixing angles.

t	R_ν	L_{ν_e}	$L_{\overline{\nu}_e}$	L_{ν_x}	$\langle E_{\nu_e}\rangle$	$\langle E_{\overline{\nu}_e}\rangle$	$\langle E_{\nu_x}\rangle$	Y_e
0.5	25	9.5	10.06	10.8	16.8	18.14	18.3	5.47×10^{-2}
2.9	16	3.28	3.4	3.74	15.8	16.3	15.8	3.23×10^{-2}

Table 1: Reference neutrino-sphere radii R_ν in km (assumed equal for all the different flavors for sake of simplicity), luminosities L_{ν_β} (in units of 10^{51} erg/s), average energies $\langle E_{\nu_\beta}\rangle$ (in MeV), and electron abundances Y_e for two different post-bounce times t (in seconds) and for each flavor ν_β (with $\beta = e, \bar{e}, x$).

The flavor evolution is described by matrices of densities for each energy mode E for ν and $\bar{\nu}$, being the diagonal entries the usual occupation numbers. The evolution of ρ_E is governed by the Liouville equations

$$i\partial_r \rho_E = [\mathsf{H}_E, \rho_E] \quad \text{and} \quad i\partial_r \bar{\rho}_E = [\bar{\mathsf{H}}_E, \bar{\rho}_E]\,, \tag{1}$$

where the overbar refers to antineutrinos and sans-serif letters denote 3×3 matrices in flavor space with initial conditions $\rho_E = \mathrm{diag}(n_{\nu_e}, n_{\nu_x}, 0)$ and $\bar{\rho}_E = \mathrm{diag}(n_{\bar{\nu}_e}, n_{\bar{\nu}_x}, 0)$. The Hamiltonian matrix contains vacuum, matter, and neutrino–neutrino terms $\mathsf{H}_E = \mathsf{H}_E^{\rm vac} + \mathsf{H}_E^{\rm m} + \mathsf{H}_E^{\nu\nu}$. Because of the presence of sterile neutrinos, the matter term includes both the charge current (CC) and the neutral current (NC) contributions: $\mathsf{H}_E^{\rm m} = \sqrt{2} G_{\rm F}\ \mathrm{diag}(N_e - N_n/2, -N_n/2, 0)$, with N_e the electron number density and N_n the neutron one in the medium. Note that being $Y_e = N_e(r)/(N_e(r) + N_n(r))$, $\mathsf{H}^{\rm m}$ is a function of Y_e and it changes as Y_e changes. While $\mathsf{H}_E^{\nu\nu}$ has all the terms involving sterile neutrinos identically equal to zero, as proved in [4].

The electron fraction, on the other hand, is altered by the charged current weak interactions by converting neutrons into protons and viceversa. Assuming β-equilibrium is reached, the electron abundance is set by the competition between $\nu_e + n \to p + e^-$ and $\bar{\nu}_e + p \to n + e^+$ and the associated reversed processes. The rate of change of Y_e on an outflowing mass element may be written as [5]

$$\frac{dY_e}{dt} = v(r)\frac{dY_e}{dr} \simeq (\lambda_{\nu_e} + \lambda_{e^+})Y_n^f - (\lambda_{\bar{\nu}_e} + \lambda_{e^-})Y_p^f\ , \tag{2}$$

where $v(r)$ is the velocity of the outflowing mass element, t is the time parameter, λ_{ν_e} ($\lambda_{\bar{\nu}_e}$) is the forward rate of (anti-)neutrinos and λ_{e^-} (λ_{e^+}) the electron (positron) capture rate on free nucleons [5]. Since Y_e is a function of the neutrino-capture rates, it depends on the neutrino flavor evolution. Therefore, we have to consider the double feedback effect due to both these effects.

3 Results: early-cooling phase

Figure 1 shows the spectra without (with) oscillations on the top (bottom) for $\Delta m_{\rm atm} < 0$. Neutrino refractive contribution on the ν_e–ν_s conversion is minimal. After the ν_e–ν_s MSW conversion, the e–x difference spectrum is very asymmetric between neutrinos and antineutrinos, essentially suppressing collective conversions.

Figure 2 shows Y_e as a function of the radius for the cases without and with neutrino oscillations. The MSW flavor conversions lower the electron abundance.

4 Results: intermediate-cooling phase

Figure 3 shows the energy fluxes for $\Delta m^2_{\rm atm} < 0$. The ν_e–ν_x refractive energy difference caused by matter is now much smaller, allowing for MSW conversions between the two active flavors, in the neutrino sector for the chosen hierarchy. The neutrino background is responsible for increasing the $\bar{\nu}_e$ flux with respect to the case with only matter and averaging out the $\bar{\nu}_x$ and $\bar{\nu}_e$ fluxes.

In Fig. 4 the electron abundance is plotted as a function of the radius. The oscillations are responsible for an asymptotic value of Y_e lower than in the case without oscillations, and in particular collective effects make it even lower. The smaller value of Y_e due to sterile neutrinos could sensitively affect the nucleosynthesis in supernovae.

5 Conclusions

Motivated by the recent hints on sterile neutrinos, we assume the existence of one sterile family with the reactor anomaly mixing parameters and discuss for the first time the impact of ν_s on two active flavor evolution and on nucleosynthesis.

The sterile neutrino production is triggered by the MSW resonance between the active and the sterile sector. However for $t = 0.5$ s, no further flavor conversion is determined by ν–ν interactions because collective oscillations are suppressed. For $t = 2.9$ s, the ν–ν interactions do trigger further flavor conversions. For both the time slices discussed, Y_e is lower than in the case without oscillations and it could affect the nuclei formation.

Acknowledgments

The results presented here have been obtained in Ref. [6] in collaboration with G.G. Raffelt, L. Hüdepohl and H.-T. Janka. I.T. acknowledges support from Alexander von Humboldt Foundation and she is grateful to HAνSE 2011 organizers for kind hospitality.

References

[1] G. Mention *et al.*, Phys. Rev. D **83** (2011) 073006.

[2] P. Huber, Phys. Rev. **C84** (2011) 024617.

[3] L. Hüdepohl, B. Müller, H.-T. Janka, A. Marek and G. G. Raffelt, Phys. Rev. Lett. **104** (2010) 251101.

[4] G. Sigl, G. Raffelt, Nucl. Phys. **B406** (1993) 423-451.

[5] G. C. McLaughlin, G. M. Fuller, J. R. Wilson, Astrophys. J. **472** (1996) 440.

[6] I. Tamborra, G. G. Raffelt, L. Huedepohl and H. T. Janka, arXiv:1110.2104 [astro-ph.SR].

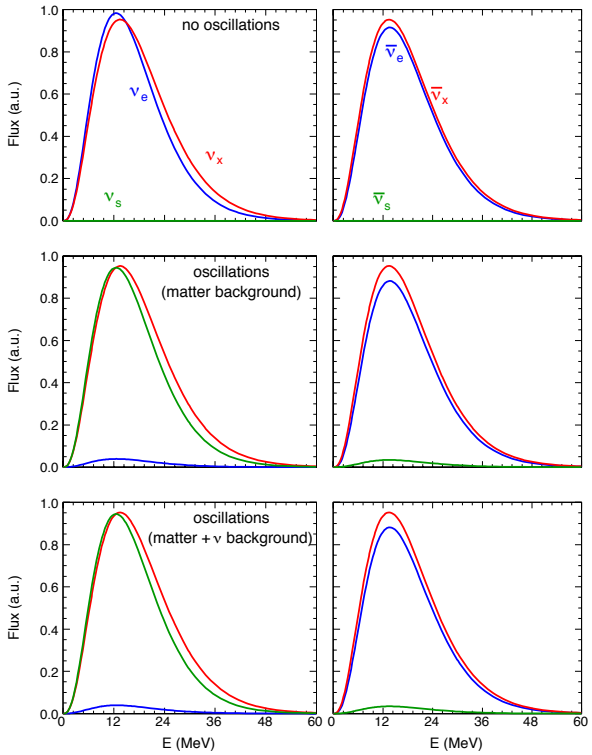

Figure 1: (color online) Spectra for neutrinos (left) and antineutrinos (right) in arbitrary unites (a.u.) for the 0.5 s model. Top: No oscillations (spectra at neutrino sphere). Middle: Oscillated spectra, including only the matter effect. Bottom: ν–ν interactions are also included, but cause no visible difference.

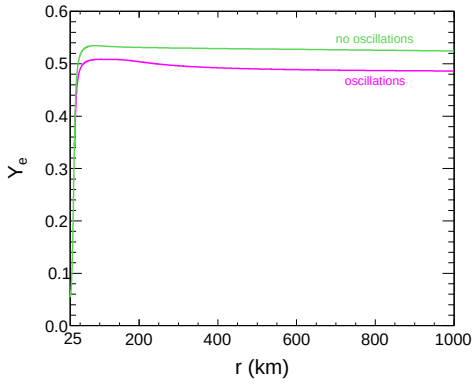

Figure 2: (color online) Electron abundance as a function of the radius at $t = 0.5$ s for the case with and without oscillations.

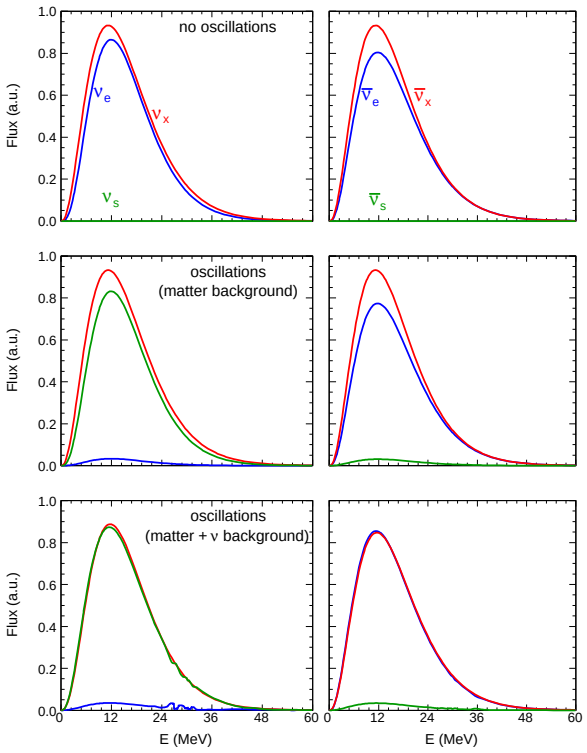

Figure 3: (color online) Energy spectra for $t = 2.9$ s, as in Fig. 1.

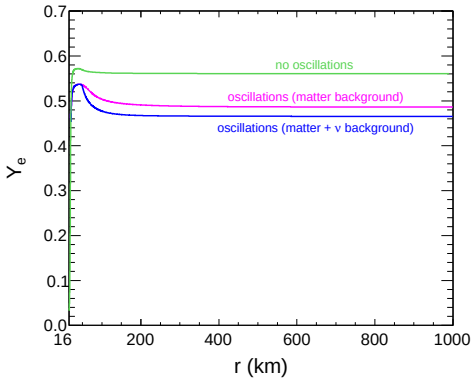

Figure 4: (color online) Electron abundance for $t = 2.9$ s, as in Fig. 2.

Turbulence and Supernova Neutrinos

James P. Kneller

Department of Physics, North Carolina State University, Raleigh,North Carolina 27695-8202, USA

DOI: http://dx.doi.org/10.3204/DESY-PROC-2011-03/kneller

As neutrinos propagate from the neutrinosphere through the mantle of a core-collapse supernova they will pass through regions of turbulence. The turbulence leads to stochastic neutrino flavor mixing thus leaving fingerprints in the Galactic supernova neutrino burst signal. In this talk I explore the effect of turbulence upon the neutrinos focusing upon the case of large amplitudes and demonstrate that the ensemble of S matrices that describe the neutrino evolution in this limit is Dyson's Circular Ensemble.

1 The signal from the next Galactic supernova

The progress in the field of supernova neutrino over the past decade has been impressive with a constant procession of important discoveries. For a review we refere the reader to Duan & Kneller [1]. We have discovered that the neutrino burst from the next supernova in our Galaxy is dynamic with information about both the neutrino and the supernova embedded within it. Decoding that signal will be a formidable challenge because of the many different processes which alter the neutrino spectra during their voyage to Earth: neutrino self interactions over the first 1000 km or so from the neutrinosphere, the effect of matter - the Mikheev-Smirnov-Wolfenstein (MSW) effect - with the added complication of turbulence, de-coherence as the neutrino propagates to Earth, and then Earth matter effects if the SN is 'shadowed' at the detector. The last two effects are well understood and are simple to account for; the first item on this list is a fascinating subject with a rich and evolving phenomenology and we refer the reader to the contributions by Baha Balantekin, Amol Dighe, Alessadro Mirizzi and Raymond Sawyer. The MSW effects too have been well studied and the expected signals of supernova features such as the shockwave have been described. That leaves the effect of turbulence (density fluctuations) which are not yet satisfactorily included in simulations of the expected neutrino signal because, a) we have little idea of what the turbulence in the supernova may look like, and b) we have no prescription for including turbulence in the signal. Having said this, the general effect of turbulence is well-known: turbulence tends to equilibrate the spectra of the different flavors. In the limit of total equilibration the spectra at Earth are a linear combination of the spectra at the neutrinosphere and thus the features in the spectra which are supposed to indicate unknown neutrino properties, neutrino phenomena such as collective effects, and supernova diagnostics such as the shock wave, are removed. A better understanding of turbulence effects upon supernova neutrinos and the implications for observables would be very desirable. This talk summarizes the work from Kneller & Volpe [3] and Kneller [4] and some more recent work which focused upon these problems.

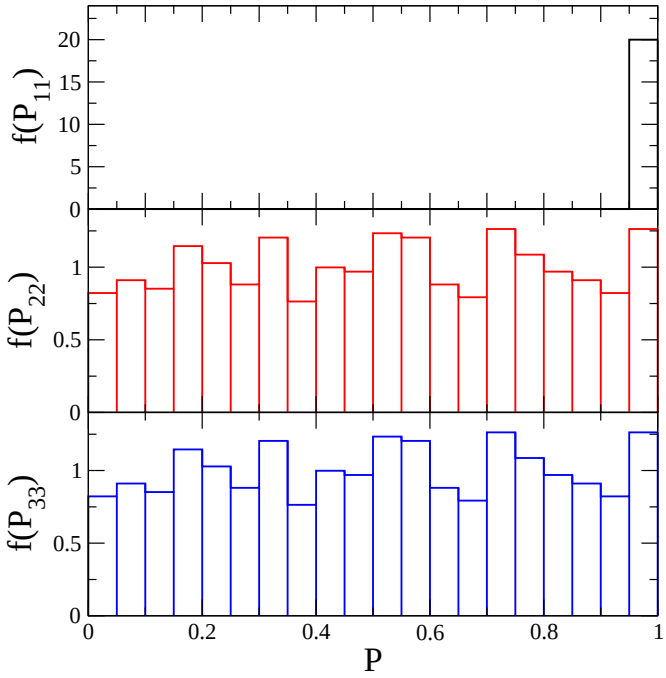

Figure 1: (color online) A normalized frequency histogram of 1012 calculations of P_{11} (top panel) P_{22} (middle panel) and P_{33} (bottom panel) for $E = 25$ MeV neutrinos. The hierarchy is normal, $\sin^2(2\theta_{13}) = 4 \times 10^{-4}$ and $C_\star^2 = 0.01$.

2 Turbulence in supernova

In multi-dimensional hydrodynamical simulations we see turbulence generated by aspherical flows through distorted shocks, convection, etc. For a description of the very interesting results of these simulations we refer the reader to the contributions by Bernhard Mueller, Stephan Bruenn, Thomas Janka and Christian Ott. In order to study the effect of this turbulence upon the neutrinos we obviously first need to have at hand density profiles with turbulence in them. Ideally we would gather such profiles from multi-dimensional hydrodynamical simulations but at present they are all focused upon the inner regions of the star and early times in order to discover the mechanism (or mechanisms) that leads to the explosion. But it is the outer regions, from ~ 1000 km to $\sim 10^7$ km, where the MSW effect occurs and where, several seconds into the signal, the shock wave will generate the turbulence that will most effect the neutrinos. Thus we are forced to take density profiles from one-dimensional simulations which do extend to the outer parts of the star and late times and insert turbulence into them. For this work we choose to model the turbulence as a Gaussian random field $F(r)$ with a rms amplitude $C_\star$ and we shall adopt a Kolmogorov power spectrum. To mimic the turbulence seen in multi-d hydro simulations we restrict the turbulence to the region between the forward and reverse shocks.

$$V_e(r) = (1 + F(r))\langle V_e(r)\rangle \tag{1}$$

The one-dimensional density profile $\langle V_e(r)\rangle$ we use here is the $t = 4.5$ s snapshot of the $Q = 3.36 \times 10^{51}$ erg model taken from Kneller, McLaughlin & Brockman [5].

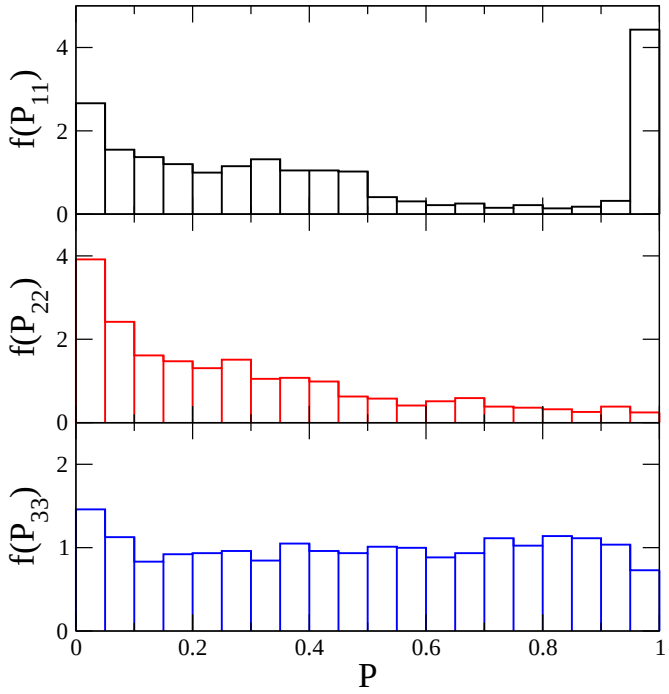

Figure 2: (color online) Normalized frequency distributions of the probabilities P_{11}, P_{22} and P_{33} of 1563 calculations. The hierarchy is normal, $C_\star^2 = 0.3$ and $E = 60$ MeV.

Now that we have our density profiles we have to run the neutrinos through them. The ν state at r is related to the initial state through an operator S and the probability that an initial state j is later detected as state i is given by the square amplitude of the appropriate element of S i.e. $P(\nu_j \to \nu_i) \equiv P_{ij} = |S_{ij}|^2$. The ideas and methods used to find S are described in Kneller & McLaughlin [2, 6]. For all results in this paper we set the oscillation frequencies and angles to $\delta m^2_{12} = 8\times10^{-5}\text{eV}^2$, $|\delta m^2_{23}| = 3\times10^{-3}\text{eV}^2$ and by $\sin^2 2\theta_{12} = 0.83$ and $\sin^2 2\theta_{23} = 1$ [7]. The value of the unknown angle θ_{13} will be given when a specific value is used in a calculation. These transition probabilities are not unique: each realization of the random field will give a different set of P_{ij}'s so in order to study the overall effect one needs to generate many many realizations and construct ensemble of S and the P_{ij}'s. From these ensembles one then extracts the transition probabilities as the neutrino exits the turbulence and construct histograms of the results. One such histogram is shown in Figure (1) for the case of relatively small turbulence amplitudes of 10%. The figure indicates that for small amplitudes the final state distributions are quasi two flavor: the transition probability P_{11} is always close to unity while the two probabilities P_{22} and P_{33} are consistent with uniform. But as we increase the amplitude of the turbulence the effect begins to change. For very large amplitudes we begin to see three-flavor effects that occur because we break HL factorization. Breaking HL factorization leads to a change in the distributions of the transition probabilities: the distributions begin to transit to a triangular shape albeit with relic quasi-two flavor features in the example shown in Figure (2).

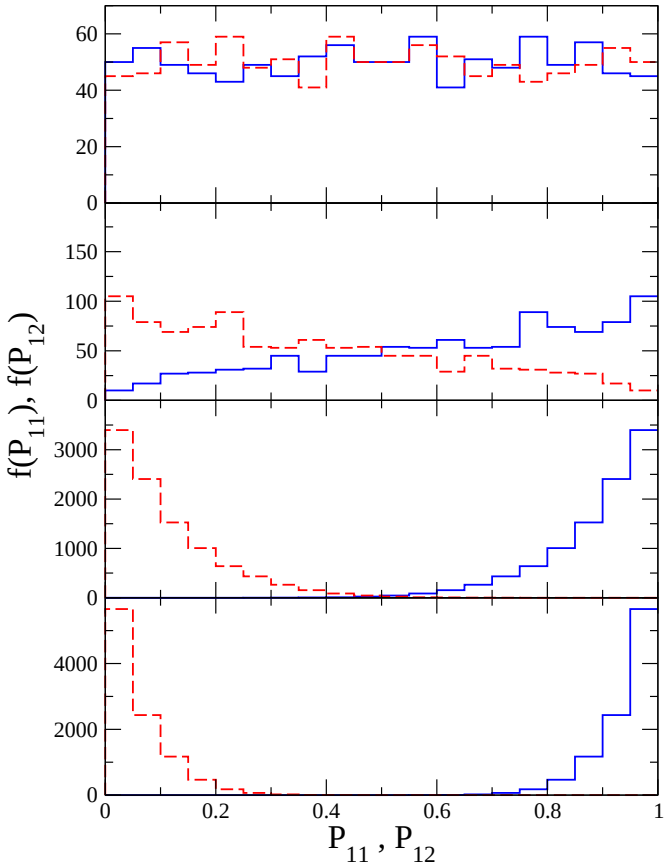

Figure 3: (color online) The distributions of the transition probabilities P_{11} (solid) and P_{12} (dashed) as a function of the number N of products of random 2×2 matrices. From bottom to top the panels are for $N = 1$, $N = 2$, $N = 10$ and $N = 100$.

3 Products of random unitary matrices

The results shown in Figures (1) and (2) correspond to two cases of flavor depolarization: one with 2 flavors and the other with 3. Depolarization means that there is no connection between the initial and final states: all final states are equally likely and when this occurs the ensemble of S matrices one has constructed is a realization of Dyson's Circular Unitary Ensemble CUE(N_f) [8] where N_f is the number of flavors. From this ansatz one can also show analytically [4] that the distribution of the set of probabilities P_{1j}, P_{2j}, ... for observing final states ν_1, ν_2 etc. is uniform over a standard N_f-1 simplex and after integrating over N_f-1 elements of the set one finds that the distribution f of a particular probability P_{ij} is $f(P_{ij}) = (N_f - 1)\,(1 - P_{ij})^{N_f - 2}$. The Circular Ensemble is also relevant to the distribution of the product of N random non-circular matrices in the limit where $N \to \infty$ which has a natural association with S matrices because S-matrices can be factored. So we can think about breaking the integration domain into N subdomains each with one MSW resonance. Each

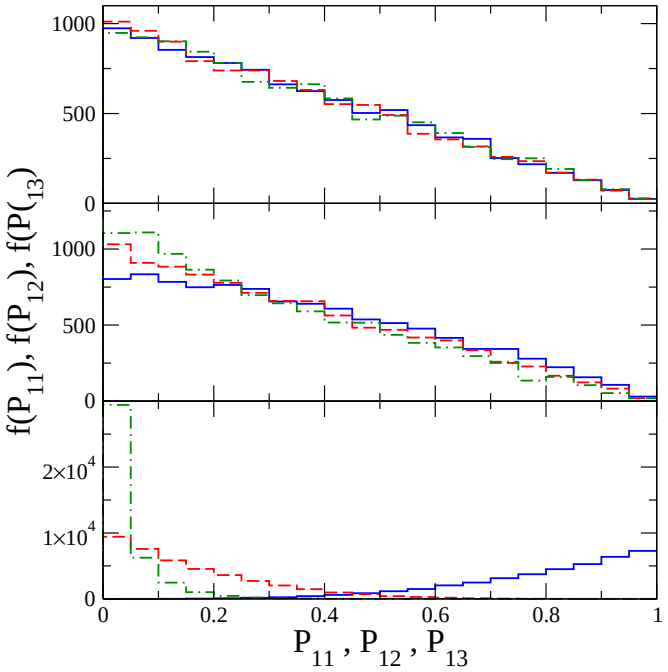

Figure 4: (color online) The distributions of the transition probabilities P_{11} (solid), P_{12} (dashed) and P_{13} (dashdot) as a function of the number N of products of random 3×3 matrices. From bottom to top the panels are for $N = 1$, $N = 10$ and $N = 100$.

domain is described by a S-matrix that we could regard as a random matrix. Thus the S matrix which describes the evolution through the entire turbulence region can be considered as the product of N random $N_f \times N_f$ matrices which individually are not necessarily from the Circular Ensemble. An ensemble of the matrix product of N random, unitary matrix factors is $CUE(N_f)$ as $N \to \infty$ for all distributions of the factors i.e. it is like the central limit theorem for random variates. An example calculation of an ensemble formed as the the product of N random 2×2 matrices is shown in Figure (3). The lowest panel shows the distribution of each matrix factor is diagonally dominant but as the number of products increases we end up with uniform distributions. Figure (4) shows the case of the product of N random 3×3 matrices and we see that as N becomes large we obtain triangular distributions.

4 Summary

The turbulence features very much depend upon the amplitude and the mixing parameters. For small amplitudes: turbulence is quasi two flavor, appears only in the H resonant channel. But for larger amplitudes turbulence breaks HL i.e. it is 3 flavor, and appears in non-resonant channel. Supernova turbulence amplitudes of order $\sim 1 - 10\%$ lead to two-flavor depolarization with uniform distributions. If the amplitudes are of order $\gtrsim 10\%$ or the turbulence extends over a much greater distance than expected then we transit to three-flavor depolarization with triangular distributions.

5 Acknowledgments

This work was supported by the DOE's Topical Collaboration in Nuclear Science "Neutrinos and Nucleosynthesis in Hot and Dense Matter".

References

[1] H. Duan and J. P. Kneller, J. Phys. G **36** 113201 (2009)

[2] J. P. Kneller and G. C. McLaughlin, Phys. Rev. D **73** 056003 (2006)

[3] J. P. Kneller, and C. Volpe, Phys. Rev. D **82** 123004 (2010)

[4] J. P. Kneller, arXiv:1004.1288 [hep-ph].

[5] J. P. Kneller, G. C. McLaughlin and J. Brockman, Phys. Rev. D **77** 045023 (2008)

[6] J. P. Kneller & G. C. McLaughlin, Phys. Rev. D **80** 053002 (2009)

[7] C. Amsler et al. [Particle Data Group], Phys. Lett. B **667** 1 (2008).

[8] F. J. Dyson, Journal of Mathematical Physics **3** 140 (1962)

Collective neutrino oscillations in supernovae: Matter suppression during the accretion phase

Alessandro Mirizzi, Sovan Chakraborty, Ninetta Saviano

II Institut für Theoretische Physik, Universität Hamburg, Luruper Chaussee 149, 22761 Hamburg, Germany

DOI: http://dx.doi.org/10.3204/DESY-PROC-2011-03/mirizzi

We carry out a detailed analysis of the supernova (SN) neutrino flavor evolution during the accretion phase (at post-bounce times $t_{pb} \leq 500$ ms), characterizing the SN ν signal by recent hydrodynamical simulations. We find that trajectory-dependent "multi-angle" effects, associated with the dense ordinary matter suppress collective oscillations, that would have been induced by $\nu - \nu$ interactions in the deepest SN regions. The matter suppression implies that neutrino oscillations will start outside the neutrino decoupling region and therefore will have a negligible impact on the neutrino heating and the explosion dynamics. Furthermore, the possible detection of the next galactic SN neutrino signal from the accretion phase, based on the usual Mikheyev-Smirnov-Wolfenstein effect in the SN mantle and Earth matter effects, can reveal the neutrino mass hierarchy in the likely case that the mixing angle θ_{13} is not very small.

1 Introduction

The total energy emitted in neutrinos (ν) and antineutrinos ($\bar{\nu}$) during a supernova (SN) explosion is of the order of several 10^{53} erg, making a stellar collapse the most powerful neutrino source in the Universe. The huge neutrino fluxes emitted from such an event represent a crucial tool to obtain information about the ν mixing parameters and to understand the dynamics of the exploding stellar core. In particular, one expects a strong sensitivity of the SN ν signal on the flavor conversions occurring in the stellar envelope. In this context, it has been recently realized that the description of neutrino flavor evolution in supernovae based on the only Mikheyev-Smirnov-Wolfenstein (MSW) effect with the ordinary matter is incomplete since SN neutrinos not only interact with the stellar medium but also with the other ν's and $\bar{\nu}$'s. It has been shown that $\nu - \nu$ interactions can give rise to collective ν flavor conversions occurring between the neutrino sphere ($r \sim 10 - 100$ km) and the MSW region ($r \sim 10^3 - 10^5$ km). The most important observational consequence of these collective oscillations would be a swap of the ν_e and $\overline{\nu}_e$ spectra with the non-electron ν_x and $\overline{\nu}_x$ spectra in certain energy ranges [1].

The development of these self-induced ν transformations crucially depends on the primary SN ν spectra. In this context, the post-bounce accretion phase of a core-collapse SN, lasting up to several hundreds of milliseconds for iron-core progenitors, might seem to offer the best opportunity to detect signatures of collective ν flavor oscillations. Indeed, the absolute ν fluxes during this phase are large with significant spectral differences between the ν species, and a flux

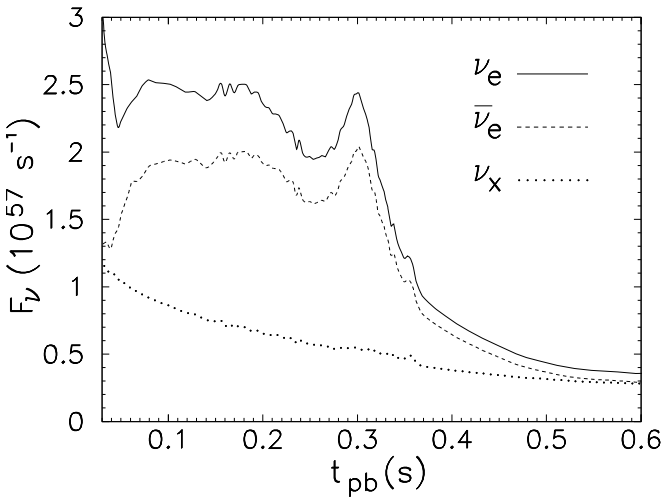

Figure 1: ν number fluxes during the accretion phase for a SN model with 10.8 $M_\odot$ progenitor mass from the Basel simulations [3].

order $F_{\nu_e} > F_{\overline{\nu}_e} \gg F_{\nu_x}$. However, the description of flavor conversions triggered by neutrino self-interactions is only in part true. In fact, as recently pointed out in [2], when the electron density n_e is not negligible with respect to the neutrino density n_ν, the large phase dispersion induced by the matter potential for ν's traveling on different trajectories will partially or totally suppress the collective oscillations through peculiar "multi-angle" effects.

Driven by this insight, we have performed a detailed study of the SN ν flavor evolution during the accretion phase, characterizing the ν signal and the matter density profiles by means of recent neutrino radiation hydrodynamics simulations [3]. Using this input, we find that the "multi-angle" effects, associated with the dense ordinary matter, suppress collective oscillations during the accretion phase. In particular, both the situations of complete (when $n_e \gg n_\nu$) or partial (when $n_e \gtrsim n_\nu$) matter suppression can be realized. In the following we will present these results and their consequences. This paper is based on our works [4, 5], to which we address the interested reader for further details.

2 Setup of the flavor evolution

We take as benchmark for the ν signal and for the matter density profile the results of the recent long-term SN simulations performed by the Basel group [3]. In Fig. 1 we show the evolution of the ν number fluxes F_{ν_α} for the different neutrino flavors ν_α up to 0.6 seconds after core bounce, for a 10.8 $M_\odot$ iron-core progenitor model.

Our description of the ν flavor conversions is based on a two-flavor scenario, driven by the atmospheric mass-square difference $\Delta m^2_{\rm atm} \simeq 2.6 \times 10^{-3}$ eV^2 and by a small (matter suppressed) in-medium mixing $\theta_{\rm eff} = 10^{-3}$. We work in the inverted ν mass hierarchy ($\Delta m^2_{\rm atm} = m^2_3 - m^2_{1,2} < 0$) and schematically we assume all the ν's to be emitted with the same energy $E = 15$ MeV. The impact of the non-isotropic nature of the ν emission on the flavor conversions is taken into account by "multi-angle" simulations, where one follows a large number [$\mathcal{O}(10^3)$]

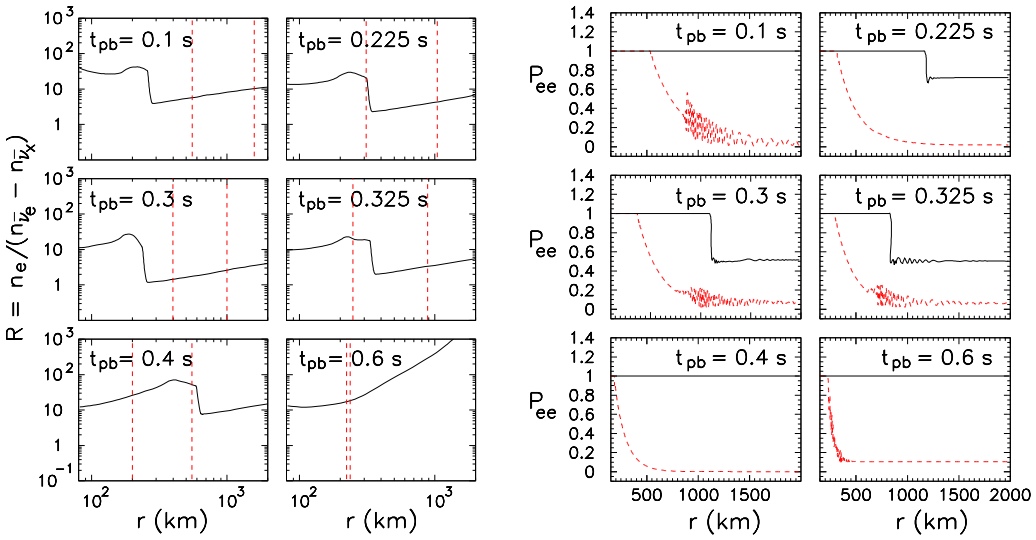

Figure 2: (color online) *Left panel*: Radial evolution of the ratio R between electron and neutrino densities at different post-bounce times. The two dashed vertical strips delimit the range where collective oscillations would arise in absence of matter effects. *Right panel*: Radial evolution of the survival probability P_{ee} for electron antineutrinos at different post-bounce times for the multi-angle evolution in presence of matter effects (continuous curve) and for $n_e = 0$ (dashed curve).

of intersecting ν trajectories.

The strength of the ν–ν interaction is given by $\mu_r = \sqrt{2} G_F \left[n_{\overline{\nu}_e}(r) - n_{\overline{\nu}_x}(r) \right]$ [6], where $n_{\nu_\alpha}(r) = F_{\nu_\alpha}/4\pi r^2$ is the number density of the species ν_α. The ν–ν potential is normalized at the neutrinosphere [$r_\nu \sim \mathcal{O}(10^2)$ km], where ν's are assumed to be isotropically emitted [6]. The matter potential is represented by $\lambda_r = \sqrt{2} G_F n_e(r)$, encoding the net electron density, $n_e \equiv n_{e^-} - n_{e^+}$.

3 Matter versus neutrino potential: analysis and results

In order to compare the strength of the matter and the neutrino potential, we show in Fig. 2 ratio $R = n_e/(n_{\overline{\nu}_e} - n_{\overline{\nu}_x})$ at selected post-bounce times (left panel). We realize that n_e is always larger than or comparable to $n_{\overline{\nu}_e} - n_{\overline{\nu}_x}$, suggesting that matter effects cannot be ignored during the accretion phase. Depending on the strength of the matter density, the matter suppression can be total, when $n_e \gg n_\nu$, or partial when the matter dominance is less pronounced. Finally, when $n_e \geq n_\nu$ the interference of the two comparable potentials leads to flavor equilibrium with a complete mixture of electron and non-electron species [2].

To validate these expectations, we show in the right panel of Fig. 2 the radial evolution of the $\bar{\nu}_e$ survival probability P_{ee} for the same post-bounce times used in the left panel. As predicted, we find that matter strongly suppresses the development of the self-induced flavor transformations. In particular, at $t_{\rm pb} = 0.1, 0.4, 0.6$ s, when $n_e \gg n_\nu$, the flavor conversions are completely blocked ($P_{ee} = 1$). Conversely, at $t_{\rm pb} = 0.225$ s, when $n_e \simeq 2 n_\nu$ in the conversions

region, the matter suppression is only partial giving a final $P_{ee} \simeq 0.75$. Finally at $t_{\rm pb} = 0.3, 0.325$ s, when $n_e \geq n_\nu$, matter effects produce a complete flavor mixture ($P_{ee} = 1/2$). This behavior suggests a time-dependent pattern for the ν conversions, i.e. complete-partial-complete suppression. For comparison, we also show the results in the case of $n_e = 0$ (light curves). One realizes that the difference with respect to the previous cases is striking.

4 Conclusions

Simulations of core-collapse SNe show that the matter density in the deepest stellar regions is large during the accretion phase before the onset the an explosion. This implies that self-induced neutrino flavor transformations are affected by the high matter density, through trajectory-dependent multi-angle effects [2]. In order to characterize the SN ν flavor evolution in this case, we performed a dedicated study, taking as benchmark for the SN neutrino emissivity and the matter profiles the results from the recent long-term core-collapse SN simulations from Ref. [3].

We find that the electron density n_e is never negligible in comparison to the neutrino density n_ν during the accretion phase. Contrarily to what shown in previous studies, based on the only ν-ν interaction effects, we find that the presence of a dominant matter term inhibits the development of collective flavor conversions. The matter suppression ranges from complete to partial, producing in principle time-dependent features. In particular, when it is complete (for post-bounce times $t_{\rm pb} \leq 0.2$ s in iron-core SNe) the ν signal will be processed only by the usual MSW effect in the SN mantle and Earth matter effects. This was the usual description before the inclusion of collective phenomena.

This *déjà vu* would reopen the possibility, prevented by self-induced effects, to reveal the neutrino mass hierarchy through the Earth matter effects on the next galactic SN neutrino burst, in the case θ_{13} is not very small. The matter suppression also implies that neutrino oscillations will start outside the neutrino decoupling region and therefore will have a negligible impact on the neutrino heating and the explosion dynamics.

Acknowledgments

This work was supported by the German Science Foundation (DFG) within the Collaborative Research Center 676 “Particles, Strings and the Early Universe”.

References

[1] G. L. Fogli, E. Lisi, A. Marrone and A. Mirizzi, JCAP **0712**, 010 (2007) [arXiv:0707.1998 [hep-ph]].

[2] A. Esteban-Pretel, A. Mirizzi, S. Pastor, R. Tomas, G. G. Raffelt, P. D. Serpico and G. Sigl, Phys. Rev. D **78**, 085012 (2008) [arXiv:0807.0659 [astro-ph]].

[3] T. Fischer, S. C. Whitehouse, A. Mezzacappa, F. K. Thielemann and M. Liebendorfer, Astron. Astrophys. **517**, A80 (2010). [arXiv:0908.1871 [astro-ph.HE]].

[4] S. Chakraborty, T. Fischer, A. Mirizzi, N. Saviano and R. Tomas, Phys. Rev. Lett. **107**, 151101 (2011) [arXiv:1104.4031 [hep-ph]].

[5] S. Chakraborty, T. Fischer, A. Mirizzi, N. Saviano and R. Tomas, Phys. Rev. D **84**, 025002 (2011) [arXiv:1105.1130 [hep-ph]].

[6] A. Esteban-Pretel, S. Pastor, R. Tomas, G. G. Raffelt and G. Sigl, Phys. Rev. D **76**, 125018 (2007) [arXiv:0706.2498 [astro-ph]].

Flavor Stability Analysis of Supernova Neutrino Fluxes Compared with Simulations

Srdjan Sarikas[1,2,3], *Georg G. Raffelt*[3]

[1]Dipartimento di Scienze Fisiche, Università di Napoli "Federico II", 80126 Napoli, Italy
[2]Istituto Nazionale di Fisica Nucleare — Sezione di Napoli, 80126 Napoli, Italy
[3]Max-Planck-Institut für Physik, Föhringer Ring 6, 80805 München, Germany

DOI: http://dx.doi.org/10.3204/DESY-PROC-2011-03/sarikas

We apply a linearized stability analysis to simplified models of accretion-phase neutrino fluxes streaming from a supernova. We compare the results with recent numerical studies and find excellent agreement. This provides confidence that a linearized stability analysis can be further applied to more realistic models.

1 Introduction

Neutrino-neutrino interactions cause the neutrino flux evolution close to a supernova (SN) core to be nonlinear and numerically very challenging [1]. The flavor instability causing collective flavor conversions can be suppressed by the "multi-angle matter effect" [2]. This point was recently investigated numerically for an accretion-phase model where the matter density near the neutrino sphere is large, using a schematic description of the neutrino fluxes [3]. On the other hand, the flavor stability can also be investigated with a linearized stability analysis, avoiding an explicit solution of the equations of motion [4]. We apply this method to the models of Ref. [3] and find excellent agreement of the stable regime identified with either method.

2 Linearized stability analysis

We describe the neutrino flavor evolution in terms of matrices $\mathsf{\Phi}_{E,u,r}$ where the diagonal elements are the usual total number fluxes and the off-diagonal elements encode phase information [2, 5]. We label the angular dependence with u, in close relation with the neutrino emission angle ϑ_R at the inner boundary radius R, $u = \sin^2\vartheta_R = (1-\cos^2\vartheta_r)\,r^2/R^2$. For semi-isotropic emission at a "neutrino sphere" with radius R, the flux is uniformly distributed on $0 \leq u \leq 1$. The equations of motion are $\mathrm{i}\partial_r \mathsf{\Phi}_{E,u,r} = [\mathsf{H}_{E,u,r}, \mathsf{\Phi}_{E,u,r}]$, with the Hamiltonian [4]

$$\mathsf{H}_{E,u,r} = \left(\frac{\mathsf{M}^2}{2E} + \sqrt{2}\,G_{\rm F}\mathsf{N}_\ell\right)\frac{1}{v_{u,r}} + \frac{\sqrt{2}\,G_{\rm F}}{4\pi r^2}\int_0^1 \mathrm{d}u' \int_{-\infty}^{+\infty} \mathrm{d}E' \left(\frac{1}{v_{u,r}v_{u',r}} - 1\right) \mathsf{\Phi}_{E',u',r}\,,$$

where M^2 is the neutrino mass-squared matrix, N_ℓ the matrix of net charged-lepton densities which in the flavor basis is $\mathsf{N}_\ell = \mathrm{diag}(n_e - n_{\bar e}, n_\mu - n_{\bar\mu}, n_\tau - n_{\bar\tau})$ and $v_{u,r}$ is the radial projection of neutrino velocity at the radius r. Antineutrinos are represented through negative-energy modes

($E < 0$) and negative negative fluxes in the matrices $\Phi_{E,u,r}$. This sign convention simplifies the formalism and obviates any distinction between neutrinos and antineutrinos.

Henceforth we drop the explicit subscript r to denote the r-dependence of all quantities. In the two flavor scenario one can write:

$$\Phi_{E,u} = \frac{\mathrm{Tr}\,\Phi_{E,u}}{2} + \frac{F^e_{E,u,R} - F^x_{E,u,R}}{2}\,\mathsf{S}_{E,u}\ ,$$

where $F^{e,x}_{E,u}$ are the differential neutrino fluxes at the inner boundary radius R for the e and x flavors. The flux summed over all flavors, $\mathrm{Tr}\,\Phi_{E,u}$, drops out of the equations of motion and is conserved in our free-streaming limit. The "swapping matrix"

$$\mathsf{S}_{E,u} = \begin{pmatrix} s_{E,u} & S_{E,u} \\ S^*_{E,u} & -s_{E,u} \end{pmatrix}\ ,$$

encodes the flavor evolution with initial conditions $s = 1$ and $S = 0$.

We expand the Hamiltonian for large distances from the core and small mixing angle. After dropping its trace we find

$$\begin{aligned}
H^{\rm vac}_{E,u} &= \frac{\mathsf{M}^2}{2E}\,v_u^{-1} \to \pm\frac{\omega}{2}\begin{pmatrix}\cos 2\theta & \sin 2\theta \\ \sin 2\theta & -\cos 2\theta\end{pmatrix} v_u^{-1} \to \pm\frac{\omega}{2}\begin{pmatrix}1 & 0 \\ 0 & -1\end{pmatrix}\left(1 + \frac{u}{2}\,\frac{R^2}{r^2}\right)\ , \\
H^{\rm m}_{E,u} &= \sqrt{2}\,G_{\rm F}\begin{pmatrix}n_e - n_{\bar e} & 0 \\ 0 & 0\end{pmatrix} v_u^{-1} \to \frac{\tilde\lambda}{2}\begin{pmatrix}1 & 0 \\ 0 & -1\end{pmatrix}\left(1 + \frac{u}{2}\,\frac{R^2}{r^2}\right)\ , \\
H^{\nu\nu}_{E,u} &\to \frac{\sqrt{2}\,G_{\rm F}\,R^2}{4\pi r^4}\int_0^1 {\rm d}u'\,\frac{u+u'}{2}\int_{-\infty}^{+\infty}{\rm d}E'\,\frac{F^e_{E,u,R} - F^x_{E,u,R}}{2}\,\mathsf{S}_{E',u'}\ .
\end{aligned}$$

where $\tilde\lambda = \sqrt{2}\,G_{\rm F}\,(n_e - n_{\bar e})$. We write the neutrino-neutrino part concisely in the form $H^{\nu\nu}_{E,u} \equiv \mu_r \int_0^1 {\rm d}u'\,\frac{1}{2}(u+u')\int_{-\infty}^{+\infty}{\rm d}E'\,g_{E,u}\,\mathsf{S}_{E',u'}$, where $\mu_r = \mu_R\,R^4/2r^4$ encodes the strength of the neutrino-neutrino interaction with the parameter $\mu_R = \sqrt{2}\,G_{\rm F}(F^{\bar\nu_e}_R - F^{\nu_x}_R)/4\pi R^4$. We further define the dimensionless flavor difference spectrum $g_{E,u} = (F^e_{E,u,R} - F^x_{E,u,R})/(F^{\bar\nu_e}_R - F^{\nu_x}_R)$ with the normalization in the antineutrino sector $\int_{-\infty}^0 {\rm d}E\int_0^1 {\rm d}u\,g_{E,u} = -1$. The integration over neutrinos (positive energies) gives $\int_0^\infty {\rm d}E\int_0^1 {\rm d}u\,g_{E,u} = (F^{\nu_e}_R - F^{\nu_x}_R)/(F^{\bar\nu_e}_R - F^{\nu_x}_R) \equiv 1 + \varepsilon$, with ε being asymmetry of the spectra.

Next we expand the equations in the small-amplitude limit $|S| \ll 1$ which implies, to linear order, $s = 1$. After switching to the variable $\omega = \Delta m^2/2E$ for the energy modes one finds [4]

$$\mathrm{i}\partial_r S_{\omega,u} = [\omega + u(\lambda + \varepsilon\mu)]\,S_{\omega,u} - \mu\int {\rm d}u'\,{\rm d}\omega'\,(u+u')\,g_{\omega' u'}\,S_{\omega',u'}\ .$$

Here $\lambda = \tilde\lambda R^2/2r^2$ encodes the imprint of multi-angle matter effect. Except for the additional two powers of r^{-1} this quantity describes the SN density profile and scales approximately as $\mu_r \propto r^{-4}$.

Writing solutions of the linear differential equation in the form $S_{\omega,u} = Q_{\omega,u}\,e^{-\mathrm{i}\Omega r}$ with complex frequency $\Omega = \gamma + \mathrm{i}\kappa$ and eigenvector $Q_{\omega,u}$ leads to the eigenvalue equation [4],

$$(\omega + u\bar\lambda - \Omega)\,Q_{\omega,u} = \mu\int du'\,d\omega'\,(u+u')\,g_{\omega' u'}\,Q_{\omega',u'}\ ,$$

where $\bar\lambda \equiv \lambda + \varepsilon\mu$. The solution has to be of the form $Q_{\omega,u} = (A + Bu)/(\omega + u\bar\lambda - \Omega)$. Solutions exist if $\mu^{-1} = I_1 \pm \sqrt{I_0 I_2}$, where $I_n = \int d\omega\,du\,g_{\omega,u}\,u^n/(\omega + u\bar\lambda - \Omega)$. The system is stable if all Ω are purely real. A possible imaginary part, κ, is the exponential growth rate.

3 Results

We aim at comparing the linearized stability analysis with the numerical solutions of Ref. [3] who numerically solved the neutrino flavor evolution for a $10.8\,M_\odot$ model at various post bounce times. They confirmed the multi-angle matter suppression of self-induced flavor conversion, but also found partial conversions at a large radius for the models $200\,\mathrm{ms} \lesssim t_{\mathrm{pb}} \lesssim 300\,\mathrm{ms}$.

We use the same schematic half-isotropic and monochromatic spectra, leading to the simple form $g_{\omega,u} = -\delta(\omega+\omega_0) + (1+\varepsilon)\,\delta(\omega-\omega_0)$. The integrals I_n can now be evaluated analytically. Then it is easy to find a solution (γ,κ) for each pair (μ,λ). Figure 1 shows the region where $\kappa \neq 0$ for two snapshots together with the κ isocontours. We also show the "SN trajectory" in the (μ,λ) plane, i.e. essentially the density profile as a function of radius because $\mu_r \propto r^{-4}$.

Our results agree with the numerical solutions of Ref. [3] for all models. Whenever the numerical solutions find no flavor conversion, our SN trajectory indeed stays clear of the unstable regime. Conversely, when it briefly enters the unstable regime as in the left panel of Fig. 1, we reproduce the onset radius for partial flavor conversion of Ref. [3]. The linear stability analysis correctly explains the numerical results.

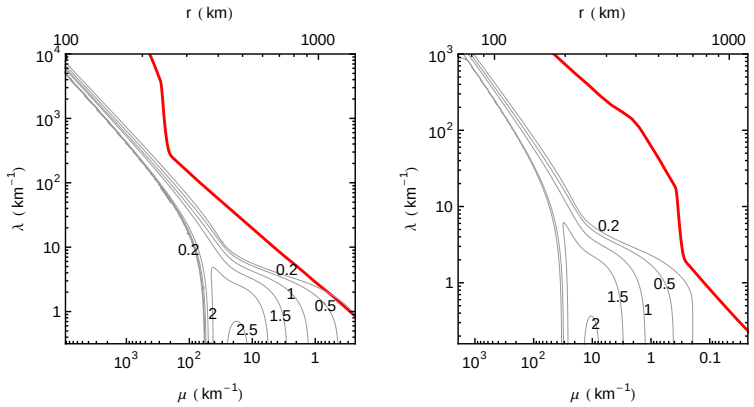

Figure 1: (color online) Contours of κ and the trajectory of SN (thick red line) at $t = 300$ ms (left) and 400 ms (right) post bounce for a $10.8\,M_\odot$ model discussed in Ref. [3].

It is interesting that in principle the SN trajectory can enter the instability region twice. As a toy model we consider the density profile $\lambda \sim 0.43\,\mu$ with half-isotropic emission at $R = 10$ km and $\mu_r = 7\times10^4\ \mathrm{km}^{-1}\ R^4/2r^4$. In Fig. 2 we show $\kappa(r)$ and the evolution of the off-diagonal element $|S|$. Indeed $|S|$ oscillates and grows in the unstable regime, only oscillates when $\kappa = 0$, and then grows again during the second instability crossing. It remains to be seen if there are realistic density profiles where such a multiple instability situation exists in practice.

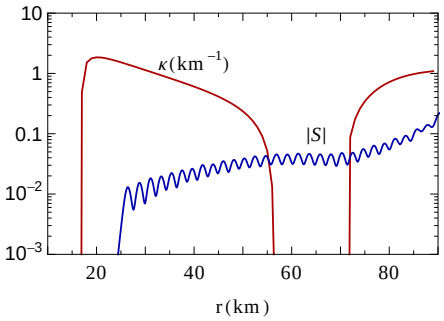

Figure 2: (color online) Growth rate κ and off-diagonal element $|S|$ for a toy model (see text).

4 Conclusions

The nonlinear neutrino flavor evolution in the SN environment can be a challenging numerical task even when it only consists of post-processing the output of a self-consistent SN simulation, not to mention solving self-consistently the multi-flavor neutrino transport. The latter is not necessary if collective oscillations do not happen in the critical region below the shock wave. The question if a given SN model with concomitant neutrino fluxes is stable against self-induced flavor conversion can be answered with a linearized stability analysis [4]. Of course, if the model is unstable, one needs to solve the equations numerically to find the final outcome. However, since neutrino fluxes during the accretion phase may well be stable because of the multi-angle matter effect, a linearized flavor stability analysis is here a useful tool.

We have applied this method to the models studied in Ref. [3] and compared with the outcome of their numerical solutions. The results are very encouraging in that we can perfectly account for the results of the numerical simulations and can also predict the onset radius for those cases where partial flavor conversion occurs at a large radius.

Meanwhile we have applied this method to an accretion-phase model with realistic energy and angle distributions [5]. We find that a stability diagram in the form of our Fig. 1 is an excellent tool to summarize the flavor stability situation of SN neutrino fluxes.

5 Acknowledgments

We thank Sovan Chakraborty and collaborators for providing us their SN models and Irene Tamborra and Javier Redondo for comments on the manuscript. We also thank the organizers of the HAνSE 2011 workshop for a very informative meeting and the opportunity to present our results on very short notice. Partial support by the Deutsche Forschungsgemeinschaft under grants TR 27 and EXC 153 is acknowledged.

References

[1] H. Duan, G. M. Fuller and Y.-Z. Qian, "Collective neutrino oscillations," Ann. Rev. Nucl. Part. Sci. **60** (2010) 569.

[2] A. Esteban-Pretel, A. Mirizzi, S. Pastor, R. Tomàs, G. G. Raffelt, P. D. Serpico and G. Sigl, "Role of dense matter in collective supernova neutrino transformations," Phys. Rev. D **78** (2008) 085012.

[3] S. Chakraborty, T. Fischer, A. Mirizzi, N. Saviano and R. Tomàs, "Analysis of matter suppression in collective neutrino oscillations during the supernova accretion phase," Phys. Rev. D **84** (2011) 025002.

[4] A. Banerjee, A. Dighe and G. G. Raffelt, "Linearized flavor-stability analysis of dense neutrino streams," Phys. Rev. D **84** (2011) 053013.

[5] S. Sarikas, G. G. Raffelt, L. Hüdepohl and H.-T. Janka, "Flavor stability of a realistic accretion-phase supernova neutrino flux," arXiv:1109.3601.

Chapter 3

Phenomenology and Detection Strategies

Convenors:

Kate Scholberg
Michael Wurm

Signatures of supernova neutrino oscillations

Amol Dighe

Tata Institute of Fundamental Research, Homi Bhabha Road, Mumbai 400005, India

DOI: http://dx.doi.org/10.3204/DESY-PROC-2011-03/dighe

After a brief review of our current understanding of neutrino flavor conversions inside a core collapse supernova, we analyze the signatures of these neutrino oscillations that can be observed at future large neutrino detectors. We examine the observability of model-independent signatures like the neutronization burst suppression, multiple spectral splits, earth matter effects, and shock wave effects. We also indicate some indirect oscillation signals, and comment on the effect of oscillations on supernova astrophysics. Finally we point out the features in the neutrino spectra that experiments should look for, even irrespective of their theoretical interpretations.

1 Introduction

Neutrinos emitted from a core collapse supernova and arriving at a detector on the earth undergo flavor conversions in three distinct regions. Inside the star, the collective effects due to neutrino-neutrino interactions [1, 2] and the MSW matter effects due to neutrino-matter interactions [3] drive the flavor transformations. Between the star and the earth, the neutrino mass eigenstates travel independently so that there are no effective flavor conversions. If the neutrinos have to pass through the earth before reaching the detector, further neutrino oscillations due to the MSW matter effects take place inside the earth.

Our understanding of the neutrino flavor conversions inside the star has undergone significant changes in the last decade, and some gaps are yet to be comprehensively filled in. The analyses around the turn of the century were carried out under the assumption that the flavor conversions mainly take place in the MSW resonance regions H and L in the mantle, around densities of $\rho_H \sim 10^{3-4}$ g/cc and $\rho_L = 1 - 10$ g/cc, respectively. The neutrino spectra arriving at the earth are then sensitive to the neutrino mass hierarchy and to the value of θ_{13}, for $\sin^2\theta_{13}$ as low as 10^{-5} [4, 5]. The flavor conversion probabilities are independent of the primary fluxes in this scenario.

However the neutrino-neutrino forward scattering interactions just outside the neutrinosphere, where $\rho \sim 10^{6-10}$ g/cc, can trigger self-induced flavor conversions [6] and give rise to significant flavor transformations [7]. These *collective effects* manifest themselves in the form of qualitatively new phenomena like synchronized oscillations [8], bipolar/pendular oscillations [9], and spectral splits [10, 11]. These collective flavor conversions are possible even for $\sin^2\theta_{13}$ as low as 10^{-10} or even lower, since the pendular oscillations can be triggered by even a small instability [12]. However the neutrino flavor conversion probabilities now depend strongly on the primary neutrino fluxes. Initial investigations into the collective effects suggested that, while these collective oscillations would be virtually ineffective for normal hierarchy (NH), in the inverted hierarchy (IH) they would result in the complete swapping of $\bar{\nu}_e$ and $\bar{\nu}_\mu$ spectra. In

addition, the ν_e and ν_μ spectra would be completely swapped for $E > E_c$ and unaffected for $E < E_c$ for a critical energy E_c [10]. The sharp change in the spectrum at $E = E_c$ is the spectral split.

It was later realized [13] that the phenomenon of a single spectral split at $E = E_c$ is a valid outcome only under special circumstances, for example, when $L_{\nu_e} \approx L_{\bar{\nu}_e} \gtrsim L_{\nu_\mu}$. In the general case, multiple spectral splits would take place, i.e. both $\nu_e \leftrightarrow \nu_y$ and $\bar{\nu}_e \leftrightarrow \bar{\nu}_y$ swaps ($\nu_y = \cos\theta_{23}\nu_\mu + \sin\theta_{23}\nu_\tau$) occur, in sharply separated energy regions. In addition, three-flavor effects [14, 15] tend to give rise to even $\nu_e \leftrightarrow \nu_x$ and $\bar{\nu}_e \leftrightarrow \bar{\nu}_x$ swaps ($\nu_x = -\sin\theta_{23}\nu_\mu + \cos\theta_{23}\nu_\tau$). The swapped and unswapped energy regions depend on primary fluxes and mass hierarchy. Combined with the MSW effects, these collective effects can give rise to many distinctive features in the ν_e and $\bar{\nu}_e$ spectra at the detector [16].

Most of the initial results with the inclusion of collective effects, both analytical and numerical, were obtained using the so-called single-angle approximation. With more detailed numerical simulations, it has become apparent that the *multi-angle* effects [7] can also have an impact: they can smoothen the flavor conversion features [17] and may even suppress the flavor conversions themselves [18, 19, 20, 21, 22]. The collective effects due to neutrino-matter interactions also come into play when multi-angle effects are included. The analytical understanding of these multi-angle effects is still a work in progress.

The aim of this talk is to analyze possible signatures of supernova neutrino oscillations at future large neutrino detectors, The first step is to determine what are the observables to look for. As we shall see, these observables can be identified with the knowledge of some broad features of the collective as well as MSW effects on neutrino oscillations. The feasibility of the relevant observations, and their interpretation in terms of neutrino mixing parameters, is where the detailed understanding of the neutrino flavor conversions becomes crucial. We shall start with a review of these flavor conversions in Sec. 2, and examine the relevant observables at the detectors in Sec. 3. We shall conclude in Sec. 4 with a summary and an outlook towards future.

2 Flavor conversions of supernova neutrinos

The simulations of supernova explosions still give rather varied predictions for the primary neutrino fluxes [23]. While they all agree on approximately thermal flavor spectra, and on the hierarchy of average energies $\langle E^0_{\nu_e}\rangle < \langle E^0_{\bar{\nu}_e}\rangle < \langle E^0_{\nu_\mu,\nu_\tau}\rangle \approx \langle E^0_{\bar{\nu}_\mu,\bar{\nu}_\tau}\rangle$, they differ in the actual values of these average energies. One typically has $\langle E^0_{\nu_e}\rangle \approx 10 - 12$ MeV, $\langle E^0_{\bar{\nu}_e}\rangle \approx 12 - 15$ MeV and $\langle E^0_{\nu_\mu}\rangle \approx 15 - 20$ MeV. These values also depend on the mass of the progenitor star. The relative luminosities of the flavors are also uncertain; though all the simulations agree on equal luminosities $L_{\nu_\mu}, L_{\nu_\tau}, L_{\bar{\nu}_\mu}$ and $L_{\bar{\nu}_\tau}$, and approximately equal luminosities L_{ν_e} and $L_{\bar{\nu}_e}$. The total energy released in neutrinos is $\sim 10^{53}$ erg. While discussing supernova neutrinos, it is convenient to talk in terms of the *flavors* ν_x and ν_y mentioned above. In the limit $\theta_{13} \to 0$, the states ν_x and ν_y are also mass eigenstates. Clearly, $\langle E^0_{\nu_x}\rangle \approx \langle E^0_{\nu_y}\rangle \approx \langle E^0_{\bar{\nu}_x}\rangle \approx \langle E^0_{\bar{\nu}_y}\rangle$ and $L_{\nu_x} \approx L_{\nu_y} \approx L_{\bar{\nu}_x} \approx L_{\bar{\nu}_y}$.

A neutrino ensemble may be described in the language of the occupation number matrices $\varrho(\vec{p})$ in the flavor basis [24, 2]. Its evolution may be described in terms of the effective

Hamiltonian $H(\vec{p}) = H_{vac}(\vec{p}) + H_{\rm MSW} + H_{\nu\nu}(\vec{p})$, where

$$\begin{aligned} H_{vac}(\vec{p}) &= M^2/(2p) \,, \\ H_{\rm MSW} &= \sqrt{2} G_F n_{e^-} diag(1,0,0) \,, \\ H_{\nu\nu}(\vec{p}) &= \sqrt{2} G_F \int \frac{d^3q}{(2\pi)^3} (1-\cos\theta_{pq}) \big(\varrho(\vec{q}) - \bar{\varrho}(\vec{q})\big) \,. \end{aligned} \tag{1}$$

Here θ_{pq} is the angle between the vectors $\vec{p}$ and $\vec{q}$. The first term $H_{vac}(\vec{p})$ arises from the neutrino mixing in vacuum, the second term $H_{\rm MSW}$ from the neutrino-matter interactions, and the last term $H_{\nu\nu}(\vec{p})$ from the neutrino-neutrino interactions. The equations of motion are

$$i\frac{\partial}{\partial t}\varrho(\vec{p}) = [H(\vec{p}), \varrho(\vec{p})] \,. \tag{2}$$

Note that $H(\vec{p})$ and $\varrho(\vec{p})$ are 3×3 matrices. The term $H_{\nu\nu}$ depends on ϱ itself, and hence makes the equations of motion nonlinear. In addition, the integration over $\vec{q}$ is rather complicated (and numerically time-consuming) due to the presence of $\varrho(\vec{q})$ terms in the integrand.

A simplifying assumption often used is the so-called *single-angle* approximation, where all the neutrinos at a given location are taken to be subject to the same average $\nu\nu$ potential, irrespective of their momentum $\vec{p}$. This is equivalent to an effective averaging of the factor of $(1-\cos\theta_{pq})$. As we shall see below, this approximation is enough to bring out many qualitative features of the evolution of the neutrino ensemble, however for a complete understanding of the flavor conversions, the complete multi-angle treatment is essential.

2.1 Oscillations due to collective effects

2.1.1 Collective effects with single-angle approximation

With the single-angle approximation, the neutrino-neutrino term in the Hamiltonian is dominant just outside the neutrinosphere, where the neutrinos have started free-streaming. The only effect of the neutrino-matter term in this region is the suppression of the effective mixing angle θ_{13}. In an iron-core supernova, the collective phenomena of synchronized oscillations, bipolar/pendular oscillations and spectral splits occur sequentially [17], followed by the MSW flavor conversions that occur mainly in the resonance layers in the mantle. The suppressed θ_{13} in matter implies that the flavor conversions are extremely small in the synchronization phase. However even a small θ_{13} is enough to cause a nonlinear instability in certain situations and start significant flavor conversions. This culminates in the formation of one or more spectral splits [10, 13].

The three-flavor effects can be roughly factorized into two-flavor effects that take place in a sequential manner [25]. The $\nu_e \leftrightarrow \nu_y$ and $\bar{\nu}_e \leftrightarrow \bar{\nu}_y$ pendular oscillations and spectral swaps are complete first, while the $\nu_e \leftrightarrow \nu_x$ and $\bar{\nu}_e \leftrightarrow \bar{\nu}_x$ pendular oscillations and spectral swaps occur later. These later swaps [14] (sometimes referred to as the *solar* swaps) are more likely to be incomplete or non-adiabatic, however they can sometimes effectively reverse the earlier $\nu_e \leftrightarrow \nu_y$ swaps, at least partially [15].

The net effect of collective oscillations is then a series of alternate swapped and unswapped regions in the ν_e and $\bar{\nu}_e$ spectra. The swaps may be incomplete in some cases. The locations and widths of the swapped/unswapped regions depend on the primary spectra. Assuming the equality of the luminosities of primary ν_e and $\bar{\nu}_e$ spectra (observed in most of the simulations),

the numerical investigation of the pattern of these swapped regions leads to the following observations [26]: When the electron flavor dominates in the primary fluxes, i.e. $L_{\nu_e} > L_{\nu_\mu}$, one obtains (i) no spectral split for NH, and (ii) single spectral splits arising from $\nu_e \leftrightarrow \nu_y$ and $\bar{\nu}_e \leftrightarrow \bar{\nu}_y$ swaps in the neutrino and antineutrino channels, respectively, for IH. On the other hand, when the non-electron flavors dominate, i.e. $L_{\nu_e} < L_{\nu_\mu}$, one gets (i) single spectral splits arising from $\nu_e \leftrightarrow \nu_y$ and $\bar{\nu}_e \leftrightarrow \bar{\nu}_y$ swaps in the neutrino and antineutrino channels, respectively, for NH, and (ii) up to two spectral splits, both in the neutrino and antineutrino channels: arising from $\nu_e \leftrightarrow \nu_y, \nu_e \leftrightarrow \nu_x$ and $\bar{\nu}_e \leftrightarrow \bar{\nu}_y, \bar{\nu}_e \leftrightarrow \bar{\nu}_x$ swaps, respectively, for IH. The incompleteness of some of the swaps may lead to a possible energy dependence in the swapped energy regime.

2.1.2 Multi-angle effects on collective oscillations

Though most of the qualitative features of the collective effects may be obtained with a single-angle approximation, the numerical multi-angle simulations have indicated that the multi-angle effects can be significant in certain situations. Typically, multi-angle effects smear the sharp features in the spectra [17]. Large neutrino densities but low $\nu - \bar{\nu}$ asymmetry may give rise to additional instabilities that would have been absent with the single-angle approximation, further leading to multi-angle decoherence [18]. Very high neutrino densities also tend to delay the onset of pendular oscillation [19]. Moreover, with multi-angle effects included, the role of matter density is not restricted to the suppression of effective θ_{13}. Indeed, large matter densities, as may be possible in the accretion phase, also tend to cause multi-angle decoherence [20]. It is possible that such large densities may lead to a complete suppression of collective oscillations deep inside the core during the accretion phase [21]. The multi-angle effects thus change the picture of when the collective oscillations start and how they develop. Recent multi-angle numerical simulations [19] seem to suggest that while the onset of large oscillations may be delayed by large multi-angle effects of the neutrino or matter background, the final spectra look like smeared versions of the single-angle predictions.

The task of analytically understanding all the features of multi-angle effects seems intractable, primarily because of the nonlinear nature of the differential equations describing the neutrino evolution. However the observation that the equations of motion may be linearized at the onset of pendular oscillations allows one to analytically examine the conditions for the onset, even with the inclusion of multi-angle effects. Such an examination for azimuthally symmetric neutrino emission reveals the following interesting features [22], which are helpful in understanding some of the numerical observations above: (i) The neutrino background potential μ and matter background potential λ appear through the combination $\bar{\lambda} = \lambda + \epsilon\mu$, where ϵ is the fractional lepton number asymmetry. (ii) When $\mu \gg \bar{\lambda}$ or $\bar{\lambda} \gg \mu$, pendular oscillations cannot start. Indeed, the instability that would start significant oscillations cannot form unless the matter potential and neutrino potential are similar in magnitude. Nontrivial angular distributions may, however, give rise to additional instabilities [27].

Most of the work so far in understanding of multi-angle effects has been numerical and exploratory, and the jury is still out on the extent of these effects. The net effects of collective oscillations cannot be directly observed as neutrinos subsequently pass through MSW resonance regions, where they may undergo further flavor conversions.

2.2 Oscillations due to the MSW effect

After the neutrinos exit the region where the collective oscillations occur, further flavor conversions occur mainly in the MSW resonance regions [4, 5]. Here the conversion probabilities are independent of the spectra themselves, and are well understood in terms of the neutrino mixing parameters and density profiles. In particular, the flavor conversion in the H resonance is completely adiabatic (non-adiabatic) for $\sin^2\theta \gtrsim 10^{-3}$ ($\lesssim 10^{-5}$), while the L resonance is always completely adiabatic [5]. The neutrino fluxes exiting the star is an ensemble of decoherent neutrino mass eigenstates in vacuum, so the flavor combination during the propagation between the star and the earth is unchanged. The neutrino fluxes F of ν_e and $\bar{\nu}_e$ arriving at the earth may be written in terms of the primary fluxes F^0 and the survival probabilities p and $\bar{p}$ of ν_e and $\bar{\nu}_e$, respectively:

$$F_{\nu_e} = pF^0_{\nu_e} + (1-p)F^0_{\nu_x} \ , \qquad F_{\bar{\nu}_e} = \bar{p}F^0_{\bar{\nu}_e} + (1-\bar{p})F^0_{\nu_x} \ . \tag{3}$$

Though p and $\bar{p}$ are in general functions of energy, they are approximately constant with energy for *small* θ_{13} ($\sin^2\theta_{13} \lesssim 10^{-5}$) and *large* θ_{13} ($\sin^2\theta_{13} \gtrsim 10^{-3}$). At intermediate θ_{13} values, the energy dependence is more complicated, however we shall not consider such a situation here.

The value of p can be directly related to the neutrino mixing pattern during the ~ 10 ms *neutronization* burst of ν_e that occurs immediately after the core bounce. During the later accretion and cooling phases, unless the primary fluxes have widely different energies, it is virtually impossible to determine p or $\bar{p}$ given only the final ν_e and $\bar{\nu}_e$ spectra. However it may be possible to distinguish between zero and nonzero values of p or $\bar{p}$ through earth matter effects. Another phenomenon that allows us to decipher p or $\bar{p}$ values is the time variation in these quantities when the shock wave passes through the MSW resonance regions. Both the earth matter effects and shock wave effects are instances of the neutrino-matter interactions affecting neutrino survival probabilities. Below we review their essential features.

2.2.1 Earth matter effects

If F_{ν_1} and F_{ν_2} are the fluxes of ν_1 and ν_2 arriving at the earth, and the net ν_e flux after the neutrinos have travelled a distance L through the earth matter is $F^D_{\nu_e}(L)$, then [5]

$$F^D_{\nu_e}(L) - F^D_{\nu_e}(0) = (F_{\nu_2} - F_{\nu_1}) \sin 2\theta^{\oplus}_{12} \sin(2\theta^{\oplus}_{12} - 2\theta_{12}) \sin^2\left(\frac{\Delta m^2_{\oplus} L}{4E}\right) \ , \tag{4}$$

where $(\Delta m^2_{\oplus}, \theta^{\oplus}_{12})$ are the values of the solar Δm^2 and mixing angle in earth matter. For antineutrinos, the right hand side changes sign.

The vanishing of neutrino survival probability p corresponds to $F_{\nu_1} = F_{\nu_2}$ and similarly $\bar{p} = 0$ corresponds to $F_{\bar{\nu}_1} = F_{\bar{\nu}_2}$. Therefore, nonzero earth matter effects require $p \neq 0$ for neutrinos and $\bar{p} \neq 0$ for antineutrinos.

2.2.2 Shock wave effects

When the shock wave passes through the MSW resonance regions, the sharp density fluctuations in the shock wave may cause the adiabatic resonances to become non-adiabatic [29]. When the shock wave is at density ρ, it affects the neutrinos with the resonant energy

$$E_{\rm res} \approx 25 \text{ MeV} \frac{600}{Y_e \rho \text{ (g/cc)}} \ . \tag{5}$$

The resonant energies increase with time, and hence the nonadiabatic regions shift to higher energies with time [30]. This will result in a time-dependent value for p and $\bar{p}$ in NH and IH, respectively, during the time of propagation of the shock wave through the resonance region $\rho_H \sim 10^{3-4}$ g/cc, i.e. around 4-5 seconds after the core collapse.

The turbulence that follows the shock wave may, if large enough, cause flavor depolarization. In the extreme case, when complete three-flavor deleptonization occurs, the fluxes of all the neutrino species – or all the antineutrino species, depending on the hierarchy – become identical [32, 33]. For low turbulence amplitude and large θ_{13}, the features of the shock effect may survive [33]. Since the extent of turbulence created during the supernova explosion is still largely uncertain, it is not possible to make a concrete statement about about the net effects of turbulence at this point of time.

3 Neutrino signals at detectors

In this section, we shall point out the features of neutrino spectra at the detectors that will act as signatures of the neutrino oscillations. We shall further comment on the feasibility of robust identification of these signatures, and what we can learn about the neutrino mixing pattern as well as the dynamics of supernova explosion.

We shall consider three main categories of large neutrino detectors: water Cherenkov, carbon-based scintillators, and liquid argon detectors. The major interaction in the first two detectors is the inverse beta decay

$$\bar{\nu}_e + p \to e^+ + n \ ,$$

which helps reconstruct the $\bar{\nu}_e$ spectrum. While the energy resolution of the water Cherenkov detectors is typically a factor of 5-10 worse than that of the liquid scintillators [34], it is easier to make larger water Cherenkov detectors, so they typically have the advantage of larger statistics. The liquid argon detector is the best detector for observing the ν_e spectrum [35], the corresponding charged current (CC) reaction being

$$\nu_e + {}^{40}\mathrm{Ar} \to {}^{40}\mathrm{K}^* + e^- \ .$$

The rule-of-thumb estimate for the number of events observed through the above reactions is ~ 300 per kt in the 10 s duration of the neutrino pulse, for a supernova at 10 kpc. The neutral current (NC) interaction

$$\nu + p \to \nu + p$$

can also be identified through the small proton recoil [36], which can be measured at scintillation detectors. There are also sub-leading interactions like

- the forward scattering $\nu + e^- \to \nu + e^-$ that occurs in all the above detectors,
- $\nu_e + {}^{16}\mathrm{O} \to X + e^-$ in water Cherenkov, and
- the NC reaction $\nu + {}^{12}\mathrm{C} \to \nu + X + \gamma(15.11\ \mathrm{MeV})$ in scintillator detectors,

which will not be discussed here.

The charged and neutral current interactions of neutrinos with a heavy nucleus like lead can release one or two neutrons free from the nuclei, through the reactions

- CC: $\nu_e + {}^{208}\mathrm{Pb} \rightarrow {}^{207}\mathrm{Bi} + n + e^-$, $\nu_e + {}^{208}\mathrm{Pb} \rightarrow {}^{206}\mathrm{Bi} + 2n + e^-$, and
- NC: $\nu + {}^{208}\mathrm{Pb} \rightarrow {}^{207}\mathrm{Pb} + n$, $\nu + {}^{208}\mathrm{Pb} \rightarrow {}^{206}\mathrm{Pb} + 2n$.

The threshold for the emission of two neutrons is higher than that for single neutron emission, thus allowing some energy discrimination on a statistical basis. Though no large detector of this type is under consideration, the HALO detector [37] has started operating already at the SNOLAB.

We shall focus on the leading charged current reactions at the large detectors above, which enable the reconstruction of the ν_e and $\bar{\nu}_e$ spectra. Following are some of the features of these spectra that can act as smoking gun signals of specific neutrino mixing scenarios.

3.1 Neutronization burst

The ~ 10 ms burst of ν_e that occurs immediately after the core bounce has a well-predicted flux [38] that is relatively free of model uncertainties. If the hierarchy is normal and $\sin^2\theta_{13} \gtrsim 10^{-3}$, the survival probability $p \approx \sin^2\theta_{13}$, so the burst signal is suppressed by a factor of $\sin^2\theta_{13}$ [5]. Such an extreme suppression (almost vanishing) of the neutronization burst signal is therefore a clear signature of this mixing scenario. However the robust identification of this signal needs a liquid Ar detector with sufficient time resolution to be able to separate the neutronization burst signal from the accretion phase fluxes that follow it.

A unique situation occurs if the progenitor of the supernova is not an iron-core star, but a O-Ne-Mg one. In such stars, the MSW resonances occur deep inside the region where the neutrinos are still undergoing collective oscillations [39]. Neutrinos of all energies then undergo the MSW resonance with the same adiabaticity [40]. In this case, the MSW resonance helps in preparing the neutrino ensemble for the spectral split. For NH this results in a single spectral split, while for IH this results in two sequential spectral splits [41]. The positions of these splits can be determined from the initial spectra and the non-adiabaticities at the resonances [42]. Recent multi-angle simulations indicate that the multi-angle effects do not change the results significantly [43]. The distortion of the neutrino spectra during the neutronization burst of a O-Ne-Mg supernova is thus unique, can identify the hierarchy even at extremely small θ_{13} values, and could be instrumental in identifying a supernova with such a light progenitor, in case an optical observation is not possible. Some more intriguing features of the neutronization burst phase of such a supernova have recently been reported in the numerical simulations [44].

3.2 Spectral split and Earth matter effects

Though the survival probability of ν_e or $\bar{\nu}_e$ changes sharply at the spectral splits, the observed signal is often diluted by the small difference between the swapping spectra. Moreover if the split is at lower energies, the smaller cross sections make the detection of the spectral split difficult. However if the primary fluxes are dominated by non-electron flavors, the splits can be at higher energies and may manifest themselves as shoulders in the ν_e or $\bar{\nu}_e$ spectra [26].

Earth matter effects provide a more practical way of determining a nonzero value of p or $\bar{p}$, since they introduce modulations of known frequency in the spectrum. Time-dependent changes in relative luminosities observed at two detectors, only one of which is shadowed by the earth, are indicators of earth matter effects [45]. On the other hand, the modulations in the ν_e or $\bar{\nu}_e$ spectra allow one to detect Earth matter effects even at a single detector [46]. While the former method needs two detectors with large fiducial masses (e.g. megaton water

Cherenkov, IceCube), the latter method needs detectors with a good energy resolution (e.g. liquid scintillator or liquid Ar).

A few remarks are in order. Typically, earth effects will be present only in a part of the spectrum due to the presence of spectral swaps. However this feature may be hard to observe. Multi-angle decoherence, turbulent effects, or small differences in primary spectra may result in the earth effects being unobservably small, so nothing may be inferred from their non-observation. However a positive identification of Earth effects would be enough to shortlist neutrino mixing patterns [26]. Relating the presence of Earth effects to the specific neutrino mixing scenarios needs a more complete understanding of the collective effects that we have at the moment.

3.3 Shock wave effects

The propagation of the shock wave through the MSW resonance region inside the star can give rise to time-dependent changes in p for NH, and in $\bar{p}$ for IH [29]. This would result in time-dependent dip/peak features in observables like $N_{\nu_e,\bar{\nu}_e}(E)$, $\langle E_{\nu_e,\bar{\nu}_e}\rangle$, $\langle E^2_{\nu_e,\bar{\nu}_e}\rangle$, etc.. Sharp changes in these observables in ν_e ($\bar{\nu}_e$) spectra at $t \gtrsim 3-4$ s testify for NH (IH) and $\sin^2\theta_{13} \gtrsim 10^{-5}$ [30, 31]. This may even allow the tracking of shock wave while it is still inside the mantle [30]. Note that probing the propagation of the shock wave at such early stages – before it breaks up the envelope of the star – is not possible through any other means (apart from possibly gravitational waves, but their detection is even harder).

If the multi-angle effects cause decoherence at such late times, or if the turbulence that follows the shock wave is large enough to cause flavor depolarization [32, 33], the spectra of all flavors may become identical and no shock effects will be observed. Thus, the non-observation of shock effects does not convey any concrete information. However, a positive observation of these effects can pinpoint the neutrino mixing pattern.

3.4 Indirect oscillation signals

So far we have focused on the oscillation signals through charge-current interactions, which are the primary reactions that allow us to reconstruct the ν_e and $\bar{\nu}_e$ spectra. However even more detailed information can be gained from complementary observables. Let us indicate some such observables in this subsection.

The detection of low energy protons recoiled from the $\nu p \to \nu p$ interaction is possible at a scintillator detector, with a threshold of ~ 0.2 MeV. The recoil spectrum of protons above this threshold can be reliably reconstructed with the superior energy resolution of such a detector. This would allow us to reconstruct the high energy tail of the sum of fluxes of all neutrinos. Clearly this will convey no direct information on neutrino oscillations. However, since the primary fluxes of non-electron neutrinos will be the major contributors to this tail, a fit to this tail would allow a measurement of the average energy $\langle E^0_{\nu_x}\rangle$ to a good accuracy [36]. This would allow a better interpretation of the primary signal observed through the charged-current interactions.

A QCD phase transition may take place in the core of the star, a few tens of a second after the core collapse. This would cause a sudden compactification of the progenitor core. At water Cherenkov detectors like Super-Kamiokande or IceCube, this will result in a prominent burst of $\bar{\nu}_e$ [47]. If a black hole is formed during the neutrino emission process, the neutrino signal will suddenly cease. Though not directly relevant to neutrino oscillations, these neutrino signals

will provide information about supernova astrophysics that is not possible through any other means.

The neutrinos emitted from all the supernova exploded in the universe till now form the diffused supernova neutrino background (DSNB). The measurement of this background should be possible within a few years at large water Cherenkov or scintillation detectors. Such a measurement would test the predictions from astrophysics and cosmology. Collective oscillations affect predictions of the DSNB fluxes by up to $\sim 50\%$ [48], and the shock wave effects can further change these predictions by $10 - 20\%$ [49]. Thus, neutrino oscillations inside the star strongly influence the predictions of the DSNB flux.

If significant neutrino oscillations take place deep inside the core, they can also affect the abundances of heavy elements in the ejecta of supernovae. The r-process nucleosynthesis that is responsible for the production of heavy elements is influenced by the densities of ν_e and $\bar{\nu}_e$ in the relevant region, since these two species take part directly in the nucleosynthesis process. In the absence of collective effects, neutrino flavor conversions occur only in the resonance layers that are out in the mantle and hence the r-process cannot be affected. With the collective effects, however, there is a possibility of neutrino oscillations in a region deeper than the r-process region. These oscillations would tend to increase the average ν_e energy, thus the ν_e cross section with nuclei, suppressing the production of heavy elements. Oscillations are thus in general detrimental to successful r-process nucleosynthesis. However the exact amount of suppression depends strongly on astrophysical conditions and no concrete predictions can be made at this stage [50].

The shock wave propagation can also be affected by neutrino oscillations if they take place deep inside the core, a possibility opened up by the collective effects. Recent explorations into this question [51] indicate no significant impact on the explosion mechanism, however this is still work in progress.

4 Concluding remarks

The neutrino signal from the explosion of a core collapse supernova carries information on primary neutrino fluxes, neutrino mixing parameters, and the shock wave propagation. This information may be extracted by various complementary probes like the neutronization burst, earth matter effects, and shock wave effects. The vanishing of neutronization burst serves for a robust determination of NH and large θ_{13}, however it needs a liquid Ar detector with a good time resolution. The spectral splits are rather difficult to identify, however the identification of earth matter effects, which manifest themselves in terms of spectral modulations, vouches for a nonzero value for the survival probabilities p and $\bar{p}$. Interpreting p and $\bar{p}$ in terms of the neutrino mixing parameters needs a better understanding of multi-angle collective effects than we have at present. The shock wave effects, that result in time-dependent sharp changes in the spectra, are independent of collective effects and can identify the hierarchy, as long as θ_{13} is not too small and turbulent convections behind the shock wave do not give rise to complete depolarization. While the charged current events form the primary signal that helps us reconstruct the ν_e and $\bar{\nu}_e$ spectra, the proton recoil signal from the neutral current events aids the reconstruction of the primary flux of non-electron neutrinos.

With the help of the above signals, one can hope to solve the *inverse supernova neutrino problem*, which consists of observing (i) the $\nu_e/\bar{\nu}_e$ spectra (ii) NC events, (iii) time variation of the signal, and (iv) earth matter effects, and drawing conclusions about (i) the primary fluxes (ii)

the shock propagation and (iii) the neutrino mixing parameters, especially the mass hierarchy. The task is not impossible, but there are many gaps yet to be filled. The major source of the gaps are the uncertainties in primary fluxes, which prevent us from a good reconstruction of the survival probabilities p and $\bar{p}$ as a function of energy, and our incomplete understanding of flavor oscillations inside the star. The details of collective oscillations including the multi-angle effects and the extent of turbulence are two issues that still remain to be resolved.

Nevertheless, it is crucial to make the following measurements: (i) reconstruction of ν_e and $\bar{\nu}_e$ spectra through CC events, (ii) NC spectra through proton recoil at scintillation detectors, (iii) single- and double-neutron events at Pb detectors, (iv) time modulation of observables like flux, average energy, and higher moments, (v) time dependent ratios of relative luminosities at large detectors, (vi) oscillatory spectral modulations from earth effects, (vii) other non-thermal features in the spectrum. Detectors should focus on the above measurements irrespective of the theoretical motivation or interpretation available presently. This has two reasons. First, a core-collapse supernova explosion in our galaxy is a rare enough event that when it happens once, the opportunity to extract whatever data from it should not be missed. Second, the history of neutrinos is full of surprises in the data that the theory had not anticipated at all.

The recent indications of a large θ_{13} [52, 53] imply some interesting consequences for the supernova neutrino analysis. In such a case, the H resonance is adiabatic, except possibly when the shock wave is propagating through the resonance region. The shock wave effects would then be prominent, the hierarchy determination easier, and shock tracking more feasible. Moreover, since the flavor transformations in the resonance regions are now known (modulo the effects of turbulence), the spectra just after the collective effects can be reconstructed from the one observed. In addition if earth effects are observed, one would know if p and $\bar{p}$ vanish or not. This would further help reconstruct the spectra before collective effects.

Of course, we first need a galactic supernova.

Acknowledgments

We would like to thank the organizers of HAνSE 2011 for getting together people working on different aspects of supernova neutrinos, and inducing useful discussions.

References

[1] J. T. Pantaleone, Phys. Lett. B **287**, 128 (1992).

[2] G. Raffelt and G. Sigl, Astropart. Phys. **1**, 165 (1993).

[3] L. Wolfenstein, Phys. Rev. D **17**, 2369 (1978); S. P. Mikheev and A. Y. Smirnov, Sov. J. Nucl. Phys. **42**, 913 (1985) [Yad. Fiz. **42**, 1441 (1985)].

[4] S. P. Mikheev and A. Y. Smirnov, Sov. Phys. JETP **64**, 4 (1986) [Zh. Eksp. Teor. Fiz. **91**, 7 (1986)].

[5] A. S. Dighe and A. Y. Smirnov, Phys. Rev. D **62**, 033007 (2000).

[6] S. Samuel, Phys. Rev. D **48**, 1462 (1993); V. A. Kostelecký and S. Samuel, Phys. Lett. B **318**, 127 (1993); V. A. Kostelecký and S. Samuel, Phys. Rev. D **52**, 621 (1995); S. Samuel, Phys. Rev. D **53**, 5382 (1996); R. F. Sawyer, Phys. Rev. D **72**, 045003 (2005); R. F. Sawyer, Phys. Rev. D **79**, 105003 (2009).

[7] H. Duan, G. M. Fuller, J. Carlson, Y. -Z. Qian, Phys. Rev. Lett. **97**, 241101 (2006); H. Duan, G. M. Fuller and Y. Z. Qian, Phys. Rev. D **74** (2006) 123004; H. Duan, G. M. Fuller, J. Carlson and Y. Z. Qian, Phys. Rev. D **74** (2006) 105014.

[8] S. Pastor and G. G. Raffelt, Phys. Rev. Lett. **89**, 191101 (2002).

[9] S. Hannestad, G. G. Raffelt, G. Sigl and Y. Y. Y. Wong, Phys. Rev. D **74**, 105010 (2006) [Erratum-ibid. D **76**, 029901 (2007)].

[10] G. G. Raffelt and A. Y. Smirnov, Phys. Rev. D **76**, 081301 (2007); G. G. Raffelt and A. Y. Smirnov, Phys. Rev. D **76**, 125008 (2007).

[11] H. Duan, G. M. Fuller and Y. Z. Qian, Phys. Rev. D **76**, 085013 (2007).

[12] B. Dasgupta, G. G. Raffelt, I. Tamborra, Phys. Rev. **D81**, 073004 (2010).

[13] B. Dasgupta, A. Dighe, G. G. Raffelt and A. Y. Smirnov, Phys. Rev. Lett. **103**, 051105 (2009).

[14] A. Friedland, Phys. Rev. Lett. **104**, 191102 (2010).

[15] B. Dasgupta, A. Mirizzi, I. Tamborra and R. Tomas, Phys. Rev. D **81**, 093008 (2010).

[16] H. Duan and J. P. Kneller, J. Phys. G **36**, 113201 (2009); H. Duan, G. M. Fuller, Y. -Z. Qian, Ann. Rev. Nucl. Part. Sci. **60**, 569-594 (2010).

[17] G. L. Fogli, E. Lisi, A. Marrone and A. Mirizzi, JCAP **0712**, 010 (2007).

[18] A. Esteban-Pretel, S. Pastor, R. Tomàs, G. G. Raffelt and G. Sigl, Phys. Rev. D **76**, 125018 (2007).

[19] H. Duan and A. Friedland, Phys. Rev. Lett. **106**, 091101 (2011).

[20] A. Esteban-Pretel, A. Mirizzi, S. Pastor, R. Tomas, G. G. Raffelt, P. D. Serpico and G. Sigl, Phys. Rev. D **78**, 085012 (2008).

[21] S. Chakraborty, T. Fischer, A. Mirizzi, N. Saviano and R. Tomas, arXiv:1104.4031 [hep-ph]; S. Chakraborty, T. Fischer, A. Mirizzi, N. Saviano and R. Tomas, Phys. Rev. D **84**, 025002 (2011).

[22] A. Banerjee, A. Dighe, G. Raffelt, Phys. Rev. **D84**, 053013 (2011).

[23] T. Fischer, S. C. Whitehouse, A. Mezzacappa, F. K. Thielemann and M. Liebendorfer, Astron. Astrophys. **517** (2010) A80; L. Hudepohl, B. Muller, H. T. Janka, A. Marek and G. G. Raffelt, Phys. Rev. Lett. **104** (2010) 251101; T. D. Brandt, A. Burrows, C. D. Ott and E. Livne, Astrophys. J. **728**, 8 (2011).

[24] A. D. Dolgov, Sov. J. Nucl. Phys. **33**, 700 (1981) [Yad. Fiz. **33**, 1309 (1981)].

[25] B. Dasgupta and A. Dighe, Phys. Rev. D **77**, 113002 (2008).

[26] S. Choubey, B. Dasgupta, A. Dighe and A. Mirizzi, arXiv:1008.0308 [hep-ph].

[27] A. Mirizzi and P. D. Serpico, arXiv:1110.0022 [hep-ph];

[28] I. Tamborra, G. G. Raffelt, L. Huedepohl and H. -T. Janka, arXiv:1110.2104 [astro-ph.SR].

[29] R. C. Schirato and G. M. Fuller, arXiv:astro-ph/0205390; G. L. Fogli, E. Lisi, D. Montanino and A. Mirizzi, Phys. Rev. D **68**, 033005 (2003).

[30] R. Tomas, M. Kachelriess, G. Raffelt, A. Dighe, H. T. Janka and L. Scheck, JCAP **0409**, 015 (2004).

[31] G. L. Fogli, E. Lisi, A. Mirizzi and D. Montanino, JCAP **0504**, 002 (2005); G. L. Fogli, E. Lisi, A. Mirizzi and D. Montanino, JCAP **0606**, 012 (2006); S. Choubey, N. P. Harries and G. G. Ross, Phys. Rev. D **74**, 053010 (2006); B. Dasgupta and A. Dighe, Phys. Rev. D **75**, 093002 (2007); J. P. Kneller, G. C. McLaughlin and J. Brockman, Phys. Rev. D **77**, 045023 (2008); J. Gava, J. Kneller, C. Volpe and G. C. McLaughlin, Phys. Rev. Lett. **103**, 071101 (2009).

[32] A. Friedland and A. Gruzinov, arXiv:astro-ph/0607244.

[33] J. P. Kneller and C. Volpe, Phys. Rev. **D82**, 123004 (2010).

[34] T. Akiri *et al.* [The LBNE Collaboration], arXiv:1110.6249 [hep-ex].

[35] I. Gil Botella and A. Rubbia, JCAP **0310**, 009 (2003); I. Gil Botella and A. Rubbia, JCAP **0408**, 001 (2004).

[36] B. Dasgupta and J. .F. Beacom, Phys. Rev. **D83**, 113006 (2011).

[37] http://www.snolab.ca/halo/index.html

[38] M. Kachelriess, R. Tomas, R. Buras, H. T. Janka, A. Marek and M. Rampp, Phys. Rev. D **71**, 063003 (2005).

[39] H. Duan, G. M. Fuller, J. Carlson and Y. Z. Qian, Phys. Rev. Lett. **100**, 021101 (2008); C. Lunardini, B. Muller and H. T. Janka, Phys. Rev. D **78**, 023016 (2008).

[40] Y. Y. Y. Wong, AIP Conf. Proc. **655**, 240 (2003).

[41] H. Duan, G. M. Fuller and Y. Z. Qian, Phys. Rev. D **77**, 085016 (2008);

[42] B. Dasgupta, A. Dighe, A. Mirizzi and G. G. Raffelt, Phys. Rev. D **77**, 113007 (2008).

[43] J. F. Cherry, G. M. Fuller, J. Carlson, H. Duan and Y. Z. Qian, Phys. Rev. D **82**, 085025 (2010).

[44] J. F. Cherry, M. -R. Wu, J. Carlson, H. Duan, G. M. Fuller, Y. -Z. Qian, arXiv:1108.4064 [astro-ph.HE]; J. F. Cherry, M. -R. Wu, J. Carlson, H. Duan, G. M. Fuller, Y. -Z. Qian, arXiv:1109.5195 [astro-ph.HE].

[45] A. S. Dighe, M. T. Keil and G. G. Raffelt, JCAP **0306**, 005 (2003); B. Dasgupta, A. Dighe and A. Mirizzi, Phys. Rev. Lett. **101**, 171801 (2008).

[46] A. S. Dighe, M. T. Keil and G. G. Raffelt, JCAP **0306**, 006 (2003); A. S. Dighe, M. Kachelriess, G. G. Raffelt and R. Tomas, JCAP **0401**, 004 (2004).

[47] B. Dasgupta, T. Fischer, S. Horiuchi, M. Liebendorfer, A. Mirizzi, I. Sagert, J. Schaffner-Bielich, Phys. Rev. **D81**, 103005 (2010).

[48] S. Chakraborty, S. Choubey, B. Dasgupta and K. Kar, JCAP **0809**, 013 (2008);

[49] S. Galais, J. Kneller, C. Volpe and J. Gava, Phys. Rev. D **81**, 053002 (2010).

[50] H. Duan, A. Friedland, G. C. McLaughlin and R. Surman, J. Phys. G **38**, 035201 (2011).

[51] B. Dasgupta, E. P. O'Connor and C. D. Ott, arXiv:1106.1167 [astro-ph.SR]; O. Pejcha, B. Dasgupta and T. A. Thompson, arXiv:1106.5718 [astro-ph.HE].

[52] K. Abe *et al.* [T2K Collaboration], arXiv:1106.2822 [hep-ex]; Z. Isvan [MINOS Collaboration], arXiv:1110.1900 [hep-ex].

[53] G. L. Fogli, E. Lisi, A. Marrone, A. Palazzo and A. M. Rotunno, arXiv:1106.6028 [hep-ph]; T. Schwetz, M. Tortola and J. W. F. Valle, arXiv:1108.1376 [hep-ph].

Low-energy Neutrino-Nucleus Cross Sections

Natalie Jachowicz

Ghent University, Department of Physics and Astronomy, Proeftuinstraat 86, B-9000 Gent, Belgium

DOI: http://dx.doi.org/10.3204/DESY-PROC-2011-03/jachowicz

We present an overview of neutrino-nucleus scattering at low energies and highlight the aspects of the study of these interactions important for supernova physics.

1 Introduction

Neutrinos are important for a type II supernova explosion in several ways. On one hand, neutrino interactions and the related energy transfers play a crucial role in the explosion dynamics and nucleosynthesis. On the other hand, the terrestrial detection of supernova neutrinos can provide a broad variety of information [1] about the neutrinos and their interactions, and about the supernova process itself. The arrival times of the neutrinos are related to their mass and can moreover hint at the fate of the star. Several reactions provide directional information, important for optical telescopes awaiting the photons in the wake of the supernova neutrino flux. The energy of the neutrinos can be inferred from the energy of the decay products. It indicates the decoupling site of the neutrinos and the temperature there. As mu and tau supernova-neutrinos do not have enough energy to produce a massive lepton in a charged-current reaction, the flavor of the arriving neutrinos can be inferred from the frequency differences between the occurrence of neutral and charge-exchange processes. Whether a neutrino or an antineutrino entered the detector can be determined by looking at the charge of the outgoing lepton for electron (anti)neutrinos or by examining the spin of the outgoing nucleon in neutral-current nucleon knockout off nuclei. When the signal in the detector is accurately resolved, the observed neutrino energies and flavors can help to disentangle the mixing scheme induced by oscillations [2, 3].

Nuclei have relatively large cross sections for neutrino reactions and are energy-sensitive in the range of interest, several particle-emission thresholds opening up with increasing incoming neutrino energies. This makes nuclear targets important as detecting material. Galactic supernova neutrinos could be detected by existing and proposed supernova neutrino detectors such as SNO [4], SuperKamiokande [5], KamLAND [1], LVD [6], MiniBooNe [7], OMNIS [8], LAND [9]. Favored detection nuclei are ^{12}C, ^{16}O, ^{56}Fe, ^{208}Pb, and deuterium. However, the signal in the detector can only be interpreted as well as the relevant neutrino-nucleus cross sections are understood. For most nuclei very little experimental neutrino data exists in the relevant energy region. This is due to the very small cross sections for weak interaction processes, and an additional limitation is caused by the fact that monochromatic neutrino beams are not available [10, 11]. This has as a consequence that for most applications one has to rely on theoretical

predictions, with their related uncertainties and model dependencies.

2 Modeling neutrino-nucleus interactions at low energies

The study of the atomic nucleus faces particular problems : generally, the atomic nucleus is a mesoscopic system, on the one hand containing too much particles to allow few-body techniques to be effective and on the other hand containing too few nucleons to enable a statistical approach of the problem. In the tens-of-MeV energy range important for supernova neutrinos, cross sections are very sensitive to nuclear structure effects.

The main methods to study neutrino scattering off nuclei at supernova-neutrino energies are the Shell Model (SM) and the Random Phase Approximation (RPA). In the former, the description of the nucleus is based on a full diagonalization of a effective interaction in a limited model space. In recent years, the shell model has been used successfully to study various weak interactions of interest to nuclear astrophysics [12]. The main disadvantage of the shell model approach is the dimension of the matrices to be diagonalized, rapidly growing with increasing model sizes.

Confronted with this drawback, a number of approximations has been designed, focusing on various aspect of the problem. Next to the Hartree-Fock approximation, considering only single-particle properties of the problem, more elaborate techniques as e.g. the RPA were developed. Contrary to mean-field descriptions were a nucleon experiences the presence of the others only through the mean-field generated by their mutual interactions, the random phase approximation allows correlations to be present even in the ground state of the nuclear system and additionally allows the particles to interact by means of the residual two-body force. The random phase approximation goes one step beyond this zeroth-order mean-field approach and describes a nuclear state as the coherent superposition of particle-hole contributions.

$$|\Psi_{RPA}\rangle = \sum_c \left\{ X_{(\Psi,C)} \ \left|ph^{-1}\right\rangle \ - \ Y_{(\Psi,C)} \ \left|hp^{-1}\right\rangle \right\}. \tag{1}$$

The summation index C stands for all quantum numbers defining a reaction channel unambiguously :

$$C = \{n_h, l_h, j_h, m_h, \varepsilon_h; l_p, j_p, m_p, \tau_z\}, \tag{2}$$

where the indices p and h indicate whether the considered quantum numbers relate to the particle or the hole state, ε_h denotes the binding-energy of the hole state and τ_z defines the isospin character of the particle-hole pair. General excited states are obtained as linear combinations of these particle-hole configurations. As the RPA approach describes nuclear excitations as the coherent superposition of individual particle-hole states out of a correlated ground state, this approach allows to account for some of the collectivity present in the nucleus. In standard RPA calculations this leads to a discrete spectrum, with several variations in the approach [13, 14, 15] in use.

In this contribution, the cross section results are illustrated using a Continuum Random Phase Approximation (CRPA), based on a Green's function approach [16, 17, 18]. The unperturbed wave-functions are generated using either a Woods-Saxon potential or a HF-calculation using a Skyrme force. The latter approach makes self-consistent HF-RPA calculations possible.

The differential cross-section for scattering of an incoming neutrino with energy ε_i is given by

$$\left(\frac{d^2\sigma_{i\to f}}{d\Omega d\omega}\right)_{\substack{\nu\\ \bar{\nu}}} = \frac{G^2\varepsilon_f^2}{\pi}\,\frac{2\cos^2\left(\frac{\theta}{2}\right)}{2J_i+1}\left[\sum_{J=0}^{\infty}\sigma_{CL}^J + \sum_{J=1}^{\infty}\sigma_T^J\right], \tag{3}$$

with

$$\sigma_{CL}^J = \left|\left\langle J_f \left|\left| \widehat{\mathcal{M}}_J(\kappa) + \frac{\omega}{|\vec{q}|}\widehat{\mathcal{L}}_J(\kappa)\right|\right| J_i\right\rangle\right|^2, \tag{4}$$

$$\begin{aligned}\sigma_T^J \;=\; & \left(-\frac{q_\mu^2}{2\,|\vec{q}|^2} + \tan^2\left(\frac{\theta}{2}\right)\right)\left[\left|\left\langle J_f\left|\left|\widehat{\mathcal{T}}_J^{mag}(\kappa)\right|\right| J_i\right\rangle\right|^2 + \left|\left\langle J_f\left|\left|\widehat{\mathcal{T}}_J^{el}(\kappa)\right|\right| J_i\right\rangle\right|^2\right] \\ & \mp \tan\left(\frac{\theta}{2}\right)\sqrt{-\frac{q_\mu^2}{|\vec{q}|^2} + \tan^2\left(\frac{\theta}{2}\right)}\;\left[2\Re\left(\left\langle J_f\left|\left|\widehat{\mathcal{T}}_J^{mag}(\kappa)\right|\right| J_i\right\rangle\left\langle J_f\left|\left|\widehat{\mathcal{T}}_J^{el}(\kappa)\right|\right| J_i\right\rangle^*\right)\right],\end{aligned} \tag{5}$$

where $\widehat{\mathcal{M}}_J$ and $\widehat{\mathcal{L}}_J$ are the Coulomb and longitudinal multipole operators, $\widehat{\mathcal{T}}_J^{mag}$ and $\widehat{\mathcal{T}}_J^{el}$ the transverse multipole operators. θ is the scattering angle of the lepton. For each multipole transition J^π only one part -vector or axial vector- of an operator is contributing. From the expression (3) it is clear that J=0 transitions are suppressed due to the lack of a transverse contribution in these channels. Still, neutrinos are able to excite 0^- states in nuclei, while electrons cannot. The second and third part of the expression show that there is interference between the Coulomb and the longitudinal (CL) terms and between both transverse contributions, but not between transverse and CL terms. The only difference between neutrino and antineutrino cross-sections is in the opposite sign of the transverse interference part. From the angular dependence of the kinematic factors, it is clear that for backwards $\theta = \pi$ scattering only transverse terms contribute, while for $\theta = 0$ CL-contributions dominate.

For charged current neutrino scattering reactions, the outgoing particle is a charged lepton. In this case, the outgoing particle has to be described by the scattering solutions in the Coulomb potential generated by the final nucleus. For the applications considered here, this can be done in an effective way introducing the Fermi function. The cross-section is then multiplied by the square of the ratio between the correct scattering solution and a plane wave for a point charge Z', evaluated at the origin.

For many applications, the direction of the outgoing lepton is irrelevant and the differential cross-section has to be integrated over the scattering angle $\Omega(\theta, \phi)$. Considering a process where the incoming neutrino energies are distributed according to a spectrum, the cross-section (3) has to be folded with this energy distribution. The total scattering cross-section is obtained by performing an integration of (3) over the excitation energies ω and summing over the different multipole contributions.

3 Cross sections

Neutrino scattering potentially constitutes a rich source of information on nuclear structure and weak interaction characteristics. But notwithstanding the experimental efforts, the extraction of information out of scattering reactions is very difficult, due to the very small interaction cross-sections. The importance of neutrinos in a variety of astrophysical situations therefore

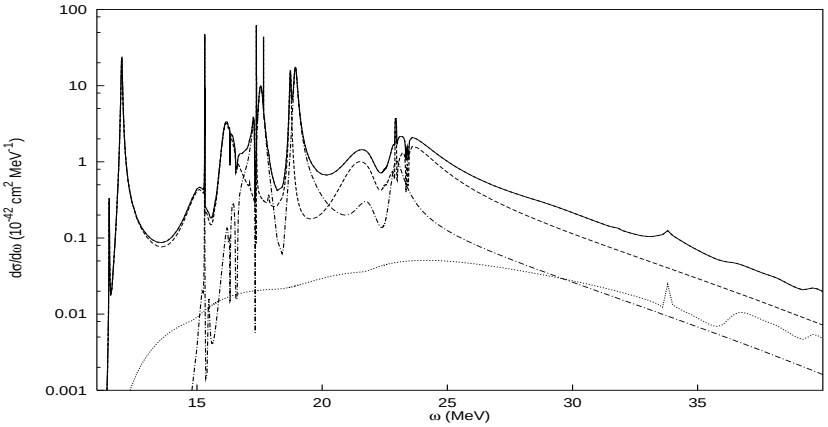

Figure 1: Cross-section for the neutral current reaction $^{16}O + \nu_{50\,MeV} \rightarrow {}^{16}O^* + \nu'$ (full line) and its dominant multipole contributions. $J^\pi = 1^-$ (dashed line), $J^\pi = 1^+$ (dashed-dotted) and $J^\pi = 2^-$ (dotted line). The total cross-section includes multipoles up to J=4. The single-particle wave-functions and energies were obtained with a Hartree-Fock calculation, as residual interaction the SkE2 parameterization was used.

represents an important additional motivation for the study of neutrino-nucleus scattering reactions.

In this section, the main characteristics of neutrino-nucleus scattering at supernova-neutrino energies are discussed using the example of neutral-current scattering of 50 MeV neutrinos off ^{16}O.

Figure 1 shows the differential cross-section for this reaction as a function of the excitation energy ω of the nucleus, and the most important multipole contributions. The differential neutrino scattering cross-sections are of the order of 10^{-42} cm^2 per MeV. The figure clearly illustrates that at energies below 20 MeV, the cross-section spectrum is sharply peaked. These peaks are related to excitations with a strong single-particle character. The resonances are however very narrow and therefore do not absorb all transition strength. At excitation energies between 20 and 25 MeV, the broad resonance structure of the giant dipole resonance shows up. For excitation energies above approximately 30 MeV the cross-section decreases almost purely quadratically as a function of the excitation energy of the nuclear system. This agrees with the energy dependence of equation (3) which shows the cross-section to be proportional to the square of the outgoing lepton energy $\frac{d\sigma}{d\omega} \sim (\varepsilon_f)^2$. This effect furthermore results in the smooth and soft broadening of the resonances for higher values of the energy of the lepton projectile.

In the calculation, multipoles up to J=4 were taken into account. Contributions of higher order multipole excitations were found to be very small at the considered energies. The J=5 transitions are suppressed by almost 5 orders of magnitude and as a consequence have negligible influence on the total cross-section. The smooth behavior of these contributions furthermore assures that the shape of the resonance structure in the excitation spectrum is not affected by the higher order multipole transitions.

The J=1 excitations are prominent, with a clear dominance of the J=1$^-$ electric dipole transition in the giant resonance region. Next to higher order multipole transitions J=3 and

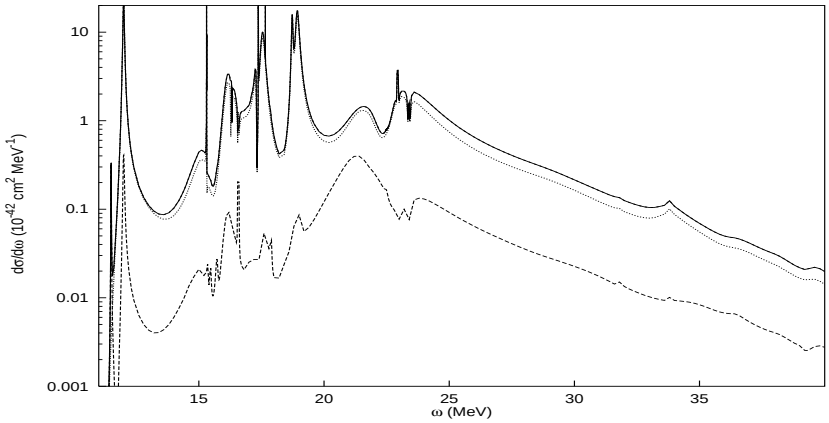

Figure 2: Comparison between the vector (dashed) and the axial vector (dotted line) contribution to the reaction $^{16}O(\nu,\nu')^{16}O^*$. The total differential cross-section is shown by the full curve.

J=4, also J=0 excitations are suppressed. This is due to the fact that only Coulomb and longitudinal terms contribute to these channels. But still, some clear 0^- resonances show up in the differential cross-sections. In general, negative parity transitions are clearly dominating the positive parity contributions. For higher excitation energies, the relative importance of higher order multipoles increases.

Figure 2 carries out a comparison between the contribution of the axial and the axial vector part of the hadronic current to the total cross-section. The axial vector current is clearly more sensitive to the weak neutrino probes. The vector contribution is suppressed by more than one order of magnitude. The splitting of the cross-section in a vector and an axial vector part excludes the interference contribution. This explains the discrepancy between the sum of both curves in figure 2 and the total cross-section.

Due to the fact that the axial vector current is completely isovector, isovector excitations will dominate isoscalar ones, as figure 4 indeed illustrates. The reason for the large suppression of the isoscalar excitations is twofold : not only is the axial vector current not contributing to isoscalar transitions, but due to the $\sin^2\theta_W$-factor the isoscalar form factors are considerably smaller than the vector ones as well. A further consequence of this isovector dominance is the large isovector contribution to the resonance at 23.6 MeV, a dominance that is clearly related to the axial vector character of this excitation (figure 2). The figure furthermore shows that, due to the repulsive character of the interaction in the isovector channels, isovector excitations are pushed towards higher energies compared to isoscalar states.

According to equation (3) it is the interference contribution that is responsible for the difference in the nuclear response to neutrino and antineutrino perturbations. The sign of the interference term determines which cross-section will be dominant. Figure 3 illustrates that generally neutrino cross-sections are slightly larger than antineutrino cross-sections. Only round 23 MeV, the interference term changes sign and antineutrino excitations become more important.

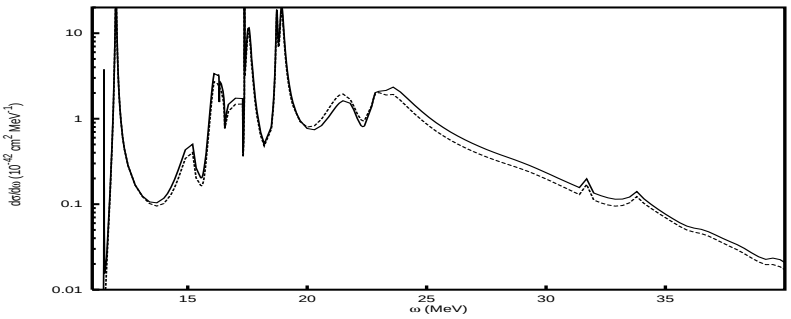

Figure 3: Cross-section for neutral current neutrino (full line) and antineutrino (dashed) scattering reactions off oxygen 16.

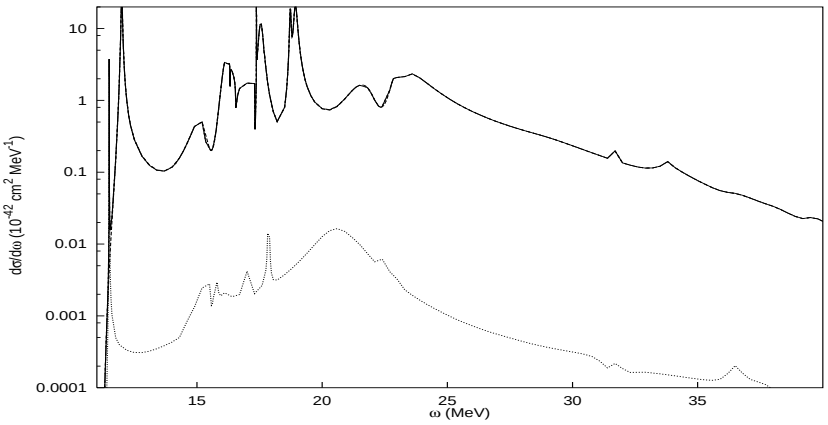

Figure 4: Comparison between the isovector (dashed line) and the isoscalar (dotted) contribution to the reaction $^{16}O(\nu,\nu')^{16}O^*$. The isovector curve almost coincides with the total cross-section.

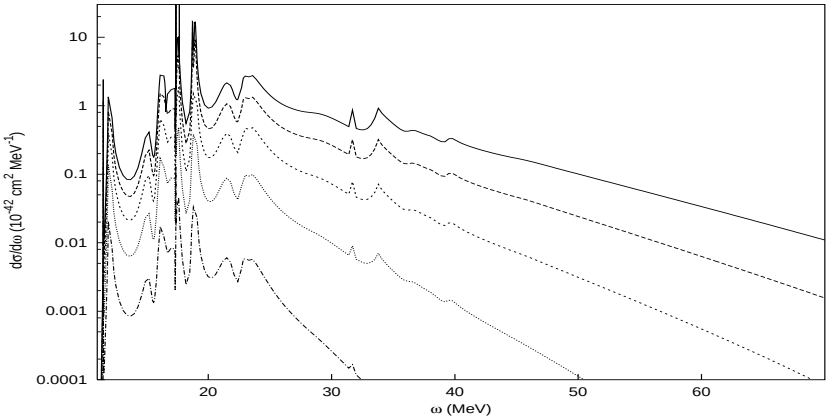

Figure 5: Differential cross-section for the neutral current reaction $^{16}O + \nu_{FD} \rightarrow {}^{16}O^* + \nu'$, averaged over neutrinos and antineutrinos and over a Fermi-Dirac distribution with temperature T and vanishing chemical potential. T=12 MeV (full line) ; T=10 MeV (dashed) ; T=8 MeV (shortdashed) ; T=6 MeV (dotted) and T=4 MeV (dashed-dotted).

4 Influence of the energy distribution

In order to obtain information about the interactions of supernova neutrinos, the cross sections have to be folded with the appropriate energy spectrum. Figure 6 shows that the folded cross section is strongly dependent on the temperature or average energy of the distribution. Traditionally, supernova-neutrino energy-distributions were parametrized using Fermi-Dirac distributions. The spectra are however not purely thermal, as the decoupling sites of the neutrinos are influenced by their flavor and energy, leading to the use of "effective temperatures" and "effective chemical potentials" in these distributions. Recent calculations showed that descriptions of a supernova neutrino spectrum are provided by a power-law distribution [19]:

$$n_{SN[\langle\varepsilon\rangle,\alpha]}(\varepsilon) = \left(\frac{\varepsilon}{\langle\varepsilon\rangle}\right)^{\alpha} e^{-(\alpha+1)\frac{\varepsilon}{\langle\varepsilon\rangle}}, \tag{6}$$

where $\langle\varepsilon\rangle$ and α represent the average energy and the width of the spectrum respectively. The average neutrino energy $\langle\varepsilon\rangle$ is related to the temperature at the decoupling site, and the effect of α is equivalent to that of the introduction of the effective chemical potential in the Fermi-Dirac distribution. Neutrino-nucleus reaction cross sections depend on the square of the incoming energy, thus rising very fast with neutrino energies. Hence, the folded cross sections reach their maximum at much higher energy values than the supernova-neutrino energy-spectrum does, as illustrated in figure 6. Typically even neutrinos with energies more than twice the average energy of the distribution make sizable contributions to the folded cross section, and integrated cross sections only converge at energies above 60 MeV [20]. This makes the high-energy tail of the spectra very important for the determination of the nuclear response.

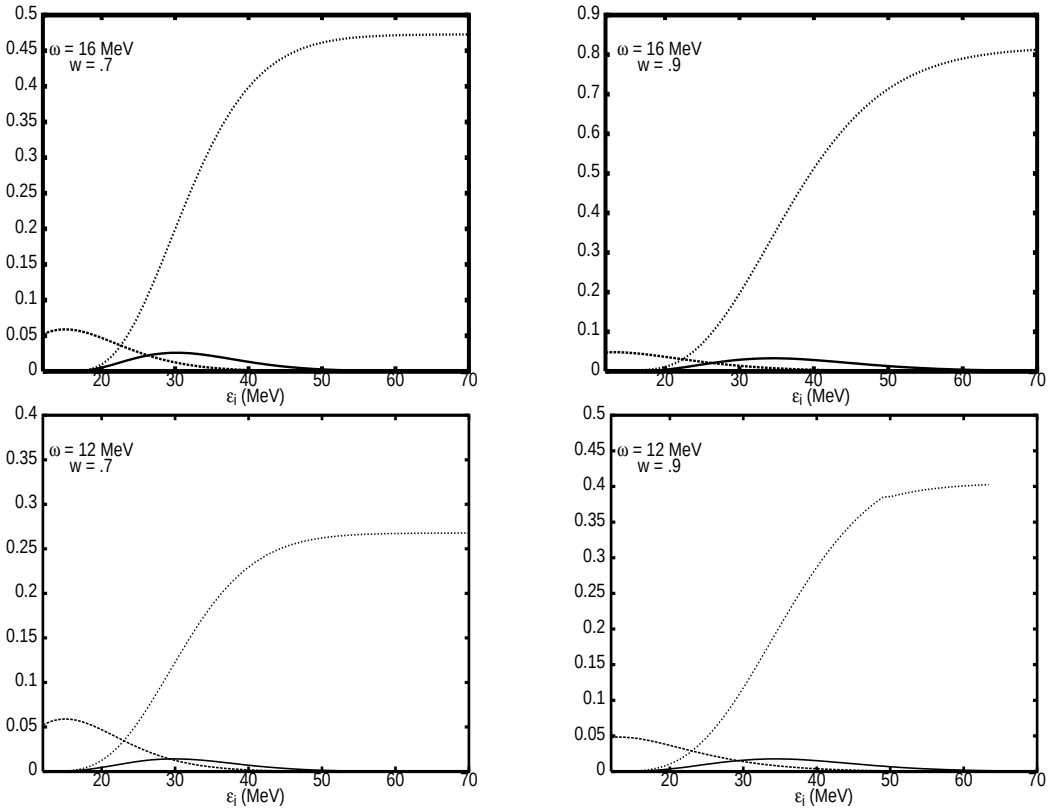

Figure 6: Influence of the supernova-neutrino energy-distribution on the folded cross section for different spectra and excitation energies of the nucleus: energy spectrum (dotted), cross section (dashed), folded cross section (full line).

5 Neutrino interactions at a low-energy beta-beam facility

Beta beams, which are neutrino beams produced by the beta decay of nuclei that have been accelerated to high gamma factor, were original proposed for high energy applications, such as the measurement of the third neutrino mixing angle θ_{13} [21]. Volpe [22, 23, 24] suggested that a beta beam run at lower gamma factor, would be useful for neutrino measurements in the tens of MeV range. The flexibility these beta-beam facilities offer [25], combined with the fact that beta-beam neutrino energies overlap with supernova-neutrino energies, allow one to construct 'synthetic' spectra that approximate an incoming supernova-neutrino energy-distribution. It can be shown that fitting 'synthetic' spectra, constructed by taking linear combinations of beta-beam spectra, to the original supernova-neutrino spectra reproduces the folded differential cross sections very accurately [26, 27]. Comparing the response in a terrestrial detector to these synthetic responses provides a direct way to determine the main parameters of the supernova-neutrino energy-distribution. Using these constructed spectra we are able to reproduce total

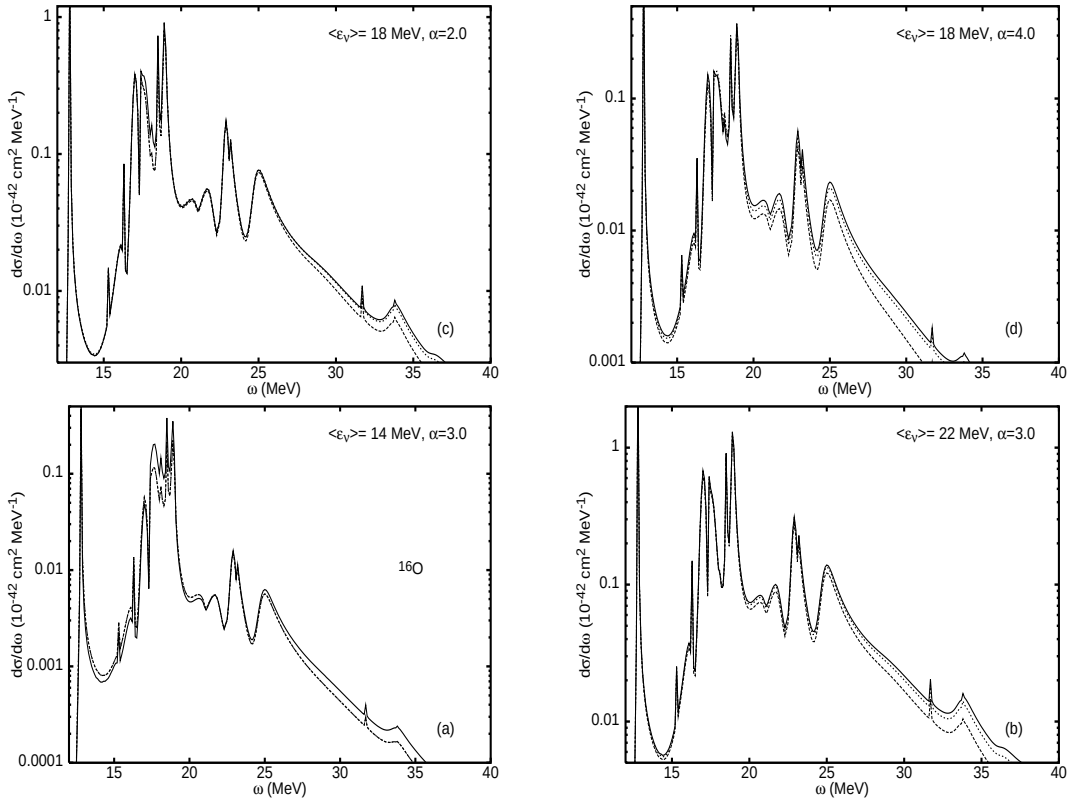

Figure 7: Comparison between differential cross sections for neutral-current scattering on ^{16}O, folded with a power-law supernova-neutrino spectrum (full line) and synthetic spectra with 3 (dashed line) and 5 components (dotted line) for different energy distributions : $\langle\varepsilon\rangle$=14, α=3 (a), $\langle\varepsilon\rangle$=22, α=3 (b), $\langle\varepsilon\rangle$=18, α=2 (c), and $\langle\varepsilon\rangle$=18, α=4 (d).

and differential folded supernova-neutrino cross-sections very accurately, as Fig.7 illustrates.

References

[1] P. Vogel, Prog. Part. Nucl. Phys. **48**, 29 (2002).

[2] G. M. Fuller, W. C. Haxton and G. C. McLaughlin, Phys. Rev. D **59**, 085005 (1999).

[3] J. Engel, G. C. McLaughlin and C. Volpe, Phys. Rev. D **67**, 013005 (2003).

[4] C.J. Clarence, the SNO Collaboration, Nucl. Phys. Proc. Suppl. **100**, 326 (2001).

[5] Y. Oyama *et al.*, Phys. Rev. Lett. 56, 2604 (1987).

[6] M. Aglietta, P. Antonioli, G. Bari, C. Castagnoli *et al.*, Nucl. Phys. Proc. Suppl. **138**, 115 (2005).

[7] M.K. Sharp, J.F. Beacom, J.A. Formaggio, Phys. Rev. D **66**, 013012 (2002).

[8] R.N. Boyd and A.St.J. Murphy, Nucl. Phys. **A688**, 386c (2001).

[9] C.K. Hargrove *et al.*, Astroparticle Physics **5**, 183 (1996).

[10] B.E. Bodmann *et al.*, Phys. Lett. **B 332**, 251 (1994).
[11] http://www.phy.ornl.gov/nusns
[12] K. Langanke, G. Martínez-Pinedo, B. Müller, H.-Th. Janka et al, Phys. Rev. Lett **100**, 011101 (2008).
[13] E. Kolbe, K. Langanke, S. Krewald and F.K. Thielemann, Nucl. Phys**A540**, 599 (1992).
[14] C. Volpe, N. Auerbach, G. Coló, T. Suzuki, N. Van Giai, Phys. Rev. C **62**, 015501 (2000).
[15] A. Samana, F. Krmpotić, N. Paar, C. Bertulani, Phys. Rev. C **83**, 024303 (2011).
[16] N. Jachowicz, K. Heyde, J.Ryckebusch, and S. Rombouts, Phys. Rev. C**59**,3246 (1999).
[17] N. Jachowicz, K. Heyde, J.Ryckebusch, and S. Rombouts, Phys. Rev. C**65**, 025501 (2002).
[18] N. Jachowicz, K. Heyde, and J. Ryckebusch, Phys. Rev. C **66**, 055501 (2002).
[19] M. Keil, G.G. Raffelt, H.-T. Janka, Astrophys. J. **590**, 971 (2003).
[20] N. Jachowicz, K. Heyde, Phys. Rev. C **68**, 055502 (2003).
[21] P. Zuchelli, Phys. Lett. **B532**, 166 (2002).
[22] C. Volpe, J. Phys. **G30**, 1 (2004).
[23] J. Serreau, C. Volpe, Phys. Rev. C **70**, 055502 (2004).
[24] G. C. McLaughlin, Phys. Rev. C **70**, 045804 (2004).
[25] http://beta-beam.web.cern.ch/beta-beam
[26] N. Jachowicz, G.C. McLaughlin, Phys. Rev. Lett. **96**, 172301 (2006).
[27] N. Jachowicz, G.C. McLaughlin, C. Volpe, Phys. Rev. **C77**, 055501 (2008).

Supernova neutrino signal in IceCube

Gösta Kroll[1]*, for the IceCube Collaboration*[2]

[1]Institut für Physik, Johannes Gutenberg-Universität, 55099 Mainz, Germany
[2]http://www.icecube.wisc.edu

DOI: http://dx.doi.org/10.3204/DESY-PROC-2011-03/kroll

IceCube has been completed in December 2010 and now forms a lattice of 5160 photomultiplier tubes covering a volume of $\sim \mathrm{km}^3$ in the deep Antarctic ice. Its main design goal is to detect neutrinos with energies greater than 100 GeV. Owing to subfreezing ice temperatures and potassium free glass, the photomultiplier dark noise rates are particularly low. Hence IceCube can also detect MeV neutrinos if they arrive in large numbers by observing a collective rise in all photomultiplier rates on top of the dark noise. Recent work has been focussed on deepening the understanding and subsequently removing several dark noise contributions. IceCubes supernova data aquisition provides a 2 ms time resolution, allowing to to track subtle features in the temporal development of a supernova neutrino burst. Assuming a supernova at the galactic center, the detector's sensitivity compares to a background-free megaton-scale supernova search experiment. The sensitivity decreases to 20 standard deviations at the galactic edge (30 kpc) and 6 standard deviations at the Large Magellanic Cloud (50 kpc). Since 2009, IceCube's supernova alert system has been sending real-time triggers from potential supernovae to the Supernova Early Warning System.

1 Detection principle

IceCube is uniquely suited to monitor our galaxy for supernovae due to its 1 km^3 size and favorable conditions of the south polar ice. With its photomultipliers surrounded by inert and cold ice at depths between (1450 – 2450) m they are partly shielded from cosmic rays and the temperature in the ice ranging from $-43\,^\circ\mathrm{C}$ to $-20\,^\circ\mathrm{C}$ leads to low average noise rates around 540 Hz.

With the inverse beta processes being the dominant interaction in water Cherenkov detectors for the typical $\mathcal{O}(10MeV)$ supernova neutrinos, the light yield per neutrino in IceCube roughly scales with E_ν^3. This accrues from the cross section of the inverse beta process showing an approximate E_ν^2 dependence, the resulting positron track lengths in ice of about $0.5\,\mathrm{cm}\cdot E_\nu/\,\mathrm{MeV}$ long and the Cherenkov light production being directly proportional to this track length. Our Monte Carlo studies yield an average number of 178 photons per MeV energy of the positron, considering only a range of wavelengths from 300 nm to 600 nm accessible to our optical modules.

The spacing between Digital Optical Modules (DOMs) of 17 m vertically and 125 m horizontally is large in comparison to the $\mathcal{O}(cm)$ positron tracks from inverse beta processes. Therefore the probability to detect light from a single interaction in more than one DOM is $\mathcal{O}(1\%)$. This gives rise to our detection principle, where small light yields in individual DOMs add up to a statistically significant collective rise in the noise rate of all 5160 photomultipliers. These noise rates are continously analyzed by an online algorithm using a maximum likelihood approach

analyzing a rolling time window.

Since September 2009, IceCube has been sending real-time datagrams to the Supernova Early Warning System (SNEWS) [3] when detecting supernova candidate events.

2 Background Noise

The Digital Optical Module (DOM) is the fundamental element in the IceCube architecture. Housed in a 13" (33 cm) borosilicate glass pressure sphere, it contains a Hamamatsu 10" hemispherical photomultiplier tube [1] as well as a custom build computer based on ARM architecture that allows each DOM to operate as a complete and autonomous data acquisition system [2].

Several effects contribute to the prevailing noise rate of 540 Hz: a Poissonian noise contribution from radioactivity, atmospheric muons and remaining thermal noise, as well as correlated noise from Cherenkov radiation and scintillation originating in the glass of the photomultiplier and the pressure vessel. The majority of hits are due to scintillation of residual cerium energized by β and α decays from trace elements in the uranium/thorium decay chains causing a series of pulses.

The observed time difference between noise hits deviates from an exponential distribution that would be expected for a Poissonian process. With typical times between correlated noise pulses of $\mathcal{O}(100\,\mu\text{s})$, the signal-to-noise ratio of the measurement can be improved by adding an artificial dead time that is configurable by a field programmable gate array in the DOM. The optimal setting for the dead time with respect to the signal over noise ratio for supernovae was found to be $\tau \approx 250\,\mu\text{s}$. This reduces the noise rate from 540 Hz to 286 Hz while introducing only 13% dead time for the signal.

In a recent study the rate distribution for data taken in 2010 after application of this artificial dead time still shows a broadening by a so called fano factor of $\sqrt{F} = \frac{\sigma}{\sqrt{<\mu>}} = 1.78$. This effectively reduces the number of DOMs by a factor of three, compared to an ideal detector with unit fano factors. In addition this correlation also broadens the width of our significance distribution. For the data from 2010 this effectively amounted to a factor of 1.43 and therefore a trigger with a measured significance 8.0 does only represent a deviation of about 5.6 standard deviations.

We believe the main reason for this broading to be the influence of correlated hits from atmospheric muons (see Fig. 1 right). We have then taken steps to eliminate this correlation by subtracting hits assiciated with atmospheric muons in an offline cleaning algorithm. We were able to reduce the fano factor from $\sqrt{F} = 1.78$ down to $\sqrt{F'} = 1.32$ and subsequently our significance distribution narrowed from a width of 1.43 to 1.05 (see Fig. 1 left).

3 IceCube performance

IceCube was completed in December 2010 and is comprised of 5160 photomultiplier tubes. Since 2009 it supersedes AMANDA in the SNEWS network. With a 250 μs artificial dead time setting, the average DOM noise rate is 286 Hz. The data taking is very reliable and covers the whole calendar year, the uptime has continuously improved and has reached 99.0 % since June 2011. IceCube's sensitivity corresponds to a megaton scale detector for galactic supernovae, triggering on supernovae with about 200, 20, and 6 standard deviations at the galactic center (10 kpc), the

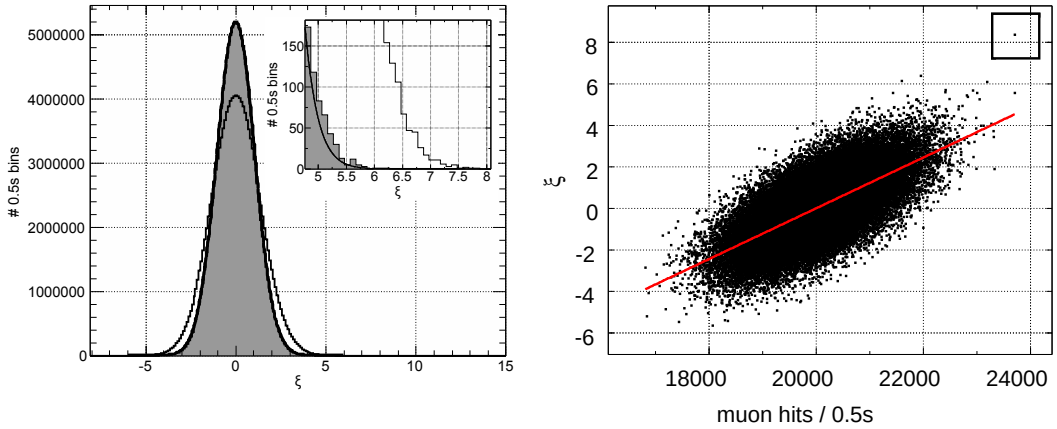

Figure 1: (color online) *Left:* This plot shows a significance distribution for data taken over 3 years, with IceCube configuration of 40, 59 and 79 strings. With offline post-processing we were able to reduce its width from originally 1.35 down to 1.05. *Right:* This correlation plot between the significance measured by IceCube's Supernova DAQ and the rate of reconstructed muons was used to rotate the significances around a "center of gravity" in order to decorrelate and thus effectivily subtract the muon influence. The 8 hour run shown contains the highest significance event before atmospheric muon subtraction.

galactic edge (30 kpc), and the Large Magellanic Cloud (50 kpc). IceCube cannot determine the type, energy, and direction of individual neutrinos and the signal is extracted statistically from rates that include a noise pedestal. On the other hand, IceCube is currently the world's best detector for establishing subtle features in the temporal development of the neutrino flux. The statistical uncertainties at 10 kpc distance in 20 ms bins around the signal maximum are about 1.5 % and 3 % for the Lawrence Livermore and Garching models, respectively.

Depending on the model, in particular the progenitor star mass, the assumed neutrino hierarchy and neutrino mixing, the total number of recorded neutrino induced photons from a burst 10 kpc away ranges between $\approx 0.17 \times 10^6$ (8.8 $M_\odot$ O-Ne-Mg core), $\approx 0.8 \times 10^6$ (20 $M_\odot$ iron core) to $\approx 3.4 \times 10^6$ for a 40 $M_\odot$ progenitor turning into a black hole. For a supernova in the center of our Galaxy, IceCube's high statistics would allow for a clear distinction between the accretion and cooling phases, an estimation of the progenitor mass from the shape of the neutrino light curve, and for the observation of short term modulation due to turbulent phenomena or forward and reverse shocks during the cooling phase. IceCube will be able to distinguish inverted and normal hierarchies for the Garching, Lawrence-Livermore and black hole models for a large fraction of supernova bursts in our Galaxy provided that the model shapes are known and $\theta_{13} > 0.9°$. The slope of the rising neutrino flux following the collapse can be used to distinguish both hierarchies in a less model dependent way for distances up to 6 kpc at 90 % C.L. As in the case of the inverted hierarchy, coherent neutrino oscillation will enhance the detectable flux considerably. A strikingly sharp spike in the $\bar{\nu}_e$ flux, detectable by IceCube for all stars within the Milky Way, would provide a clear proof of the transition for neutron to a quark star as would be the sudden drop of the neutrino flux in case of a black hole

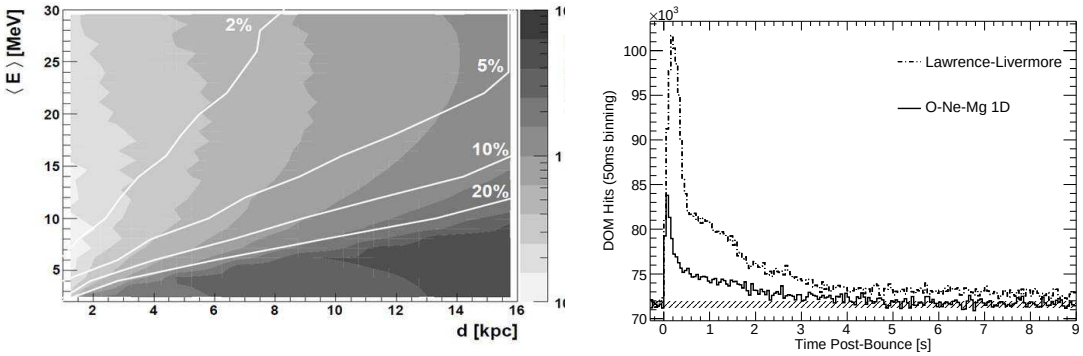

Figure 2: (color online) *Left:* This plot shows the result of a recent Monte Carlo study [4], where we were able to infer an average energy through the ratio between single and multiple coincidence hits. The ratio between the mean energy shown on the y-axis and its error shown as contour color gives the relative precision of our measurement shown as white contour lines. *Right:* This plot shows a comparison of expected supernova signal for two different models, the Lawrence Livermore [6] and the Hüdepohl/Garching model [5]. A 1 sigma-band corresponding to the measured detector noise is shown as a hatched area.

formation.

4 Outlook

As of late several projects concerning further optimizations to the data acquisition, analysis and Monte Carlo have started. We will upgrade IceCube's low level data processing logic to not only read out time binned scaler data, but to also store all photomultiplier hits with their respective timestamps in case of a high significance alert (i.e. the one we would sent to SNEWS). This will enable us to improve the time resolution beyond the current 2 ms and will pave the way for energy estimations using coincidences (see Fig. 2). As a first step, we consider the following nearest neighbour coincidences: **"1+0"** (single hit, no coincidence), **"1+1"** (double hit, two DOMs) and **"2+0"** (double hit on one DOM). Our calculations [4] show a clear energy dependence of the ratios $(1+1)/(1+0)$ and $(2+0)/(1+0)$. We found for the $(1+1)/(1+0)$ ratio a statistical error of 5% corresponding to an energy resolution of about 1 MeV, assuming a SN flux from a 8.8 solar mass Garching model [5] and 10 kpc distance.

References

[1] Abbasi, R., et al. 2010, Nucl. Instrum. Meth. A618, 139

[2] Abbasi, R., et al. 2009, Nucl. Instrum. Meth. A601, 294

[3] Antonioli, P., et al. 2004, New J. Phys., 6, 114

[4] Demiroers, L., Ribordy, M. & Salathe, M. 2011, arXiv:astro-ph/1106.1937v2

[5] Hudepohl L., Muller B., Janka H. -T.,Marek A., Raffelt G. G., Phys. Rev. Lett. 104, 251101 (2010).

[6] Totani, T., Sato, K., Dalhed, H. E., Wilson, J. R. 1998, Astrop. Phys., 496, 216

Supernova Neutrinos in Liquid Scintillator Detectors by means of neutrino-proton elastic scattering

Aldo Ianni[1]

[1]INFN, Laboratori Nazionali del Gran Sasso, S.S. 17bis km 18+910, 67010 Assergi, Italy

DOI: http://dx.doi.org/10.3204/DESY-PROC-2011-03/ianni

A brief review of supernova neutrino detection by massive underground liquid scintillators is presented. Prominence is given to the neutrino-proton elastic scattering detection channel which is unique for such detectors.

1 Introduction

In this paper we deal with massive underground liquid scintillator detectors which might search for supernova neutrinos. An organic liquid scintillator is made of carbon and hydrogen atoms and neutrinos from a core collapse supernova can be detected by a number of interaction channels (see also [1]): inverse-beta decay, neutrino-proton elastic scattering, neutrino-electron elastic scattering, charged current and neutral current on carbon nuclei. Among these interaction processes the *golden* detection channel is the inverse-beta decay for electron anti-neutrinos: $\bar{\nu}_e + p \rightarrow e^+ + n$. This interaction has the largest cross-section and a threshold equal to 1.806 MeV. Moreover, it offers an important tagging through the delayed signal provided by the capture reaction: $n + p \rightarrow d + \gamma(2.22\ \mathrm{MeV})$. This reaction can be thought of as background free in liquid scintillators.

For a standard supernova at 10 kpc [2] we predict about 300-400 events for a target mass with 10^{32} protons in the inverse-beta decay channel. Another important interaction channel is the neutral current on carbon nuclei: $\nu_x + ^{12}C \rightarrow \nu_x + ^{12}C + \gamma(15.11\ \mathrm{MeV})$. For this reaction we predict about 70 events for 10^{32} ^{12}C nuclei and for a standard supernova. This is also a background free reaction and will provide an unambiguous signal of supernova neutrinos. Yet, it will not be possible to disentangle the degeneracy between the supernova luminosity and temperature. Charged current interactions on ^{12}C and neutrino-electron elastic scattering will

Detector	N_p	Design
LVD	9.3×10^{31}	segmented
Borexino	1.7×10^{31}	unsegmented
KamLAND	5.9×10^{31}	unsegmented
Baksan	1.2×10^{31}	segmented
MiniBooNE	5.2×10^{31}	unsegmented
SNO+(*)	5.9×10^{31}	unsegmented
LENA(**)	3.3×10^{33}	unsegmented

Table 1: Liquid scintillator detectors which might detect supernova neutrinos. (*) SNO+ is planned to be operational in 2013. (**) LENA is in an advanced proposal stage.

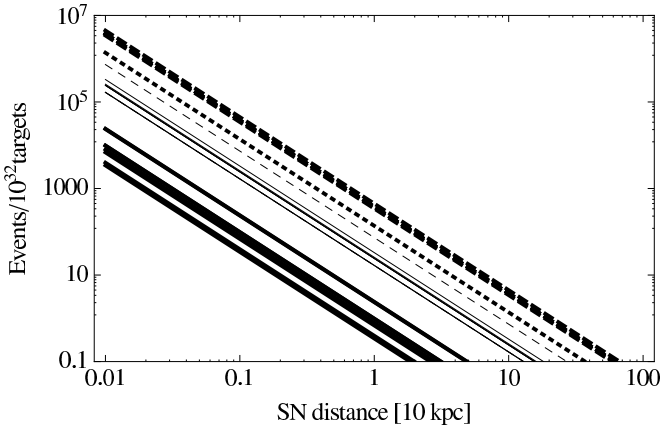

Figure 1: Predicted number of events for a standard supernova against the supernova distance. Black thick dashed lines: inverse-beta decay. Black thick dotted line: neutrino-proton elastic scattering. Black dashed: NC on ^{12}C. Black solid lines: CC on ^{12}C. Black thick solid lines: neutrino-electron elastic scattering.

play a minor role in the detectors in operation. The technology of massive liquid scintillators underground has been developed over the last 20 years. In Tab. 1 we report the list of detectors which make use of an organic liquid scintillator. One main design feature can be outlined: some detectors have a segmented structure, others not. This is an important aspect for supernova neutrinos due to the fact that in a segmented detector the duty cycle is often larger. However, an unsegmented detector can work better for other neutrino sources such as solar neutrinos, geo-neutrinos and electron antineutrinos from reactors, as an example. The possibility to search for just a rare event as that of a supernova cannot justify the construction of a massive underground neutrino detector nowdays. Therefore, the detectors listed in Tab. 1 have other main research goals besides supernova neutrinos.

In Fig. 1 we report a summary of the expected number of events for a standard supernova in a liquid scintillator detector. This figure includes the effect of neutrino oscillations with direct and inverted hierarchy. A galactic supernova can be as far as about 30 kpc with a most likely distance around 10 kpc. The SN1987A was at about 50 kpc.

In liquid scintillators at present electron neutrinos will produce only a minor signal. This could be different with the very massive LENA detector. The signal from electron neutrinos is important to probe the early neutrino production during the collapse. One possibility to disentangle electron neutrinos could come from the CC interaction on ^{12}C: $\nu_e + ^{12}C \rightarrow e^- + ^{12}N$ with a threshold equal to 17.34 MeV. This reaction is followed by the β-decay of ^{12}N which can provide a delayed tagging. However, in spite of the prompt-delayed signals, the rate in a kton scale detector is of the order of 10-20 events for a 10 kpc supernova. Moreover the CC channel on electron antineutrinos will make the measurement difficult with a small statistic data sample due to an overlap of the two visible spectra from ν_e and $\bar{\nu}_e$.

2 Neutrino-proton elastic scattering for supernova neutrinos

The idea to search for neutrino-proton elastic scattering was introduced by J. Beacom, W. Farr and P. Vogel in 2002 [3]. This work has been recently revised [4] to make use of quenching measurements and more realistic detector features. For this detection channel the visible energy is due to the recoiled protons. The yield of an ionizing proton in a liquid scintillator is affected by a non-radiative energy transfer. This effect is accounted for with a quenching factor which depends on the energy [5]. For a 20 MeV incoming neutrino the recoiled proton will have an energy of about 1 MeV and a visible energy of 0.2 MeV. Therefore, in order to exploit such a detection channel, the experimental apparatus needs a sub-MeV threshold. At present Borexino is working with a 0.2 MeV threshold to search for sub-MeV solar neutrinos [6]. The quenching of protons has been measured in KamLAND by means of a dedicated test facility [7] and in Borexino by means of an AmBe source deployed inside the detector. In Fig. 2 we show the expected spectrum for this interaction channel where $\nu_{\mu,\tau}$ in the supernova model have an average energy of 20 MeV. From this figure it is possible to see that the spectrum of ν_e and $\bar{\nu}_e$ are shifted below threshold due to the quenching effect: only $\nu_{\mu,\tau}$ can be detected above 200 keV. In Borexino, which has the smallest target size among the detectors listed in Tab. 1, we expect about 30 events for a 10 kpc supernova. From Borexino data [6] one expects about 3 accidental counts in 10 seconds which is the duration of the supernova burst. Therefore, we could claim that with the present technology developed for massive underground and high radiopurity liquid scintillators it is feasible to detect such supernova neutrinos. The neutrino-proton channel is a feature of liquid scintillators and is particularly important due to the fact that allows to break the degeneracy between temperature and binding energy for $\nu_{\mu,\tau}$ neutrinos. As a matter of fact, the temperature or average energy and the binding energy are related to the number of events detected: $N_{ev} \propto \langle\sigma\rangle E_{binding}/\langle E_{\nu_x}\rangle$. It turns out that the measurement of the spectrum of recoiled protons can break this degeneray and provide fundamental information about the supernova mechanism. In order to perform an accurate measurement it can be shown that the knowledge of the quenching at the level of a few %'s is important to disentangle the average neutrino energy. In a few years SNO+ with about 800 tons of target mass should also be able to detect sub-MeV energies.

3 Conclusions

Present massive liquid scintillators are ready to observe some 100-400/10^{32}targets neutrino events for a standard supernova at 10 kpc. The *golden* detection channel is the inverse-beta decay which probes $\bar{\nu}_e$. The neutrino-proton elastic scattering provide a unique investigation tool for $\nu_{\mu,\tau}$ neutrinos with high purity massive underground liquid scintillators detectors. Neutral current on carbon nuclei will offer an unambiguous signal of supernova neutrinos with about 70 events/10^{32}targets. Liquid scintillators at present cannot offer a good detection channel for electron neutrinos. This could be a goal for future super-massive detectors such as LENA.

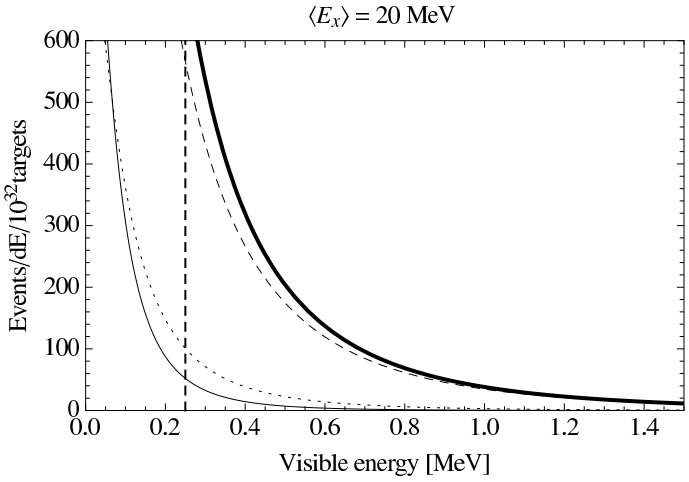

Figure 2: Expected visible spectrum for a 10 kpc supernova in the neutrino-proton elastic scattering detection channel. Back thin line: ν_e. Black dotted thin line: $\bar{\nu}_e$. Black thin dashed line: $\nu_{\mu,\tau}$

4 Acknowledgments

The author would like to acknowledge the organizing Committee for the nice atmosphere and the outstanding workshop.

References

[1] C. Virtue, *Supernova neutrino detection technologies*, this meeting.

[2] J. Raffelt, *Supernovae as laboratories for particle physics*, this meeting.

[3] J. Beacom, W. Farr and P. Vogel, Phys. Rev. D **66** 033001 (2002).

[4] B. Dasgupta and J. Beacom, Phys. Rev. D **66** 033001 (2002).

[5] J.B. Birks, *Photophysics of Aromatic Molecules*, Wiley-Interscience, London, 1970.

[6] Borexino collaboration, Physical Review Letters 107, 141302 (2011).

[7] S. Yoshida et al., NIM A bf 622 574-582 (2010).

SN neutrinos in LVD

Walter Fulgione[1,2] *for the LVD Collaboration*

[1]INFN, Torino, Italy
[2]INAF, IFSI-Torino, Italy

DOI: http://dx.doi.org/10.3204/DESY-PROC-2011-03/fulgione

The Large Volume Detector (LVD) in the INFN Gran Sasso National Laboratory (LNGS), Italy, is a ν observatory mainly designed to study low energy neutrinos from the gravitational collapse of galactic objects. The experiment has been monitoring the Galaxy since June 1992, under increasing larger configurations: in January 2001 it has reached its final active mass $M = 1$ kt. Next year it will celebrate twenty years of operation. No burst candidate has been found over 6314 days of live-time, since $June\ 6^{th}$ 1992 to $March\ 27^{th}$ 2011, resulting 90% c.l. upper limit to the rate of gravitational stellar collapses in the Galaxy ($D \leq 20$ kpc) is 0.13 y^{-1}.
Since July 2005 LVD participates to the Supernovae Early Warning System (SNEWS), the network of SN neutrino observatories whose main goal is to provide the astronomical community with a prompt alert for the next galactic core collapse supernova explosion.
Since 2006 acts as a far beam monitor for the Cern Neutrinos to Gran Sasso (CNGS) project, the high energy, wide band ν_μ beam, set up at Cern and sent towards the LNGS. Possible upgrade of the experiment have been studied and discussed in the last years.

1 The LVD Detector

The Large Volume Detector (LVD), located in the hall A of the INFN Gran Sasso National Laboratory, Italy, consists of 1000 tons of liquid scintillator arranged in a modular geometry. The major purpose of LVD is the search for neutrinos from Gravitational Stellar Collapses (GSC) in our Galaxy [1].
The detector consists of an array of 840 scintillator counters, 1.5 m^3 each. The whole array is divided in three identical "towers" consisting of 35 "modules" hosting a cluster of 8 counters. Each counter is viewed from the top by three photomultipliers (PMTs). The main neutrino reaction in LVD is $\bar{\nu}_e p \rightarrow e^+ n$, which gives two detectable signals: the prompt one, due to the e^+, followed by the signal from the (n,p) capture ($E_\gamma = 2.2$ MeV) with a mean delay of $\simeq 185$ μs.
The trigger logic is optimized for the detection of both products of the inverse beta decay and is based on the three-fold coincidence of the PMTs of a single counter. Each PMT is discriminated at two different thresholds resulting in two possible levels of coincidence between a counter's PMTs: H and L, corresponding to $\mathcal{E}_H \simeq 4$ MeV and $\mathcal{E}_L \simeq 500$ KeV.
The iron support structure of the detector can also act as a target for neutrinos and antineutrinos. The products of the interaction can exit iron and be detected in the liquid scintillator. The signal observable in LVD, in different reactions and due to different kinds of neutrinos, besides providing astrophysical informations on the nature of the collapse, is sensitive to intrin-

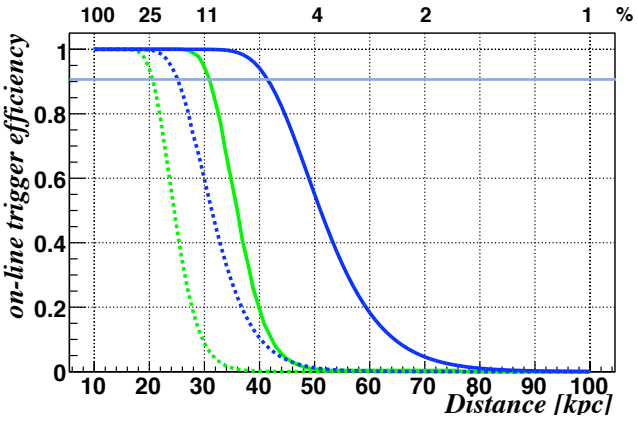

Figure 1: (color online) Trigger efficiency versus distance (lower scale) and percentage of SN1987A signal at 10 kpc (upper scale) for E_{cut}=7-10MeV (light green and dark blue lines, respectively) and M=300t (dotted) and 1000t (continuous) for LVD stand alone.

sic ν properties, as oscillation of massive neutrinos and can give an important contribution to define some of the neutrino oscillation properties still missing. We have studied [2] how neutrino oscillations affect the signal detected by LVD and also evaluated the impact on the signal of the astrophysical parameters of the supernova explosion mechanism, such as the total energy emitted in neutrinos, the star distance, the neutrino–sphere temperatures and the partition of the energy among neutrino flavors.
However, being aware of the fact that the astrophysical parameters of the supernova mechanism are up to now not well defined, to compute the detector sensitivity expressed in terms of source distance or emitted neutrino flux we adopted the following conservative values for the astrophysical parameters [3],[4]: average $\bar{\nu}_e$ energy $\langle E_{\bar{\nu}_e} \rangle$=14 MeV; total radiated energy $E_b = 2.4{\cdot}10^{53}$ erg and average non-electron neutrino energy 20% higher than $\bar{\nu}_e$. Concerning neutrino oscillations we conservatively considered normal mass hierarchy and non-adiabaticity. Taking into account Poisson fluctuations in the cluster multiplicity, we derived the trigger efficiency shown in figure 1 as a function of the distance for LVD working stand-alone [5].

2 Results

LVD has been taking data since June 1992 with increasing mass configurations (sensitive mass being always greater than 300 t), enough to monitor the whole Galaxy ($D \leq 20$ kpc)[1]. In fig. 2 we show sensitive mass and duty cycle of the experiment since $June\ 6^{th}$ 1992 to $March\ 27^{th}$ 2011. The search for ν burst candidates is performed by studying the temporal sequence of triggers and looking for clusters. Preliminary cuts are applied to reject muons and events with an energy release lower than 7 MeV to avoid threshold effects. The neutrino burst candidate selection, widely discussed in [5], requires that the bulk of the events in the

[1]The results of this search have been periodically updated and published in the ICRC and Neutrino Conference Proceedings, since 1993 till 2011. [6].

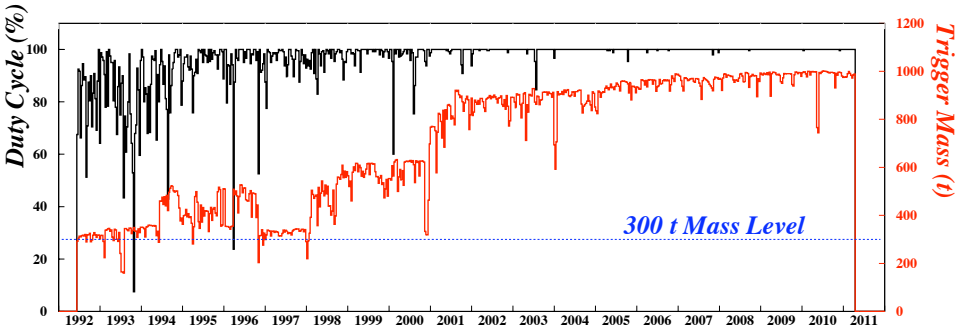

Figure 2: (color online) LVD sensitive mass and duty cycle during 1992-2011.

cluster is contained in a time window of duration 10 sec (relaxed to 100 sec in the off-line analysis) and that events are uniformly distributed inside the array. The candidate is simply characterized by its multiplicity m, i.e. the number of pulses detected in Δt. All the other characteristics of the cluster are left to a subsequent independent analysis. The search for burst candidates is performed, on-line, simultaneously for two values of the energy cut: $\mathrm{E}_{cut} = 7$ MeV ($f_{bk} = 0.2$ Hz) and $\mathrm{E}_{cut} = 10$ MeV ($f_{bk} = 0.03$ Hz). The chosen imitation frequencies, F_{im}, below which the detected cluster will be a candidate supernova event, is 1 per 100 year working stand-alone while it is relaxed to 1 per month working in coincidence with other detectors (SNEWS),[2] and 1 per day for monitoring task. After this pure statistical selection a complete analysis of each detected cluster with $F_{im} \leq 1$/day is performed, to test its consistency with a ν burst through the study of the topological distribution of events inside the array, energy spectrum and time distribution of events in the cluster and time distribution of delayed low energy pulses, signature of $\bar{\nu}_e$ interactions.
No candidates have been found since 1992, see detail in table 1. Since the LVD sensitivity is higher than expected from GSC models (even if the source is at a distance of 20 kpc and for soft neutrino energy spectra), the resulting 90% c.l. upper limit to the rate of gravitational stellar collapses in the Galaxy ($D \leq 20$ kpc) is 0.13 y^{-1}.

3 Possible upgrades

During the last years we have investigated possible upgrades of the detector. In particular we studied the possibility to improve the detector capability in distinguish different neutrino interactions by adding Gd to the liquid scintillator and the possibility of LVD to act as an active shielding and veto with respect to an internal volume.
Doping the liquid scintillator with a small ($\sim 0.15\%$ in weight) quantity of Gd definitely improves the performance of the LVD tank in the neutron detection, because Gd has a huge cross

[2]The SNEWS (SuperNova Early Warning System) [7] project is an international collaboration including several experiments sensitive to a core-collapse supernova neutrino signal in the Galaxy and neighbourhood.

Table 1: LVD run.

RUN	SINCE	TO	LIVE TIME	DUTY CYCLE	MASS
1	6-6-1992	5-31-1993	285 days	60 %	310 t
2	8-4-1993	3-11-1995	397 days	74 %	390 t
3	3-11-1995	4-30-1997	627 days	90 %	400 t
4	4-30-1997	3-15-1999	685 days	94 %	415 t
5	3-16-1999	12-11-2000	592 days	95 %	580 t
6	12-12-2000	3-24-2003	821 days	98 %	842 t
7	3-25-2003	2-4-2005	666 days	> 99 %	881 t
8	2-4-2005	5-31-2007	846 days	> 99 %	936 t
9	5-31-2007	4-30-2009	669 days	> 99 %	967 t
10	5-1-2009	3-27-2011	696 days	> 99 %	981 t
Σ	6-6-1992	3-27-2011	6314 days		

section for n-capture due, essentially, to the two isotopes ^{155}Gd and ^{157}Gd. In particular the mean n-capture time results highly shortened and the gamma cascade generated in n-captures on Gd has a total energy of about 8 MeV to be compared with 2.2 MeV of gamma quanta from (n,p) captures [8]. Accordingly, doping with Gd the LVD liquid scintillator, we could increase the signal to noise ratio of a factor of several hundreds maintaining the present neutron capture detection efficiency, simply increasing the energy threshold for neutron detection and shortening the time window for the coincidence.

The improvements that LVD could obtain if all its active scintillator mass was doped with this small amount of Gadolinium has been evaluated in [9]. It results that the detection probability of a neutrino burst from a core collapse in the Large Magellanic Cloud would be as high as 90%, while it is currently around 50%. The sensitivity that is achieved when Gd doping the whole detector is comparable to that which we would obtain doubling the mass of LVD.

It is well known that the muon-induced high energy neutrons limit the possibility of searches for rare events, like neutrinoless double beta decay or WIMP dark matter interactions. Underground laboratories provide the overburden necessary to reduce this background, by attenuating cosmic-ray muons and their progenies. If the depth of the underground laboratory is not enough to reach the necessary background reduction, the high energy neutron flux can be shielded and/or actively vetoed. An inner region inside the LVD structure with a volume of about 30 m^3 could be realized causing a negligible impact on LVD operation and sensitive mass and could be effectively exploited by a compact experiment for the search of rare events [10].

We have evaluated the shielding power of LVD working both as an active veto for muons that generate high energy neutrons, and as a passive shield and moderator for the low energy gamma and neutron background. From the results of a dedicated simulation [11] it appears that, with LVD behaving as a muon veto, the flux of high energy un-vetoed neutrons at the surface of the inner region is reduced by a factor 50, that is equivalent to the muon-induced neutron flux at the equivalent vertical depth of 6 km w.e (i.e. the Sudbury mine).

References

[1] LVD Collaboration, Il Nuovo Cimento **A105** (1992) 1793

[2] N. Yu. Agafonova *et al.*, Astropart. Phys. **27**, 254-270 (2007) [arXiv: hep-ph/0609305].

[3] G. Pagliaroli, F. Vissani, M. L. Costantini, and A. Ianni, Astropart. Phys. **31**, 163 (2009)

[4] M.L. Costantini, A. Ianni and F. Vissani, Phys. Rev. D **70** (2004) 043006.

[5] N. Yu. Agafonova *et al.*, Astropart. Phys. **28**, 516-522 (2008) [arXiv:0710.0259].

[6] W.Fulgione *et al.*, Proceedings of the $\mathbf{32}^{nd}$ ICRC, 2011.

[7] P. Antonioli *et al.*, New Journal of Physics **6** (2004) 114 [http://hep.bu.edu/∼snnet/]

[8] I.R. Barabanov *et al.*, JINST **5** (2010) P04001, e-Print: arXiv:0803.1577 [physics.ins-det]

[9] G.Bruno *et al.*, JCAP **06** (2011) 024

[10] F.Arneodo and W.Fulgione JCAP **02** (2009) 028

[11] M.Selvi et al., IDM 2008, Stockholm, Sweden, 18-22 Aug 2008. e-Print: arXiv:0811.2884 [hep-ex]

Supernova Neutrino Signal at HALO: Learning about the Primary Neutrino Fluxes

Daavid Väänänen, Cristina Volpe

Institut de Physique Nucléaire,
F-91406 Orsay cedex, CNRS/IN2P3 and University of Paris-Sud, France

DOI: http://dx.doi.org/10.3204/DESY-PROC-2011-03/vaananen

We predict the numbers of one- and two-neutron charged and neutral-current electron-neutrino scattering on lead events including collective effects due to the neutrino-neutrino interactions and the Mikheev-Smirnov-Wolfenstein (MSW) effect due to the neutrino interactions with the background matter. We show that the ratios of one- to two-neutron events are sensitive to the pinching parameters of neutrino fluxes at the neutrinosphere, almost independently of the presently unknown neutrino properties. Besides, such events have an interesting sensitivity to the spectral split features that depend upon the presence/absence of energy equipartition among neutrino flavors.

1 Introduction

The features of the *primary* (i.e. at the neutrinosphere) neutrino fluxes encode information on supernova dynamics, including the microscopic processes determining the neutrino transport within the supernova core and the equation of state of the neutron star. The details of the neutrino spectra at the surface of the star depend upon such primary neutrino fluxes and upon unknown neutrino parameters – in particular the mass hierarchy and the third neutrino mixing angle. Extracting information on the primary fluxes from future observations, in spite of the unknowns and of the complexity of flavor conversion phenomena in such media, represents an important test of supernova models. Important progress has been made in our understanding of flavor conversion in these environments (for a recent review on $\nu\nu$ interaction effects, see e.g. [1]). However, several aspects still need a full understanding. Work is also needed to finally assessing its phenomenological impact in a future core-collapse supernova signal.

Most of the existing and proposed observatories, with a capability to detect supernova neutrinos, are sensitive to electron anti-neutrinos through scattering on protons. While liquid argon and scintillator detectors like LENA are sensitive to ν_e, a new detector is currently under construction at SNOLAB: the Helium And Lead Observatory (HALO). This dedicated supernova neutrino detector is able to observe the neutrons emitted from electron-neutrino scattering on lead from charged- and neutral-current events.

In this contribution, we discuss the information that can be extracted, with a detector like HALO, on the characteristics of the neutrino spectra at the neutrinosphere, taking into account the existing uncertainties from the unknown neutrino properties and from the different supernova simulations. More details on this work can be found in [2].

2 Neutrino flavor evolution: the formalism

We follow the neutrino flavor evolution from the neutrinosphere of an iron core-collapse supernova (SN) up to Earth. We propagate probabilities using the approximation of factorized dynamics. This allows us to use analytical expressions to compute the fluxes. Such an approximation has been shown to be reliable if one is not considering phase effects (from shock wave or from the Dirac CP violating phase [3]), which is our case. The primary neutrino fluxes at the neutrinospheres can be expressed using modified power law energy distribution as

$$F^0_\nu(E_\nu) \propto \frac{L_\nu}{\langle E^0_\nu \rangle} E^{\alpha_\nu}_\nu \exp\left[-(\alpha_\nu + 1) \frac{E_\nu}{\langle E^0_\nu \rangle} \right] ,$$

where L_ν is neutrino luminosity, $\langle E^0_\nu \rangle$ average neutrino energy and α_ν characterizes pinching.

In the collective region, we follow the results of the full three flavor numerical calculations with/without equipartition for the neutrino luminosity (as in [4]). These calculations show that after the collective effects there can be no splits, one low (or high) energy split or both low and high energy splits in (anti)neutrino spectra, depending on the neutrino flux parameters and mass hierarchy. We have assumed all the splits in energy to be sharp. In the computation of event numbers we have used numerical values $E^s_l = 8$ MeV and $E^s_h = 23$ MeV (E^s_l and E^s_h are the low and high split energies, respectively), when appropriate. Non-electron-type (anti)neutrino fluxes are assumed to be equal.

After the collective effects have ceased, the neutrinos enter the MSW region. In this region, neutrino flavor evolution depends on how the MSW resonances are crossed. The measured values of the solar parameters make the flavor transition at the low resonance always adiabatic for typical density profiles from supernova simulations. We consider the still unknown mixing angle θ_{13} to be very small (0.001) or close to the present Chooz limit (0.1). This implies that all the processes at the high resonance are assumed to be completely adiabatic (large) or non-adiabatic (very small θ_{13}). For the other mixing angles we use the values $\sin^2 2\theta_{12} = 0.86$, $\sin^2 2\theta_{23} = 0.99$. We set the Dirac CP phase to zero.

Once the (anti)neutrinos have reached the surface of the star as mass eigenstates ν_i ($i = 1, 2, 3$), they travel up to Earth and are detected as flavor eigenstates ν_ℓ ($\ell = e, \mu, \tau$). The probabilities of a certain flavor neutrino ν_ℓ being in a given mass eigenstate ν_i is given by $|U_{\ell i}|^2 = |\langle \nu_\ell | \nu_i \rangle|^2$, where $U_{\ell i}$ is an element of the Pontecorvo-Maki-Nakagawa-Sakata (PMNS) mixing matrix $U_{\rm PMNS}$.

3 Expected events in the Helium and Lead Observatory

The detector is currently under construction and should start to be operating soon [5]. In phase-I HALO is made of 79 tons of lead while in phase-II the mass is planned to be increased to 1 kton. Such a detector exploits the following detection channels:

$$\begin{array}{ll} \nu_e + {}^{208}\mathrm{Pb} \to {}^{207}\mathrm{Bi} + n + e^- & \nu_x + {}^{208}\mathrm{Pb} \to {}^{207}\mathrm{Pb} + n + \nu_x \\ \nu_e + {}^{208}\mathrm{Pb} \to {}^{206}\mathrm{Bi} + 2n + e^- \ , & \nu_x + {}^{208}\mathrm{Pb} \to {}^{206}\mathrm{Pb} + 2n + \nu_x \end{array}$$

where neutrons are detected using ^{3}He counters as done for SNO experiment. In phase-I, one-neutron ($1n$-) and two-neutron ($2n$-) detection efficiencies are about 50 % and 25 %, respectively, while the detector will have a good time resolution of about 30 ms. Since HALO does not identify

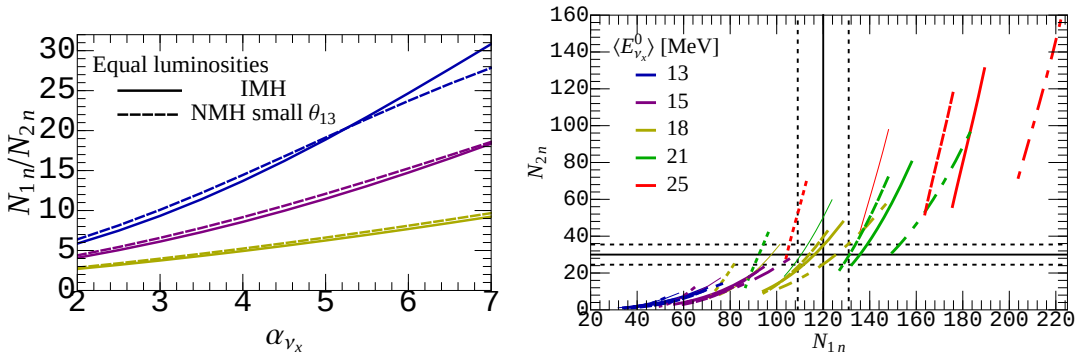

Figure 1: (color online) Left: Ratios of one- (N_{1n}) to two-neutron (N_{2n}) event rates as a function of primary non-electron neutrino pinching parameter α_{ν_x} with different primary non-electron-type neutrino average energies. Here equal luminosities and IMH are assumed. Average energies are from top to bottom $\langle E^0_{\nu_x}\rangle = 13, 15$ and 18 MeV. Right: One- and two-neutron event rates with different values of α_{ν_x}: at the top (bottom) of each curve $\alpha_{\nu_x} = 2$ (7). Solid lines are for equal luminosities (thick IMH, thin NMH with small θ_{13}), others for $L_{\nu_x} = 2L_{\nu_e}$: dotted IMH, dashed NMH with large θ_{13} and dash-dotted NMH with small θ_{13}.

the outgoing lepton, the total event rates are given by the sum of charged- and neutral-current event rates. The neutrino-lead cross sections we use are from a microscopic calculation based on the Random Phase Approximation (RPA) (see table I of ref.[6]).

In ref. [2] we have performed new predictions for the $1n$- and $2n$-events (from galactic supernova at 10 kpc) going beyond the previous calculations [6, 7] and including collective effects. In all of our calculations we assume a 100 % detection efficiency and consider HALO phase-II (1 kton). Since $1n$- and $2n$-events can be well identified, it is attractive to consider the corresponding ratio which is independent of common normalization factors (see e.g. left panel of Figure 1 valid for equal luminosities and IMH). From the figure it is clear that these ratios are sensitive to the pinching regardless of the physical scenario i.e. luminosities, neutrino mass hierarchy and the value of θ_{13}. The measured ratio would allow to identify different degenerate combinations of non-electron-type primary neutrino average energies and pinching parameters (even without a precise knowledge of the physical scenarios and common flux parameters). By knowing (or assuming) the non-electron-type primary neutrino average energy, it would be possible to give tight constraints on pinching.

We have summarized our results in the right panel of Figure 1 in which all the $1n$- and $2n$-events, in our considerations, are shown. The values are taken for a typical cooling phase (the total time-integrated luminosity is 10^{53} erg). The straight lines correspond to an example where 120 one-neutron events and 30 two-neutron events are measured during the explosion, with the associated statistical errors. This example case shows that while from the point of view of neutrino properties (mass hierarchy and θ_{13}) all scenarios are possible, rather tight constraints on the primary flux parameters – average energy and pinching parameter – can be obtained. However, notice that, if the $1n$- and $2n$-event numbers are e.g. 220 and 140, respectively (corresponding to $\langle E^0_{\nu_x}\rangle \approx 25$ MeV and $\alpha_{\nu_x} \approx 2-4$), one can obtain also a clear indication on the mass hierarchy, the value of θ_{13} and the luminosity case: the most favorable would be $L_{\nu_x} = 2L_{\nu_e}$ and NMH with small θ_{13}.

4 Conclusions

We have presented new predictions of the expected neutrino events from iron core-collapse supernovae in a lead-based observatory, such as Helium and Lead Observatory (HALO) under construction at SNOLAB. Our calculations include collective flavor conversion and the MSW effects while possible shock wave, turbulence or Earth matter effects are not considered.

We have shown that the measurement of $1n$- and $2n$-event rates as well as of their ratio is particularly sensitive to the non-electron neutrino primary average energy and pinching parameter. Using information from other detectors, the combination of $1n$- and $2n$-event rates should allow to identify degenerate solutions of average energies and pinching values. Moreover, from the ratio of these events, HALO alone can be used to give constraints on these parameters. Furthermore, from the combination of $1n$- and $2n$-event rate measurement it may be possible to give an indication on the presence/absence of the energy equipartition among neutrino flavors.

The present work emphasizes the interest of having more information on the characteristics of the high-energy component of the neutrino distributions at the neutrinosphere from future supernova simulations. It also furnishes a good example of how, having a network of detectors with different energy thresholds, constitute a unique tool to probe different components of the neutrino fluxes from a supernova explosion and to unravel interesting information on the neutrino emission and on neutrino properties. However, to be able to extract the most from future observations, a precise measurement of neutrino-lead cross sections is called for. This could be realized either at a low energy beta-beam facility [8], or nearby one of the future intense Spallation Sources [9].

References

[1] Huaiyu Duan, George M. Fuller, and Yong-Zhong Qian. Collective Neutrino Oscillations. *Ann.Rev.Nucl.Part.Sci.*, 60:569–594, 2010.

[2] Daavid Vaananen and Cristina Volpe. The neutrino signal at HALO: learning about the primary supernova neutrino fluxes and neutrino properties. 2011. * Temporary entry *.

[3] Akif Baha Balantekin, J. Gava, and C. Volpe. Possible CP-Violation effects in core-collapse Supernovae. *Phys.Lett.*, B662:396–404, 2008.

[4] Sandhya Choubey, Basudeb Dasgupta, Amol Dighe, and Alessandro Mirizzi. Signatures of collective and matter effects on supernova neutrinos at large detectors. 2010.

[5] *One can follow the status from the HALO website: http://www.snolab.ca/halo/.*

[6] J. Engel, G.C. McLaughlin, and C. Volpe. What can be learned with a lead based supernova neutrino detector? *Phys.Rev.*, D67:013005, 2003.

[7] George M. Fuller, Wick C. Haxton, and Gail C. McLaughlin. Prospects for detecting supernova neutrino flavor oscillations. *Phys.Rev.*, D59:085005, 1999.

[8] Cristina Volpe. What about a beta beam facility for low-energy neutrinos? *J.Phys.G*, G30:L1–L6, 2004.

[9] R. Lazauskas and C. Volpe. Low energy neutrino scattering measurements at future Spallation Source facilities. *J.Phys.G*, G37:125101, 2010.

Supernova Neutrino Detection via Coherent Scattering

E. Bougamont[1], *P. Colas*[1], *A. Dastgheibi-Fard*[1], *J. Derre*[1], *I. Giomataris*[1], *G. Gerbier*[1], *M. Gros*[1], *P. Magnier*[1], *X.F. Navick*[1], *P. Salin*[2], *I. Savvidis*[3], *G. Tsiledakis*[1], *J.D. Vergados*[4]

[1]CEA-Saclay, France
[2]APC University of Paris, France
[3]University of Thessaloniki, Greece
[4]University of Ioannina, Greece

DOI: http://dx.doi.org/10.3204/DESY-PROC-2011-03/tsiledakis

Development of large mass detectors for low-energy neutrinos and dark matter may allow supernova detection via neutrino-nucleus elastic scattering. The Spherical Proportional Counter, recently developed, allows to instrument large target masses with good energy resolution and sub-keV energy threshold. This detector filled with a high pressure and high Z noble gas, can be employed to detect typical supernova neutrinos in our galaxy. Here we provide feasible measured signal rates and describe further developments optimizing the electric field configuration around the central electrode of the detector.

1 Introduction

The question of detecting and exploiting neutrinos from both terrestrial and extra terrestrial sources has become central to physics and astrophysics. Coherent neutrino-nucleus scattering is a famous but as yet untested prediction of the Standard Model [1, 2]. The process is mediated by neutral currents (NC), and hence is flavor-blind. Despite having relatively high rates, neutrino-nucleus scattering is difficult to observe because its only signature is a small nuclear recoil of energy $\sim$ keV (for MeV neutrinos). Because the neutrino is light, the nuclear recoil energy is extremely small leading to a signal below threshold for conventional solid or liquid state detectors. Thus, the challenge is to achieve a very low energy threshold (typically below 100 eV). Perhaps, the "ultimate" supernova detector involves neutrino-nucleus elastic scattering. The cound rate in such a detector could be very high because the coherent elastic cross section is large and all six neutrino components contribute to the signal. The detection might be feasible using large mass detectors [3].

A new gaseous detector based on a spherical geometry, the Spherical Proportional Counter (SPC), has been developed that combines large mass, sub-keV energy threshold and good energy resolution. This new concept has been proven to operate in a simple and robust way and allows reading large volumes with a single read-out channel. In the next session a short description and details of its performance will be provided. Then, new developments concerning the electrostatics of the SPC will be shown. Finally, we will present an estimation of the number of expected neutrino events for a typical supernova at 10 kpc, using this novel detector.

2 Detector description and performance

The detector consists of a large spherical copper vessel 1.3 m in diameter and a small metallic ball 16 mm in diameter located at the center of the drift vessel, which is the proportional counter. The ball is maintained in the center of the sphere by a stainless steel rod and is set at high voltage. A second electrode (umbrella-shaped) that is placed 24 mm away from the ball along the rod, is powered with an independent but lower high voltage, serving as electric field corrector. The detector operates in a seal mode: the spherical vessel is first pumped out and then filled with an appropriate gas at a pressure from few tens of mbar up to 5 bar. Detailed description of the detector, its electronics, its operation and its performance could be found in references [4, 5, 6].

Ultra low energy results taken with this counter are shown in reference [7, 8], leading to an energy threshold as low as 25 eV and a single electron detection sensitivity. The bench mark result is the observation of a well resolved peak at 270 eV due to carbon fluorescence, which is a unique performance for such large massive detector. Its moderate cost, simplicity and robustness, make this technology a promising approach to NC based detection of reactor and astronomical neutrinos and opens a new window in dark matter searches.

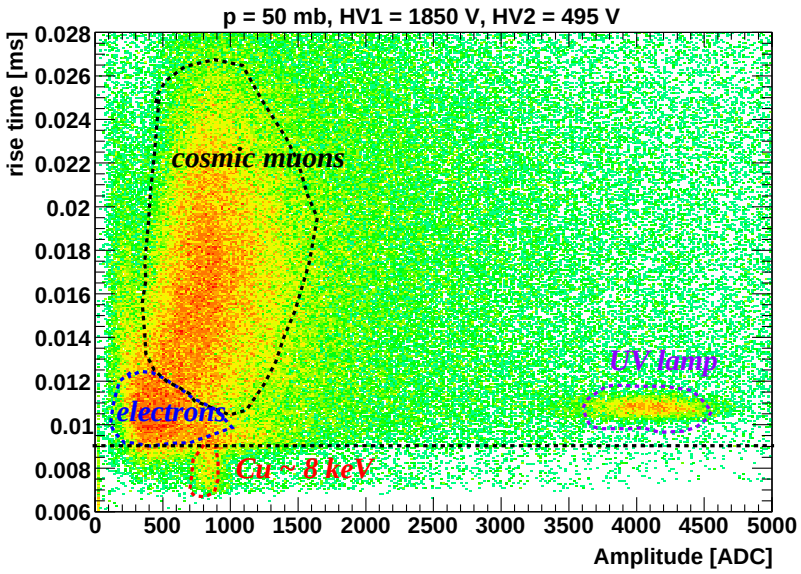

Figure 1: (color online) The rise time (rt) versus the amplitude for a gas mixture of Ar-CH_4 2% where a UV lamp is attached on the sphere.

A run is performed with the present detector, using a gas filling of Argon with 2% admixture of CH_4 and having a UV flash lamp installed in one of the sphere openings. The scatter plot of the rise time (rt) versus the amplitude of the signal is shown in Figure 1. The rise time of the signal actually provides the depth of the ionized electrons produced in the gas. We can observe on Figure 1 cosmic muons that are crossing the chamber having large rise time, electrons or low rise time X-rays that are absorbed in the periphery of the SPC, the photoelectrons created by the lamp which have the maximum drift time and the 8 keV line which is an induced

fluorescence at the copper vessel. By applying a cut at rt $\leq$ 0.009 ms, we keep only volume events and observe a spectacular background reduction, from $\sim$300 Hz to $\sim$4.5 Hz, with $\sim$1.5 Hz in Cu (keeping $\sim$70% of the signal). The observed background at the relevant region for supernova neutrino detection (a few keV) is already quite low at ground. Keeping in mind that the needed mass to observe 100 events from a local SN is about 6000 times higher than the mass involved in present run, we anticipate that a shield might be needed.

2.1 Current developments configuring the electrostatics of the SPC

Current efforts focus on the design of an electrostatic structure that allows bringing the high voltage to the internal sphere with minimal distortion of the spherical field, both for purposes of drift and homogeneous amplification all around the small sphere [6]. The electric field configuration of the entire system has been numerically simulated and optimized, using COMSOL Multiphysics[1]. Figure 2 shows the electric field in a circle at a distance of 0.2 mm far from

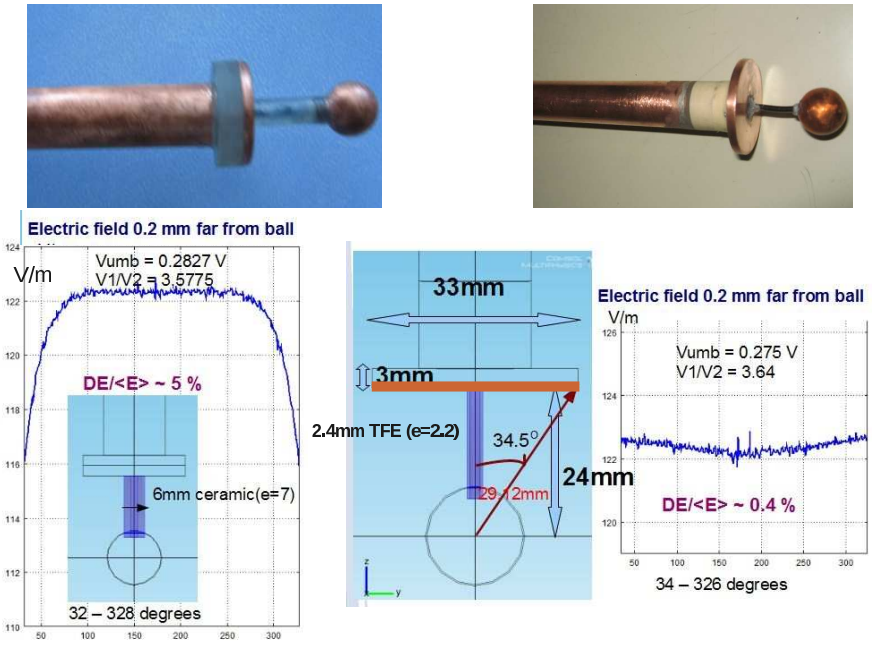

Figure 2: (color online) The simulated variation of the electric field 0.2 mm far from the ball for two different sensors.

the central electrode (ball) where an electric potential of 1 V is applied. In the first case the insulator that connects the two electrodes is made by ceramic of 6 mm thickness and in the second by teflon of 2.4 mm. The simulation proves that in the second case the variation of the electric field around the ball is significantly smaller, leading to a conclusion that material of low dielectric constant combined with a small thickness should be used. Preliminary results given in Figure 3 look very promising. The energy resolution in the 8 keV line of copper when a single cable is used is 6% (FWHM), compared to 11%.

[1]COMSOL Multiphysics, http://www.comsol.com

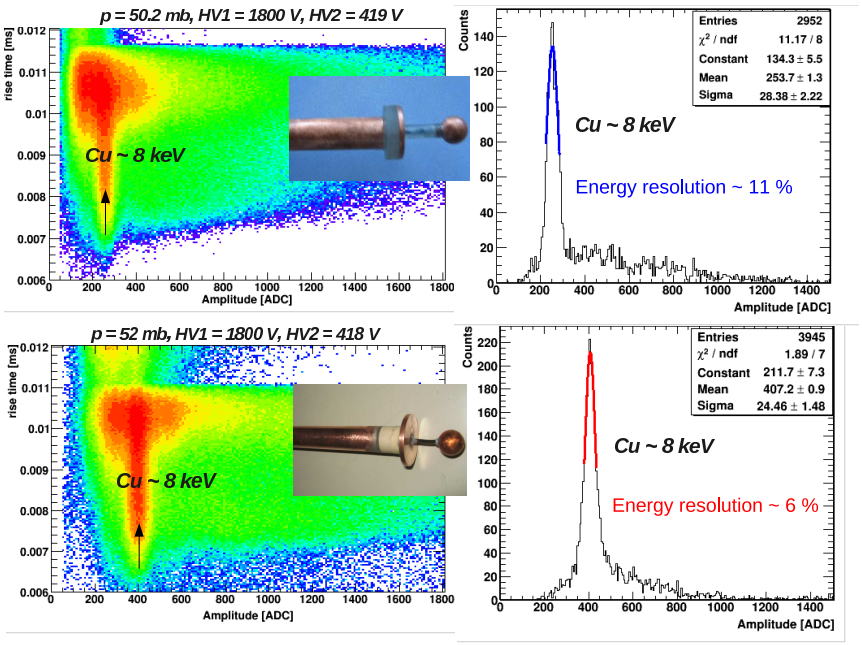

Figure 3: (color online) The rise time (rt) versus the amplitude as well as the energy spectra ($7 \leq$ rt $\leq 8\mu$s) for two different sensors where a gas mixture of Ar-CH_4 2% is used.

3 Supernova detection

In [9] it has been shown that it is feasible to detect typical supernova neutrinos in our galaxy. The idea is to employ the Spherical Proportional Counter filled with a high pressure noble gas. An enhancement of the neutral current component is achieved via the coherent effect of all neutrons in the target. The peak energies of the emitted neutrinos are approximately 15, 25 and 35 MeV for electron neutrinos, electron antineutrinos and all other flavors respectively. A detector of radius 2 m filled with Xe gas at a pressure of 10 Atm will detect about 100 events for a typical supernova explosion at 10 kpc. A world wide network of several such simple, stable and low cost supernova detectors is proposed [9].

References

[1] D.Z. Freedman *et al.*, Ann. Rev, Nucl. Sci. **27** 167 (1977).
[2] A. Drukier and L. Stodolsky, Phys. Rev. **D30** 2295 (1984).
[3] C.J. Horowitz, K.J. Coakley and D.N. McKinsey, Phys. Rev. **D68** 023005 (2003).
[4] S. Aune *et al.*, AIP Conf. Proc. **785** 110-118 (2005).
[5] I. Giomataris *et al.*, Nucl. Phys. Proc. Suppl. **150** 208-213 (2006).
[6] I. Giomataris *et al.*, JINST **3** P090007 (2008).
[7] E. Bougamond *et al.*, arXiv:1010.4132 [physics.ins-det], to be published at JMP (2010).
[8] E. Bougamont *et al.*, J.Phys. Conf. Ser. **309** 012023 (2011).
[9] I. Giomataris and J.D. Vergados, Phys. Lett. **B634** 23-29 (2008).

Chapter 4

Summary Talk

Neutrino Forecast: Mostly Sunny, with a Good Chance of Supernovas

Mark R. Vagins

Institute for the Physics and Mathematics of the Universe, Todai Institutes for Advanced Study, University of Tokyo, 5-1-5 Kashiwanoha, Kashiwa, Chiba 277-8583, Japan

DOI: http://dx.doi.org/10.3204/DESY-PROC-2011-03/vagins

A very personal view of the near-term prospects for non-terrestrial neutrino detection is presented in this somewhat unconventional, conference-concluding talk. The bottom line: thanks to new technologies currently under development, a steady supply of supernova neutrinos should soon be available for study in the not-too-distant future.

1 Okay, Let's Get the Ground Rules Straight

This article is a record of what was presented as the concluding talk of the HAνSE 2011 supernova neutrino workshop, which was held at DESY in Hamburg, Germany, in July of that year. The final talk was not meant, intended, or expected to be a summary of what had been shown at the meeting up to that point, but rather was designated by the organizers to be a hopefully entertaining, definitely upbeat expression of my personal views on the prospects for supernova neutrino detection, circa mid-2011.

Therefore, in what follows I speak only for myself. For the purposes of that talk and this article I am not "Prof. Mark Vagins for the *XYZ* Collaboration"; rather, consider this to be merely the sound of a lone experimentalist's voice in the wilderness.

Fair warning: this article contains cartoons, sarcasm, and a dash of salty language. Proceed into these Proceedings at your own risk.

2 A Snide Aside

Now that we have the ground rules established, I would like to thank the organizers of this conference, not just for inviting me to give a sunny concluding talk, but also for setting a good example in the appropriate use of our beloved "ν".

Sure, the Greek letter *nu* rather looks like the English letter "v". However, as illustrated in Figure 1, it is most certainly pronounced with an "n" sound. You know, like that sound at the beginning of the word *neutrino*. And indeed, HAνSE is properly pronounced (and sometime written) as

Figure 1: "This just in: v and ν are not, as previously believed, interchangeable!"

"HANSE", a quite resonant word in Northern German history.

Why bother to point this out? Well, recently there has been an unfortunate tendency in our field to ignore the fact that "ν" is a proper Greek letter carrying a specific pronunciation. Instead, it is being used as if it's some clever, insider way to insert a "v" into an acronym. That's right, NOνA and MINERνA, I'm talking to you! Or perhaps I should say NONA and MINERNA. There will be more about acronyms later.

3 Why So Serious?

So, what's not to love about supernova neutrinos? They carry unique information about one of the most dramatic processes in the stellar life-cycle, a process responsible for the production and dispersal of all the heavy elements (i.e., just about everything above helium) in the universe, and therefore a process absolutely essential not only to the look and feel of the universe as we know it, but also to life itself.

As a gauge of the community's level of interest in these particular particles, it is worth noting that, based upon the world sample of twenty or so neutrinos detected from SN1987A (by Kamiokande, IMB, and BAKSAN), there has on average been a paper published once every ten days... for the last twenty-four years! After a quarter of a century, this handful of events remain the only recorded neutrinos known to have originated from a more distant source than our own Sun (by an easily-remembered factor of 10^{10}).

Figure 2: Regarding supernova neutrinos, the waiting is the hardest part... primarily because of, well, *death.* No one wants to be that guy on the right. The other guy's probably not having such a great time, either.

My talk was given on July 23$^{\text{rd}}$, 2011. In other words, this decidedly optimistic presentation about seeing supernova neutrinos took place exactly 406 years and 287 days since a supernova was last conclusively observed in our own galaxy. That was SN1604, often known as "Kepler's supernova". Of course, no neutrino observatories were online that mid-October day in 1604, but it was probably a type Ia explosion, anyway.

Not surprisingly, the next nearby core collapse supernova is eagerly awaited by experimentalists, observers, and theorists alike. Unfortunately, over the last 1800 years there have been just six such explosions seen in our galaxy. So the really big question, of course, is: *when will the next one happen?* The most serious problem is that none of us has an unlimited time in which to wait, as I have quite helpfully (and graphically) depicted in Figure 2.

Yes, it has certainly been a long, cold winter for supernova neutrino watching. But I am here to tell you, to *testify,* my weakly-interacting brothers and sisters, that there is hope!

4 The Good News

Now, anyone who knows me knows that I am usually a pretty happy, optimistic guy, especially when there is cake in the vicinity (see Figure 3). Would I lie to you about cake? Never!

But it is not only cake about which I am optimistic. I also feel quite certain that we will soon have some more supernova neutrinos to study. As a matter of fact, I expect a never-ending stream of them.

How can this be? There have been just six core collapse supernovas, i.e., the type which produce neutrinos, seen in our galaxy in 1800 years, right?

Well, first of all, one should not underestimate the power of six events. As luck would have it, there were exactly six events in my Ph.D. thesis experiment on the double Dalitz decay of the long-lived neutral kaon [1]. There were also just six fiducial events in the already famous nonzero-θ_{13} paper from the T2K experiment [2].

It should be remembered that those six supernova events were just the ones which could be seen with the naked eye for which records were made and, critically, whose records *survived* to the present day. Undoubtedly there were many, many more explosions during this time period, all of which would have been quite easily observed by a functioning neutrino telescope, had one but been available during, say, the Dark Ages.

Figure 3: A happy guy with cake at IPMU's 1$^{\text{st}}$ anniversary party.

Indeed, it is believed that the core collapse supernova rate in the Milky Way galaxy is somewhere between one and three per century. Still not great, cheating death-wise, but considerably better than one per three hundred years, which would pretty much come up as a win in Death's column most of the time.

But you know what? Screw all this waiting around stuff! I have a better idea...

5 Having Your Cake and Eating It, Too

Supernovas in our galaxy may be relatively rare on a human timescale, but supernovas themselves are not rare at all. On average, somewhere in the universe *there is a supernova explosion once every second.* What's more, all of the neutrinos which have ever been emitted by every supernova since the onset of stellar formation suffuse the universe. These comprise the so-called "diffuse supernova neutrino background" [DSNB], also known as the "relic supernova neutrinos." They have not yet been seen, but if they proved to be observable they could provide a steady stream of information about not only stellar collapse and nucleosynthesis but also on the evolving size, speed, and nature of the universe itself.

And yet, in terms of the non-terrestrial neutrino forecast, there is no doubt that "sunny" is the key word. The flux of solar ^{8}B neutrinos is some 10^6 times the subtle DSNB flux.

In 2003, Super–Kamiokande [Super–K, SK] published the results of a search for these supernova relic neutrinos [3]. However, this study was strongly background limited, especially by the many low energy events below 19 MeV which swamped any possible DSNB signal in that

most likely energy range, as well as by Michel electrons from sub-Cherenkov threshold muons produced by atmospheric neutrino interactions in the detector. Consequently, this previous SK study could see no statistically significant excess of events and therefore was only able to set the world's most stringent upper limits on the relic flux.

In the time between my talk at DESY and this article's writing, a new Super–K relic paper has come out sporting a new, improved analysis and much more data [4]. However, even with improved cut efficiencies and a lower threshold of 16 MeV the backgrounds still dominate, and the resulting relic flux limits are depressingly quite similar to those from eight years ago. Oy.

But didn't I say there would be cake at this party? All right then, one cake, coming up!

6 Doing Something About the (Neutrino) Weather

In order to finally see the elusive DSNB signal, theorist John Beacom and I are proposing to introduce a water-soluble gadolinium [Gd] compound, gadolinium chloride, $GdCl_3$, or the less reactive though also less soluble gadolinium sulfate, $Gd_2(SO_4)_3$, into the Super–Kamiokande detector (shown in Figure 4). As neutron capture on gadolinium produces an 8.0 MeV gamma cascade, the inverse beta decay reaction, $\overline{\nu}_e + p \rightarrow e^+ + n$, in such a Gd-enriched Super–K will yield coincident positron and neutron capture signals. This will allow a large reduction in backgrounds and greatly enhance the detector's response to both supernova neutrinos (galactic and relic) and reactor antineutrinos.

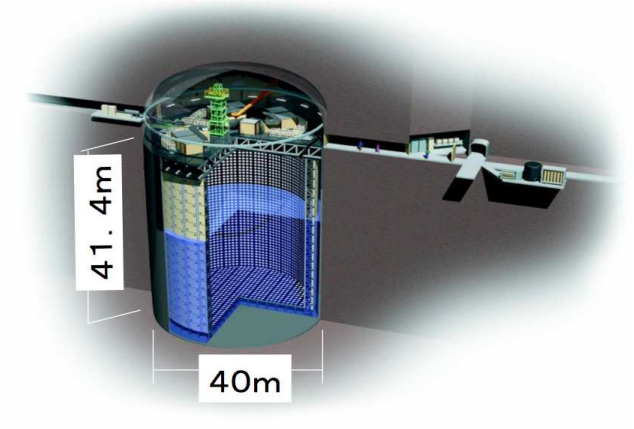

Figure 4: The Super–Kamiokande detector, located one kilometer underground in Mozumi, Japan. At 50,000 tons of water, it's large: the Statue of Liberty would fit inside.

The gadolinium must compete with the hydrogen in the water for the neutrons, as neutron capture on hydrogen yields a 2.2 MeV gamma, which is essentially invisible in Super–K. So, by using 100 tons of gadolinium compound we would have 0.1% Gd by mass in the SK tank, and just over 90% of the inverse beta neutrons would be visibly caught by the gadolinium. Figure 5 is an artist's (okay, *my*) conception of how the gadolinium will be delivered.

Figure 5: "I got 1999 more of these here 50 kilo fellers out in the truck. Yup, it's a pretty big truck."

Due to a collapse in the price of gadolinium as a result of large-scale production facilities operating in Inner Mongolia, adding this much gadolinium to Super–K should cost no more than $600,000 today, though it

would have cost a staggering $400,000,000 back when SK was first designed. This is primarily due to the fact that the rare earth elements are found blended together in nature, and when refining one of them the others are inevitably produced, with or without an accompanying commercial market demand (see Figure 6).

Figure 6: Where rare earths are concerned, if you've refined one, you've refined 'em all.

Figure 7: Mark Vagins and John Beacom working on GADZOOKS!. In case you're wondering, this drawing shows us as we appeared back in 2003. Sigh.

We call this new project "GADZOOKS!". In addition to being an expression of surprise as well as an archaic swear word dating back to 1694 (but as such *still* nearly a century more recent than the last galactic supernova), it's also a sweet acronym: Gadolinium Antineutrino Detector Zealously Outperforming Old Kamiokande, Super!

People tend to either love this name or hate it, but no one forgets it, which is important when promoting a new idea. The basics of this load-SK-with-Gd proposal are detailed in our *Physical Review Letters* article [5], the creation of which I've whimsically depicted in Figure 7. The relationship between gadolinium loading and the percentage of neutrons which the Gd will capture is plotted in Figure 8.

7 Supernova ν Signals? We Gotcha' Signals Right *Here!*

7.1 DSNB Signal: Betting On a Sure Thing

Adding $Gd_2(SO_4)_3$ to Super–Kamiokande will make it possible to look for coincident signals, i.e., for a positron's Cherenkov light followed shortly – within 50 microseconds – and in the same spot – easily within SK's best vertex fitter's position resolution – by the gamma cascade of a captured neutron. Once this happens, then troublesome spallation singles backgrounds could be eliminated and the analysis threshold lowered far below the old 19 MeV cutoff or even the present one at 16 MeV. This would be accomplished by simply applying most of the same techniques used in SK's usual solar neutrino analysis [6], the only major difference being that a search for pairs of correlated events would allow extraction of the inverse beta signal.

Note that without neutron tagging, after the normal cuts are applied only three neutrino-like singles events per cubic meter per *year* remain (see Figure 9), so requiring pairs of events to fall within 50 μs and 50 cm will essentially wipe out most non-inverse beta backgrounds.

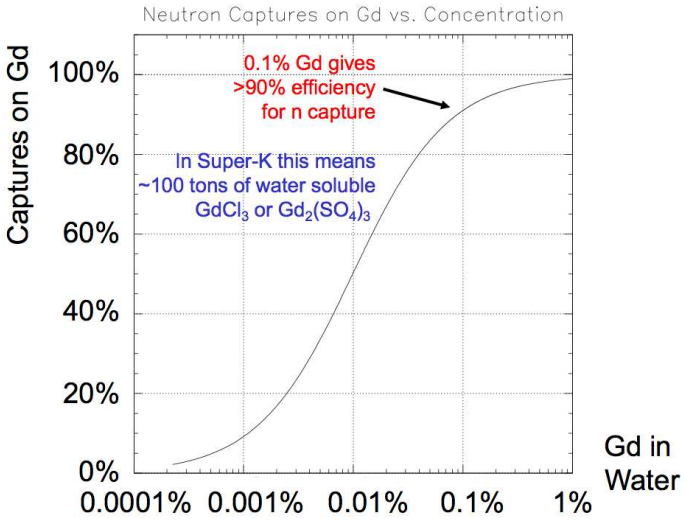

Figure 8: (color online) Neutron capture efficiency vs. gadolinium loading. The remaining neutrons get caught by the H in all that H_2O.

Figure 9: After the usual solar cuts, Super–K is left with only three neutrino-like events per cubic meter per year. That's all, folks!

Going lower in energy will not only allow a detection of the so-far unseen DSNB flux, but it will also allow the extraction of important – and unique, barring a galactic supernova – information regarding the neutrino emission parameters of supernovas. The sparse SN1987A data is in disagreement regarding the average luminosity and energy of the supernova $\overline{\nu}_e$'s.

DSNB models vary, and there is in fact some tension between the models (and their proponents), but according to a rather definitive modern review of the topic, Super–K with gadolinium should see about five of these supernova events every year [7]. This rate, if correct, would allow a rather prompt (within one year) discovery of the DSNB by SK [8] and hence lead to correspondingly rapid solutions to a number of long-standing questions, including the seemingly incompatible SN1987A neutrino data sets, the actual rate of optically dark explosions, the correct heavy metal production model, and the average supernova neutrino emission parameters. Furthermore, with fresh supernova neutrino data in hand for the first time in a generation, such an observation will undoubtedly stimulate new theoretical (and perhaps even experimental) developments in the neutrino and cosmology communities.

Figure 10 shows the expected spectrum of neutron-tagged positrons – signal and background – in a Gd-enriched Super–K. The width of the band labeled "DSNB" reflects the remaining allowed range of theoretical flux predictions for the relic signal. The scale of the expected reactor signal is uncertain at best right now, as what is shown assumes normal operations of all Japanese reactors, which is probably unlikely (to say the least) anytime soon. However, note that the lower bound on the DSNB window would be only marginally reduced by up to a 90% cut in reactor flux; even if all the Japanese reactors are turned off there will still be some

operating on the Korean peninsula... yes, on both sides of the DMZ!

At any rate, we expect to see a (few?) thousand or so coincident reactor antineutrino events in a gadolinium-enriched Super–K each year, along with about five coincident supernova relic neutrinos events. Remaining coincident backgrounds from atmospheric neutrinos which contribute to the DSNB flux will be small, less than one a year, and their number decreases with falling energy while the flux of supernova neutrinos rises. The remaining spallation background will lie under the huge reactor flux and will therefore be negligible.

The net result? A steady stream of supernova neutrinos without the annoying wait!

7.2 Galactic Supernova Signal: Hey, It's Gotta Happen Eventually

If we are fortunate enough to observe a nearby supernova in the coming decades, it would be most beneficial to have $Gd_2(SO_4)_3$ in the water of the large water Cherenkov detectors which are online when the resulting neutrino wave sweeps across the planet. This is primarily because their most copious supernova neutrino signal by far (∼88%) comes from inverse beta events. These are only produced by one of the six species of neutrinos and antineutrinos which are generated by a stellar collapse, and so if we could be tag them individually by their follow-on neutron captures then we could extract the $\overline{\nu}_e$ time structure of the burst precisely, gaining valuable insight into the dynamics of the burst. What's more, we could then subtract them away from the more subtle non-$\overline{\nu}_e$ signals, uncovering additional information that would otherwise be lost from this once-in-a-lifetime (we should be so lucky) happening.

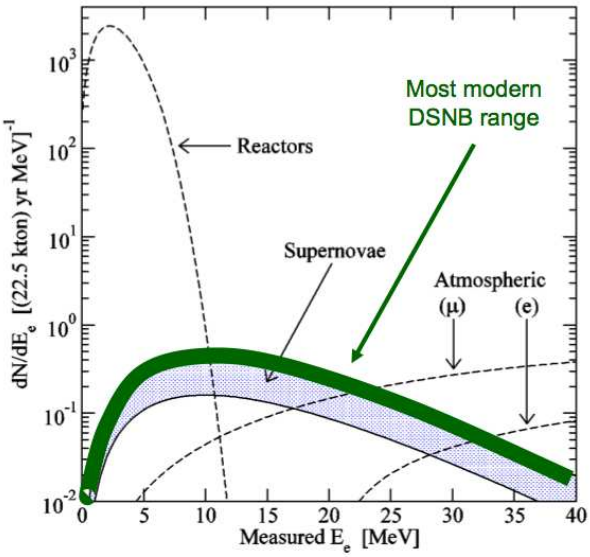

Figure 10: (color online) Expected positron spectrum tagged by neutron captures in a Gd-enriched Super–Kamiokande. One year of data is shown, with SK's energy resolution and all known backgrounds taken into account. Note the clear window for observing the relic supernova neutrinos between the reactor and atmospheric neutrino events.

For example, being able to tag the $\overline{\nu}_e$ events would immediately double SK's pointing accuracy back to the progenitor star. This is merely the result of statistics, since the elastic scatter events (about 3% of the total) would no longer be sitting on a large background in angular phase space [9]. Super–Kamiokande is the only running detector with useful neutrino pointing capability; reducing the error on this quantity by a factor of two would reduce the amount of sky to be searched by a factor of four. This could prove quite important for the narrow-field astronomical instruments which would be attempting, assuming of course that Super–K can get the word out in time, to see the first light from the new supernova.

At the same time, this event-by-event subtraction would allow identification of the initial electron neutrino pulse from the neutronization of the infalling stellar matter, a key input in understanding supernova dynamics.

Oh, and here's a really neat trick: if

the exploding star was big and rather close (∼two kiloparsecs or less) we would get an early warning of its impending collapse [10]. Approximately a week before exploding, the turn-on of silicon fusion in the core would raise the temperature of the star sufficiently that electron-positron annihilations within its volume would begin to produce $\overline{\nu}_e$ just above inverse beta threshold. The sub-Cherenkov positrons would be invisible, but in SK the captures of the resulting neutrons on gadolinium would result in a sudden, dramatic, and monotonically increasing singles rate. As early as six days before collapse there would be a five sigma excursion in SK's low energy singles rate in the case of Betelgeuse nearing the end of its lifetime. The continuing increase in singles rate would clearly indicate a coming explosion, ensuring that no one would intentionally turn off Super–K for calibration or maintenance and thereby miss the big event. Only Super–K with effective neutron tagging can receive this early warning; no other existing detector can do this.

In addition, a gadolinium-enriched Super–K would be sensitive to very late black hole formation following a supernova explosion anywhere within our galaxy, since the distinctive coincident inverse beta signals from the cooling phase could be distinguished from the usual singles backgrounds. An abrupt cutoff of these coincident signals occurring even many minutes or hours after the main burst would be the conclusive signature of a singularity being born. Direct observation of such an event – witnessing (and thereby measuring) the actual moment of a black hole's creation – would clearly be of great value, especially when eventually correlated with electromagnetic signals from X-ray or gamma-ray observatories, or gravitational wave signals.

8 Gadolinium R&D – Or, How I Became a Plumber

8.1 Selective Water Filtration in Sunny Southern California

Since maintaining the excellent light transmission of a water Cherenkov detector is a crucial requirement, the insertion of any chemical compound is a challenging task. Simply put, we want to shovel 100 tons of something into ultrapure water without screwing up its clarity. And there is another immediate challenge to making GADZOOKS! work in the real world:

In detectors such as Super–Kamiokande, the long mean free path of light (∼100 meters) is maintained by constant recirculation of the water through a water purification system. The existing SK purification system would dutifully and rapidly eliminate any added gadolinium along with the contaminants that are currently removed to maintain optical clarity. Crap!

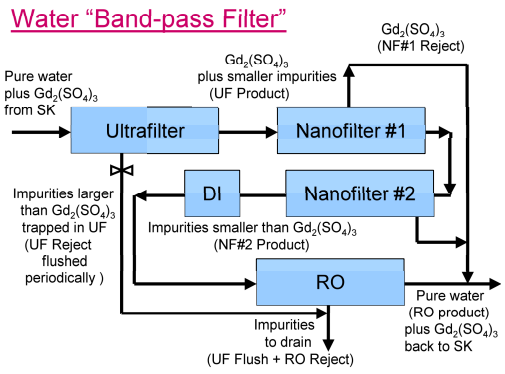

Figure 11: Selective water filtration conceptual design. Looks pretty simple, huh?

To solve this fundamental problem, I had to do something which had not been done before: invent a molecular "Band-pass Filter," a system capable of *selectively* filtering the water to retain the Gd while removing the impurities. To this end, a scaled-down version of the SK water filtration system was built under my direction at the University of California, Irvine [UCI], where I hold a joint appointment. The essential idea is as follows: there are a variety of commercially produced, membrane-based filters on the market. Rated by the size of pores in the membrane, they

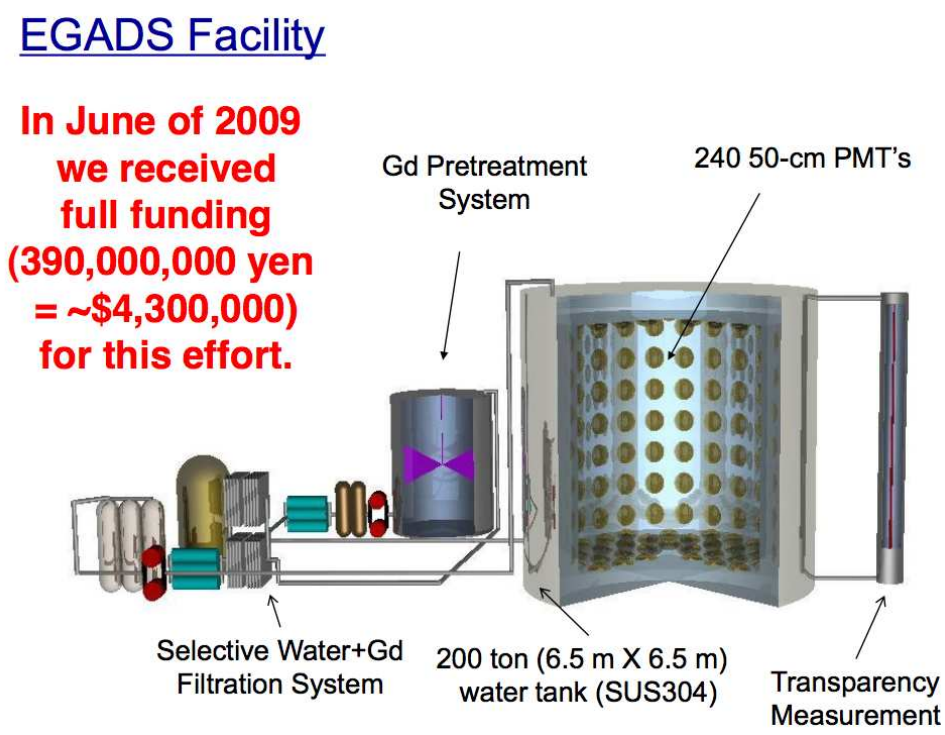

Figure 12: EGADS, the new large-scale gadolinium test facility in the Kamioka mine.

reject contaminants larger than these holes, while passing those which are smaller into the product water stream. By using a suitable sequence of filters, and by introducing nanofiltration, a new membrane intermediate in pore size between reverse osmosis (which rejects all gadolinium and everything larger) and ultrafiltration (which passes all gadolinium and everything smaller), I hypothesized – a fancy science word for "guessed" - that a fundamentally new type of filtration system could be assembled. It would selectively extract $Gd_2(SO_4)_3$ from the water stream and return it to the tank, while allowing all other impurities to be removed via the usual combination of reverse osmosis [RO] and deionization [DI]. This concept is shown schematically in Figure 11.

Amazingly, the damn thing worked. Chemical analysis on the prototype system at UCI showed that a particular two-stage nanofilter separated all Gd and SO_4 ions from the main water stream and allowed de-ionizing of that main water stream while maintaining the transparency of the water. Even after one thousand passes of the water through the system there was no detectable drop in gadolinium concentration – holy crap! Then it was time for the next step.

8.2 EGADS: In the Hall of the Mountain King

Although a small, sealed, gadolinium-loaded calibration device has already been deployed in Super–Kamiokande to verify the detector's predicted response to Gd neutron capture gammas [11], before Gd can be introduced into SK itself I must first demonstrate that the selective

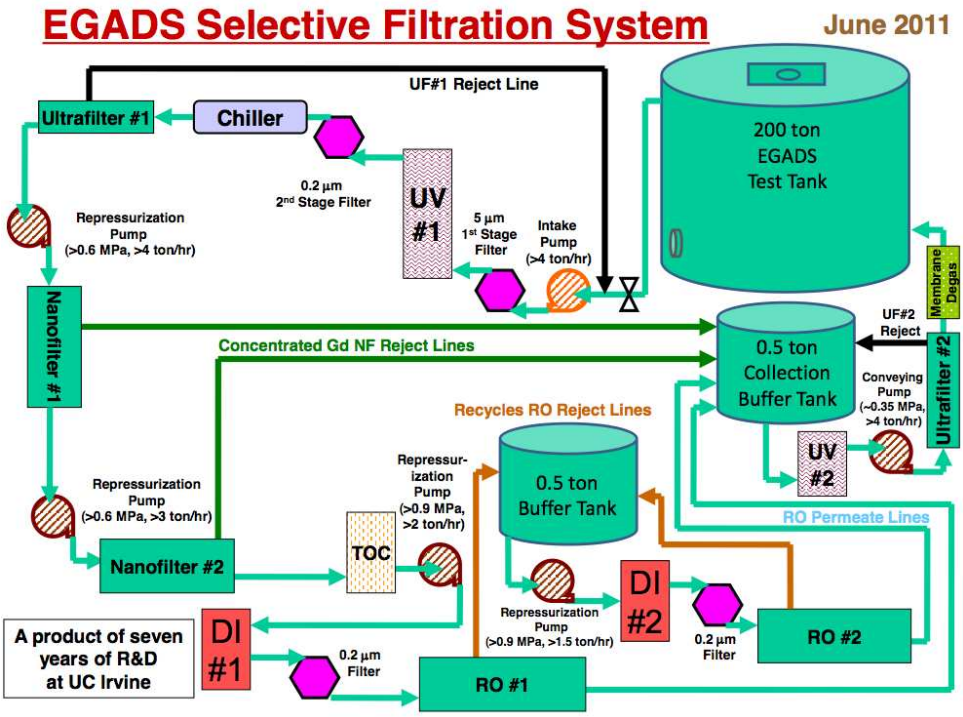

Figure 13: The selective filtration water system for EGADS. It will be capable of processing 100 tons of gadolinium-loaded water each day.

water recirculation technique works on a massive scale and that light transmission will only be marginally reduced by the presence of dissolved $Gd_2(SO_4)_3$. To this end, a new experimental chamber has been excavated in the Kamioka mine, located close to Super–Kamiokande. There, a dedicated, large-scale gadolinium test facility and water Cherenkov detector (essentially a ∼200 ton scale model of Super–K) is being built as depicted in Figure 12.

Known as EGADS (Evaluating Gadolinium's Action on Detector Systems), it will be used to make absolutely sure that the introduction of Gd will not interact with the detector materials and to certify the viability of the Gd-loading technique on a large scale, closely matched to the final Super–K requirements.

Funding for the new facility has been obtained in Japan to the tune of 390,000,000 yen (about $4,300,000 at the current exchange rate); construction began in September of 2009. Within nine months we had gone from solid rock to an excavated hall with a total volume of about 2.5 kilotons ready for physics occupancy, complete with a 200 ton stainless steel tank. Six months after that a significantly scaled-up version of my UCI selective water filtration system had been assembled and installed. It started running with pure water in January of 2011, and has been filtering dissolved gadolinium sulfate since August of that year.

The flow chart of the EGADS selective filtration system can be seen in Figure 13; it has certainly gotten a bit more complicated than the conceptual design shown in Figure 11, but this is what it takes to make things work in the real world. An additional requirement which the

underground EGADS version of my system had to meet was that it do its job in a nearly lossless fashion – and indeed, note that there are no drain lines in Figure 13. Instead, all rejected water is cleaned and recycled. But guess what? This lossless design works, too!

A custom data acquisition system is currently being assembled and tested, and in the spring of 2012 a total of 240 calibrated 50-cm photomultiplier tubes, the same design as those being used in Super–K, will be installed in the tank.

Comparative studies both with and without dissolved gadolinium in the 200 ton tank will take place during 2012 and 2013. If all goes well, we should be ready to introduce gadolinium into Super–Kamiokande sometime within the next few years. The ultimate goal is to be able to make the world's first conclusive DSNB observation by 2016. Gadzooks, indeed!

9 My Fearless Extended Forecast

Figure 14: Got a kilo of Chinese white gadolinium powder concealed in your carry-on bags at the airport? Hey kids, don't try this; it might not end well.

As one who has spent, over the last eight years, many a long day and longer night covered with gadolinium dust (don't worry, it's [mostly] harmless), I can state with certainty that it has been a long, strange trip trying to get Gd into Super–Kamiokande. There have been exciting breakthroughs and discoveries along the way.

A series of important discoveries I made: a) it is an exceedingly bad idea to put any large quantity of gadolinium in your carry-on bags when traveling internationally, because b) Gd is opaque to X-rays, and c) airport personnel get very upset indeed (see Figure 14) when they find a kilogram of mysterious white powder from China in someone's luggage. Oh, and d) it will not improve your situation one bit to cry out to the security folks who are pointing automatic weapons at you and pawing your precious container of highly-refined gadolinium, "Don't open that! It's very pure!"

This incident took place, I kid you not, at John Wayne Airport (yes, named after the actor who usually played gun-toting cowboys) in Orange County, California. At any rate, I was eventually released from police custody, and progress on enriching Super–K with Gd could continue.

The Japanese-backed funding and rapid construction of EGADS, not to mention its very promising early results, indicates that the goal is finally within sight. If adding gadolinium to Super–K is a success, then I am convinced that – almost overnight – selective filtration will become part of the standard technology suite for all future water Cherenkov detectors, taking its place alongside such venerable components as phototubes and high voltage supplies.

Already, as I have been laboring away deep underground, the GADZOOKS! concept has gained significant traction around the world. Note that this is the only method of detecting neutrons which can be extended to the tens-of-kilotons scale and beyond, and at reasonable expense – adding no more than 2% to the capital cost of detector construction – as well. Given the additional physics reach neutron detection makes possible (for supernova studies as well as

other, unrelated topics like proton decay), getting this capability for minimal extra cost is an enticing possibility.

This is probably why all of the major proposed next-generation water Cherenkov detectors either are officially retaining Gd-loading as an option (LBNE in the US [12]) or simply assume it as part of their baseline design (Hyper–Kamiokande in Japan [13] and MEMPHYS in Europe [14]). The recent Hyper-Kamiokande Letter of Intent [13] even went so far as to include the benefits of gadolinium in its Executive Summary.

Any one of these new detectors, once enriched with gadolinium, will be able to record on the order of *one hundred relic supernova neutrinos every year.* They will therefore accumulate statistics comparable to the total number of events seen from SN1987A by Kamiokande every single month they are in operation.

As if that's not enough to make one giddily optimistic, having one or more such giant, Gd-enhanced detectors awaiting the next galactic supernova is also a truly exciting prospect. In other words: delicious cake for everyone!

So, I think it is safe to predict that the extended outlook for supernova neutrinos is remarkably bright and sunny indeed.

References

[1] M. R. Vagins, R. K. Adair, H. B. Greenlee, H. Kasha, E. B. Mannelli, K. E. Ohl, M. P. Schmidt and E. Jastrzembski *et al.*, "Measurement of the branching ratio for K(L) → e+ e- e+ e-," Phys. Rev. Lett. **71**, 35 (1993).

[2] K. Abe *et al.* [T2K Collaboration], "Indication of Electron Neutrino Appearance from an Accelerator-produced Off-axis Muon Neutrino Beam," Phys. Rev. Lett. **107**, 041801 (2011) [arXiv:1106.2822 [hep-ex]].

[3] M. Malek *et al.* [Super-Kamiokande Collaboration], "Search for supernova relic neutrinos at SUPER-KAMIOKANDE," Phys. Rev. Lett. **90**, 061101 (2003) [hep-ex/0209028].

[4] K. Bays *et al.* [Super-Kamiokande Collaboration], "Supernova Relic Neutrino Search at Super-Kamiokande," arXiv:1111.5031 [hep-ex].

[5] J. F. Beacom and M. R. Vagins, "GADZOOKS! Anti-neutrino spectroscopy with large water Cherenkov detectors," Phys. Rev. Lett. **93**, 171101 (2004) [hep-ph/0309300].

[6] J. Hosaka *et al.* [Super-Kamiokande Collaboration], "Solar neutrino measurements in super-Kamiokande-I," Phys. Rev. D **73**, 112001 (2006) [hep-ex/0508053].

[7] J. F. Beacom, "The Diffuse Supernova Neutrino Background," Ann. Rev. Nucl. Part. Sci. **60**, 439 (2010) [arXiv:1004.3311 [astro-ph.HE]].

[8] S. Horiuchi, J. F. Beacom and E. Dwek, "The Diffuse Supernova Neutrino Background is detectable in Super-Kamiokande," Phys. Rev. D **79**, 083013 (2009) [arXiv:0812.3157 [astro-ph]].

[9] R. Tomas, D. Semikoz, G. G. Raffelt, M. Kachelriess and A. S. Dighe, "Supernova pointing with low-energy and high-energy neutrino detectors," Phys. Rev. D **68**, 093013 (2003) [hep-ph/0307050].

[10] A. Odrzywolek, M. Misiaszek and M. Kutschera, "Detection possibility of the pair - annihilation neutrinos from the neutrino - cooled pre-supernova star," Astropart. Phys. **21**, 303 (2004) [astro-ph/0311012].

[11] H. Watanabe *et al.* [Super-Kamiokande Collaboration], "First Study of Neutron Tagging with a Water Cherenkov Detector," arXiv:0811.0735 [hep-ex].

[12] T. Akiri *et al.* [LBNE Collaboration], "The 2010 Interim Report of the Long-Baseline Neutrino Experiment Collaboration Physics Working Groups," arXiv:1110.6249 [hep-ex].

[13] K. Abe, T. Abe, H. Aihara, Y. Fukuda, Y. Hayato, K. Huang, A. K. Ichikawa and M. Ikeda *et al.*, "Letter of Intent: The Hyper-Kamiokande Experiment — Detector Design and Physics Potential," arXiv:1109.3262 [hep-ex].

[14] A. de Bellefon, J. Bouchez, J. Busto, J. -E. Campagne, C. Cavata, J. Dolbeau, J. Dumarchez and P. Gorodetzky *et al.*, "MEMPHYS: A Large scale water Cerenkov detector at Frejus," hep-ex/0607026.

List of Authors

List of Participants

Arcones, Almudena (Basel University)
Balantekin, A. Baha (Wisconsin University)
Bruenn, Stephen (Florida Atlantic University)
Cardall, Christian (Oak Ridge National Laboratory)
Chakraborty, Sovan (Hamburg University)
Chavarria, Alvaro (Princeton University)
Dighe, Amol (TIFR Mumbai)
Espinoza, Maria Catalina (IPN Orsay)
Fogli, Gianluigi (Bari University)
Fulgione, Walter (INAF & INFN Torino)
Hagner, Caren (Hamburg University)
Heereman, David (IIHE VUB-ULB Brussels)
Jachowicz, Natalie (Gent University)
Janka, Hans-Thomas (MPA Garching)
Keum, Yong-Yeon (Seoul National University)
Kneller, James P. (North Carolina State University)
Kroll, Gösta (Mainz University)
Liebendörfer, Matthias (Basel University)
Ianni, Aldo (LNGS Assergi)
Lisi, Eligio (INFN Bari)
Lund, Tina (North Carolina State University)
McLaughlin, Gail (North Carolina State University)
Marrone, Antonio (Bari University)
Mirizzi, Alessandro (Hamburg University)
Molinaro, Andrea (INFN Torino)
Montanino, Daniele (Lecce University)
Mornas, Lysiane (University Oviedo)
Müller, Bernhard (MPA Garching)
Nunokawa, Hirsoshi (Rio de Janeiro University)
Ott, Christian (Caltech)
Palazzo, Antonio (TUM Munich)
Raffelt, Georg (MPP Munich)
Sakuda, Makoto (Okayama University)
Sawyer, Raymond (Santa Barbara University)
Saviano, Ninetta (Hamburg University)
Scholberg, Kate (Duke University)
Serpico, Pasquale Dario (LAPTH Annecy-le-vieux)

Sigl, Günter (Hamburg University)
Sarikas, Srdjian (MPP Munich)
Shen, Gang (Los Alamos National Laboratory)
Surman, Rebecca (Union College, New York)
Tamborra, Irene (MPP Munich)
Tomàs, Ricard (Hamburg University)
Tsiledakis, Georgios (CEA/Irfu Saclay)
Väänänen, Daavid (IPN Orsay)
Vagins, Mark (IPMU, Tokyo)
Virtue, Clarence (Laurentian University & SNOLAB)
Wurm, Michael (Hamburg University)
Zhou, Shun (MPP Munich)


WISSENS
WERTE.
Öffentlicher Abendvortrag im Rahmen der HAνSE 2011
HAνSE 2011
Rätselhafte Supernovae –
den Geheimnissen der größten
kosmischen Explosionen auf der Spur
Dr. Hans-Thomas Janka


Background (DSAB)
• Axions with $m_a \sim 10$ meV
near SN 1987A energy-loss limit
• Provide DSRB with comparable
energy density as DSNB and EBL
• No obvious detection channel
Raffelt, Redondo & Viaux
work in progress (2011)
HAνSE ★ 2011


HAνSE 2011
Universität Hamburg
Particles, Strings, and the Early Universe
LEXI

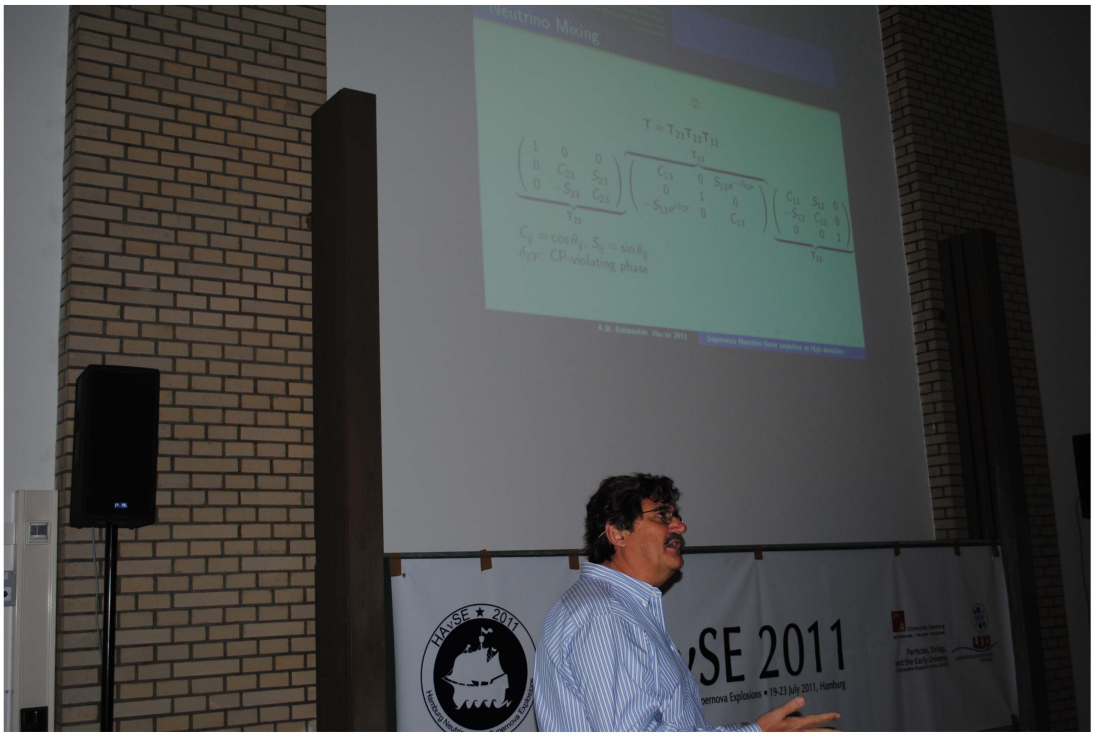
Neutrino Mixing
$T = T_{23}T_{13}T_{12}$
$C_{ij} = \cos\theta_{ij}, S_{ij} = \sin\theta_{ij}$
δ_{CP}: CP-violating phase
HAνSE 2011

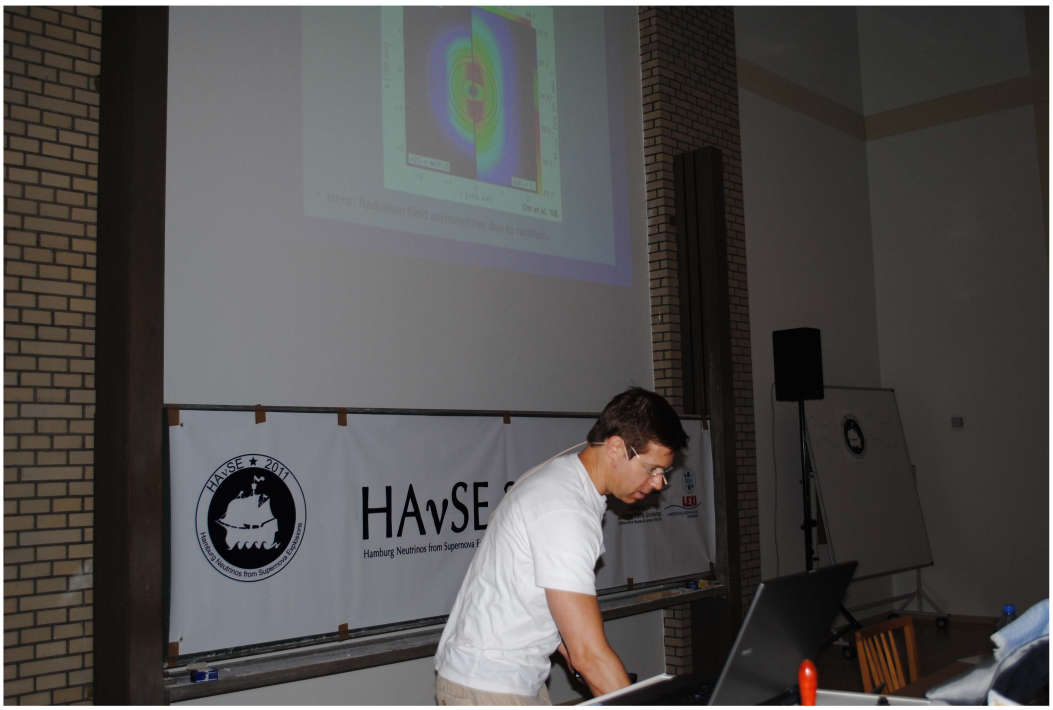
HAvSE
Hamburg Neutrinos from Supernova


HAvSE 2011
Hamburg Neutrinos from Supernova Explosions • 19-23 July 2011, Hamburg